PROBING BASE METAL COORDINATION COMPLEXES USING ELECTROSPRAY IONIZATION QUADRUPOLE TIME-OF-FLIGHT MASS SPECTROMETRY

Jessica J. Martin

SUBMITTED IN PARTIAL FULFILLMENT
FOR THE DEGREE OF MASTER OF SCIENCE

Department of Chemistry and Biomolecular Sciences | Département de Chimie et Sciences Biomolécularies
University of Ottawa | Université d'Ottawa
Ottawa, Ontario K1N 9B4

ABSTRACT

Presently, much research has been completed focusing on metal coordination complexes in the liquid phase but very little in terms of the gas phase. The purpose of this research is to further investigate these conditions and learn more about the reactions that can occur using Electrospray Ionization Quadrupole Time-of-Flight Mass Spectrometry (ESI QToF MS). This research focuses on Nickel (II) and Iron (III) Nitrate solutions in combination with five ligands: 2,2'-Bipyridine, 4,4'-Bipyridine, 2,2'-Bipyridine-4,4'-Dicarboxylic Acid, 1,10-Phenanthroline and the Baker Group's SNS Ligand. Observations of these complexes were restricted to the monocations. Those combinations that successfully coordinated in the gas phase were subjected to further analysis to determine their fragmentation pathways under specific conditions. To investigate their interactions, studies were conducted using three different mixing techniques. These techniques included a pre-mixed single-spray solution, a dual-spray injection method, and the TRESI (time-resolved electrospray ionization) method. By using all three methods, the compounds' ability to react in solution over time can be compared to real-time mixing in both the gas and liquid phases, via dual-spray and TRESI techniques respectively. Further experimentation took place on target complexes, created by each of the ten combinations of starting compounds, to further investigate the gas phase properties and fragmentation patterns that exist. It was observed that most experiments with the Nickel (II) Nitrate solution were successful with all three methods, while the Iron (III) Nitrate however created some problems. In general, single-spray analysis gave the best results compared to dual-spray, which was ineffective for some combinations, particularly the 2,2'-Bipyridine-4,4'-Dicarboxylic Acid and SNS ligands. It was found that both the 2,2'-

Bipyridine and 4,4’-Bipyrdine combinations produced very similar results despite their respective bidentate and bridging coordination tendencies. The TRESI method provided limited information due to the delayed reaction times with some combinations. Overall, this work proved useful in its ability to compare metal coordination complex formation in solution and gas phases.

ACKNOWLEDGMENTS

This research was conducted at the University of Ottawa in Ottawa, Ontario, Canada out of the John L. Holmes Mass Spectrometry Facility. I would like to thank the John L. Holmes Mass Spectrometry Facility for the use of the equipment.

I would especially like to thank Dr. Sharon Curtis, Dr. Paul Mayer and my supervisor, Dr. R. Tom Baker. Thank you for your endless advice, guidance and encouragement during this project, as well as the opportunity itself. Your support and patience throughout the process have been invaluable. The knowledge and skills I have learned through my studies under your supervision have truly been an inspiration and I cannot thank you enough.

I would like to thank my thesis committee, for their time and energy in providing support and feedback in this process. I would like to also thank and acknowledge the members of both the Baker and Mayer research groups for their help and support during my time here. It was a pleasure to work with everyone, to learn and grow together even through these difficult times.

Finally, I would like to thank my friends and family for their love, encouragement and patience throughout this journey. I could not have gotten to where I am today without the help of those closest to me.

TABLE OF CONTENTS

LIST OF TABLES

LIST OF FIGURES

GLOSSARY

CID	Collision Induced Dissociation
Fragment Ion	A charged compound formed from the fragmentation of a precursor ion during the tandem mass spectrometry process.
DS	Dual-Spray
ESI	Electrospray Ionization
MS	Mass Spectrometry
Precursor Ion	A molecular ion that later fragments during tandem mass spectrometry.
QToF	Quadrupole Time-of-Flight
Resonant Ion	The ion selected for detection when using the quadrupole technique in the mass spectrometry process.
TRESI	Time-Resolved Electrospray Ionization

CHAPTER 1 – INTRODUCTION AND BACKGROUND

1.1 Introduction

Mass spectrometry is a significant and versatile technique that can be used to analyze a wide range of chemical compounds. It is an extremely helpful technique as it can identify unknown compounds and aid in the discovery of their structure by determining the elemental composition of a molecule.[1–3] In doing so, combinations of samples can be investigated and new unknown molecules can be identified using a variety of techniques mass spectrometry has to offer. Using mass spectrometry as a method of experimentation allows researchers to employ a variety of techniques and parameters within the instrument in order to achieve the best results possible.

Although it is a destructive technique, very little sample is required to acquire extremely precise results.[4] Additionally, mass spectrometry can be used on both inorganic and organic molecules, including those of organometallic nature, as long as they are volatile enough to fragment into molecular ions.[4,5] Oftentimes, electrospray ionization is coupled with mass spectrometry when working with metal coordination complexes and other covalent compounds.[3,5,6] Therefore, electrospray ionization mass spectrometry is an advantageous technique to employ when studying mixtures of organometallic compounds.

1.2 Background

1.2.1 Coordination Compounds

Coordination compounds are created by the covalent bonding of a ligand to a central metal atom. They are the product of a Lewis acid-base reaction whereby a metal cation accepts an electron pair from a neutral or anionic ligand.[4] Some transition metals have a higher affinity to specific elements present in these ligands, such as nickel which has a higher affinity for nitrogen-containing ligands.[7] These complexes are extremely important as they are often used in catalysis and biochemistry.[8,9]

Coordination chemistry was first discovered in 1891 by Alfred Werner.[10,11] His early work, for which he won the Nobel Prize for in 1913, laid the foundation for what is now referred to as a coordination number.[4,8] Up until his discovery, it was assumed that the valence number of a metal was the same as its coordination number.[8] Werner referred to these as the primary and secondary valence numbers, respectively.[8] Werner's theories of geometric isomerism within coordination compounds led to monovalent [M]X, divalent $[M]X_2$ and trivalent $[M]X_3$ complex configurations.[10] This was the basis for the Bloomstrand-Jorgensen's chain theory of bonding in coordination compounds that also accounted for the three-dimensional nature of compounds and their stereochemistry.[11]

Coordination numbers can range from two to nine, depending on the metal.[8] Those with low coordination numbers have a greater energy difference in their stereochemical arrangements when compared to complexes with higher coordination numbers.[8]

There is little research conducted in regard to coordination chemistry analysis in the gas phase, specifically using mass spectrometry techniques. There are several studies involving metal-ligand synthesis in aqueous media, specifically involving nickel

coordination and other metals such as cobalt, copper, iron and zinc.[12–14] These studies detail the findings of the coordination in solution using techniques such as IR (infrared) and UV-Vis (ultraviolet-visible) spectroscopy, DFT (discrete Fourier transform) analysis, IRMPD (infrared multiple photon dissociation) action spectroscopy, NMR (nuclear magnetic resonance) spectroscopy and X-ray crystallography.[12,15–20] All of these studies focus specifically on the physical analysis of the synthesized complexes in their aqueous or solid phases. However, there are limited studies that have used mass spectrometry as an analysis technique. Beginning with a study conducted in March 2000, the researchers did in fact use collision-induced dissociation techniques within an electrospray ionization quadrupole ion trap mass spectrometer (ESI QTrap MS).[21] Their results indicated a decrease in the coordination number of the metal in relation to the loss of a coordinated functional group and the formation of such product ions, as is to be expected when using this technique.[21] Those that did not decrease in coordination number assumes that the lost functional group is not involved in the coordination to the metal complex.[21] A study conducted in May 2005, again uses quadrupole ion trap mass spectrometry (QTrap MS).[22] Their results indicated that the gas-phase kinetics of the reactions are influenced by the functional groups bound to the metal ion, depending on their electron density.[22] They also found that these ligand groups can be displaced very easily in the gas phase.[22] A study from 2010, focusing on electrospray mass spectrometry found that aqueous solutions of divalent transition metals (MX_2), when mixed with a nitrogen containing ligand led to monocations with the coordinated monovalent counterion $[M(L)_mX]^+$.[7] The mass spectra also typically showed a large signal for the protonated ligand complex (LH^+).[7] Finally, a study from 2018 that used dual-electrospray synthesis concluded that many

unique species are formed in the gas phase, including those with two additional hydrogen atoms for many of the ligands studied.[23] Although few studies exist, the results are expected to be consistent throughout the course of this research.

There are also very few mentions of these specific compounds of interest studied in the literature. Although there are several studies that use the ligands of interest in this research, there were limited studies found to support all the combinations of complexes used. Nickel and iron metals have been found to be successful when creating ligand-coordinated complexes as well as their derivatives.[14] Phenanthroline is a common compound used in a variety of different contexts including in the coordination to nickel.[24,25] A study from March 2021 used Nickel (II) Nitrate in its study and the complex coordination proved to be successful.[24] Pyridine and dipyridyl ligands are also popular choices to synthesize complexes with iron, nickel and other transition metals.[26–28] Of the above mentioned research papers, none use mass spectrometry as an analysis method. Therefore, no judgments can be made as to the effectiveness of the coordination of these complexes in the gas phase as opposed to the previously used liquid phases.

1.2.2 Mass Spectrometry

In general, mass spectrometers measure the mass-to-charge ratio of ions.[4] A mass spectrometer is made of three components; the ionizer, the ion analyzer and the detector.[29] In the ionizer or ion source, the sample is converted into gas-phase ions. The analyzer then sorts the ions according to their mass to charge ratios (*m/z*). Finally, the detector measures the ions and reports them in the form of a mass spectrum.

Many types of mass analyser techniques exist including, but not limited to, time-of-flight (ToF), quadrupole (Q), magnetic sector, ion trap and tandem mass spectrometry

(MS/MS).[29] There are also several types of ionization methods such as electron impact (EI), electrospray ionization (ESI), atmospheric pressure chemical ionization (APCI) and matrix assisted laser desorption ionization (MALDI).[29] Each technique and method have their own advantages and disadvantages, depending on the type of sample being analysed.

The theory of mass spectrometry (MS) was first developed in 1912 and has been a crucial part of the scientific world ever since.[30] It was developed by J.J. Thomson and called a parabola spectrograph that he used to report the first evidence of non-radioactive isotopes.[30] In Thomson's model, today's concepts of mass-to-charge ratios still applied although denoted as *e/m* rather than today's abbreviation of *m/z*.[31] He determined these ratios based on the positive ions formed in cathode ray tubes when an electrostatic field was applied.[30,31] In 1946, the first concept of the time-of-flight-mass spectrometer was presented at an American Physical Society meeting in Massachusetts by William Stephens.[30,31] Up until this time, mass spectrometers were predominantly used by physicists and it was not until the 1940s that these instruments were commercially available to more scientists, specifically industrial chemists.[31] The quadrupole mass filter and ion trap were introduced in 1953 by Wolfgang Paul.[31] In the 1960s, the resolution was improved by the development of electrospray ionization and further again in 1985 by the development of matrix-assisted laser desorption/ionization.[30]

1.2.2.1 Electrospray Ionization

Electrospray ionization (ESI) is a great tool for analysing organometallic compounds that are soluble in a polar solvent.[32,33] It is an easy way of introducing organometallic complexes to the gas face and providing reproducible and reliable results when compared to other techniques.[5]

Electrospray ionization is known as a soft ionization method.[29] In other words, little energy is used in the fragmentation of molecules so to preserve the integrity of the complex. This is achieved by ionizing droplets of the molecules that are further desolvated in the instrument.[34] In ESI, gas-phase ions are created by spraying the solution through a charged capillary needle while using a nebulizer gas, which is often nitrogen, to produce either positively or negatively charged droplets.[3,4] As the droplets leave the sprayer, the vacuum chamber evaporates the solvent, leaving behind individually charged ions as seen in Figure 1.1.[4]

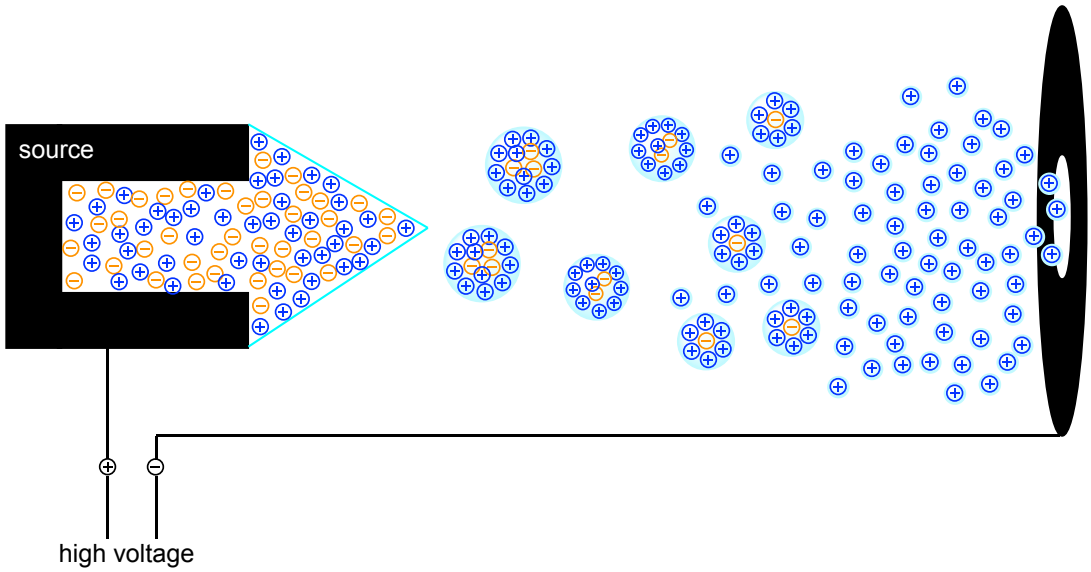

Figure 1.1 Overview of positive mode electrospray ionization.

With each method, only molecules with at least one respective charge can be detected.[35] In positive mode, basic analytes that are easily ionized make adducts with protons, meaning that the precursor ion still contains all original atoms, with the addition of a proton.[35] These ions can be singly or multiply protonated although usually found as singly protonated when in the lower total mass range, typically below 2000 Da.[5,35]

1.2.2.2 Quadrupole Time-of-Flight Mass Spectrometry

In a quadrupole time-of-flight mass spectrometer (QToF), there are two different mass analysers that the sample must pass through before reaching the detector. The first being the quadrupole which provides good sensitivity while the time-of flight portion provides high resolution.[36]

Within the quadrupole chamber there are four parallel circular electrodes that use a combination of alternating current (AC) and direct current (DC) to filter ions of a particular mass range.[36–38] Only ions that are within the set mass range, the resonant ions, will oscillate within the rods with a constant amplitude in order to exit the quadrupole and move through the instrument.[36] All others, the non-resonant ions, are filtered out and do not move forward.

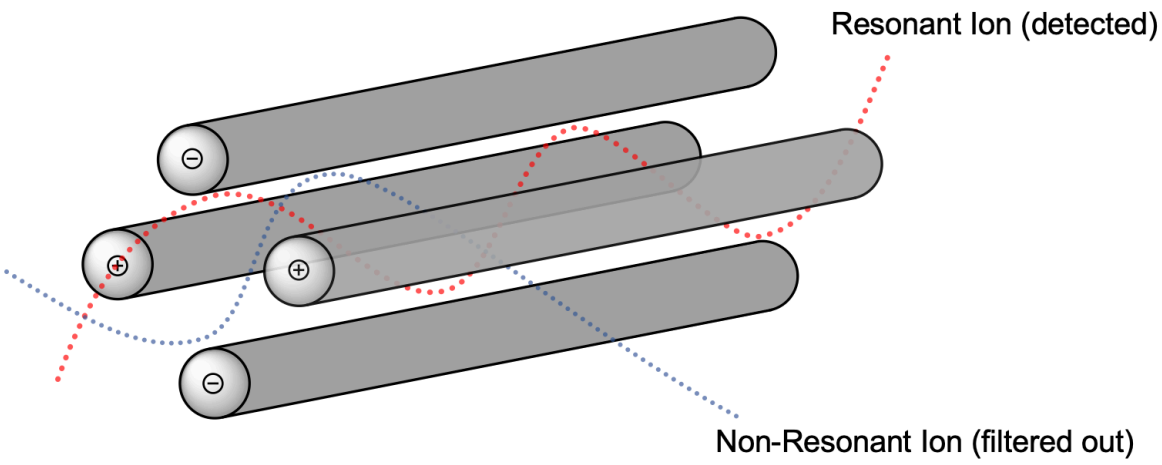

Figure 1.2 Quadrupole mass analyser.

In the time-of-flight portion, ions are separated based on their kinetic energy and velocity.[38] This is achieved by using a flight or drift tube and allowing the ions to travel through. Ions from the source are exposed to an electric field which accelerates their movement as they enter the tube, all to similar kinetic energies proportional to their charge.[36,39] As the ions travel through the tube, those with smaller masses and mass-to-charge ratios have a greater velocity and will reach the detector first while the larger ions will travel the slowest, as seen in Figure 1.3.[36,39,40] This overall process occurs quite quickly where tens of thousands of flights can occur per second.[39]

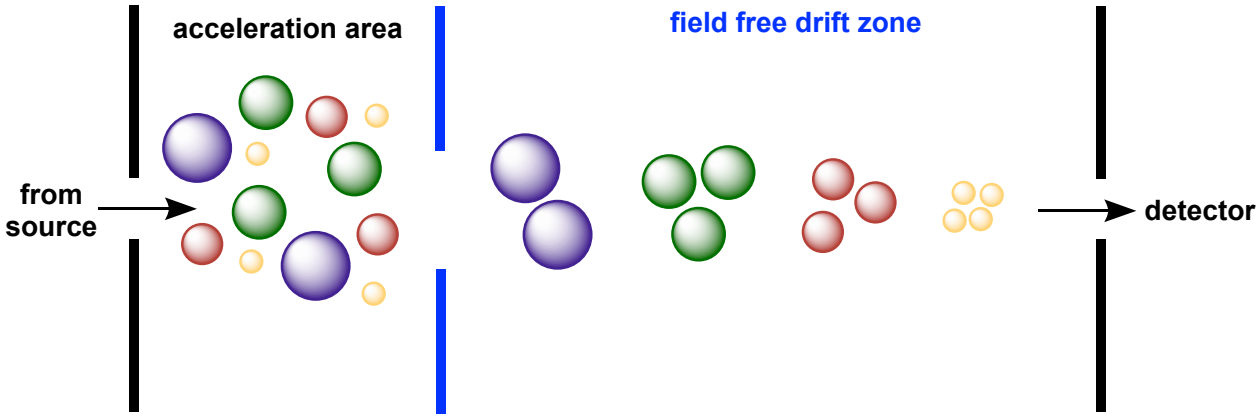

Figure 1.3 Overview of time-of-flight mass spectrometry.

By using the reflectron as seen in Figure 1.4, the resolution of the time-of-flight analyser is increased without lengthening the drift tube or losing sensitivity.[38,40] By applying an electric potential to an ion mirror, the ions are reflected back in the opposite direction, towards the detector.[40]

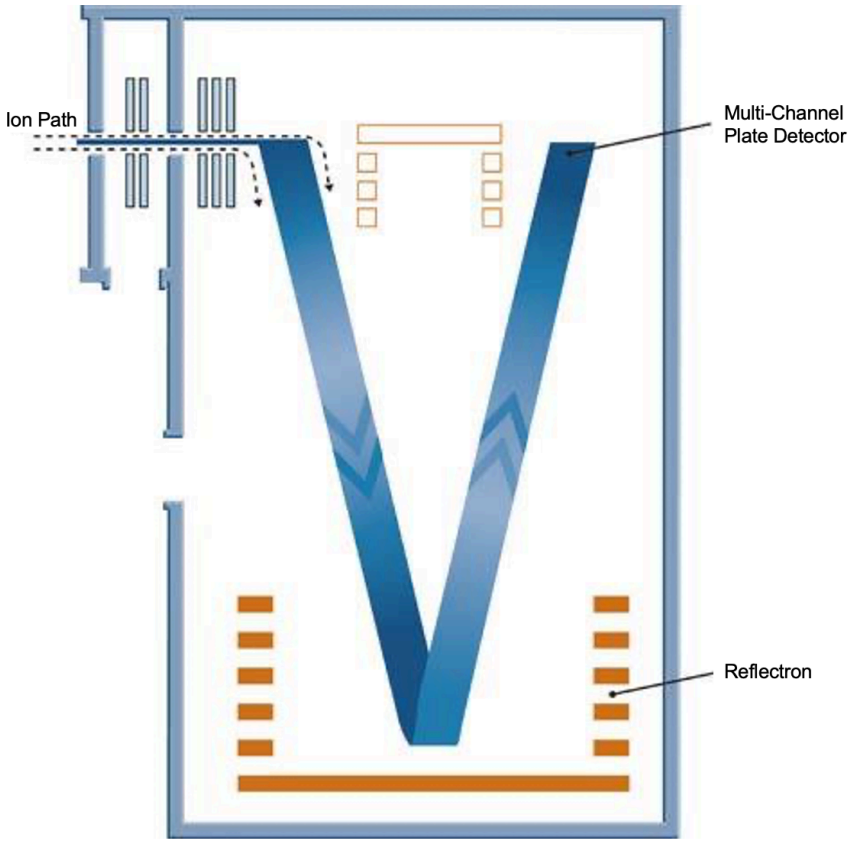

Figure 1.4 Time-of-flight drift tube employed in the Waters Synapt instrument.[36]

1.2.3 Time-Resolved Electrospray Ionization

In time-resolved electrospray ionization (TRESI), two syringes are connected together using a three-way junction allowing the monitoring of the reaction times of two solutions mixed together as they enter the instrument, as seen in Figure 1.5.[41,42] Each syringe is connected to a capillary tube, one outer and one inner. While the outer tube has a fixed conformation, the inner tube can be adjusted to increase the allotted reaction time. When the inner capillary is pulled back, the mixing volume is increased and therefore the sample has a longer reaction time before it enters the source.[41,42] This technique

allows the user to monitor milli-second timescale reactions.[41] This technique was modeled after the previously completed work by the lab of Derek Wilson of York University.

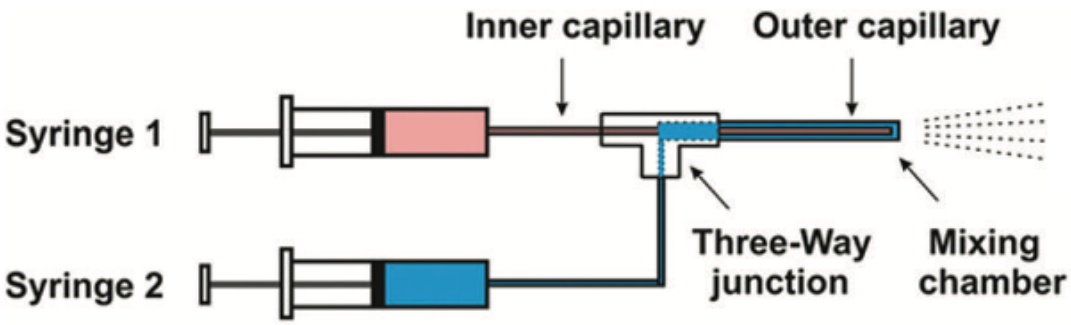

Figure 1.5 TRESI device setup.[41]

1.2.4 Collision Induced Dissociation

Collision induced dissociation (CID) is one of the most common activation techniques used today.[43] It is a method of fragmentation that breaks the chemical bonds of the precursor ion in order to form smaller pieces or fragments.[36] An applied electric potential gives the molecules high kinetic energy from which a portion is used in the collision.[36,44] This typically happens under vacuum in the instrument where the ions can collide with a neutral gas such as nitrogen or argon and the kinetic energy causes the bond to break and product or fragment ions to form.[36,43,44] This can be performed at varying energies with single or multiple collisions.[43] This information is extremely useful as it demonstrates to the researcher the structure of the precursor and fragments ions as well as the relative energies of the bonds themselves.[44]

1.3 Goals

The aim of this research project was to use mass spectrometry as a technique to further investigate base metal complexes and ligand coordination, particularly focusing on nitrogen containing ligands. To do so, we wanted to use a variety of different combinations of metals and ligands to observe the possible interactions of each mixture. We also wanted to use different techniques in order to have multiple points of comparison within the sample groups. By replicating these experiments with a variety of combinations, much can be learned from the results of these studies. This will include comparing mixing in the gas versus liquid phases, as well as real-time mixing versus extended reaction times in solution.

The goals of this study are outlined as follows. First, to investigate the stability of the target complexes in solution and in the gas phase. Second, to compare the ability of mass spectrometry as a technique to detect the target complexes of interest. Lastly, to determine the fragmentation patterns and breakdown pathways of the target complexes using mass spectrometry. By making these comparisons, it should become evident as to which combinations and techniques result in the most stable complexes and which provide the most clear fragmentation pathways when subject to specific conditions. It will also indicate which complexes perform best using mass spectrometry and under which conditions and states. It can be hypothesised that the size, type of functional group, acidity, solubility and other properties of the complexes will play a role in determining their effectiveness to be analysed via mass spectrometry techniques.

It is important to note that only the monocations were studied during this research. Doubly and triply charged ions typically create smaller peak clusters than those that are

singly charged.[45] Doubly charged molecules can be distinguished by their half-integer values when determining their mass-to-charge (*m/z*) ratios. However, complexes with even molecular weights will have their doubly charged ions found at one half the value, for dinuclear complexes this is the same mass peak as the singly charged ion.[45] For these reasons, only singly-charged ions were chosen to be the focus and for the purpose of simplicity when comparing results. Although the metals of interest will form double and triple charged ions, limiting the scope of this research to monocations will simplify the data generated.

1.3.1 Project Development

The focus for this research project was inspired by the research conducted by Shaan Rashid and Paul Mayer published in their paper *Dual-electrospray synthesis: A method of studying unique coordination complexes in the gas phase.*[23] In attempting to recreate this paper to observe the mass spectrometry techniques of the dual-spray method with Iron (II) Oxalate and 2,2'-Bipyridine solutions that were previously used, we were unable to observe the same results. This was attributed to the degradation of the stored oxalate sample over time. Instead, we chose to proceed with the 2,2'-Bipyridine ligand and experiment with the metal complex.

During the development process, Iron (II) Oxalate, Iron (III) Oxalate and Tin (II) Oxalate were all unsuccessful in creating the expected metal-ligand compounds when dual-sprayed with the 2,2'-Bipyridine ligand. It was determined that the stored samples of oxalate materials were no longer useable for research purposes. Finally, Nickel (II) Nitrate was used and found to be successful and was therefore chosen to use moving forward.

Iron (III) Nitrate was also chosen due to its nitrate group as well as its relation to the Baker Group research with Iron-SNS complexes.

Based on the success of the 2,2'-Bipyridine ligand, three other ligands were chosen to investigate for their similar chemical structures. Of course, 1-10-Phenanthroline was chosen as it was also used in the 2017 paper, in addition to 4,4'-Bipyridine and 2,2'-Bipyridine-4,4'-Dicarboxylic Acid. Furthermore, we chose to experiment with the Baker Group SNS ligand to further investigate our research goals.

1.4 Compounds of Interest

The compounds of interest for this research project are as follows; Nickel (II) Nitrate, Iron (III) Nitrate, 2,2'-Bipyridine, 4,4'-Bipyridine, 1,10-Phenanthroline, 2,2'-Bipyridine-4,4'-Dicarboxylic Acid, and the Baker Group's SNS ligand. It is important to note that unlike the other ligands, the SNS ligand exists as a cyclic proligand that binds to metals in its "open" form.[46] Chemical structures for these compounds can be found in Figure 1.6. All relevant information including chemical formula and molecular weight, as well as additional information pertaining to each compound can be found in Table 1.1 and 1.2.

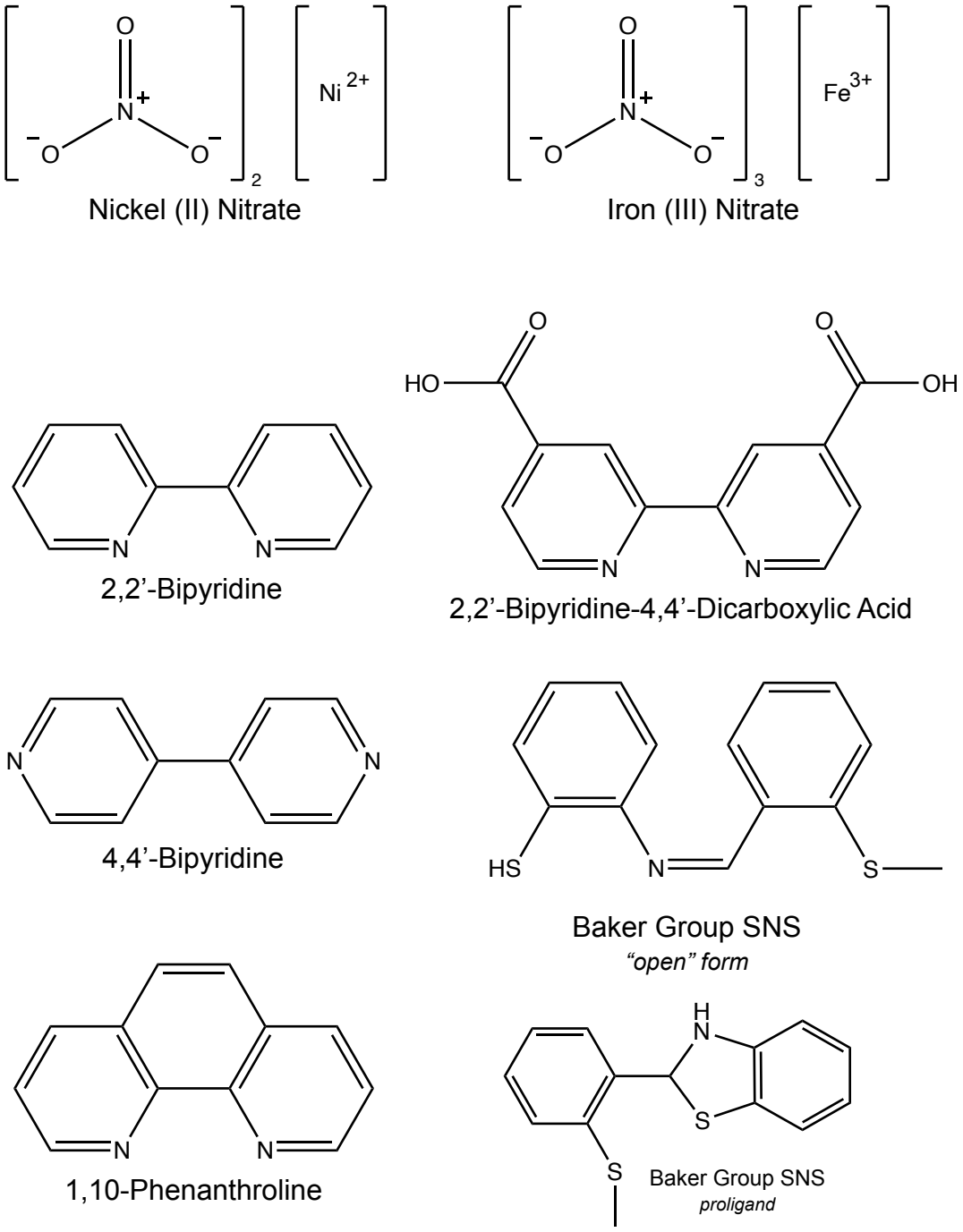

Figure 1.6 Chemical structures of all compounds of interest.

Table 1.1 Metal compounds of interest.[47–51]

Compound	Chemical Formula	Molecular Weight (g/mol)	Density (g/cm^3)	Boiling Point (ºC)	Melting Point (ºC)	Key Features	Main Uses
Nickel (II) Nitrate Hexahydrate	$Ni(NO_3)_2 \cdot 6H_2O$	182.70 *	2.05	136.7	56.7	A corrosive, non-combustible and oxidative compound, usually found in the form of solid green crystals.[47,48]	Often used to make nickel catalysts for the manufacturing of other chemicals.[47]
Iron (III) Nitrate Nonahydrate	$Fe(NO_3)_3 \cdot 9H_2O$	241.86 *	1.68	47	125	An oxidative and non-combustible material in small quantities, usually found in the form of solid violet crystals.[49,50]	Often used for chemical analysis and in medicine.[50]

* Indicates the molecular weight of the compound without water.

Table 1.2 Ligands of interest.[52–59]

Compound	Chemical Formula	Molecular Weight (g/mol)	Density (g/cm^3)	Boiling Point (ºC)	Melting Point (ºC)	Main Uses
2,2'-Bipyridine	$C_{10}H_8N_2$	156.18	~1.3	72	273.5	Often used in the determination of metals.[52]
4,4'-Bipyridine	$C_{10}H_8N_2$	156.18	~1.3	305	112	Often used in the preparation of polymers.[54]
2,2'-Bipyridine-4,4'-Dicarboxylic Acid	$C_{12}H_8N_2O_4$	244.20	~1.3	387	310	Often used in chemical synthesis.[55]
1,10-Phenanthroline	$C_{12}H_8N_2$	180.20	~1.3	300	117	Often used as an enzyme inhibitor, cathode buffer, chelator and versatile ligand.[58,59]
Baker Group SNS	$C_{14}H_{13}NS_2$	259.38				

CHAPTER 2 – MATERIALS AND METHODS

2.1 Reagents and Supplies

All samples and reagents were provided by the J. L. Holmes Mass Spectrometry Facility and the University of Ottawa. Samples were all purchased from Sigma-Aldrich or Strem Chemicals. All reagents used were HPLC grade.

2.1.2 Sample Preparation

All samples were weighed using an analytical balance. Each solution was made to a concentration of approximately 0.5 mg/mL. Stock solutions were made as required and in HPLC grade methanol unless otherwise stated. All solutions were analysed each day prior to experimentation to ensure stability and that no degradation occurred.

A 50:50 v/v mixture of HPLC water and methanol was used to clean all laboratory equipment and HPLC acetonitrile was used to clean the instrument so as to prevent cross-contamination and carryover.

2.2 Instrumentation

The instrument of choice was the Waters Synapt G1 High-Definition Mass Spectrometer (Figure 2.1). High performance tandem mass spectrometry is achieved by the inclusion of the triwave components as well as time-of-flight (TOF) analyser.[60] After the sample enters the source, the configuration of the trap, ion mobility separation (IMS) and transfer T-Wave cells control the ion trapping and separation of molecules to be analysed in the time-of-flight chamber in a W or V pattern.

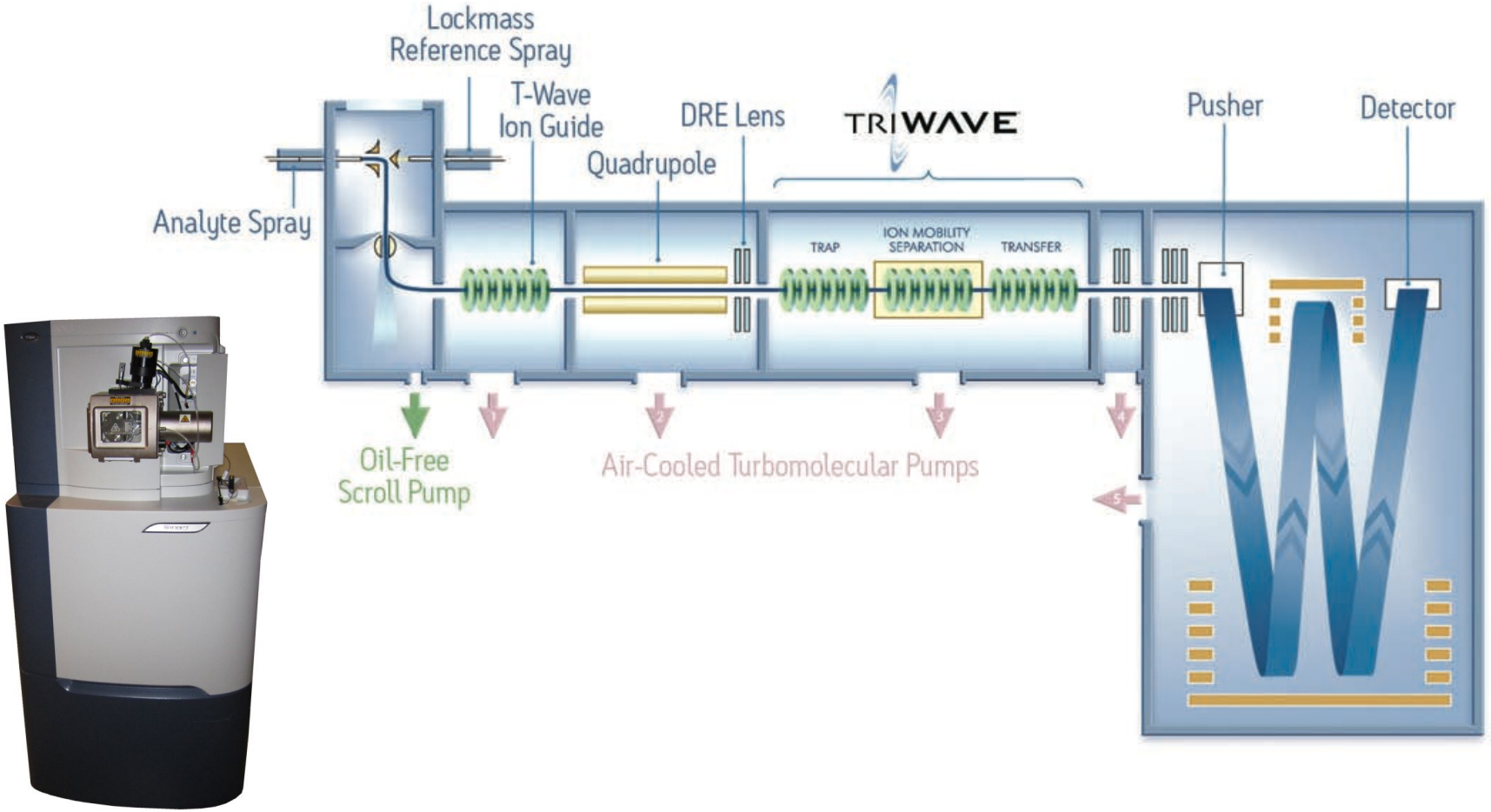

Figure 2.1 Waters Synapt G1 High Definition Mass Spectrometer (Electrospray Ionization) instrument and operation diagram.[60]

For the purpose of this research, the trap and transfer T-Wave cells were the main focus. All samples were analysed in positive mode electrospray ionization (ESI+) in a V pattern in the TOF analyser. A full list of instrument parameters can be found in Table 2.1. Automated syringe pumps operating at 20 µL/min were used in order to ensure precision and accuracy within sample runs.

Table 2.1 Waters Synapt G1 High Definition Mass Spectrometer (Electrospray Ionization) Default Operation Parameters

ES+	
Source	
Capillary (kV)	3.00
Sampling Cone	50
Extraction Cone	2.0
Temperatures (ºC)	
Source	100
Desolvation	250
Cone	40 L/h
Desolvation	176 L/h

Instrument	
Collision Energy	
Trap CE	6.0
Transfer CE	4.0
Source	18 mL/min
Trap	1 mL/min
TOF	
Detector	1900
Resolving Quadrupole	
LM Resolution	15.0

2.3 Data Analysis

Data analysis was conducted using the MassLynx Software. Screen captures of the output spectra are included throughout this document.

2.4 Experiment Overview

Ni^{2+} and Fe^{3+} were the metal ions of interest for this research in the form of Nickel (II) Nitrate and Iron (III) Nitrate. Each metal was analysed with a series of five ligand compounds using multiple methods: 2,2'-Bipyridine, 4,4'-Bipyridine, 1,10-Phenanthroline,

2,2'-Bipyridine-4,4'-Dicarboxylic Acid, and the Baker Group's SNS ligand, pictured previously in Figure 1.6.

Each of the analysis outputs for the following methods can be compared within its metal group as well as across ligand groups, and between other methods of analysis.

2.4.1 Single-Spray Analysis (SS)

The first method uses a prepared solution 50:50 v/v mixture of each metal-ligand combination (approximately 0.5 mg/mL), analysed via positive mode Electrospray Ionization Quadrupole Time-of-Flight Mass Spectrometry (QToF MS). In this method of analysis, the compounds are mixed in the liquid phase and allowed to go to completion. The reaction time and stability of each mixture was tested at one, 24 and 48 hours after mixing. After such time, the solutions are injected into the instrument and analysed. The most effective reaction time was chosen based on the greatest signal intensity of peaks of interest. By comparing all four target complexes in the mass spectrum in relation to their change in intensity over time, the ideal reaction time could be decided. The spectra that had the greatest signal intensity on average at all four target masses, without a significant amount of distortion from background noise or other formed complexes was chosen moving forward. This mixture was used for further experimentation.

2.4.2 Dual-Spray Analysis (DS)

This method uses two stock solutions, one metal and one ligand at approximately 0.5 mg/mL each, analysed via positive mode Electrospray Ionization Quadrupole Time-of-Flight Mass Spectrometry (QToF MS). In this method of analysis, the compounds are

mixed in the gas phase as they enter the source, leaving much less time for the reactions to go to completion before analysis occurs.

2.4.3 Collision-Induced Dissociation (CID)

Within each of these sample runs for both single-spray and dual-spray analysis, Collision-Induced Dissociation (CID) experiments were performed on each of the four masses and their major isotopes; the metal and one ligand, the nitrated metal and one ligand, the metal and two ligands, and the nitrated metal and two ligands (Table 2.2).

Table 2.2 Metal-ligand combinations and their major isotope masses to be analysed.

Nickel (II) Nitrate								
	Mass (Da)							
	Metal + One Ligand		*Nitrated Metal + One Ligand*		*Metal + Two Ligands*		*Nitrated Metal + Two Ligands*	
2,2'-Bipyridine	213.9	215.9	275.9	277.9	370.0	372.0	432.0	434.0
4,4'-Bipyridine	213.9	215.9	275.9	277.9	370.0	372.0	432.0	434.0
1,10-Phenanthroline	237.9	239.9	299.9	301.9	418.0	420.0	480.0	482.0
2,2'-Bipyridine-4,4'-Dicarboxylic Acid	301.9	303.9	363.9	365.9	544.9	546.9	607.9	609.9
SNS	316.9	318.9	378.9	380.9	576.0	578.0	638.0	640.0

Iron (III) Nitrate				
	Mass (Da)			
	Metal + One Ligand	*Nitrated Metal + One Ligand*	*Metal + Two Ligands*	*Nitrated Metal + Two Ligands*
2,2'-Bipyridine	211.9	274.0	368.0	430.0
4,4'-Bipyridine	211.9	274.0	368.0	430.0
1,10-Phenanthroline	235.9	297.9	416.0	478.0
2,2'-Bipyridine-4,4'-Dicarboxylic Acid	299.9	361.9	542.9	605.9
SNS	314.9	376.9	574.0	636.0

Unless otherwise stated, samples were run at increasing increments of 5 eV in each the trap and transfer until the signal was lost or 100 eV was reached. When the signal was lost, this indicated that the amount of voltage applied exceeded the amount required to fragment the precursor ion and still detect its fragments. While experimenting in the trap, the transfer cell was maintained at 4 eV with the trap gas increased to 5 mL/min. While experimenting in the transfer, the trap cell was maintained at 6 eV and the trap gas at 1 mL/min. Argon gas is used in the trap when performing these experiments while Nitrogen gas is always used in the source.

Using this data, breakdown diagrams were creating for each of the experiments conducted. The intensities of each of the peaks of interest was recorded and normalized according to the data set. This was done by dividing the intensity of each peak by the total sum of intensities for a given collision energy, seen in the following equation:

$$Relative\ Intensity = \frac{Peak\ Intensity}{Sum\ of\ Intensities\ at\ Given\ Collision\ Energy}$$

This value was plotted on the y-axis. On the x-axis, the Centre of Mass Frame, or the real collision energy, was plotted. The collision energy determined by the instrument is a theoretical amount of kinetic energy which does not consider the other parameters in the lab. By using the following equation, we can take into account the types of gases used as well as the precursor ion (PI) of focus in each experiment to find the real collision energy, which is the experimental amount of kinetic energy given.

$$E_{COM} = E_{LAB}\left(\frac{m_{Ar}}{m_{Ar}+m_{PI}}\right)$$

2.4.4 Time-Resolved Electrospray Ionization Analysis (TRESI)

This method again used two stock solutions, one metal and one ligand at approximately 0.5 mg/mL, and analysed via Quadrupole Time-of-Flight Mass Spectrometry (QToF MS). In this final method, the compounds are mixed in the liquid phase but immediately enter the source as seen in the previous Figure 1.5.

The time at which the solutions are allowed to mix can be varied, increasing the reaction time before the solution enters the instrument. Table 2.3 displays the factors involved in the TRESI method based on the standard flow rate of 20 µL/min used in these experiments. CID experiments were not conducted on these combinations.

Table 2.3 TRESI mixing volumes and reaction times for each capillary length at a flow rate of 20 µL/min.

Length (cm)	*Volume (µL)*	*Time (sec)*
0	0.00	0.00
1	2.03	6.09
2	4.06	12.18
3	6.09	18.27
4	8.12	24.36
5	10.15	30.45
6	12.18	36.54
7	14.21	42.63
8	16.24	48.72
9	18.27	54.81
10	20.30	60.90

CHAPTER 3 – METHOD COMPARISON: SINGLE-SPRAY, DUAL-SPRAY AND TRESI

Three different injection methods were chosen for the purpose of this research. The first method was a single-spray of a pre-mixed solution of the metal-ligand mixture. The second was using simultaneous dual-spray injections of both the metal and ligand solutions. The third used a time-resolved device known as the TRESI which involved mixing the solutions as they enter the instrument.

For the single-spray method, a 50:50 *v/v* mixture of each ligand and metal combination was made in methanol and analysed via positive mode ESI QToF after one, 24 and 48 hours. Within this experiment, the appropriate reaction time for each individual solution was discovered using a stability study. The ideal reaction time was determined to be when the signal for the mass-to-charge ratios (*m/z*) of interest were large enough to perform further experimentation but before the signal began to drop out, having other minor peaks dominate the spectrum. By comparing the mass spectrums, focused on the four target complexes, a visual comparison could be made to select the time scale with the most intense peaks on average to undergo further experimentation. This time varied by combination, but most solutions completed their reaction within the first hour. An example of such spectra can be seen in Figure 3.1 below.

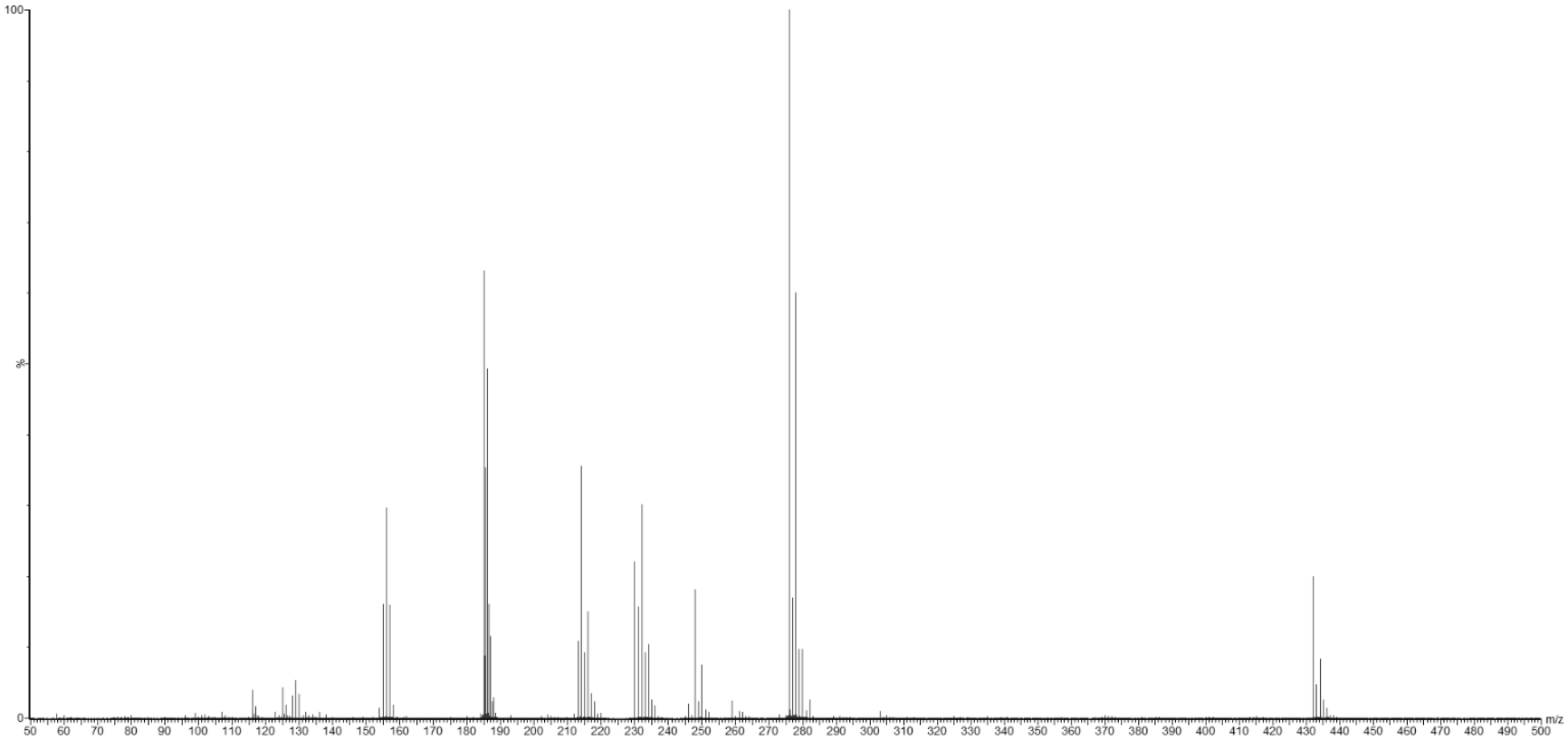

Figure 3.1 Sample single-spray spectrum of Nickel (II) Nitrate 2,2'-Bipyridine 50:50 *v/v* mixture in methanol (50-500 Da) taken using Electrospray Ionization (QToF) Mass Spectrometry.

Using this information, a sample spectrum was taken and used to confirm the formation of the four target *m/z* to be analysed. This included the 1:1 metal to ligand complex, the nitrated 1:1 metal to ligand complex, the 1:2 metal to ligand complex and the nitrated 1:2 metal to ligand complex, for each combination respectively. The target masses for each combination can be found in Table 2.2. A sample spectrum can be seen in Figure 3.2 below.

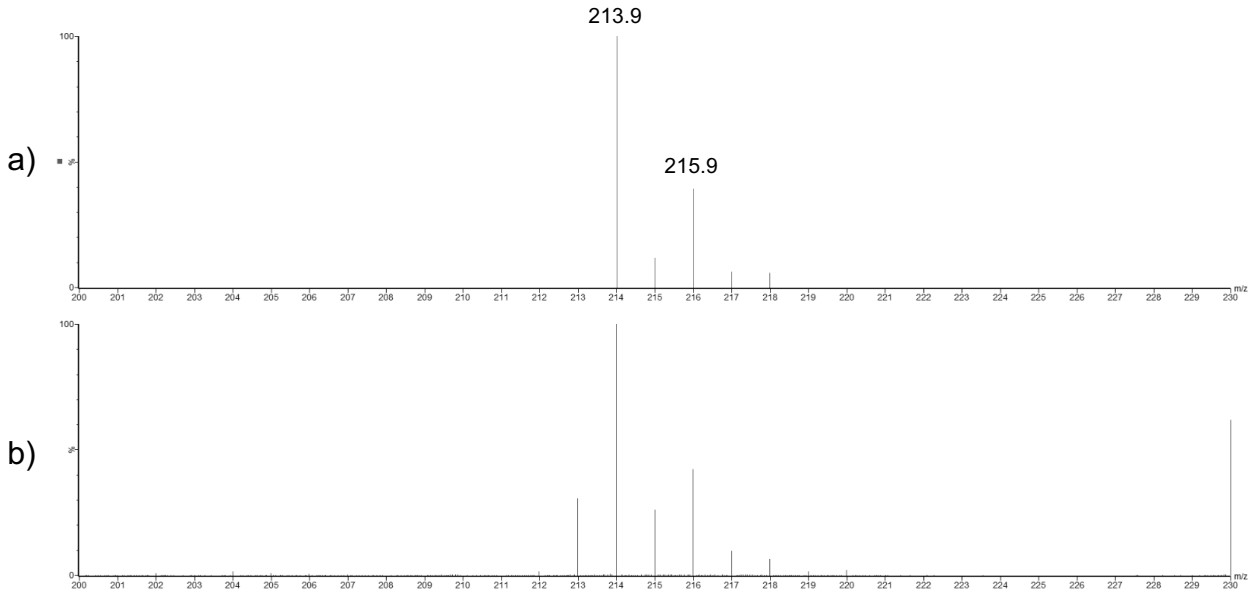

Figure 3.2 Sample single-spray spectrum of Nickel (II) Nitrate 2,2'-Bipyridine 50:50 *v/v* mixture in methanol focused on the 1:1 metal to ligand complex at 213.9 *m/z* and its isotope at 215.9 *m/z* taken using Electrospray Ionization (QToF) Mass Spectrometry comparing a) the expected isotope pattern as generated by the MassLynx software isotope modeling tool, to b) the acquired sample.

For the dual-spray method, two syringes containing either the ligand or metal solutions in methanol were injected simultaneously and analysed via positive mode ESI QToF. Within this experiment, each sample spectra for the same four target *m/z* were taken as the solutions mixed in the gas phase of the source. The spectral outputs look similar to that of the single-spray mixtures seen in Figures 3.1 and 3.2.

Finally, in the TRESI method, a single mixture entered the source after each ligand and metal solution in methanol mixed in the liquid phase using the TRESI device as seen in Figure 1.5. Again, the samples were analysed via positive mode ESI QToF. Samples were analyzed for one minute increments, starting at 0cm, before the inner tubing was pulled back 1 cm further from the point of contact. This was repeated several times for each experiment in order to increase the mixing volume within the device and increase the allotted reaction time for each of the samples. Parameters can be found in Table 2.3. Figure 3.3 below shows a sample mass spectra for the TRESI technique. Additional spectra can be found in the appendix.

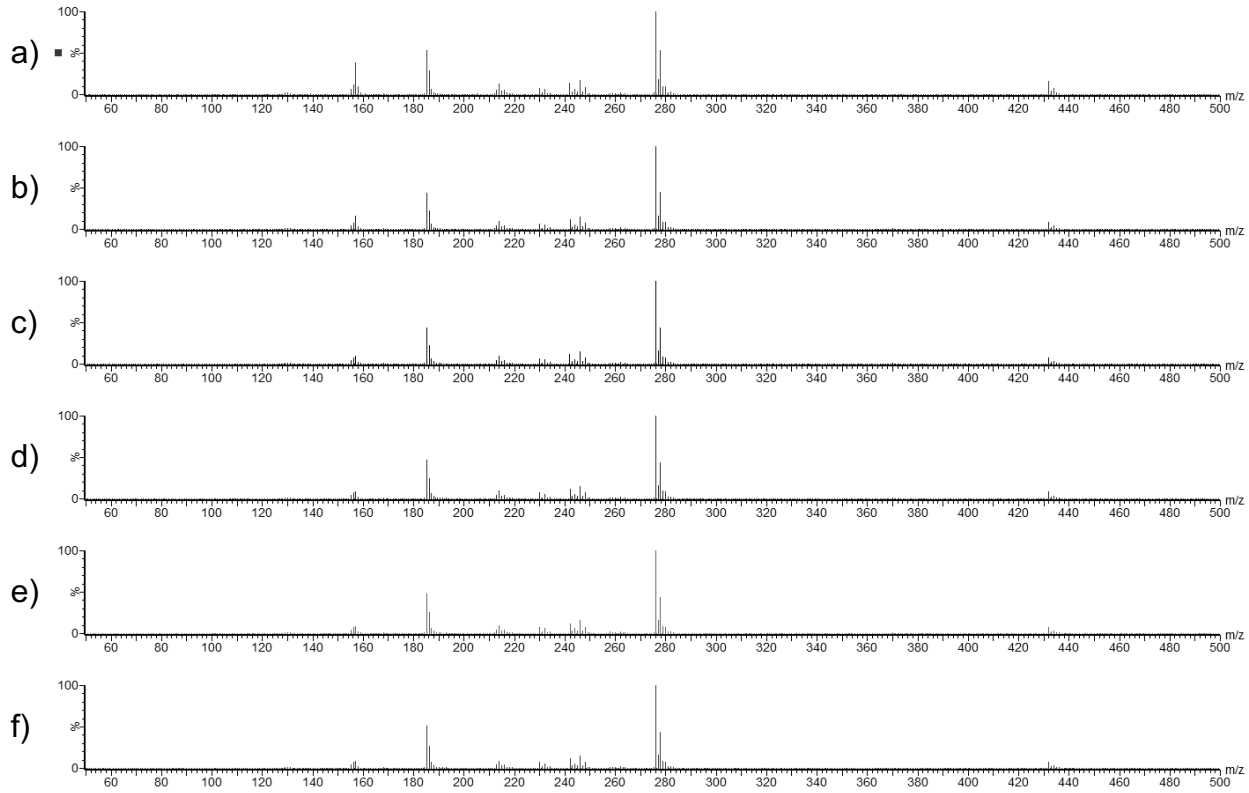

Figure 3.3 Sample TRESI mass spectra of Nickel (II) Nitrate 2,2'-Bipyridine 50:50 *v/v* mixture in methanol taken using Electrospray Ionization (QToF) Mass Spectrometry at a) 0 cm, b) 1 cm, c) 2 cm, d) 3 cm, e) 4 cm, and f) 5 cm.

3.1 Metal Solutions

Nickel (II) Nitrate, $Ni(NO_3)_2$, has a molecular mass of 182.70 g/mol. Figure 3.4 below displays the mass spectrum (50-1000 Da) taken of the compound when mixed in methanol at a concentration of approximately 0.5 mg/mL. Although the entire complex is not visible intact, the peak cluster at 57.9 *m/z* can be seen and confirms the presence of the Nickel ion (Ni^+) and its major isotope at 59.9 *m/z*.

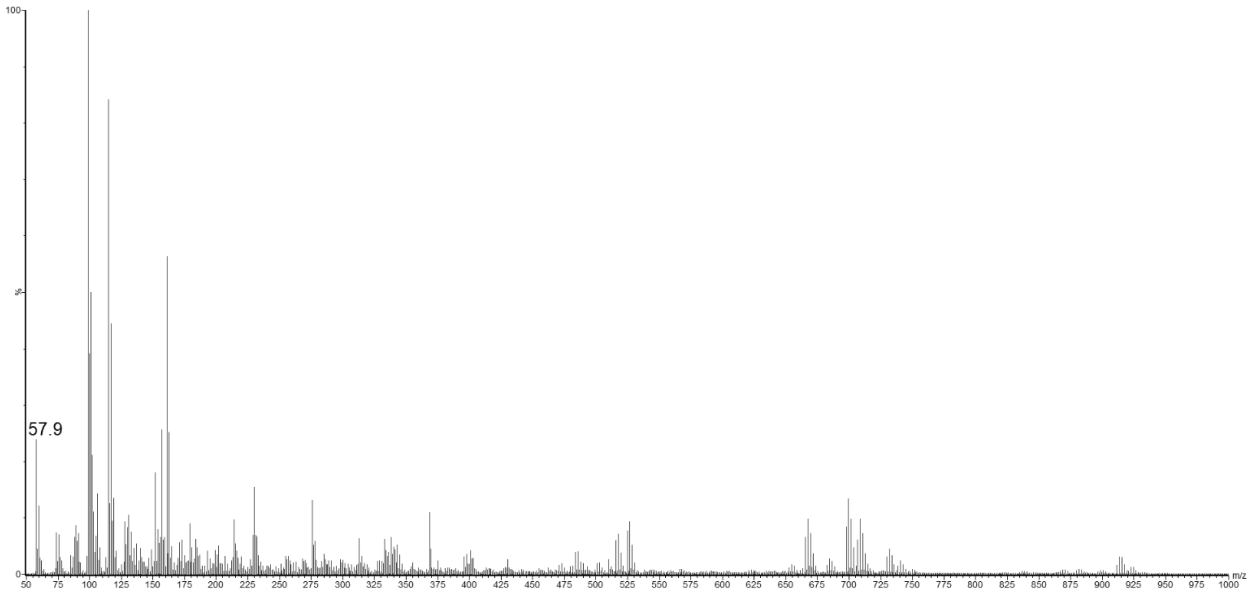

Figure 3.4 Spectrum of Nickel (II) Nitrate in methanol taken using Electrospray Ionization (QToF) Mass Spectrometry.

Iron (II) Nitrate, $Fe(NO_3)_3$, has a molecular mass of 241.86 g/mol. Figure 3.5 below displays the mass spectrum (50-1000 Da) taken of the compound when mixed in methanol at a concentration of approximately 0.5 mg/mL.

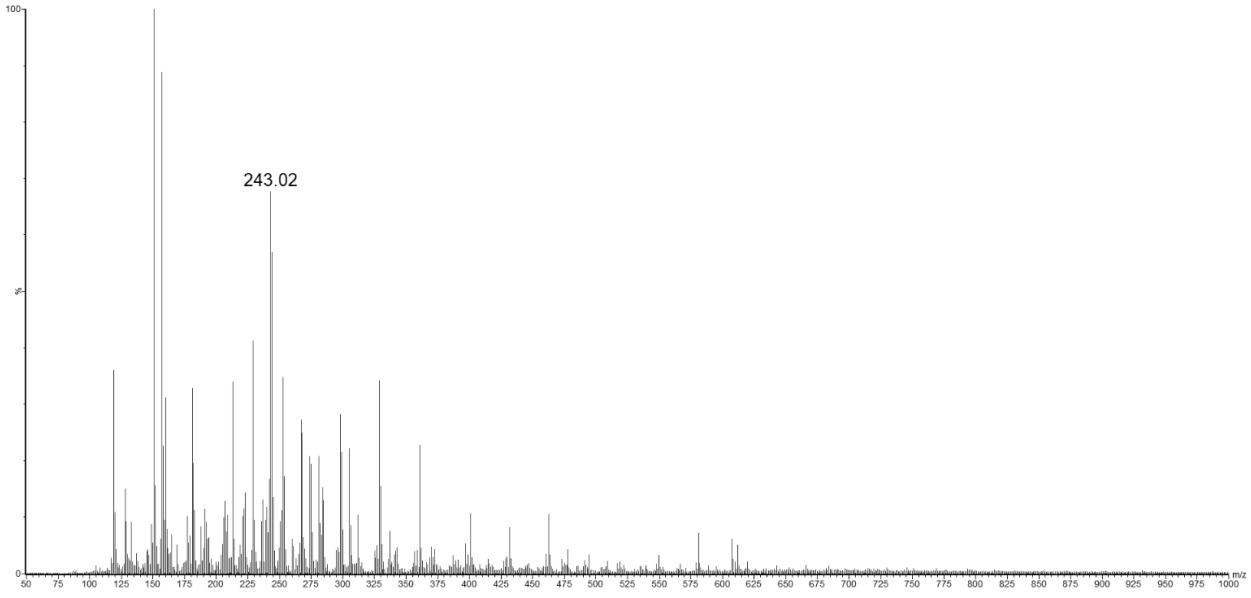

Figure 3.5 Spectrum of Iron (III) Nitrate in methanol taken using Electrospray Ionization (QToF) Mass Spectrometry.

There are several other peaks present in both Figure 3.4 and Figure 3.5. They are likely due to the many possible fragments of each of the complexes, as well as the interaction of other particles present within the instrument at the time of the sample analysis. The overall pattern of each of the clusters is at most times consistent, meaning that the metal isotopes are indeed present in each of those clusters. These types of patterns indicate the compound is not stable in solution and may not be totally dissolved.

3.2 2,2'-Bipyridine

2,2'-Bipyridine, $C_{10}H_8N_2$, has a molecular mass of 156.18 g/mol. Figure 3.6 below displays the mass spectrum (50-400 Da) taken of the compound when mixed in methanol at a concentration of approximately 0.5 mg/mL.

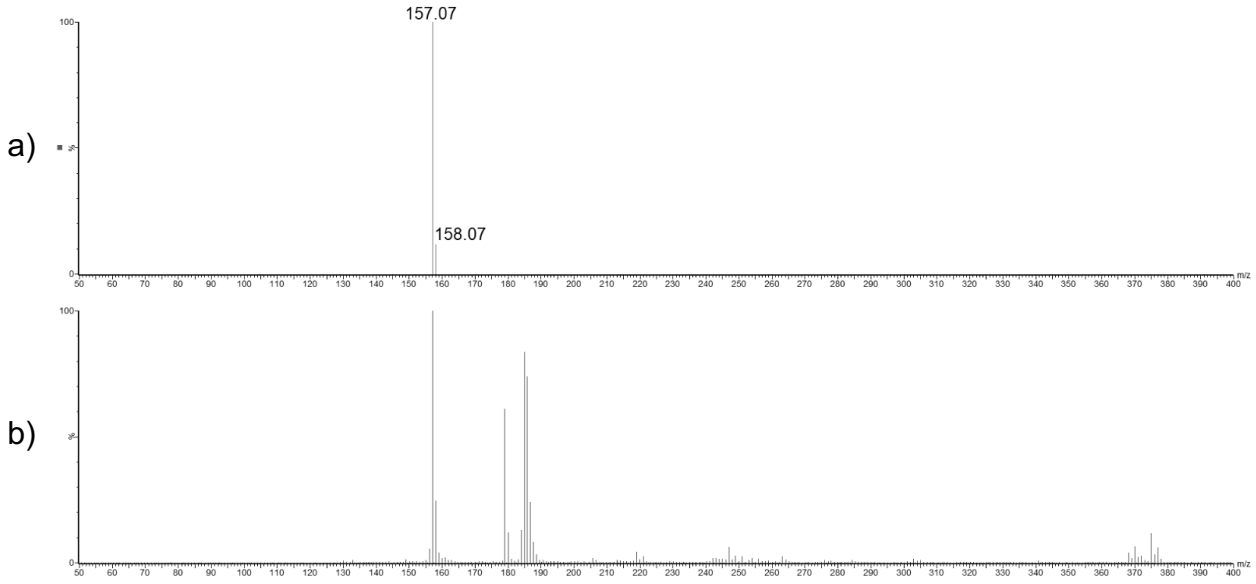

Figure 3.6 Spectrum of 2,2'-Bipyridine in methanol focused on the $C_{10}H_8N_2H^+$ ion focused at 157.0 and 158.0 *m/z* taken using Electrospray Ionization (QToF) Mass Spectrometry comparing a) the expected isotope pattern as generated by the MassLynx software isotope modeling tool, to b) the acquired sample.

After mixing the 2,2'-Bipyridine solution with the Nickel (II) Nitrate solution 50:50 *v/v*, a stability study was performed, the results of which can be seen in Figure 3.7 below. The stability study of the Iron (III) Nitrate and 2,2'-Bipyridine 50:50 *v/v* solution can be found in Figure 3.8.

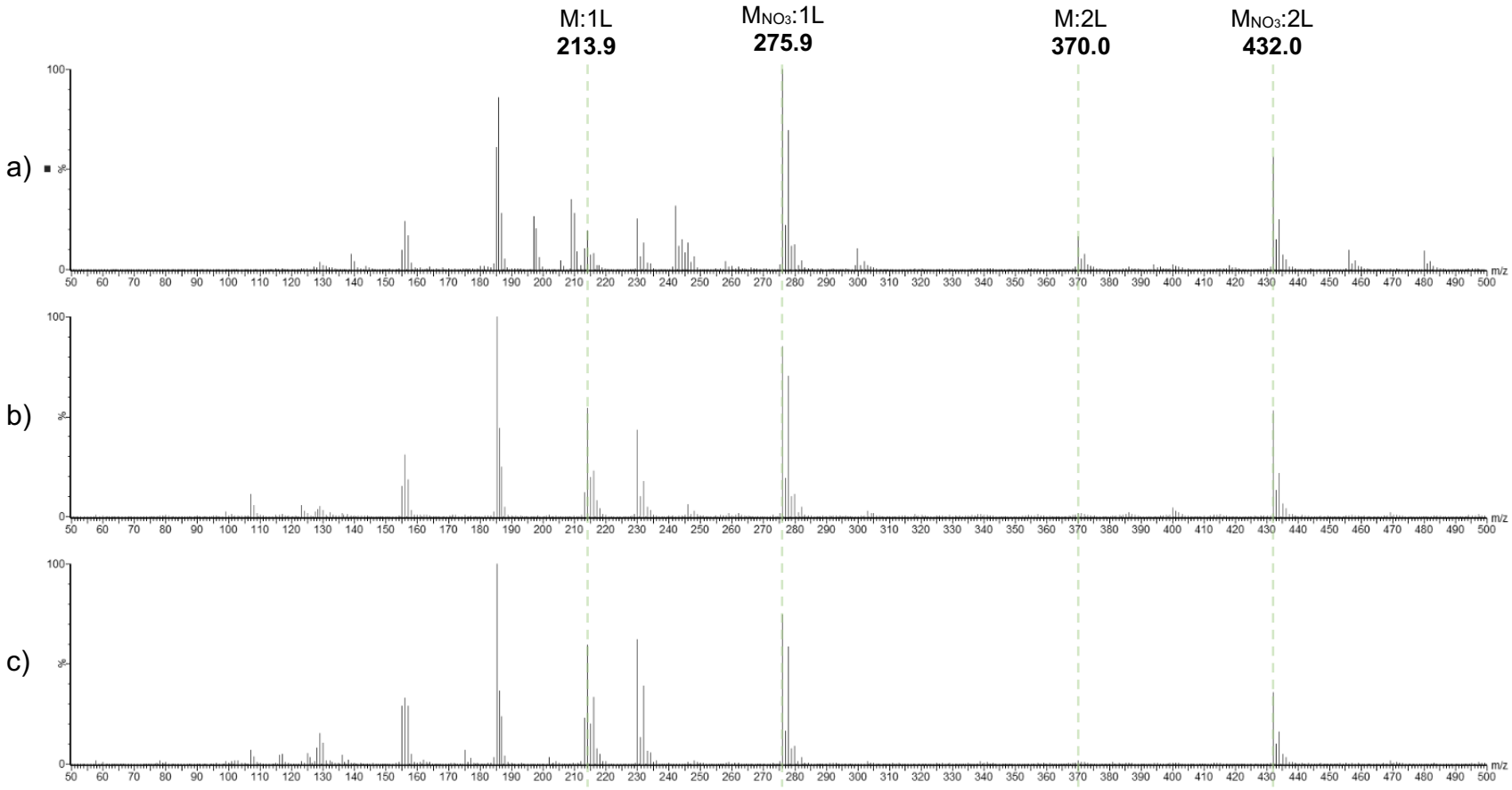

Figure 3.7 Stability study of Nickel (II) Nitrate 2,2'-Bipyridine 50:50 *v/v* mixture in methanol at a) one, b) 24, and c) 48 hours.

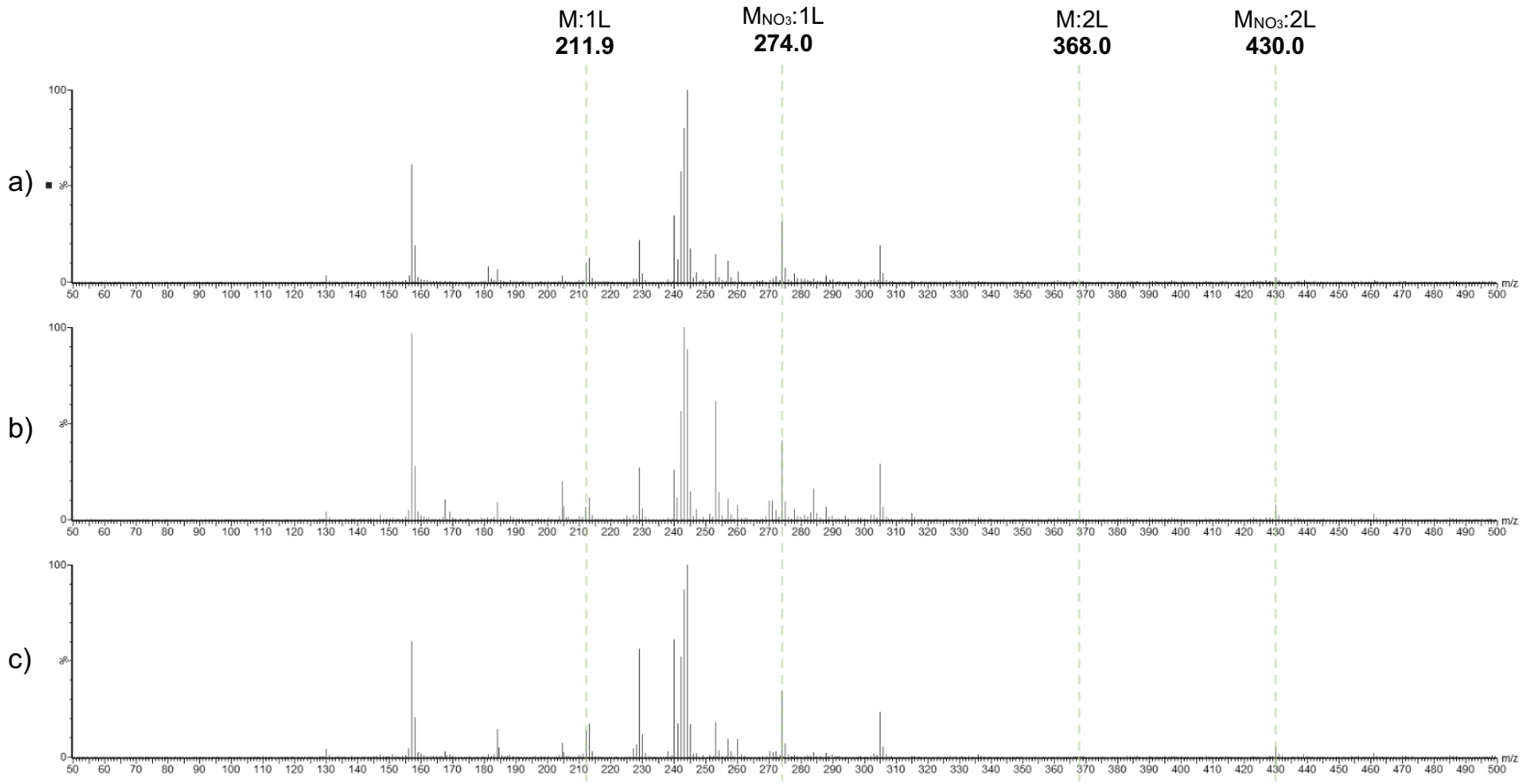

Figure 3.8 Stability study of Iron (III) Nitrate 2,2'-Bipyridine 50:50 *v/v* mixture in methanol at a) one, b) 24, and c) 48 hours.

It was determined that the reaction of Nickel (II) Nitrate 2,2'-Bipyridine reached completion within the first hour after mixing. The signal intensity begins to drop in the higher *m/z* regions after the first 24 hours. At the 24 hour mark, it can be seen that many of the lower intensity clusters have dropped out, specifically the 1:2 complex ($NiC_{10}H_8N_2C_{10}H_8N_2^+$) at 370.0 *m/z* and the cluster at approximately 242 *m/z*. Also, everything less than 150 *m/z* and greater than 450 *m/z* has significantly decreased in intensity. After 48 hours, many of the clusters have disappeared and those with medium intensities after one hour have now started to disappear while some have significantly increased in intensity. Therefore, less than 24 hours was determined to be the ideal reaction time for this mixture to undergo further experimentation.

When looking at the mixture with Iron (III) Nitrate, the same conclusion was made. After one hour, there is a signal of both compounds of interest with the 1:1 metal to ligand ratios, $FeC_{10}H_8N_2^+$ and $FeC_{10}H_8N_2NO_3^+$. There is very little signal at the compounds with the 1:2 ratio, however the signal does not increase significantly with time. It is important to note that a visible colour change was observed in the solution within the first hour after mixing, as shown in Figure 3.9.

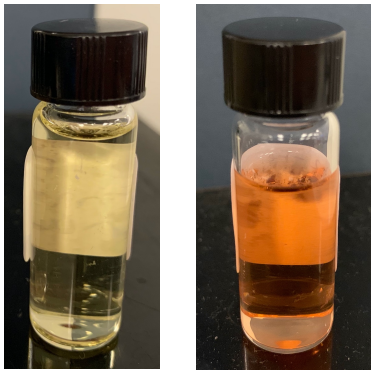

Figure 3.9 Iron (III) Nitrate 2,2'-Bipyridine solution approximately one minute after mixing (left) as compared to approximately one hour after mixing (right).

It is understood that this colour change indicates an oxidation reaction has occurred. The speed at which this took place proves the overall reaction also occurred quite quickly. At the 24 hour mark, other peaks have started to grow in and distort the signal of the compounds of interest. After 48 hours, many of the lower intensity clusters have begun to disappear. The most prominent peaks throughout the spectra include the Iron (III) Nitrate cluster, $Fe(NO_3)_3H^+$, at 243.0 *m/z* and the 2,2'-Bipyridine ligand, $C_{10}H_8N_2H^+$, at 157.0 *m/z*. Overtime, the ligand cluster does begin to decrease in intensity, but the pattern of the 243.0 *m/z* cluster begins to shift and distort. Therefore, less than 24 hours was determined to be the ideal reaction time for this mixture.

Figures 3.10 and 3.11 below compare the three methods of injection overall, the single-spray mixture, dual-spray and TRESI with both the Nickel and Iron solutions respectively.

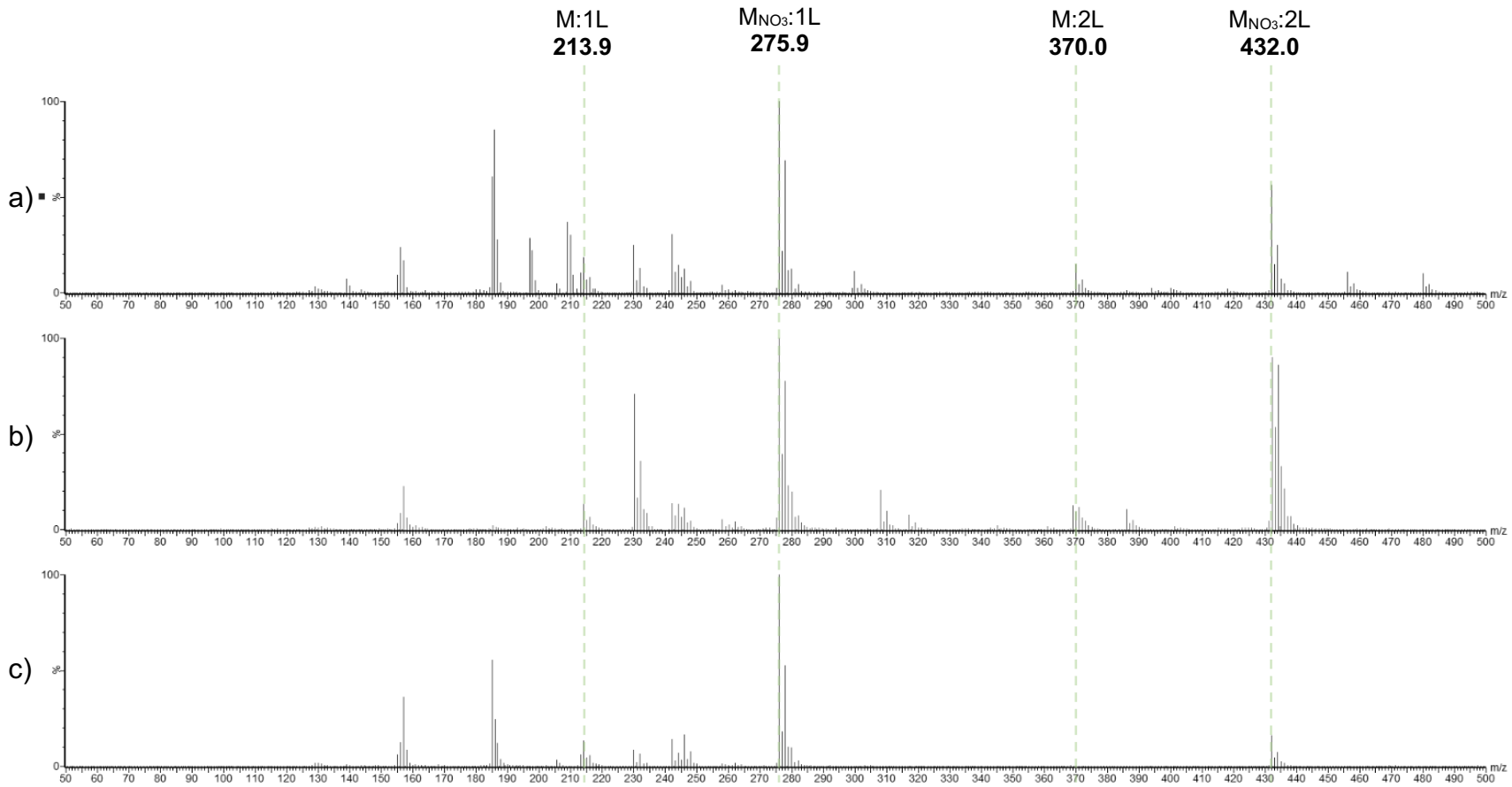

Figure 3.10 A comparison study of the spectra of Nickel (II) Nitrate 2,2'-Bipyridine for a) 50:50 v/v mixture in methanol, b) the dual-spray method, and c) the TRESI method.

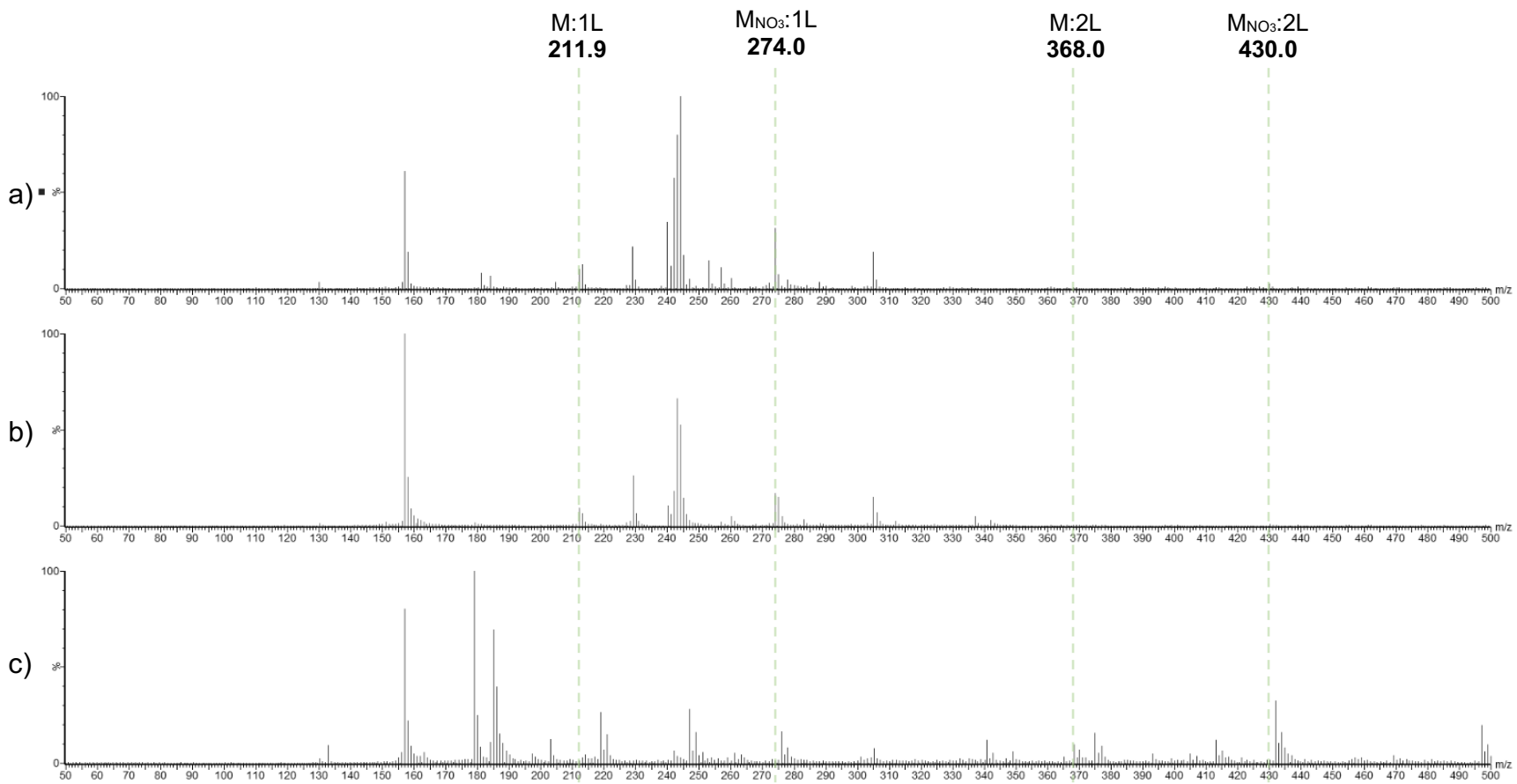

Figure 3.11 A comparison study of the spectra of Iron (III) Nitrate 2,2'-Bipyridine for a) 50:50 v/v mixture in methanol, b) the dual-spray method, and c) the TRESI method.

In terms of the Nickel (II) Nitrate mixture from Figure 3.10, it is clear that the single-spray mixture had the greatest intensity for all four target masses overall after letting the reaction occur for between one and 24 hours. The dual-spray method produced a large amount of nitrated compounds in comparison to the non-nitrated, although they were still present. The TRESI method produced similar results as the nitrated 1:1 complex had the greatest intensity, followed by the nitrated 1:2 complex, however the 1:1 complex has almost no ion counts at all. In all three techniques, the ligand alone is notably present.

From this data, it can be concluded that the combination of these two solutions needs some time to react properly. Although the instant mixing in the gas phase via-dual-spray does produce ions of interest, the nitrogen gas strongly influences the mixing resulting in the high intensity of the nitrated complexes. However, the intensity ratios are comparable to that of the single-spray mixture. When the compounds mix in the liquid phase, much fewer complexes are formed. As previously stated, the nickel metal has a high affinity for nitrogen-containing compounds, which could explain the larger intensity of the formed nitrated complexes. Overall, all three methods were relatively effective at creating the complexes of interest for the Nickel (II) Nitrate 2,2'-Bipyridine combination.

When looking at the Iron (III) Nitrate mixture from Figure 3.11, it can be learned that the single- and dual-spray techniques produced roughly the same amount of target ions. This included a medium intensity cluster at both 1:1 complexes and very little to none at the 1:2 complexes. As for the TRESI technique, the target clusters appear at slightly higher mass-to-charge ratios than was expected. In general, the TRESI method had the least amount of Iron (III) Nitrate ions lingering in solution, likely meaning more

particles had reacted which could explain the abundance of clusters in the 179-190 *m/z* range. In all three techniques, the ligand alone is again notably present.

These two solutions needed very little time to react. The almost immediate change in colour helps explain the similarities between the single- and dual-spray methods. Also similar to the nickel solution, the presence of nitrogen gas influences the mixture by giving the nitrated compound at 274.0 *m/z* ($FeC_{10}H_8N_2NO_3^+$) a higher intensity than the non-nitrated 1:1 complex at 211.9 *m/z* ($FeC_{10}H_8N_2^+$). Overall, the TRESI method was very ineffective at creating the target compounds while both single- and dual-spray techniques were both moderately effective.

3.3 4,4'-Bipyridine

4,4'-Bipyridine, $C_{10}H_8N_2$, has a molecular mass of 156.18 g/mol. Figure 3.12 below displays the mass spectrum (50-400 Da) taken of the compound when mixed in methanol at a concentration of approximately 0.5 mg/mL.

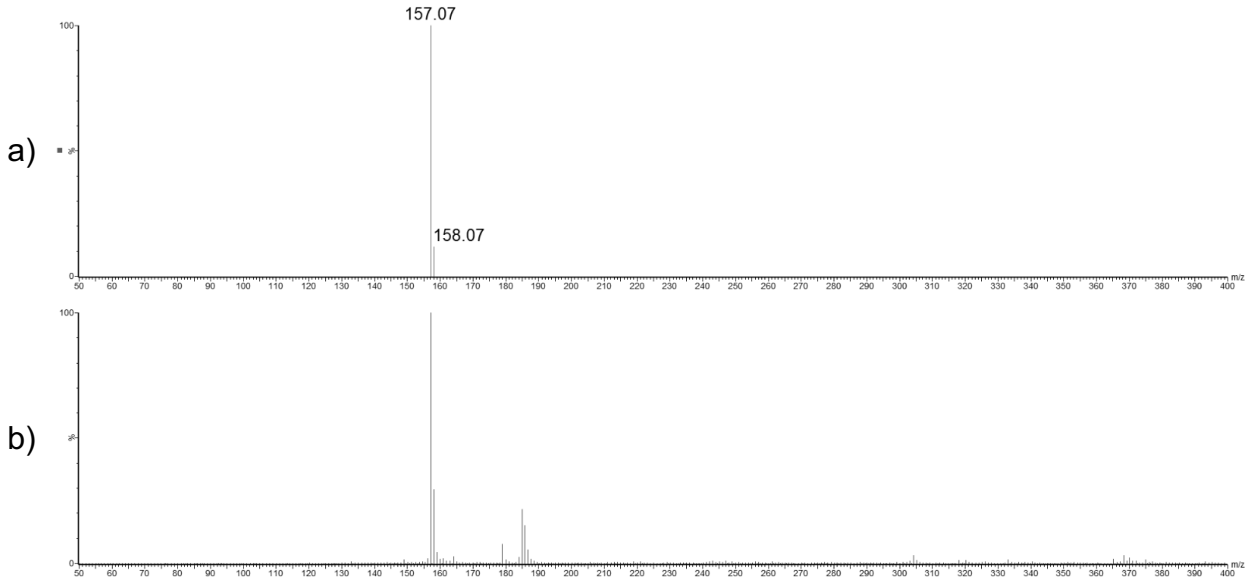

Figure 3.12 Spectrum of 4,4'-Bipyridine in methanol focused on the $C_{10}H_8N_2H^+$ ion focused at 157.0 and 158.0 *m/z* taken using Electrospray Ionization (QToF) Mass Spectrometry comparing a) the expected isotope pattern as generated by the MassLynx software isotope modeling tool, to b) the acquired sample.

After mixing the 4,4'-Bipyridine solution with the Nickel (II) Nitrate solution 50:50 *v/v*, a stability study was performed, the results of which can be seen in Figure 3.13 below. It is important to note the difference between the 4,4'-Bipyridine mixture and the 2,2'-Bipyridine mixture previously discussed. In this mixture, the non-nitrated 1:2 complex has one less hydrogen, $NiC_{10}H_8N_2C_{10}H_7N_2^+$, for a *m/z* ratio of 369.0 instead of 370.0 as seen in the previous 2,2'-Bipyridine mixture. These compounds are almost identical and therefore no reasonable explanation for this difference is evident. A stability study of the ligand and Iron (III) Nitrate 50:50 *v/v*, was also completed and displayed in Figure 3.14.

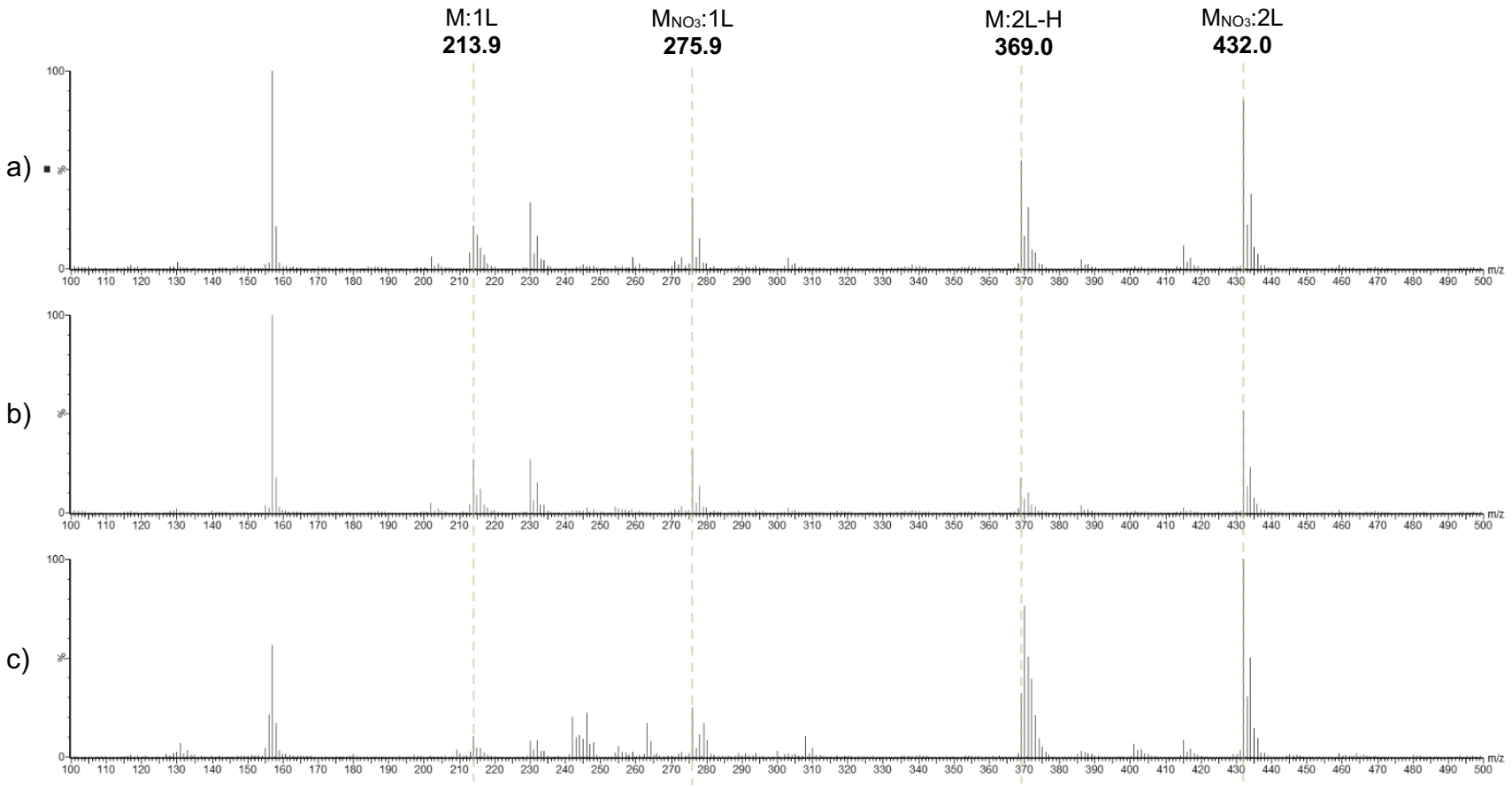

Figure 3.13 Stability study of Nickel (II) Nitrate 4,4'-Bipyridine 50:50 *v/v* mixture in methanol at a) one, b) 24, and c) 48 hours.

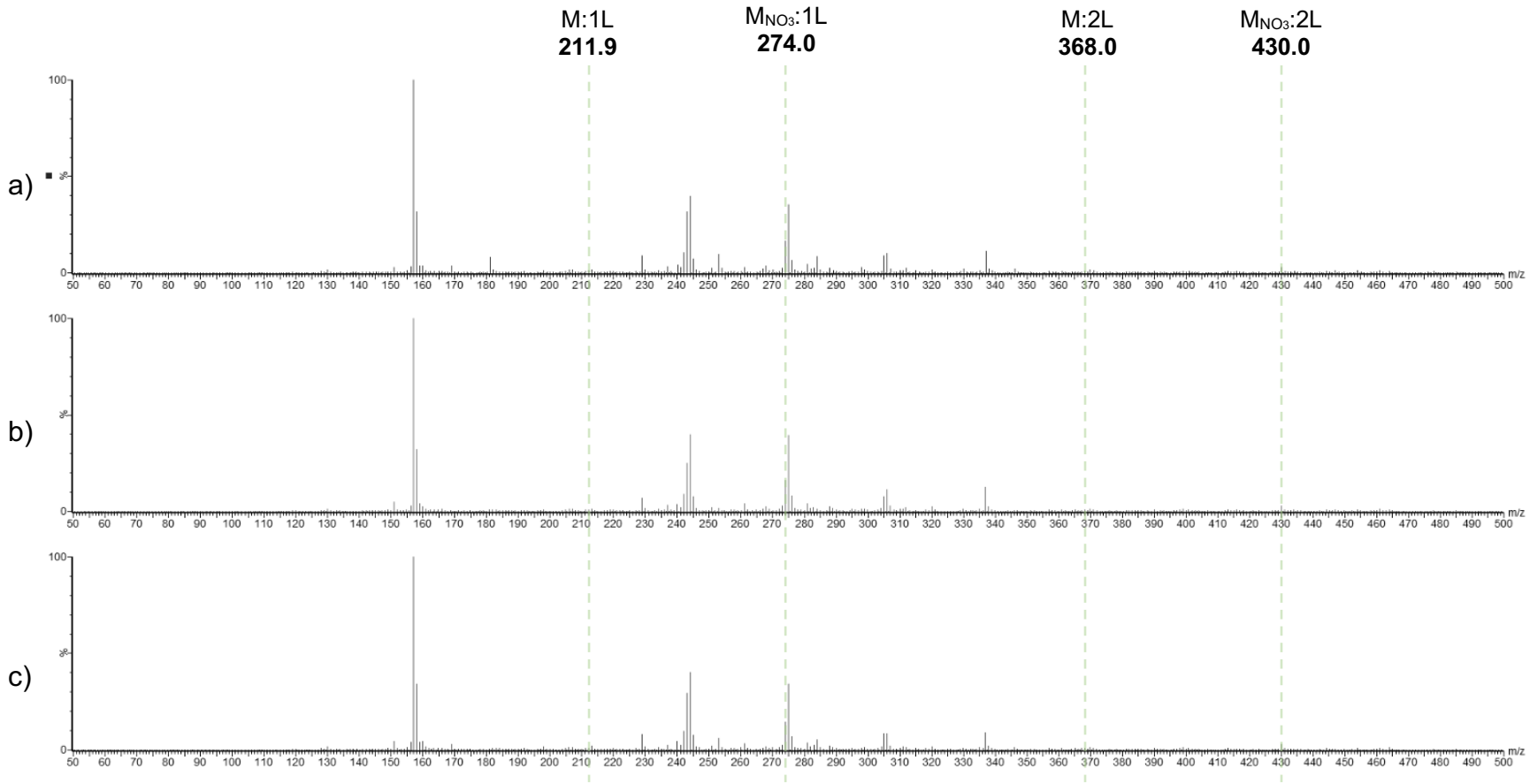

Figure 3.14 Stability study of Iron (III) Nitrate 4,4'-Bipyridine 50:50 *v/v* mixture in methanol at a) one, b) 24, and c) 48 hours.

It was determined that from Figure 3.13, the reaction of Nickel (II) Nitrate 4,4'-Bipyridine reached completion within the first hour after mixing. After the first 24 hours, the signal intensity of the higher *m/z* regions begins to drop while it increases in the lower *m/z* regions. At the 24 hour mark, it can be seen that many of the mid *m/z* range clusters have begun to drop out, specifically the 200-400 *m/z* region. After 48 hours, many of the clusters have disappeared or have significantly decreased in intensity. However, the two clusters at 369.0 *m/z* ($NiC_{10}H_8N_2C_{10}H_7N_2^+$) and 432.0 *m/z* ($NiC_{10}H_8N_2C_{10}H_8N_2NO_3^+$) have increased considerably in intensity. Therefore, between one and 24 hours was determined to be the ideal reaction time for this mixture to undergo further experimentation.

In Figure 3.14, it is discovered that the reaction of Iron (III) Nitrate 4,4'-Bipyridine also reached completion within the first hour after mixing. There is little to no change after one, 24 and 48 hours of analysis indicating this mixture is quite stable over time. This is confirmed by the lack of colour change in solution as depicted in the figure below.

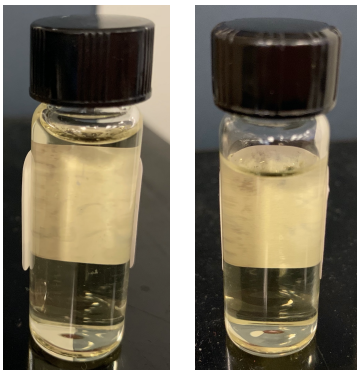

Figure 3.15 Iron (III) Nitrate 4,4'-Bipyridine solution approximately one minute after mixing (left) as compared to approximately one hour after mixing (right).

However, only the nitrate 1:1 complex produced a significant signal intensity while the other three compounds of interest are barely visible. Again, the ligand alone dominates the spectra at 157.0 *m/z*, $C_{10}H_8N_2H^+$.

Figures 3.16 and 3.17 below compare the three methods of injection overall, the single-spray mixture, dual-spray and TRESI with both the Nickel and Iron solutions respectively.

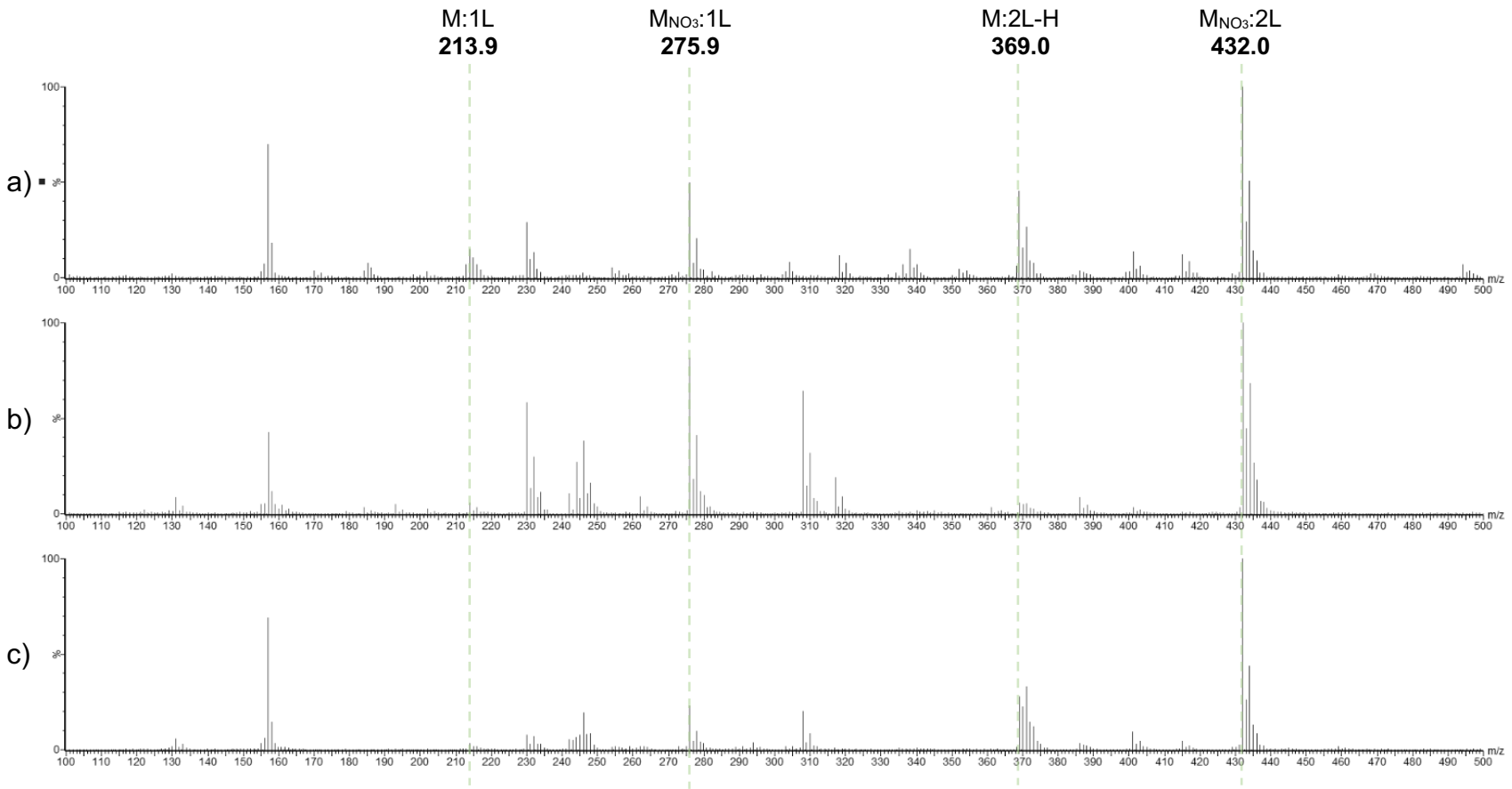

Figure 3.16 A comparison study of the spectra of Nickel (II) Nitrate 4,4'-Bipyridine for a) 50:50 *v/v* mixture in methanol, b) the dual-spray method, and c) the TRESI method.

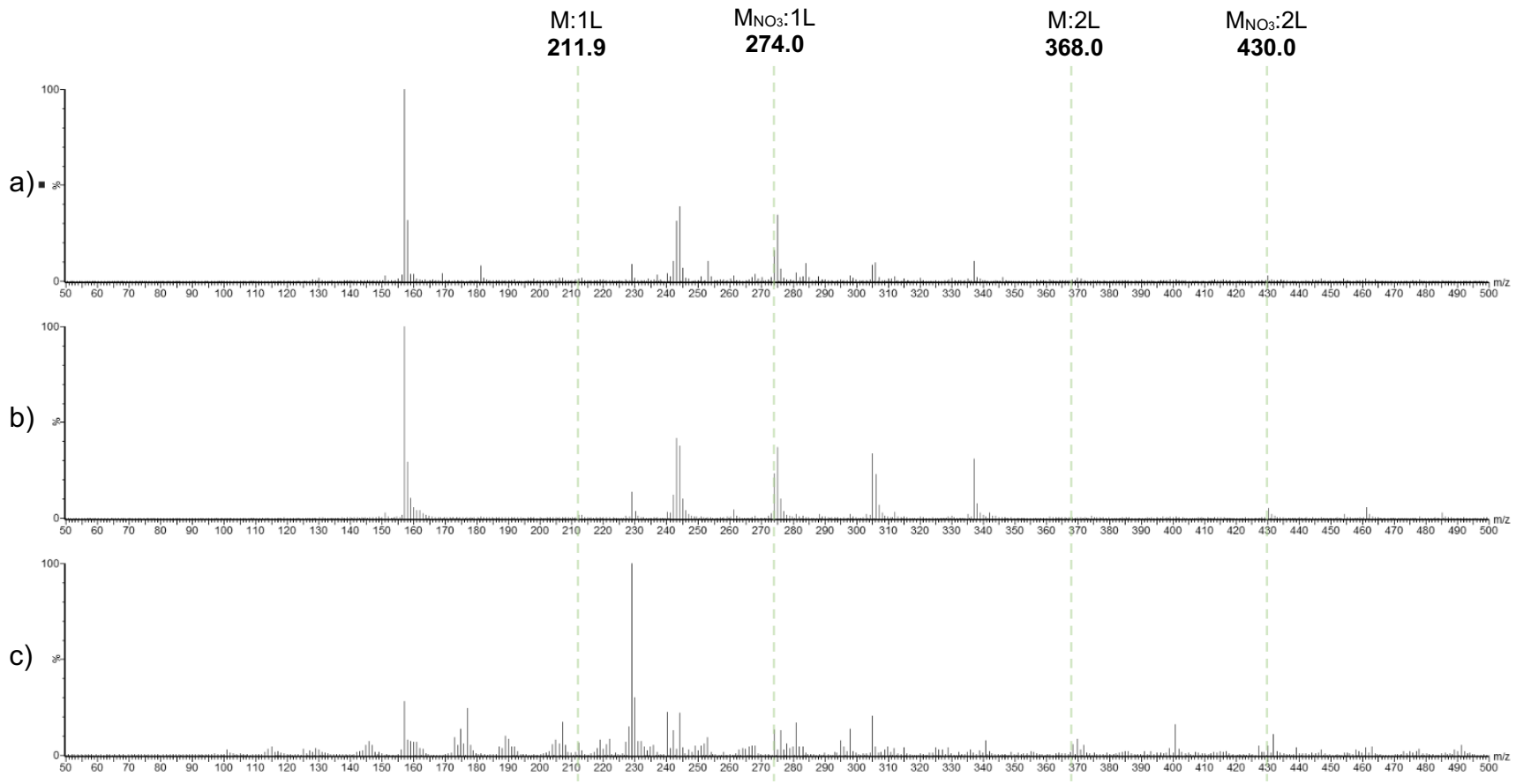

Figure 3.17 A comparison study of the spectra of Nickel (II) Nitrate 4,4'-Bipyridine for a) 50:50 *v/v* mixture in methanol, b) the dual-spray method, and c) the TRESI method.

From Figure 3.16, it is clear that once again the single-spray mixture had the greatest intensity for all four target masses overall after letting the reaction occur for between one and 24 hours for the Nickel (II) Nitrate mixture. Although still visible, the non-nitrated compounds show significantly less intensity than their nitrated counterparts when examining the dual-spray method. The TRESI method also showed greater intensity when nitrated but only in the 1:2 complex ($NiC_{10}H_8N_2C_{10}H_8N_2NO_3^+$) while the other three are very low in intensity. Again, in all three techniques, the ligand alone is notably present.

It can be determined from the above data that like the 2,2'-Bipyridine mixture, these two solutions need time to completely react. Both the real-time mixing in the liquid and gas phases did produce complexes of interest, however the single-spray mixture overall worked most effectively. Both real-time methods had higher intensities with the nitrated complexes as seen previously and attributed to nickel's affinity for nitrogen-containing compounds. It is interesting to note that both dual-spray and TRESI methods made little to no ions for the 1:1 complex at 213.9 *m/z* ($NiC_{10}H_8N_2^+$), as well as the non-nitrated 1:2 ($NiC_{10}H_8N_2C_{10}H_8N_2^+$) complex at 369.0 *m/z* only in the dual-spray method. Overall, all three methods were relatively effective at created the complexes of interest.

For the Iron (III) Nitrate combination in Figure 3.17, it can be learned that the single- and dual-spray techniques are both moderately effective at producing the compounds of interest. Both spectra look quite similar, indicated that the mixing in the gas phase is equally as effective as a pre-mixed solution. The TRESI method also produced compounds of interest but created many other clusters as well, making the spectrum extremely noisy. In all three spectra, the ligand is once again present.

When specifically looking at target complexes, all three methods seem to be relatively effective meaning they are not limited by reaction time. However, in both the single- and dual-spray methods, the ligand alone is the dominant peak. In the TRESI method, the cluster of 229.0 *m/z* dominates the spectrum. It is clear that the real-time mixing in the liquid phase creates a different resulting spectrum. Many of the medium intensity clusters are present in very low quantities in the other two spectra or simply not present at all. Overall, all three methods were relatively effective at creating the complexes of interest although the TRESI spectrum was not as clean as the others.

3.4 2,2'-Bipyridine-4,4'-Dicarboxylic Acid

2,2'-Bipyridine-4,4'-Dicarboxylic Acid, $C_{12}H_8N_2O_4$, has a molecular mass of 244.20 g/mol. Figure 3.18 below displays the mass spectrum (50-400 Da) taken of the compound when mixed in methanol at a concentration of approximately 0.5 mg/mL. It can be noted that the entire complex is not visible in the expected *m/z* region. However, fragments of the overall compound are visible at both 202.0 *m/z* ($C_{11}H_8N_2O_2H_2^+$) as well as 157.0 *m/z* ($C_{10}H_8N_2H^+$), which confirm the complex is present in solution.

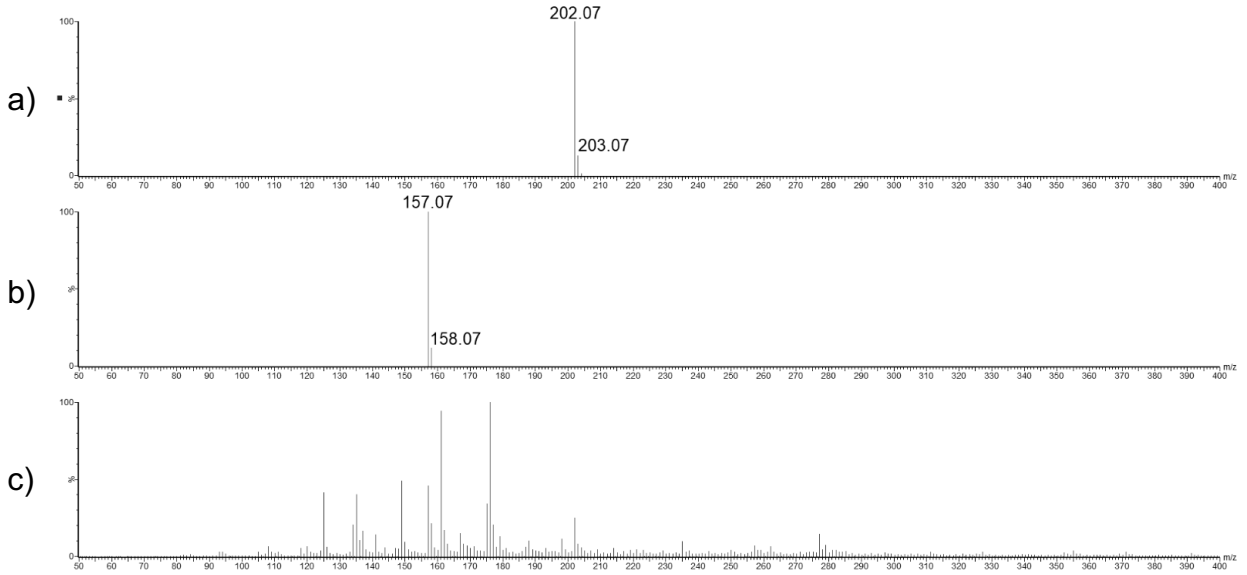

Figure 3.18 Spectrum of 2,2'-Bipyridine-4,4'-Dicarboxylic Acid in methanol taken using Electrospray Ionization (QToF) Mass Spectrometry comparing a) the expected isotope pattern of $C_{11}H_8N_2O_2H_2^+$ at 202.0 and 203.0 *m/z* as generated by the MassLynx software isotope modeling tool, and b) the expected isotope pattern of $C_{10}H_8N_2H^+$ and at 157.0 and 158.0 *m/z* from MassLynx, to c) the acquired sample.

After mixing the 2,2'-Bipyridine-4,4'-Dicarboxylic Acid with the Nickel (II) Nitrate solution 50:50 *v/v*, a stability study was performed, the results of which can be seen in Figure 3.19 below. A stability study with Iron (III) Nitrate was also completed and shown in Figure 3.20.

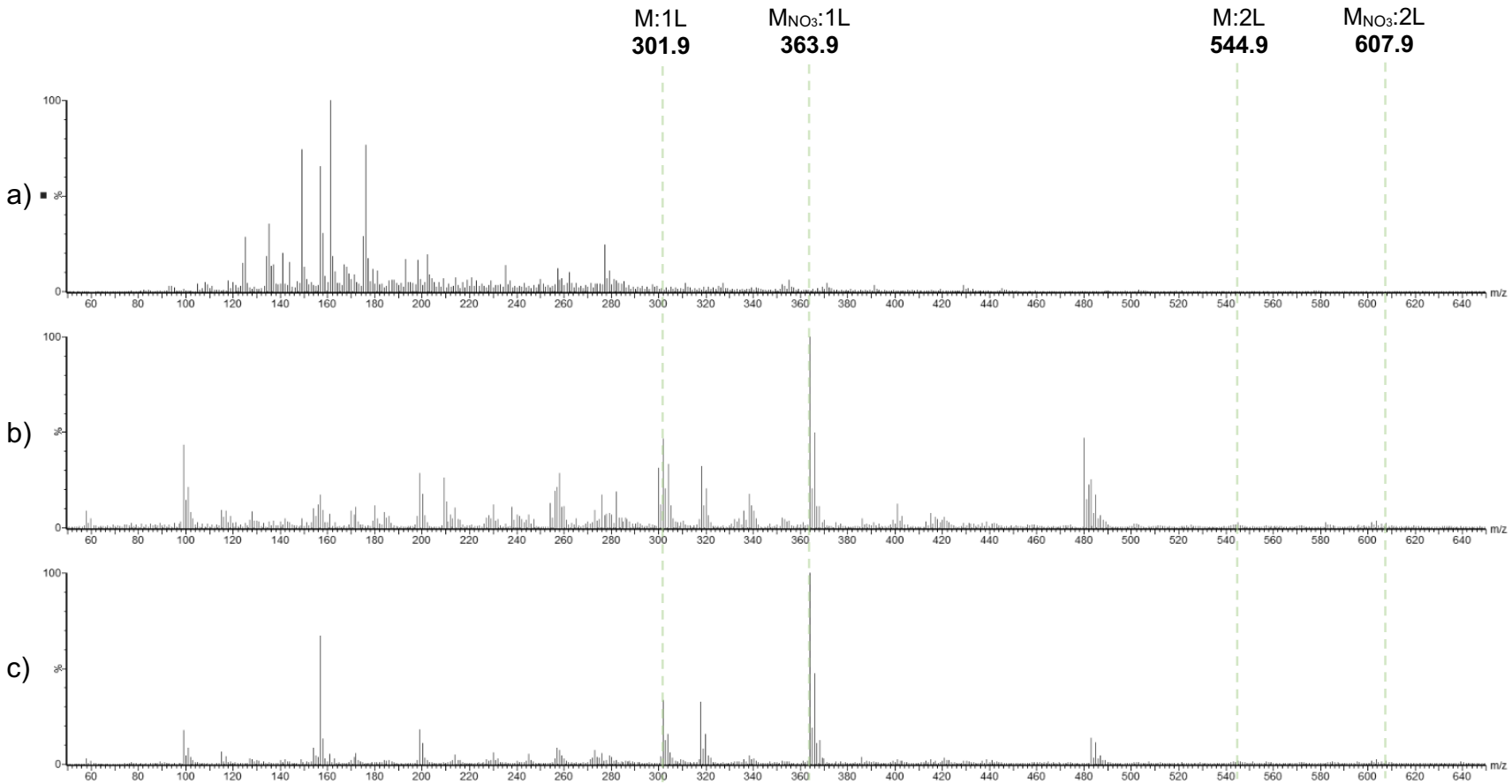

Figure 3.19 Stability study of Nickel (II) Nitrate 2,2'-Bipyridine-4,4'-Dicarboxylic Acid 50:50 *v/v* mixture in methanol after a) one, b) 24, and c) 48 hours.

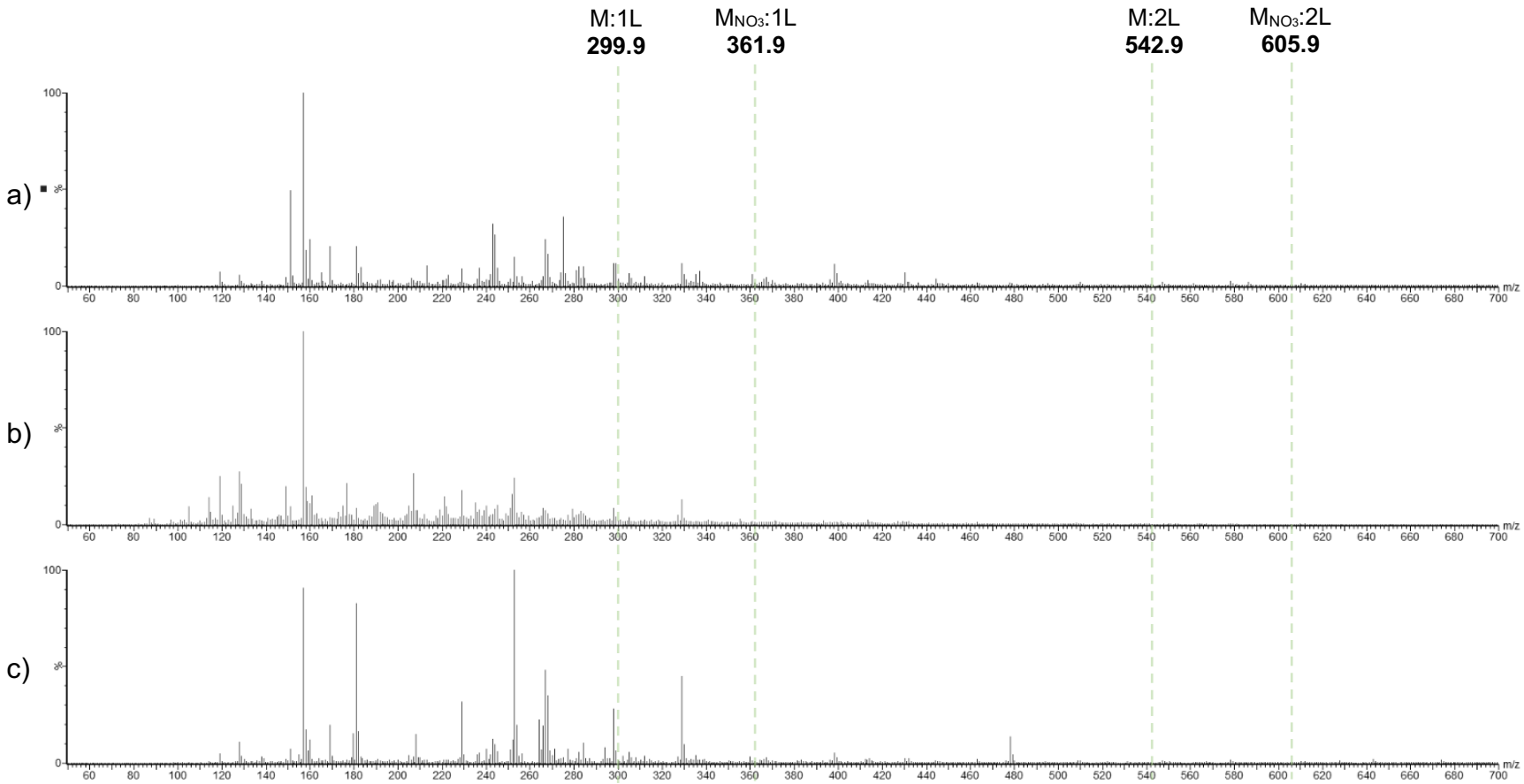

Figure 3.20 Stability study of Iron (III) Nitrate 2,2'-Bipyridine-4,4'-Dicarboxylic Acid 50:50 *v/v* mixture in methanol after a) one, b) 24, and c) 48 hours.

It was determined from Figure 3.19 that the reaction of Nickel (II) Nitrate 2,2'-Bipyridine-4,4'-Dicarboxylic Acid reached completion between 24 and 48 hours after mixing. After the first hour, there are no target complexes formed and very little ions above the 300 *m/z* region. After 24 hours, the signal intensities of the 1:1 complexes are quite strong. There are also very small signals for the 1:2 complexes at this time and it is clear that a reaction has occurred. After 48 hours, the signal intensities of complexes above the 380 *m/z* region begin to disappear and any other signals of medium intensity begin to drop out. Although the signal of the nitrated 1:1 complex ($NiC_{12}H_8N_2O_4NO_3^+$) still appears strong, the non-nitrated 1:1 complex ($NiC_{12}H_8N_2O_4^+$) and the 1:2 complexes are less visible. In all three spectra, the bipyridine portion of the ligand is present, however in much lower quantities at the 24 hour mark. This could potentially mean that more of the ligand had reacted with the metal solution at this point. However, after 48 hours, more of the ligand began to appear, meaning the new complexes were no longer stable. Therefore, between 24 and 48 hours was determined to be the ideal reaction time for this mixture to undergo further experimentation.

From Figure 3.20 it is learned that very little reaction has occurred, if at all, for the Iron (III) Nitrate 2,2'-Bipyridine-4,4'-Dicarboxylic Acid combination. The bipyridine portion of the ligand was a dominating cluster in all three spectra, also suggested very little of the solution had reacted with the metal. This is confirmed by Figure 3.21 which shows no observable change in the solution. The cloudiness of the solution suggests the two solutions did not mix well and therefore would not produce a reaction.

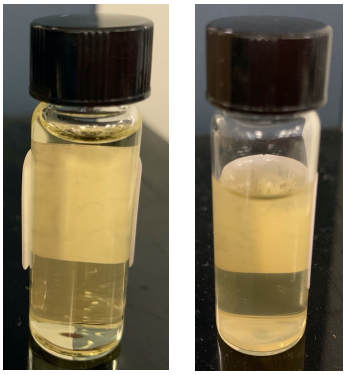

Figure 3.21 Iron (III) Nitrate 2,2'-Bipyridine-4,4'-Dicarboxylic Acid solution approximately one minute after mixing (left) as compared to approximately one hour after mixing (right).

After one and 24 hours, the spectra look fairly similar with small intensity clusters around the 1:1 ($FeC_{12}H_8N_2O_4^+$) complex as well as the nitrated 1:1 complex ($FeC_{12}H_8N_2O_4NO_3^+$). There is no signal at the expected 1:2 complex *m/z* regions. At the 24 hour mark, many of the low intensity peaks have grown in creating a noisy and unclear spectra. After 48 hours, the signals of the two clusters became more intense, however the *m/z* is slightly off from the expected pattern. Therefore, a reaction time between one and 24 hours was used for further experimentation.

Figures 3.22 and 3.23 below compare the three methods of injection overall, the single-spray mixture, dual-spray and TRESI with both the Nickel and Iron solutions respectively.

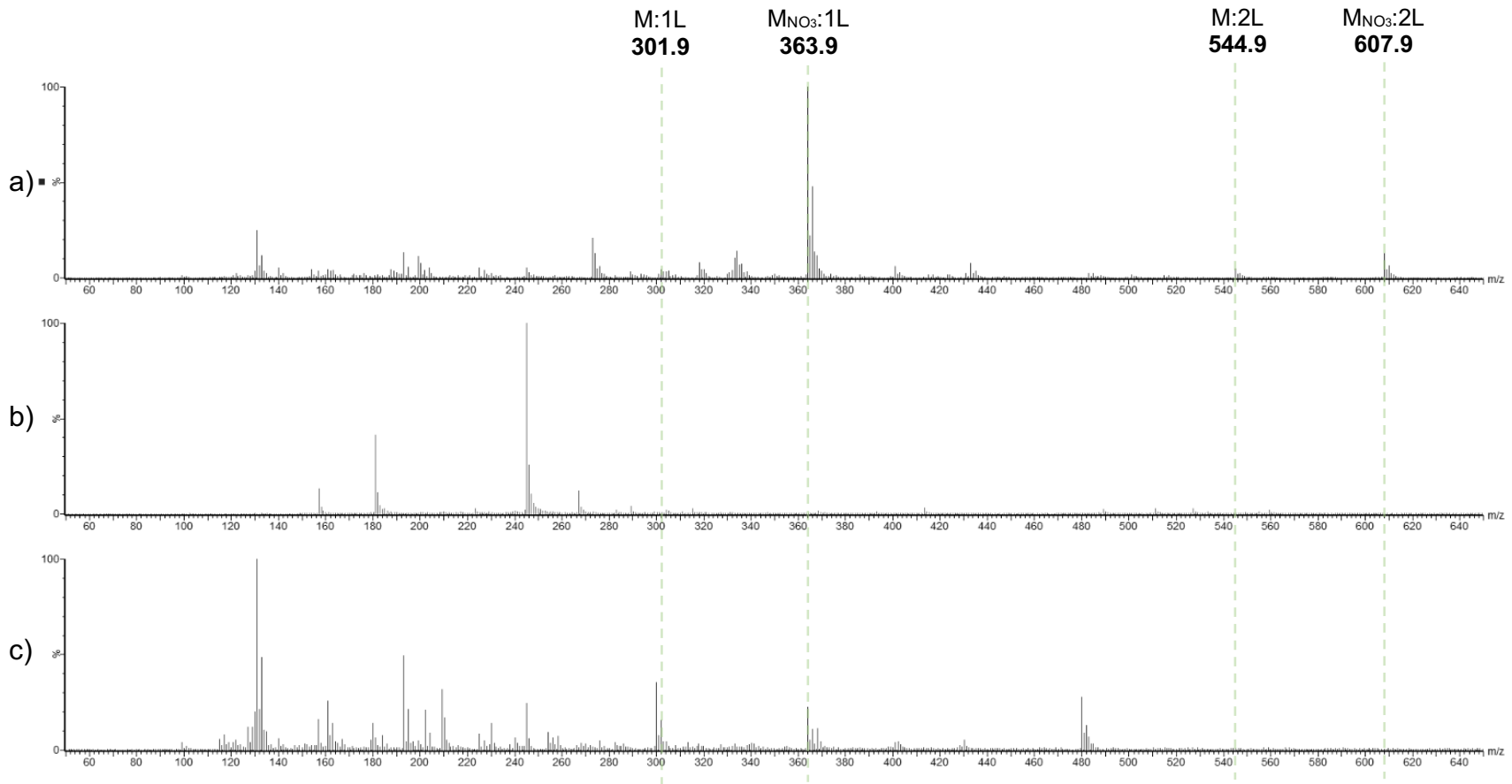

Figure 3.22 A comparison study of the spectra of Nickel (II) Nitrate and 2,2'-Bipyridine-4,4'-Dicarboxylic Acid for a) 50:50 *v/v* mixture in methanol, b) the dual-spray method, and c) the TRESI method.

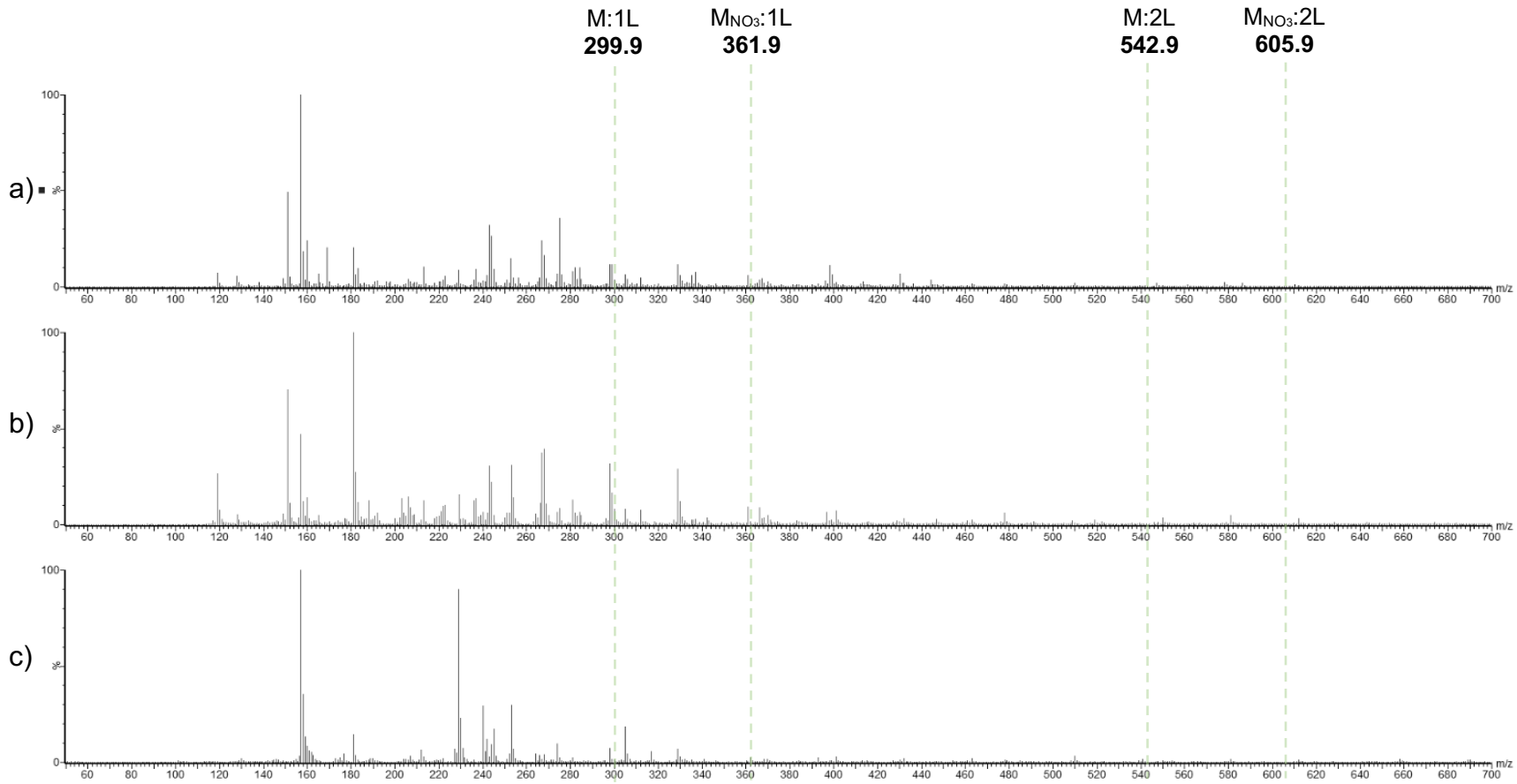

Figure 3.23 A comparison study of the spectra of Iron (III) Nitrate and 2,2'-Bipyridine-4,4'-Dicarboxylic Acid for a) 50:50 *v/v* mixture in methanol, b) the dual-spray method, and c) the TRESI method.

From Figure 3.22, it can be learned that the single-spray mixture method is the only relatively effective method of analysing the combination of Nickel (II) Nitrate and 2,2'-Bipyridine-4,4'-Dicarboxylic Acid. As determined by the stability study, the reaction needed a minimum of 24 hours to go to completion, making the real-time methods insignificant. It is clear that the dual-spray method of mixing compounds in the gas phase produced little to no ion complexes of interest. However, it is surprising to note that the TRESI method of mixing ions in the liquid phase did indeed produce some target complexes. The figure shows that there is signal produced for the 1:1 complexes at the 301.9 *m/z* ($NiC_{12}H_8N_2O_4^+$) and 363.9 *m/z* ($NiC_{12}H_8N_2O_4NO_3^+$) regions. Overall, only the single-spray mixture method was effective while the TRESI method had some success and the dual-spray method had little to no success at creating the complexes of interest.

It is seen in Figure 3.23 both the single- and dual-spray methods of the Iron (III) Nitrate combination were both relatively ineffective at creating target complexes. Although some 1:1 complexes are present, there is very little signal in these regions and the *m/z* is one or two mass units lower than expected in each case. When looking at the TRESI method, only a small signal is produced at the non-nitrated 1:1 complex around 299.9 *m/z*, $FeC_{12}H_8N_2O_4^+$. As determined by the stability study, very little reaction occurred over time, if at all. With that knowledge it is not unexpected that the real-time mixing in both the liquid and gas phases did not produce any viable signal. Therefore, no method tested was successful in creating the target compounds of interest.

3.5 1,10-Phenanthroline

1,10-Phenanthroline, $C_{12}H_8N_2$, has a molecular mass of 180.20 g/mol. Figure 3.24 below displays the mass spectrum (50-400 Da) taken of the compound when mixed in methanol at a concentration of approximately 0.5 mg/mL.

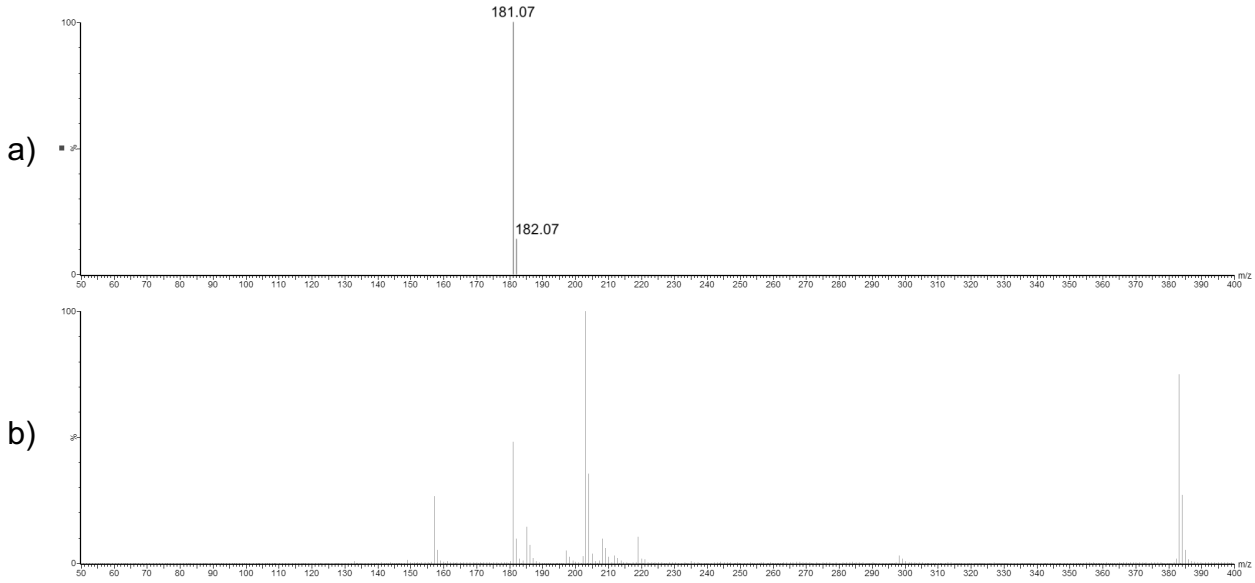

Figure 3.24 Spectrum of 1,10-Phenanthroline in methanol focused on the $C_{12}H_8N_2H^+$ ion at 181.0 and 182.0 *m/z* taken using Electrospray Ionization (QToF) Mass Spectrometry comparing a) the expected isotope pattern as generated by the MassLynx software isotope modeling tool, to b) the acquired sample.

After mixing the 1,10-Phenanthroline with the Nickel (II) Nitrate solution 50:50 *v/v*, a stability study was performed, the results of which can be seen in Figure 3.25 below. The stability study of the Iron (III) Nitrate and 1,10-Phenanthroline 50:50 v/v solution can be found in Figure 3.25.

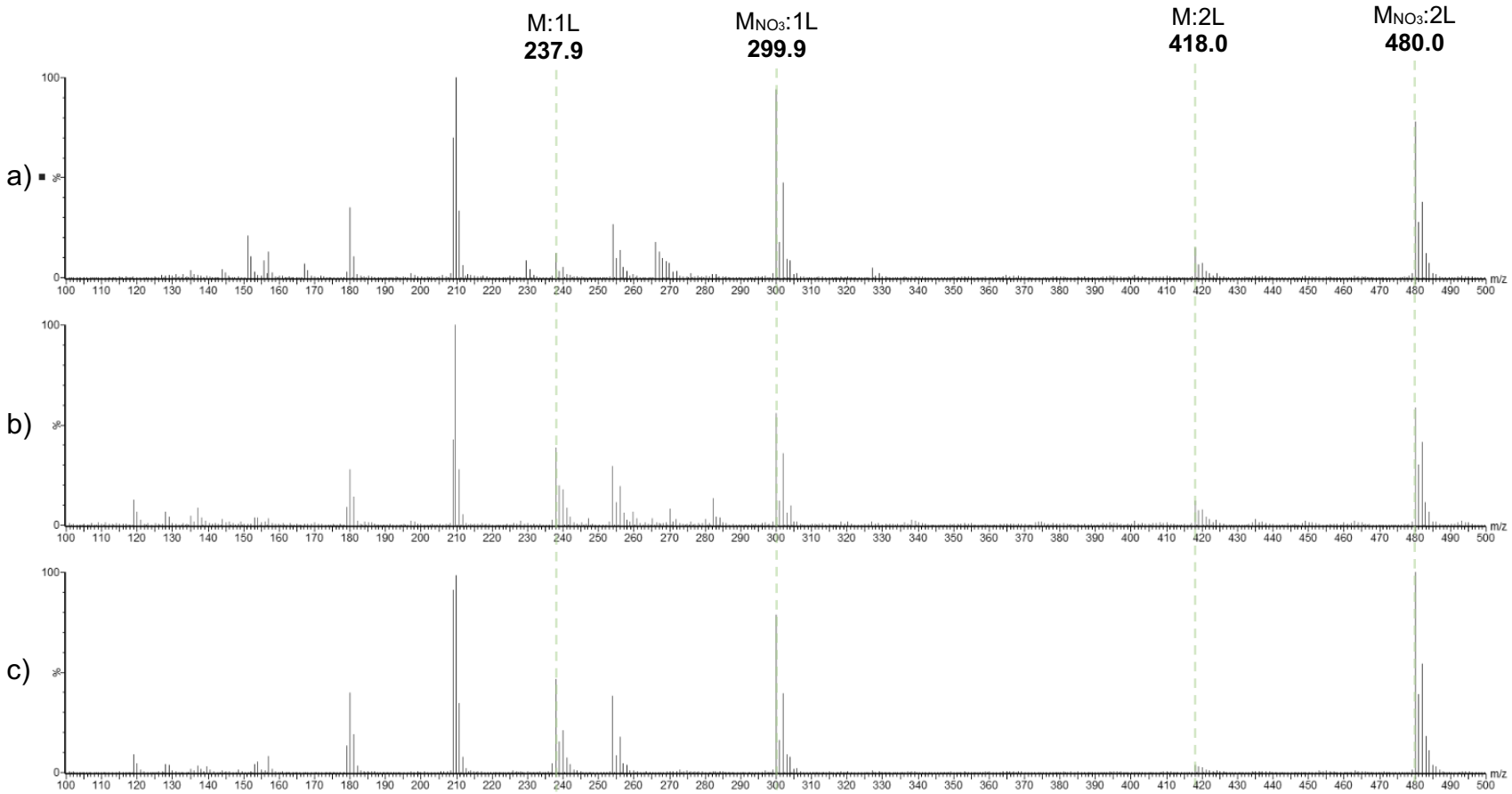

Figure 3.25 Stability study of Nickel (II) Nitrate 1,10-Phenanthroline 50:50 *v/v* mixture in methanol after a) one, b) 24, and c) 48 hours.

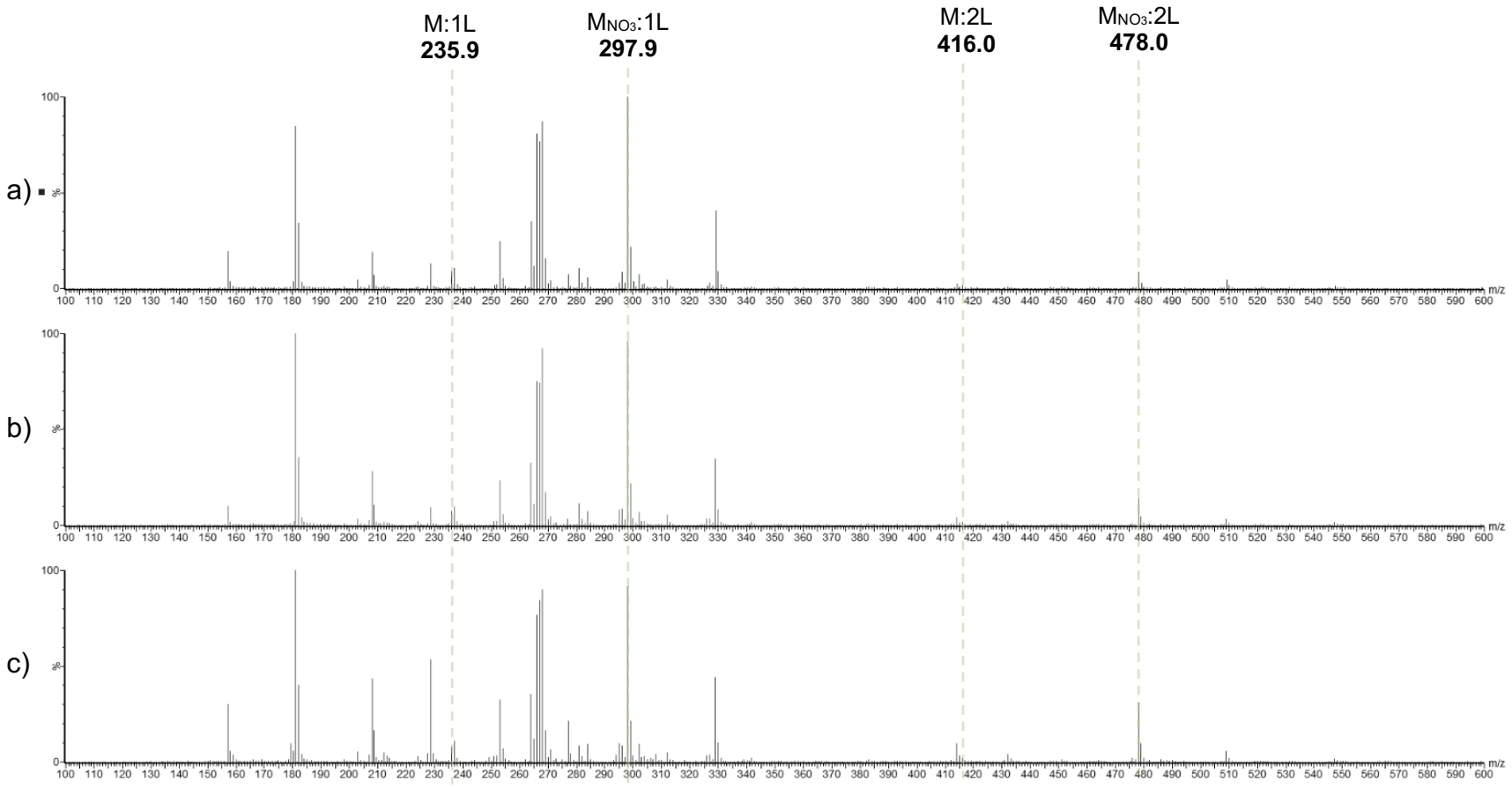

Figure 3.26 Stability study of Iron (III) Nitrate 1,10-Phenanthroline 50:50 *v/v* mixture in methanol after a) one, b) 24, and c) 48 hours.

It was determined from Figure 3.25 that the reaction of Nickel (II) Nitrate 1,10-Phenanthroline was complete within the first 24 hours after mixing. After the first hour, all complexes of interest are present, but the non-nitrated compounds are at very low signal intensities. After 24 hours, the signal of the non-nitrated 1:1 complex seems to improve but not the 1:2. There is little to no intensity lost for any other compounds present with the addition of a few more ions in the lower *m/z* regions. After 48 hours, there is a drop in intensity for the non-nitrated 1:2 complex as well as those compounds in the lower *m/z* regions. The ligand is present in all three spectra, but at the lowest intensity in the 24 hour spectra, suggesting more of the compound had reacted. Generally, there is very little difference in the stability of the mixture overtime, but between one and 24 hours was the ideal reaction time for this combination to undergo further experimentation.

From Figure 3.26 it is learned that there is very little change over time for the Iron (III) Nitrate 1,10-Phenanthroline combination. One hour after mixing, there are signals present at each of the four target complexes and in very similar ratios to the Nickel solution. Again, the non-nitrated 1:1 and 1:2 complexes have very little intensities. After 24 hours, the intensities increase slightly but become distorted by the 48 hour mark, specifically the non-nitrated 1:2 complex. Figure 3.27 confirms the quick reaction time by the colour change beginning in the first hour of mixing. Again, this suggests an oxidation reaction and the rapid change indicates the completion of the reaction fairly early on.

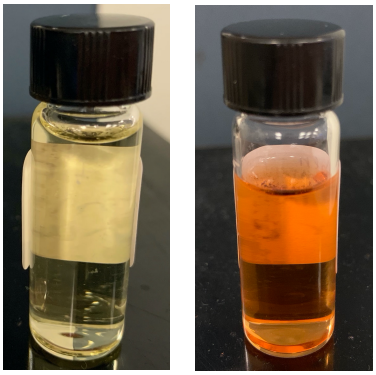

Figure 3.27 Iron (III) Nitrate 1,10-Phenanthroline solution approximately one minute after mixing (left) as compared to approximately one hour after mixing (right).

Taking the colour change and relative intensities of the spectra into account, it was decided that between one and 24 hours was the ideal reaction time for this mixture.

Figures 3.28 and 3.29 below compare the three methods of injection overall, the single-spray mixture, dual-spray and TRESI with both the Nickel and Iron solutions respectively.

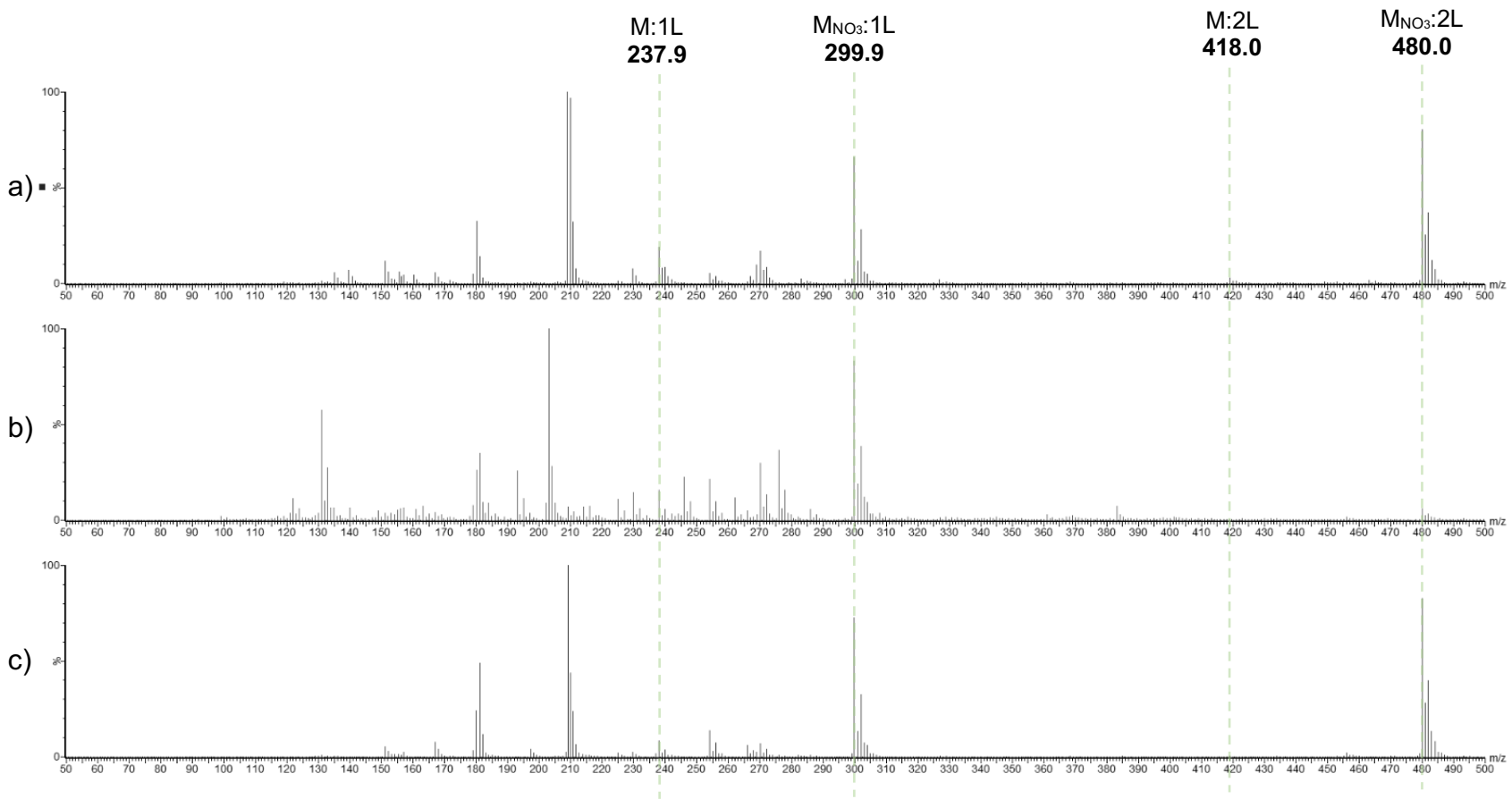

Figure 3.28 A comparison study of the spectra of Nickel (II) Nitrate 1,10-Phenanthroline for a) 50:50 *v/v* mixture in methanol, b) the dual-spray method, and c) the TRESI method.

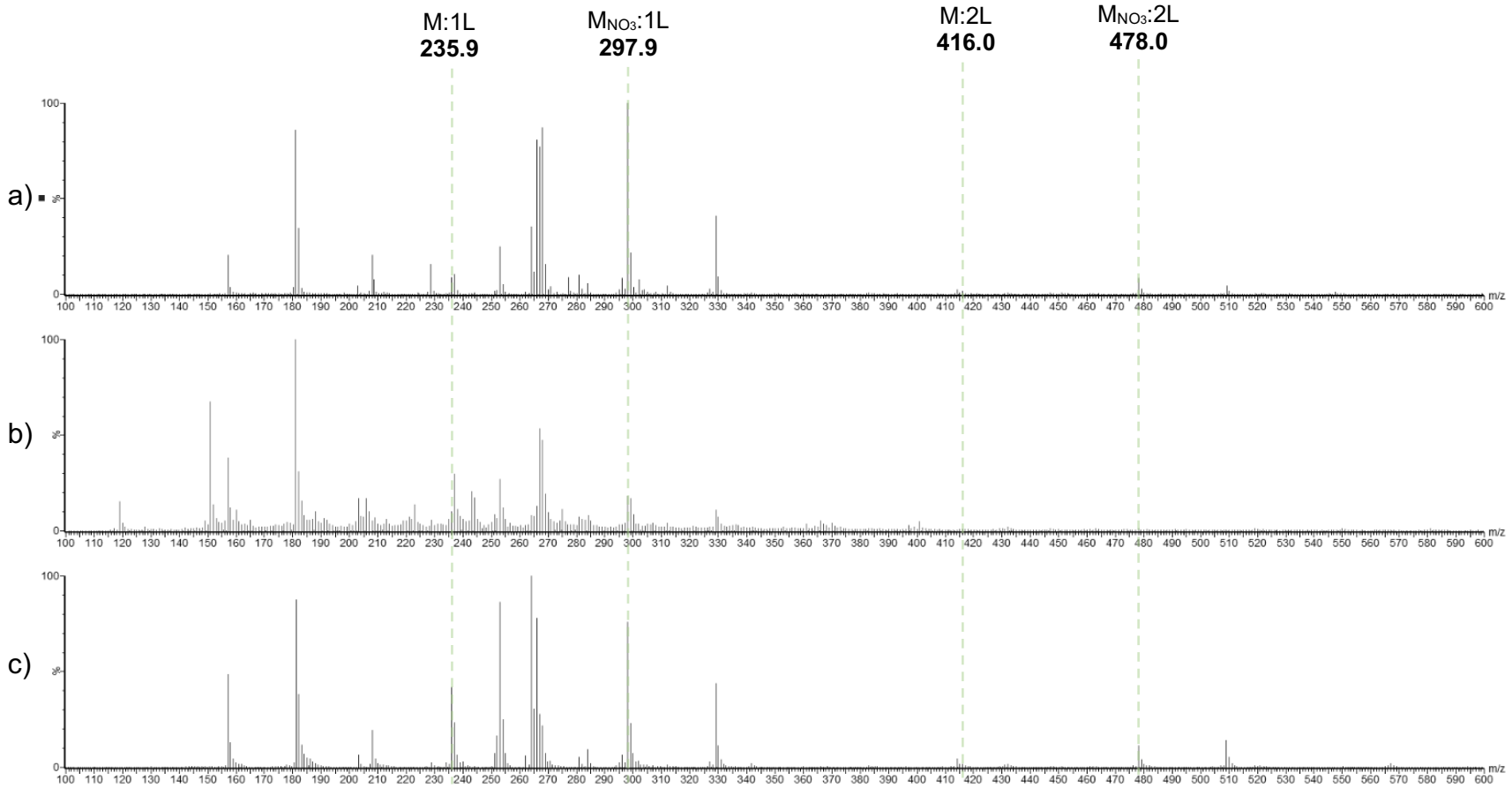

Figure 3.29 A comparison study of the spectra of Iron (III) Nitrate 1,10-Phenanthroline for a) 50:50 *v/v* mixture in methanol, b) the dual-spray method, and c) the TRESI method.

From Figure 3.28, the single-spray mixture method of Nickel (II) Nitrate Phenanthroline again seems to be the most effective method of analysing this combination. Although very similar to the spectrum from the TRESI method, the intensities of both non-nitrated compounds are larger in the single-spray method. This is also true for the dual-spray method, both non-nitrated complexes have little to no intensity. However, the nitrated 1:2 complex also has very little intensity. In all three techniques, the ligand alone is notably present.

It is known that the 1,10-Phenanthroline mixture also takes some time to complete its reaction. Mixing with the Nickel (II) Nitrate in both the liquid and gas phases did however produce some ions for the complexes of interest, just in lower intensities than with the pre-mixed solution. Overall, only the single-spray mixture method was effective while the TRESI method had some success and the dual-spray method had very little success at creating the complexes of interest.

In Figure 3.29, it is seen that the Iron (III) Nitrate Phenanthroline combination produces similar results to the Nickel combination. While the single-spray method is quite effective, the TRESI method is also very effective, specifically when looking at the 1:1 complexes. Both methods produced greater signals for the 1:1 complexes than for the 1:2 complexes. Interestingly, the TRESI method produced a much more intense signal with a more complete isotope pattern for the non-nitrated 1:1 complex ($FeC_{12}H_8N_2^+$) than the single-spray method. However, when observing the 1:2 complexes, both methods produced significantly less intense signals and the TRESI method was much more distorted at the non-nitrated 1:2 complex ($FeC_{12}H_8N_2C_{12}H_8N_2^+$) than was the single-spray mixture. Furthermore, the dual-spray method produced some signal for the 1:1 complexes

but little to no signal for the 1:2 complexes. Also, the spectrum is very noisy and somewhat unclear in the 150-400 *m/z* range making the data less reliable.

Knowing that the mixture needed some time to react, it is no surprise that the real-time mixing in the gas phase produced little usable results in the dual-spray method. It is surprising however that the TRESI method of real-time mixing in the liquid phase was so successful. It produced very similar if not better results than the pre-mixed solution and single-spray method. Clearly these compounds react very well in the liquid phase and not as much in the gas phase. Overall, the single-spray and TRESI methods were very effective in creating the target compounds of interest while the dual-spray method had very little success.

3.6 SNS

The Baker Group's SNS Ligand, $C_{14}H_{13}NS_2$, has a molecular mass of 259.38 g/mol. Figure 3.30 below displays the mass spectrum (50-400 Da) taken of the compound when mixed in methanol at a concentration of approximately 0.5 mg/mL.

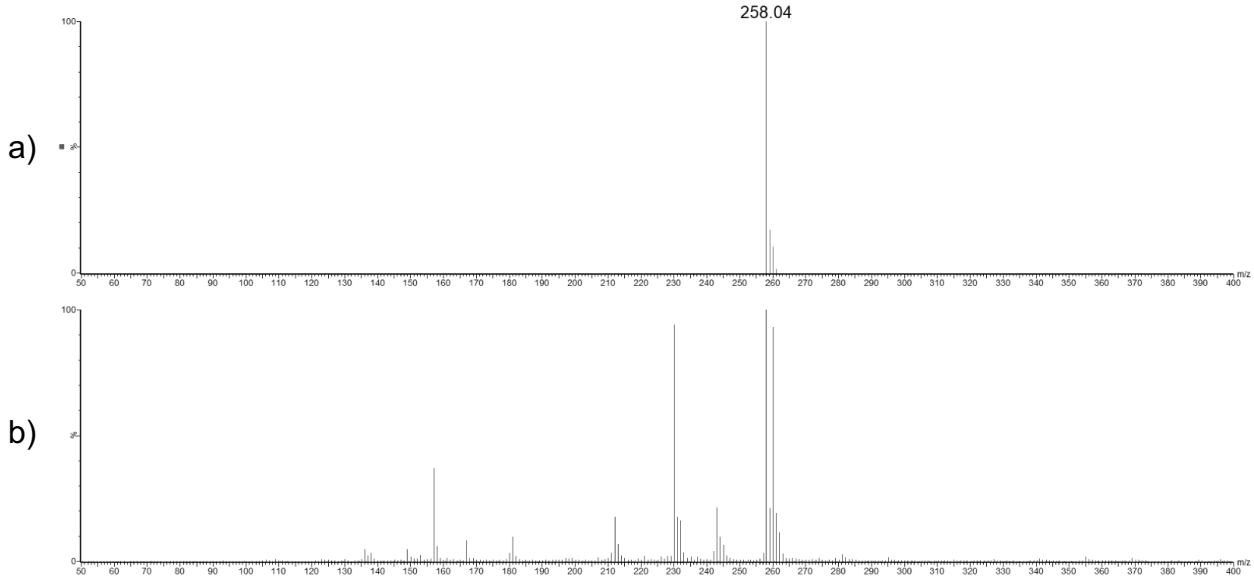

Figure 3.30 Spectrum of SNS Ligand, less one hydrogen ($C_{14}H_{12}NS_2^+$), in methanol taken using Electrospray Ionization (QToF) Mass Spectrometry comparing a) the expected isotope pattern as generated by the MassLynx software isotope modeling tool, to b) the acquired sample.

After mixing the SNS Ligand with the Nickel (II) Nitrate solution 50:50 *v/v*, a stability study was performed, the results of which can be seen in Figure 3.31 below. The stability study of the Iron (III) Nitrate and the SNS Ligand 50:50 v/v solution can be found in Figure 3.31.

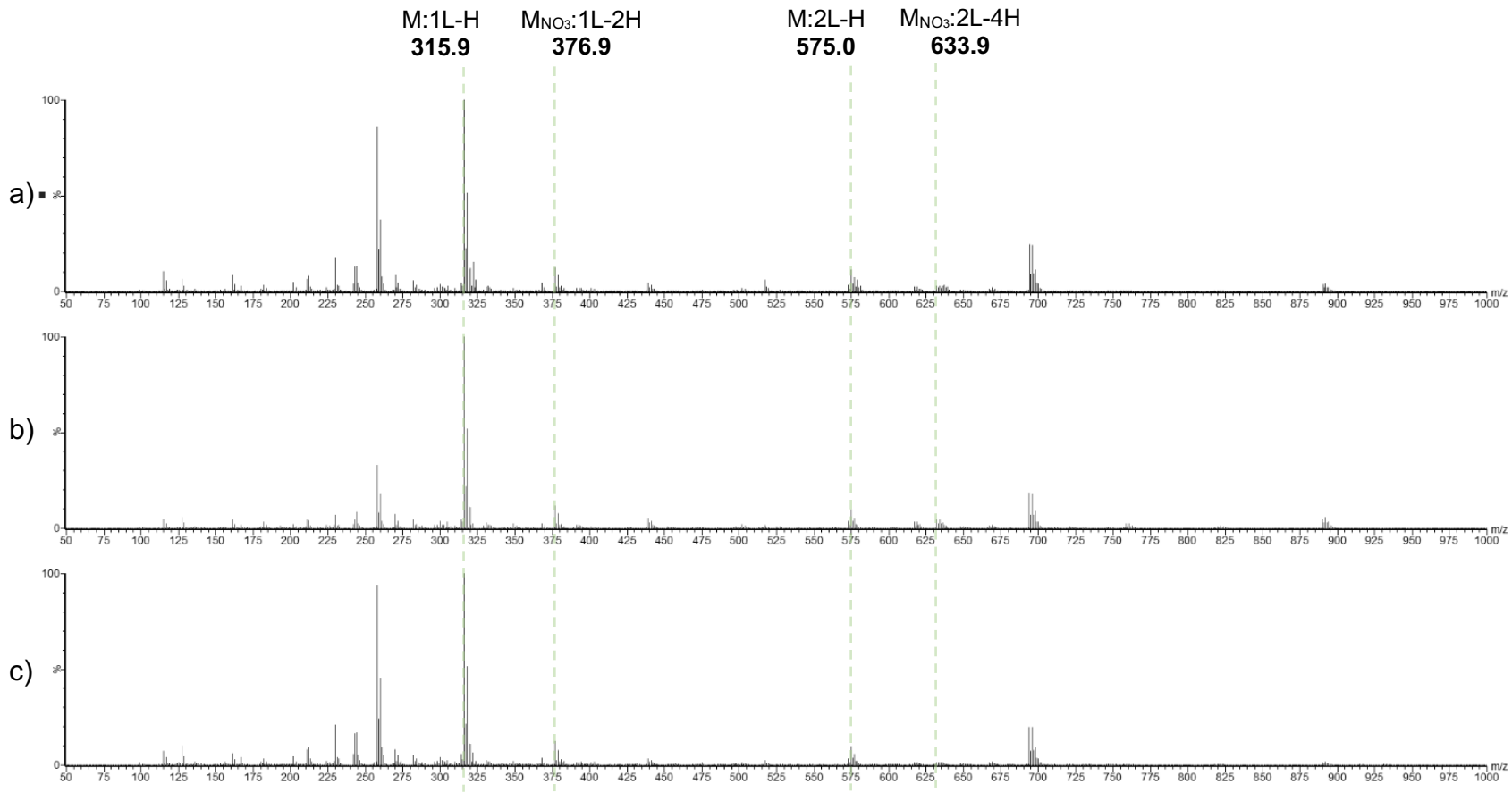

Figure 3.31 Stability study of Nickel (II) Nitrate SNS 50:50 *v/v* mixture in methanol at a) one, b) 24, and c) 48 hours.

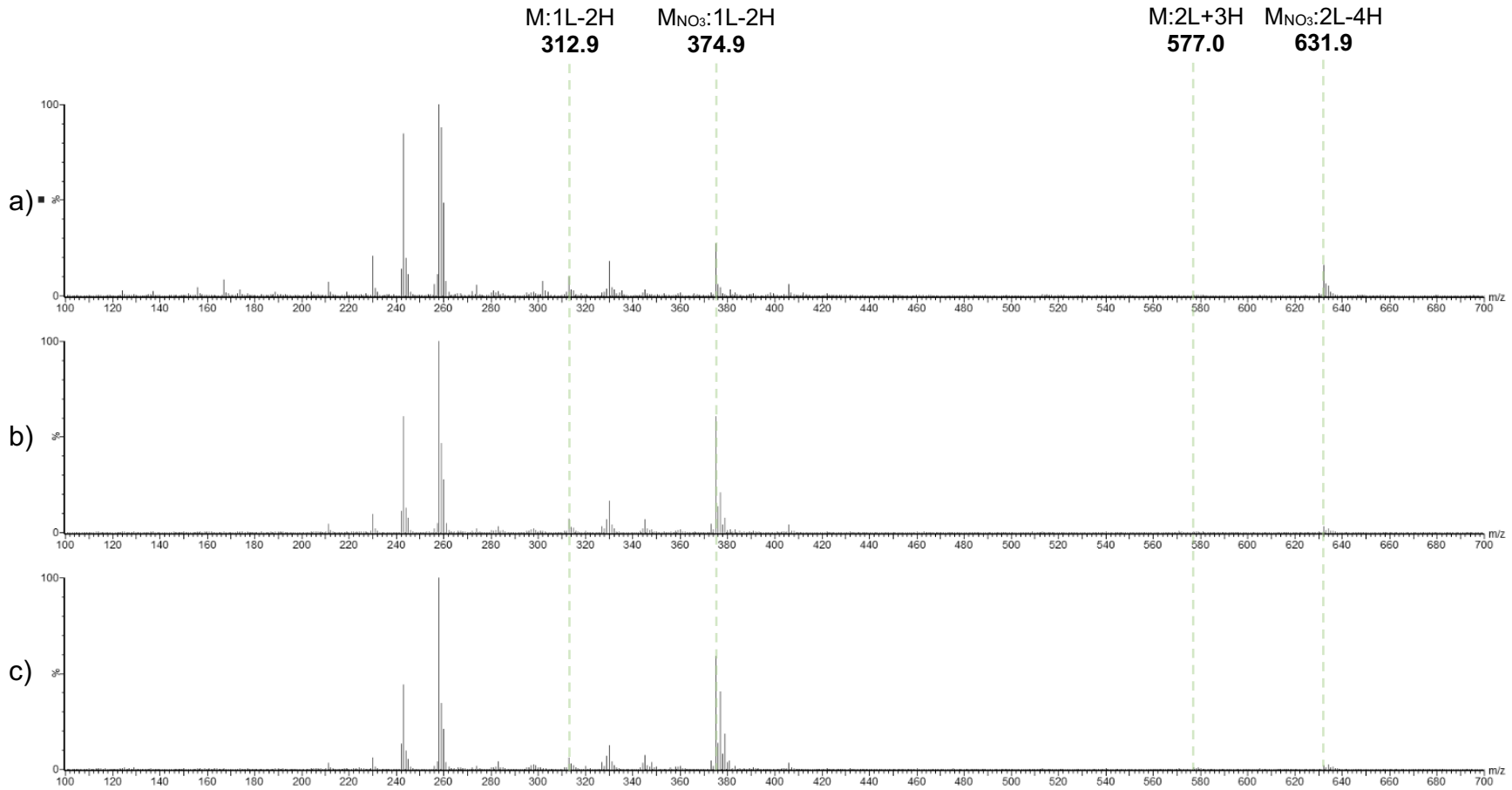

Figure 3.32 Stability study of Iron (III) Nitrate SNS 50:50 *v/v* mixture in methanol at a) one, b) 24, and c) 48 hours.

It was determined that the reaction of Nickel (II) Nitrate SNS was complete within the first hour after mixing. After the first hour, all complexes of interest are present, although in very low intensities compared to the dominant peak of the non-nitrated 1:1 complex ($NiC_{14}H_{12}NS_2^+$). After both 24 and 48 hour periods, very few changes occur within the spectrum meaning that this mixed complex is quite stable over time. The ligand alone less one hydrogen, $C_{14}H_{12}NS_2^+$, is also visible with a relatively high intensity at 258 *m/z* at all analyzed times. Knowing the ligand is only visible missing one mass unit less due to a hydrogen atom loss, it is no surprise that the non-nitrated 1:1 and 1:2 complexes are also found one mass unit less. When looking at the nitrated 1:1 complex, $NiC_{14}H_{11}NS_2NO_3^+$, it is found at 376.9 *m/z*, meaning it has lost two hydrogen atoms. The same pattern follows for the nitrated 1:2 complex as it is found to have lost four hydrogen atoms, $NiC_{14}H_{11}NS_2C_{14}H_{11}NS_2NO_3^+$ at 633.9 *m/z*. The ligand less one hydrogen, $C_{14}H_{12}NS_2^+$, is visible in all three spectra. Therefore, one hour was chosen to be the ideal reaction time for this mixture to undergo further experimentation.

When looking at Iron (III) Nitrate SNS, the same conclusion was made. The spectrum after one hour has the greatest average intensity of all four complexes of interest. Again, both nitrated complexes have lost two and four hydrogens respectively as seen in the nickel mixture, $FeC_{14}H_{11}NS_2NO_3^+$ and $FeC_{14}H_{11}NS_2C_{14}H_{11}NS_2NO_3^+$. This time, the 1:1 non-nitrated complex appears two hydrogens less than expected, $FeC_{14}H_{11}NS_2^+$, but the 1:2 non-nitrated appears three hydrogens more, $FeC_{14}H_{13}NS_2C_{14}H_{16}NS_2^+$. At 577.0 *m/z,* it has very little intensity after one hour but does not increase with time. It also does not follow the pattern of the rest and likely means the complex is not the target of interest. Although the nitrated 1:1 complex does increase over

time, the nitrated 1:2 complex signal significantly decreases after the first hour. The 1:1 complex at 312.9 *m/z*, $FeC_{14}H_{11}NS_2^+$, is fairly consistent throughout the spectra. There is no image of the solution for this mixture. The ligand less one hydrogen $C_{14}H_{12}NS_2^+$, is again visible in all three spectra. Therefore, one hour was chosen for this mixture as well to be the ideal reaction time to undergo further experimentation.

Figures 3.33 and 3.34 below compare the three methods of injection overall, the single-spray mixture, dual-spray and TRESI with both the Nickel and Iron solutions respectively.

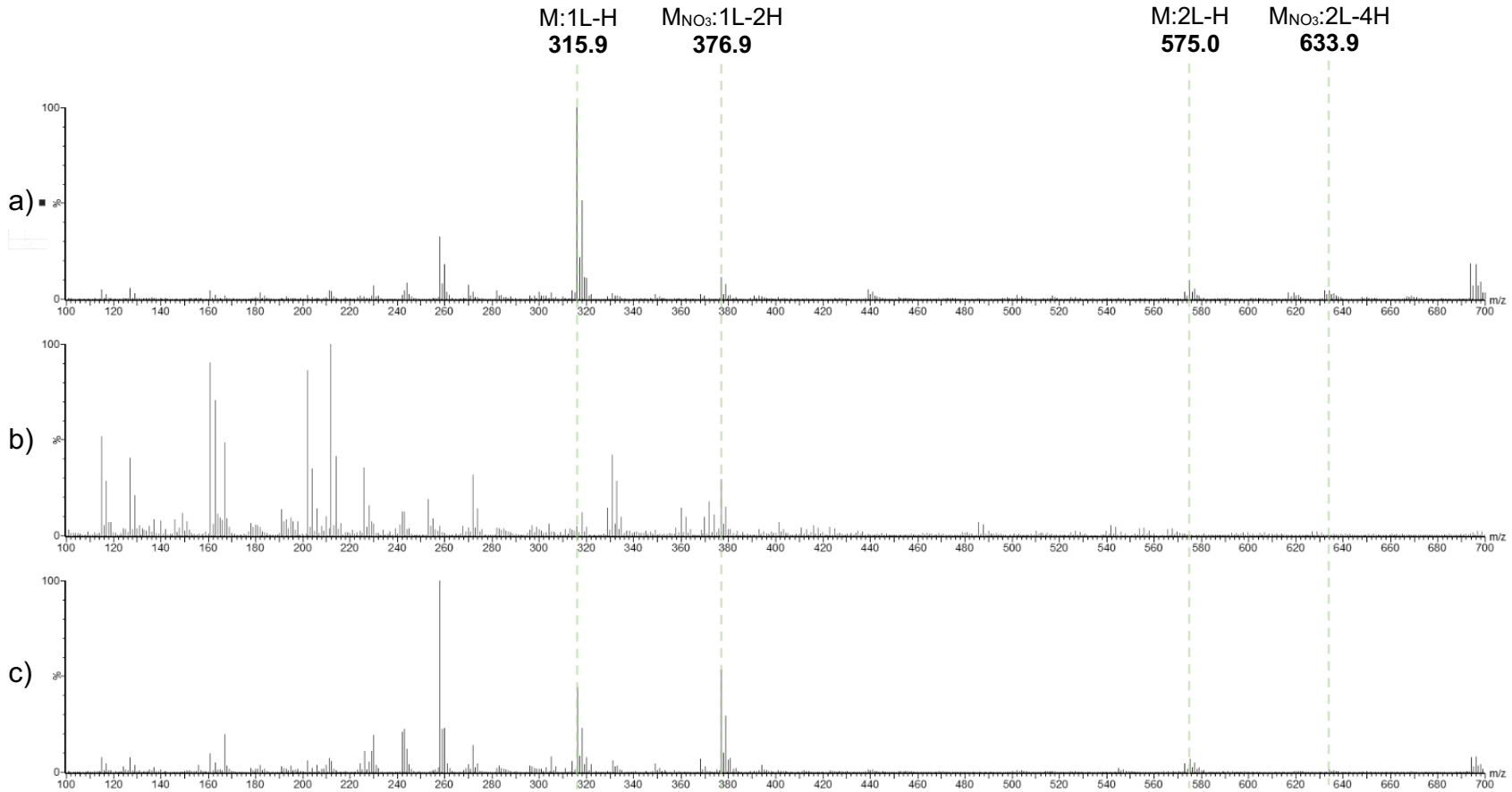

Figure 3.33 A comparison study of the spectra of Nickel (II) Nitrate SNS for a) 50:50 *v/v* mixture in methanol, b) the dual-spray method, and c) the TRESI method.

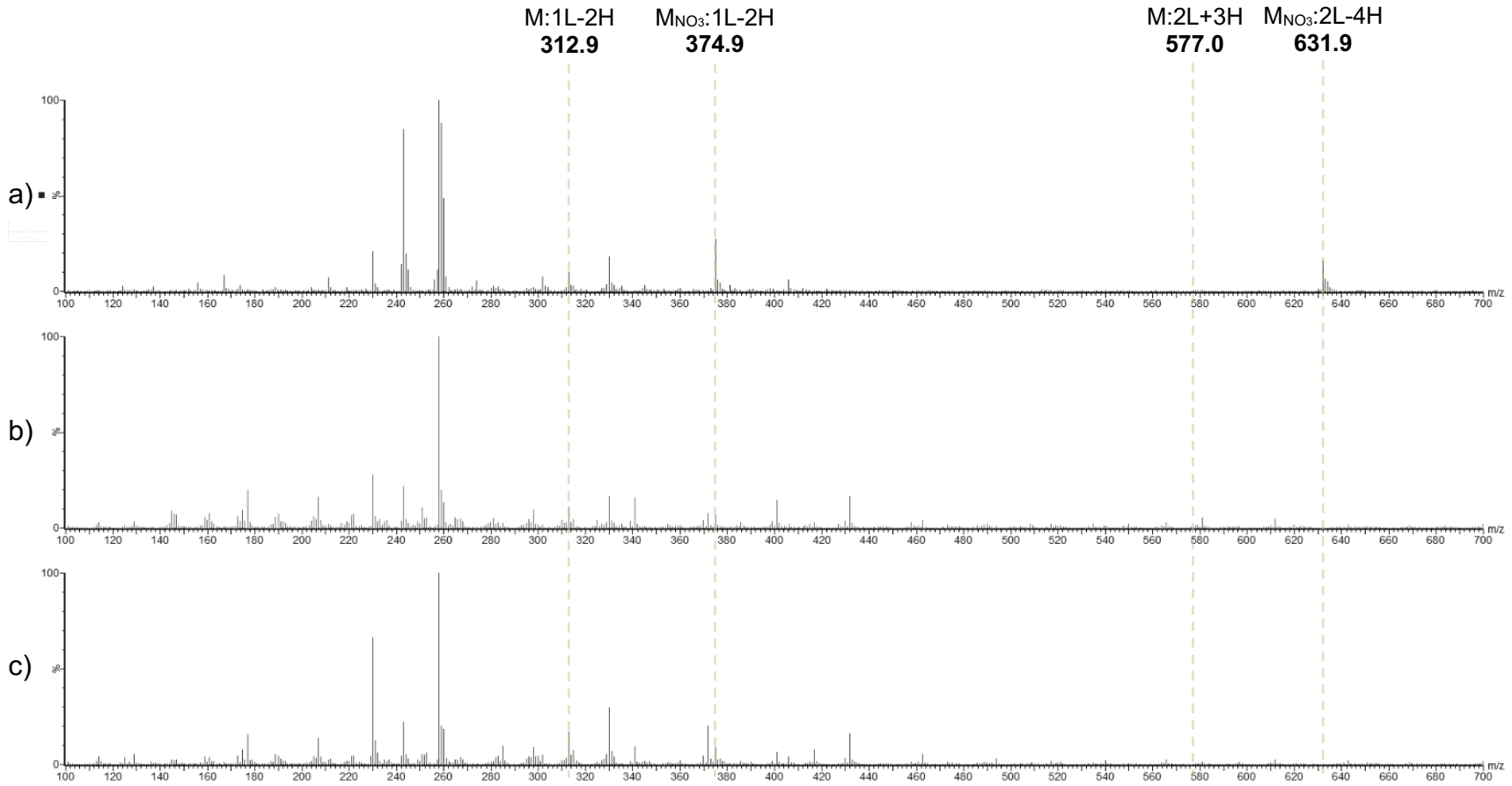

Figure 3.34 A comparison study of the spectra of Iron (III) Nitrate SNS for a) 50:50 *v/v* mixture in methanol, b) the dual-spray method, and c) the TRESI method.

From Figure 3.33, it can be learned that the single-spray mixture method and the TRESI method are almost equally as effective when analysing this combination. In the single-spray mixture, only the 1:1 complex has a relatively high intensity while the other three are present but in low quantities. In the TRESI method, both the non-nitrated and nitrated 1:1 complexes are present in similar intensities but much lower than other intense peaks within the spectra. Also, the non-nitrated 1:2 complex is present with a small intensity while the nitrated 1:2 shows little to no ions produced. Alternatively, the dual-spray method shows little to no ions of interest produced overall. There is a small signal produced for the 376.9 *m/z*, the nitrated 1:1 complex ($NiC_{14}H_{11}NS_2NO_3^+$), but the spectrum is mainly comprised of other compounds in the lower *m/z* regions. Overall, only the single-spray was relatively effective as was the TRESI method while the dual-spray method had little to no success at creating the complexes of interest.

When looking at the Iron (III) Nitrate SNS combination from Figure 3.34, similar patterns are present. The single-spray mixture and TRESI method similarly produced moderate ions of interest while the dual-spray method produced little to no target signals overall. Both nitrated complexes appear at higher intensities with the single-spray method over the TRESI method, but each method would still be considered successful. Therefore, the dual-spray method was the least effective, followed by the TRESI method, making the single-spray method the most effective technique to create complexes of interest.

3.7 Summary of Results

Below is a summary of the previous results, indicating which techniques were relatively successful at created complexes of interest versus those that were unsuccessful.

Table 3.1 Summary of method comparison results.

Nickel (II) Nitrate			
Ligand	*Single-Spray*	*Dual-Spray*	*TRESI*
2,2'-Bipyridine	✓	✓	✓
4.4'-Bipyridine	✓	✓	✓
2,2'-Bipyridine-4,4'-Dicarboxylic Acid	✓	✗	✗
1,10-Phenanthroline	✓	✓	✓
SNS	✓	✗	✓

Iron (III) Nitrate			
Ligand	*Single-Spray*	*Dual-Spray*	*TRESI*
2,2'-Bipyridine	✓	✓	✗
4.4'-Bipyridine	✓	✓	✓
2,2'-Bipyridine-4,4'-Dicarboxylic Acid	✗	✗	✗
1,10-Phenanthroline	✓	✓	✓
SNS	✓	✗	✓

CHAPTER 4 – GAS PHASE REACTIVITY OF METAL COMPLEXES: BIPYRIDINE LIGANDS

Collision Induced Dissociation (CID) experiments were performed within both the single- (mixture) and dual-spray methods. They were performed on each of the four target complexes. In the case of Nickel, the experiments were repeated on both dominant isotopes, the 57.9 and 59.9 *m/z* containing compounds. Each experiment was performed by adjusting parameters in both the trap and transfer cells unless otherwise stated. This began at 5 eV and continued until the signal was lost or 100 eV was reached. The data was then analysed, and breakdown diagrams were created to display such results, plotting relative intensity against the E_{COM} (eV) values of the known *m/z*. Complexes marked with an asterisk (*) indicate the presence of Nickel as confirmed by the breakdown diagram of the second isotope containing complex (see appendix).

Each of the three bipyridine ligands, 2,2'-Bipyridine, 4,4'-Bipyridine and 2,2'-Bipyridine-4,4'-Dicarboxylic Acid gave somewhat similar results which will be discussed in this chapter.

The following figures and tables detail the possible skeletal fragments observed in the mass spectra. It is important to note that they are merely potential dissociation pieces and do not reflect the final form of the ion. They were simply posed as possibilities based on the calculated mass of the elemental composition of each peak of interest in the performed experiments.

4.1 2,2'-Bipyridine

In the single-spray (mixture) method with the Nickel (II) Nitrate solution, the 1:1 metal: ligand complex, $NiC_{10}H_8N_2^+$, was observed at 213.9 and 215.9 *m/z*. The nitrated 1:1 complex, $NiC_{10}H_8N_2NO_3^+$, was observed at 275.9 and 277.9 *m/z*. The 1:2 complex, $NiC_{10}H_8N_2C_{10}H_8N_2^+$, was observed at 370.0 and 372.0 *m/z*. Finally, the nitrated 1:2 complex, $NiC_{10}H_8N_2C_{10}H_8N_2NO_3^+$, was observed at 432.0 and 434.0 *m/z*. All results can be found in the following figures, as well as in the appendix.

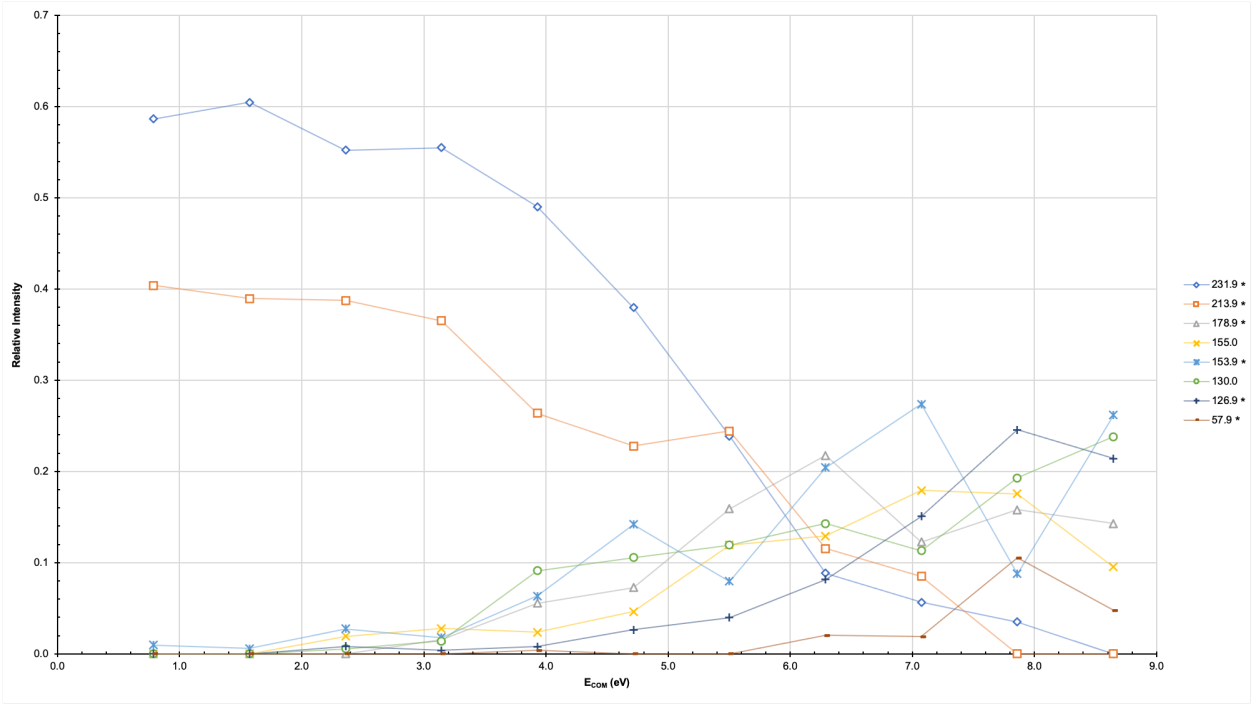

Figure 4.1 Breakdown diagram for the 1:1 complex of Nickel (II) Nitrate and 2,2'-Bipyridine ($NiC_{10}H_8N_2^+$) at 213.9 *m/z* in the trap from 0-55eV, single-spray.

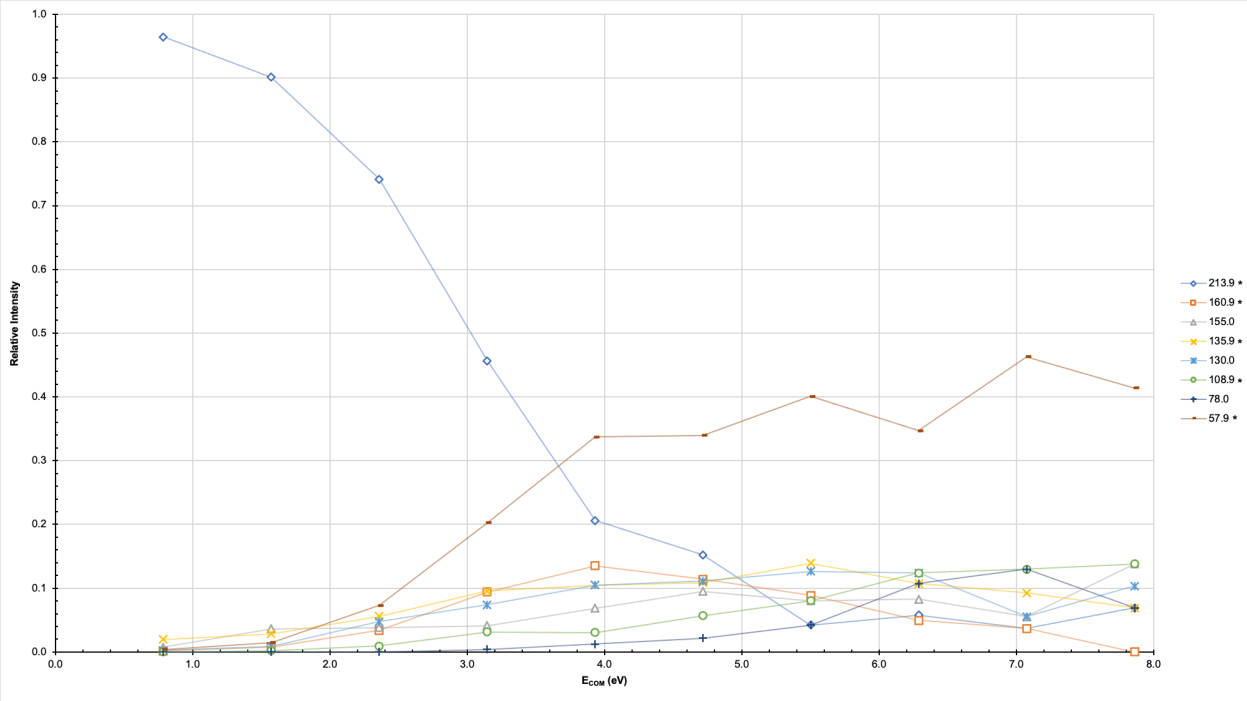

Figure 4.2 Breakdown diagram for the 1:1 complex of Nickel (II) Nitrate and 2,2'-Bipyridine ($NiC_{10}H_8N_2^+$) at 213.9 *m/z* in the transfer from 0-50eV, single-spray.

From Figures 4.1 and 4.2, it can be seen that the single-spray experiment in the transfer gives much more clear results than that of the trap. It was discovered that when the experiment is performed in the trap, the resulting fragments coordinate to water molecules before reaching the detector, creating signals with an additional 18.0 Da such as the fragment at 231.9 *m/z*.

In the dual-spray method with the Nickel (II) Nitrate solution, the same compounds as previously stated were also observed with the exception of the 1:2 compound observed at 369.0 and 371.0 *m/z*, resulting in $NiC_{10}H_8N_2C_{10}H_7N_2^+$ from the loss of a hydrogen atom. Due to the coordination of water and to yield better results, these experiments were only performed in the transfer cell. The results of the first complex can be seen below in Figure 4.3.

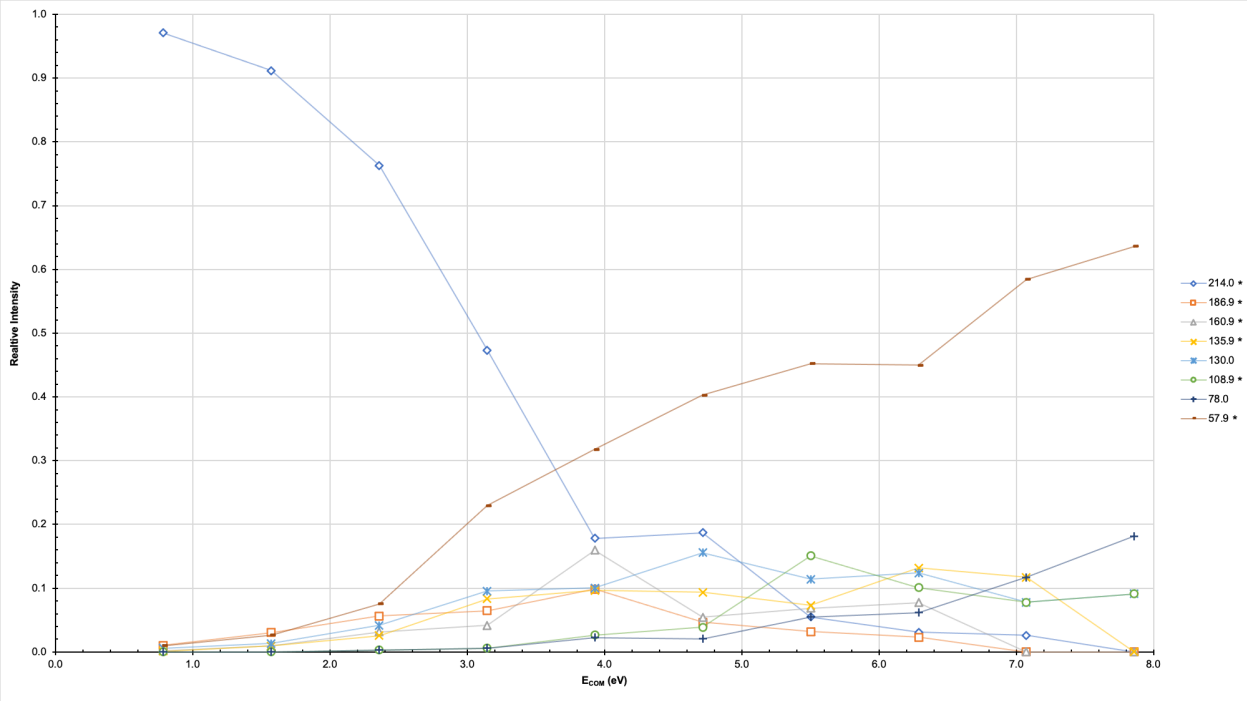

Figure 4.3 Breakdown diagram for the 1:1 complex of Nickel (II) Nitrate and 2,2'-Bipyridine ($NiC_{10}H_8N_2^+$) at 214.0 *m/z* in the transfer from 0-50eV, dual-spray.

All three experiments prove to give very similar results. Several of the same fragments can be observed within each of the experiments. By the end of the experiment, almost all of the initial complex has been fragmented into the nickel ion (Ni^+) at 57.9 *m/z* as to be expected. Other fragments to note can be found in Table 4.1. Some of the potential structures of these fragments can be found in Figure 4.4.

Table 4.1 Nickel (II) Nitrate and 2,2'-Bipyridine fragment mass-to charge values and their possible molecular formulas.

Mass-to-Charge Value	*Possible Molecular Formula*
231.9*	$NiC_{10}H_8N_2H_2O^+$
213.9*	$NiC_{10}H_8N_2^+$
186.9*	$NiC_9H_7N_2^+$
178.9*	$NiC_8H_{11}N_2^+$
160.9*	$NiC_7H_5N_2^+$
155.0	$C_{10}H_7N_2^+$
135.9*	$NiC_5H_4N^+$
130.0	$C_9H_8N^+$
126.9*	$NiC_4H_7N^+$
108.9*	NiC_3HN^+
78.0	$C_5H_4N^+$
57.9*	Ni^+

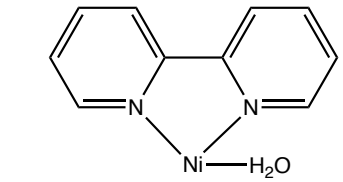

Chemical Formula: $C_{10}H_{10}N_2NiO^+$
Exact Mass: 232.0147

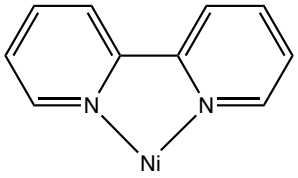

Chemical Formula: $C_{10}H_8N_2Ni^+$
Exact Mass: 214.0041

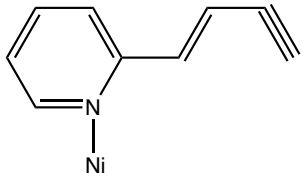

Chemical Formula: $C_9H_7NNi^+$
Exact Mass: 186.9932

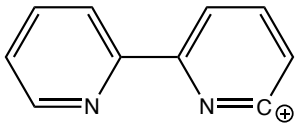

Chemical Formula: $C_{10}H_7N_2^+$
Exact Mass: 155.0604

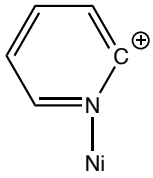

Chemical Formula: $C_5H_4NNi^+$
Exact Mass: 135.9692

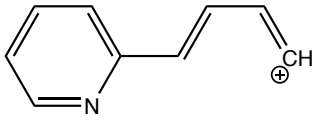

Chemical Formula: $C_9H_8N^+$
Exact Mass: 130.0651

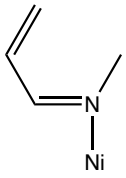

Chemical Formula: $C_4H_7NNi^+$
Exact Mass: 126.9932

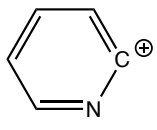

Chemical Formula: $C_5H_4N^+$
Exact Mass: 78.0338

Figure 4.4 Possible skeleton ion fragments formed by collision induced dissociation of Nickel (II) Nitrate and 2,2'-Bipyridine.

The following figures depict the single- and dual-spray experiments for the nitrated 1:1 complex.

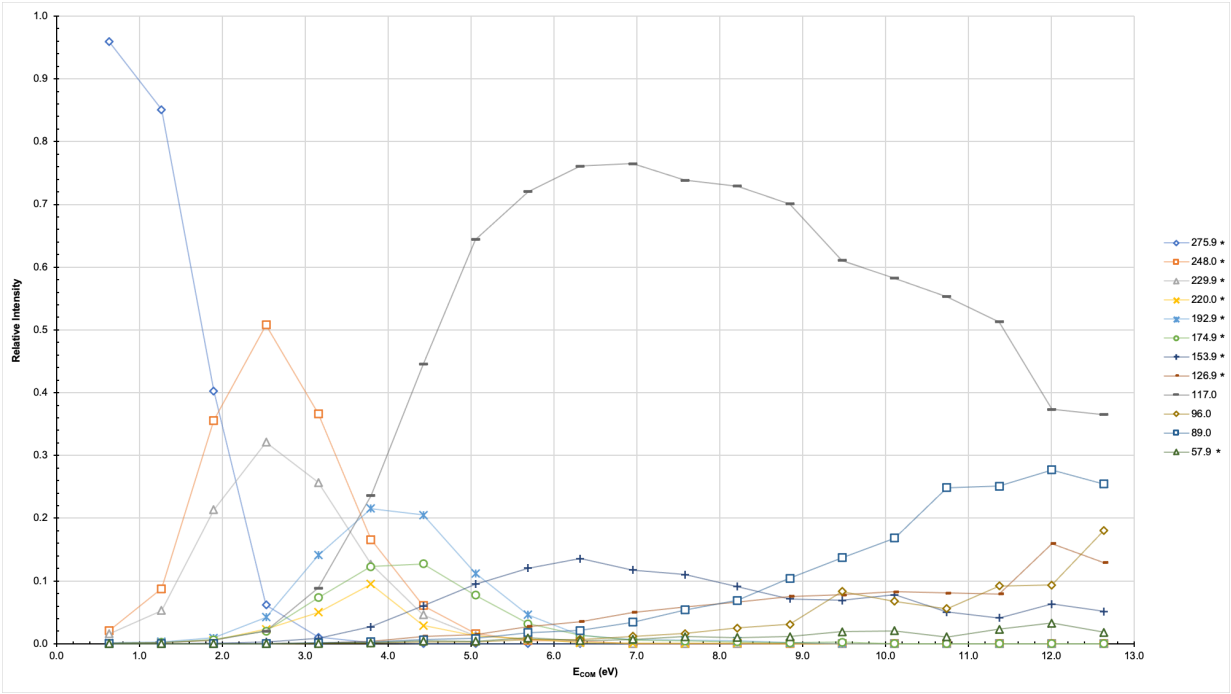

Figure 4.5 Breakdown diagram for the nitrated 1:1 complex of Nickel (II) Nitrate and 2,2'-Bipyridine ($NiC_{10}H_8N_2NO_3^+$) at 275.9 *m/z* in the trap from 0-100eV, single-spray.

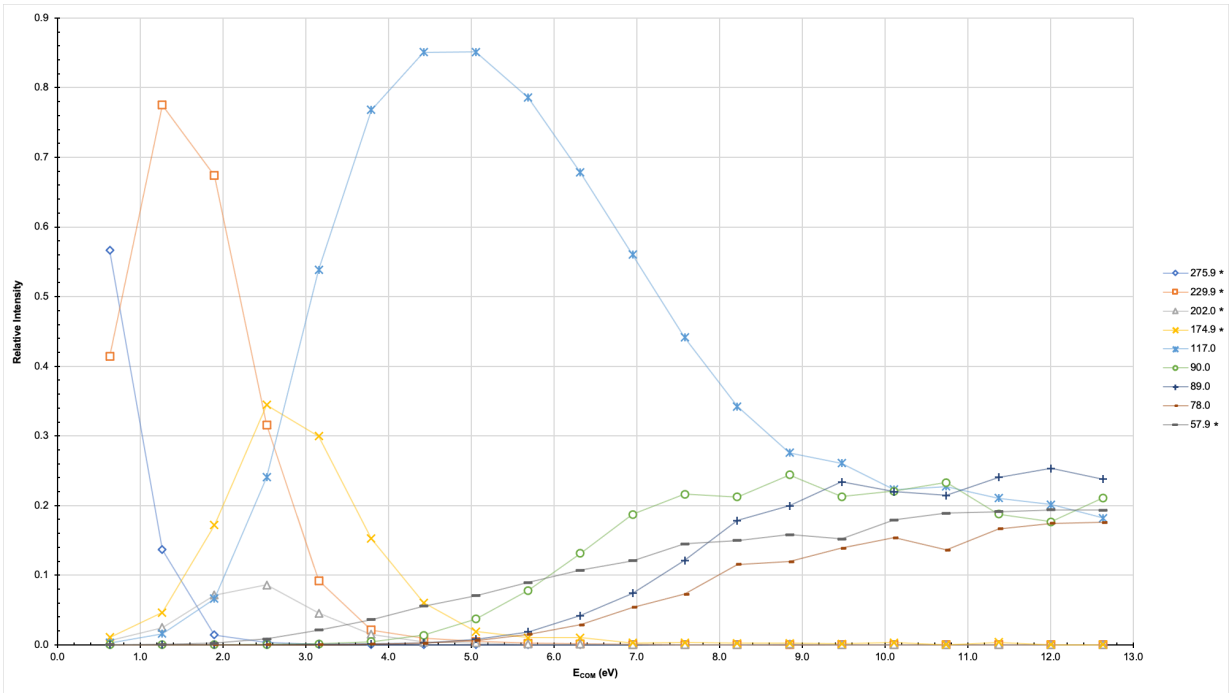

Figure 4.6 Breakdown diagram for the nitrated 1:1 complex of Nickel (II) Nitrate and 2,2'-Bipyridine ($NiC_{10}H_8N_2NO_3^+$) at 275.9 *m/z* in the transfer from 0-100eV, single-spray.

From Figures 4.5 and 4.6, it can be seen that the results from the trap and transfer cells are much more similar and significantly more clear than that of the previous complex. Again, as per the previous discovery, the dual-spray experiment was only performed in the transfer to avoid the coordination of water.

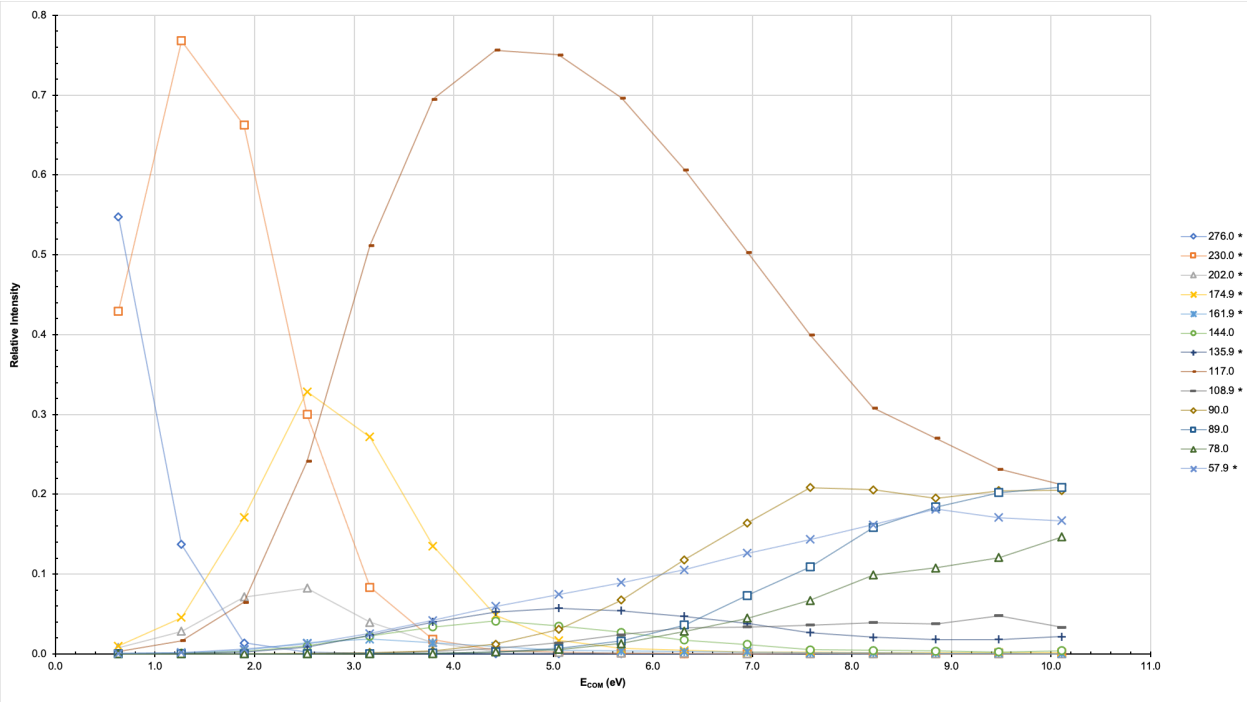

Figure 4.7 Breakdown diagram for the nitrated 1:1 complex of Nickel (II) Nitrate and 2,2'-Bipyridine ($NiC_{10}H_8N_2NO_3^+$) at 276.0 *m/z* in the transfer from 0-80eV, dual-spray.

When comparing the results from single- and dual-spray experiments, the general trend of each graph looks fairly similar. Also, many of the same fragments appear in all three breakdown diagrams. Several of these fragments also appear in the previous set of experiments. As they are only seen in the trap, the fragments at 248.0, 220.0, 192.9, 153.9 and 126.9 *m/z* can be explained by the addition of water to fragments at 229.9, 202.0, 174.9, 135.9 and 108.9 *m/z* respectively, which are also visible in the other diagrams. Additional fragments to note can be found in Table 4.2. Some of the potential structures of these fragments can be found in Figure 4.8.

Table 4.2 Nickel (II) Nitrate and 2,2'-Bipyridine fragment mass-to charge values and their possible molecular formulas, continued.

Mass-to-Charge Value	*Possible Molecular Formula*
275.9*	$NiC_{10}H_8N_2NO_3^+$
229.9*	$NiC_6H_{10}N_2NO_3^+$
202.0*	$NiC_4H_6N_2NO_3^+$
174.9*	$NiC_8H_7NNO_3^+$
161.9*	$NiC_2H_4NNO_3^+$
144.0	$C_9H_8N_2^+$
117.0	$C_8H_7N_2^+$
96.0	$C_5H_8N_2^+$
90.0	$CH_2NNO_3^+$
89.0	$CHNNO_3^+$

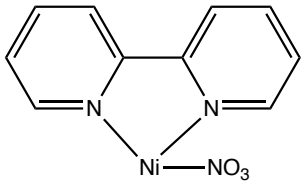

Chemical Formula: $C_{10}H_8N_3NiO_3^+$
Exact Mass: 275.9919

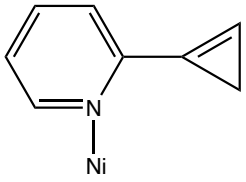

Chemical Formula: $C_8H_7NNi^+$
Exact Mass: 174.9932

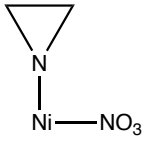

Chemical Formula: $C_2H_4N_2NiO_3^+$
Exact Mass: 161.9575

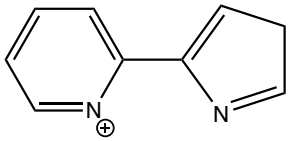

Chemical Formula: $C_9H_8N_2^+$
Exact Mass: 144.0682

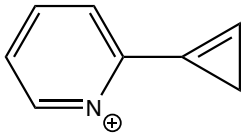

Chemical Formula: $C_8H_7N^+$
Exact Mass: 117.0573

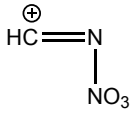

Chemical Formula: $CHN_2O_3^+$
Exact Mass: 88.9982

Figure 4.8 Possible skeletal ion fragments formed by collision induced dissociation of Nickel (II) Nitrate and 2,2'-Bipyridine, continued.

Moving to the 1:2 complex, the results are as follows.

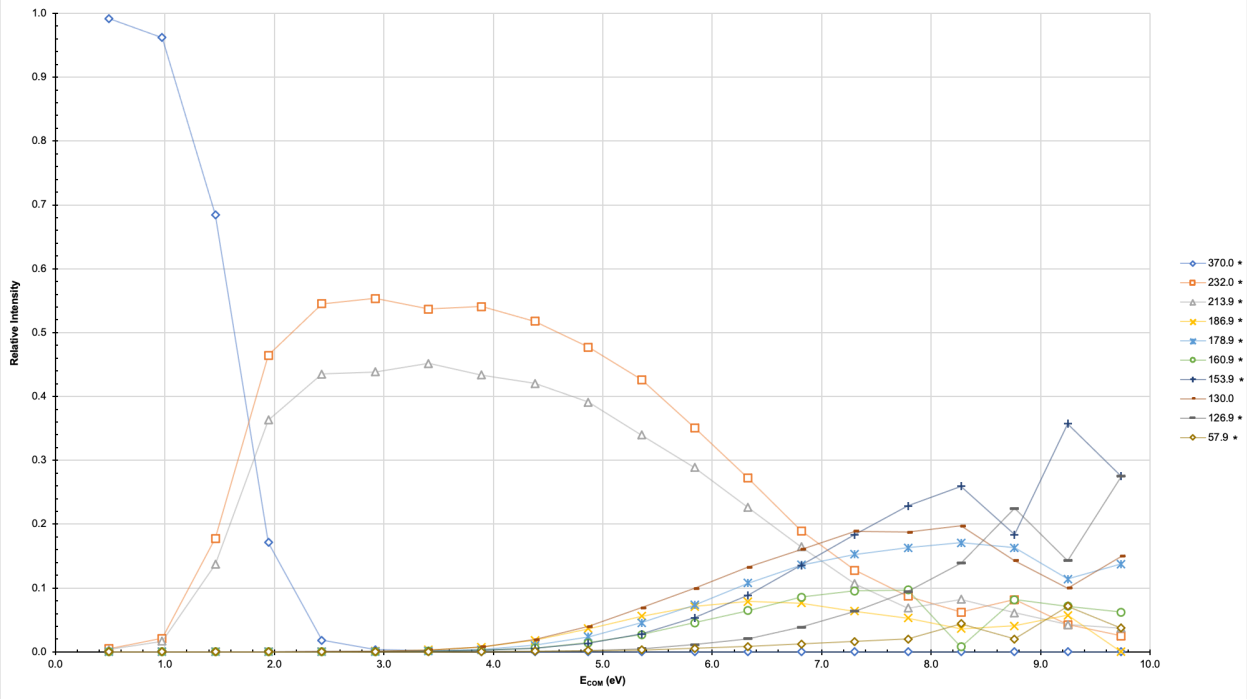

Figure 4.9 Breakdown diagram for the 1:2 complex of Nickel (II) Nitrate and 2,2'-Bipyridine ($NiC_{10}H_8N_2C_{10}H_8N_2^+$) at 370.0 *m/z* in the trap from 0-100eV, single-spray.

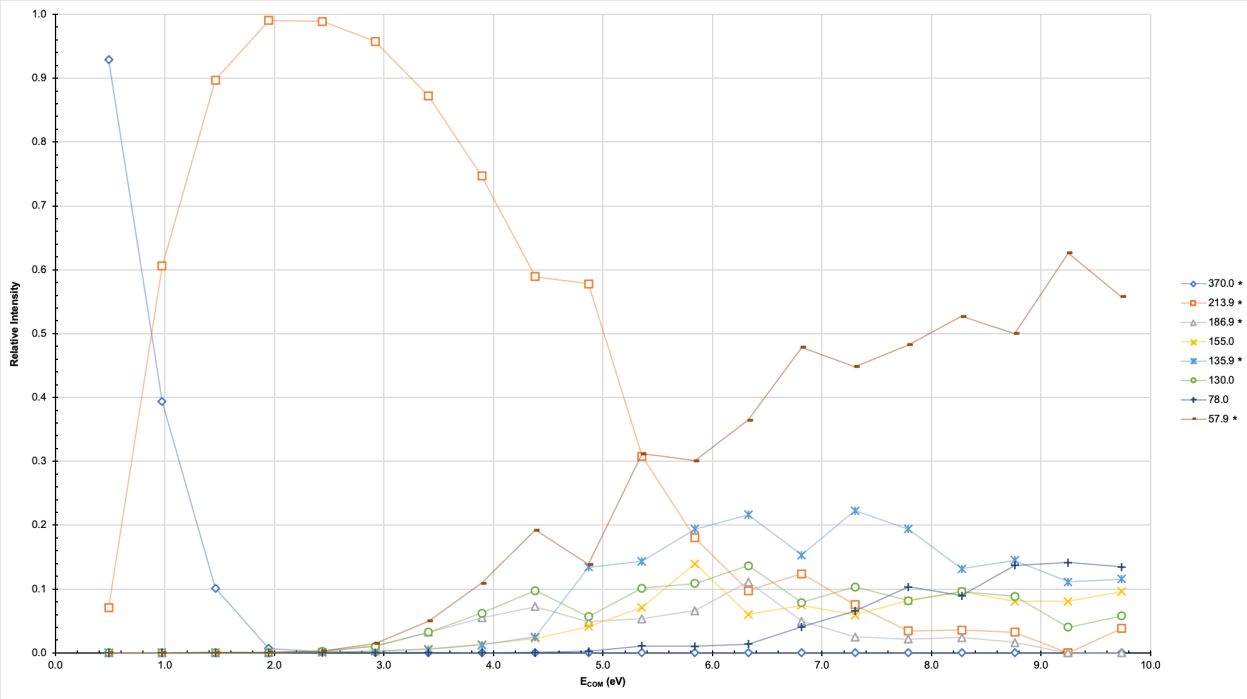

Figure 4.10 Breakdown diagram for the 1:2 complex of Nickel (II) Nitrate and 2,2'-Bipyridine ($NiC_{10}H_8N_2C_{10}H_8N_2^+$) at 370.0 *m/z* in the transfer from 0-100eV, single-spray.

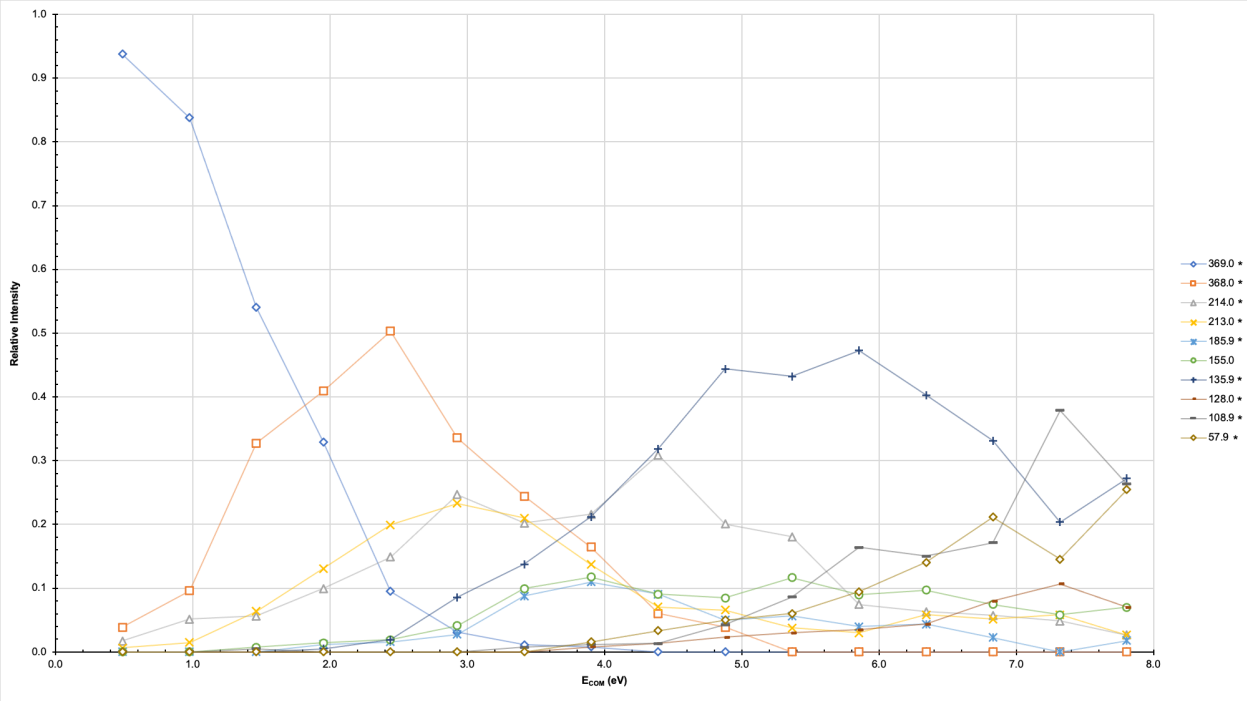

Figure 4.11 Breakdown diagram for the 1:2 complex of Nickel (II) Nitrate and 2,2'-Bipyridine ($NiC_{10}H_8N_2C_{10}H_7N_2^+$) at 369.1 *m/z* in the transfer from 0-100eV, dual-spray.

Again, we see the coordination of water in the trap cell with fragments 232.0, 178.9, 153.9 and 126.9 *m/z*. For the single-spray experiments the 1:1 complex is the dominant fragment of each of the breakdown diagrams almost immediately. With increasing collision energy, the Nickel ion slowly starts to appear and dominates the transfer cell experiment. This confirms the main breakdown pathways of these complexes as well as helps in proving the reproducibility of these experiments. It is interesting to note that in the dual-spray experiment, the target complex was one hydrogen less than what as expected, and this trend continues within the breakdown diagram. The dominant peaks to start were at 369.0 and 368.0 *m/z*, likely after the loss of another hydrogen. Within the graph it is seen that there is again a pair of fragments at the 213.0 and 214.0 *m/z*, indicating the 1:1 complex fragment also followed the same pattern. The molecular structures of the added complexes can be seen in Figure 4.12.

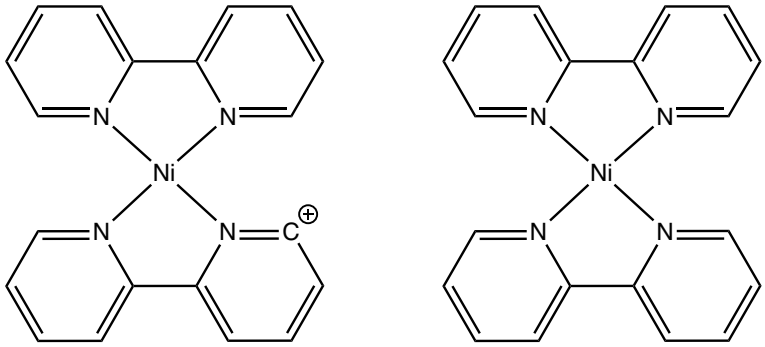

Chemical Formula: $C_{20}H_{15}N_4Ni^+$
Exact Mass: 369.0645

Chemical Formula: $C_{20}H_{16}N_4Ni^+$
Exact Mass: 370.0728

Figure 4.12 Possible skeletal ions made from the Nickel (II) Nitrate and 2,2'-Bipyridine analysis.

Finally, the nitrated 1:2 complex results are found below.

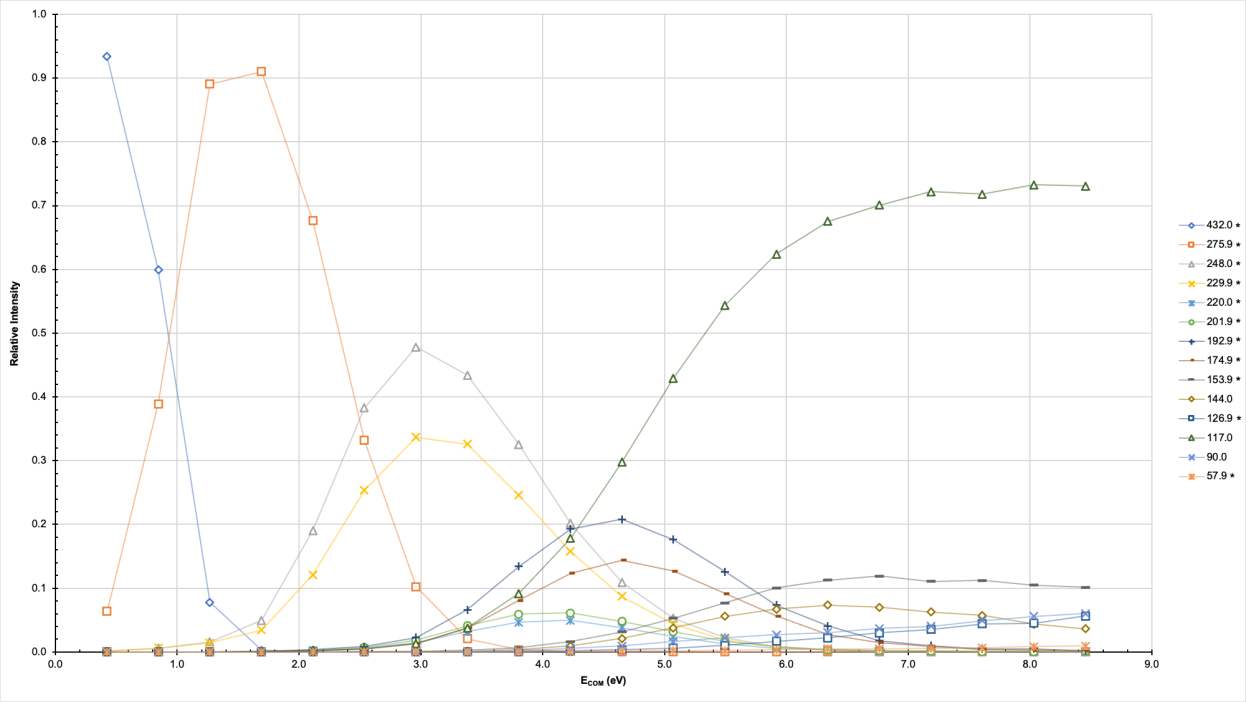

Figure 4.13 Breakdown diagram for the nitrated 1:2 complex of Nickel (II) Nitrate and 2,2'-Bipyridine ($NiC_{10}H_8N_2C_{10}H_8N_2NO_3^+$) at 432.0 *m/z* in the trap from 0-100eV, single-spray.

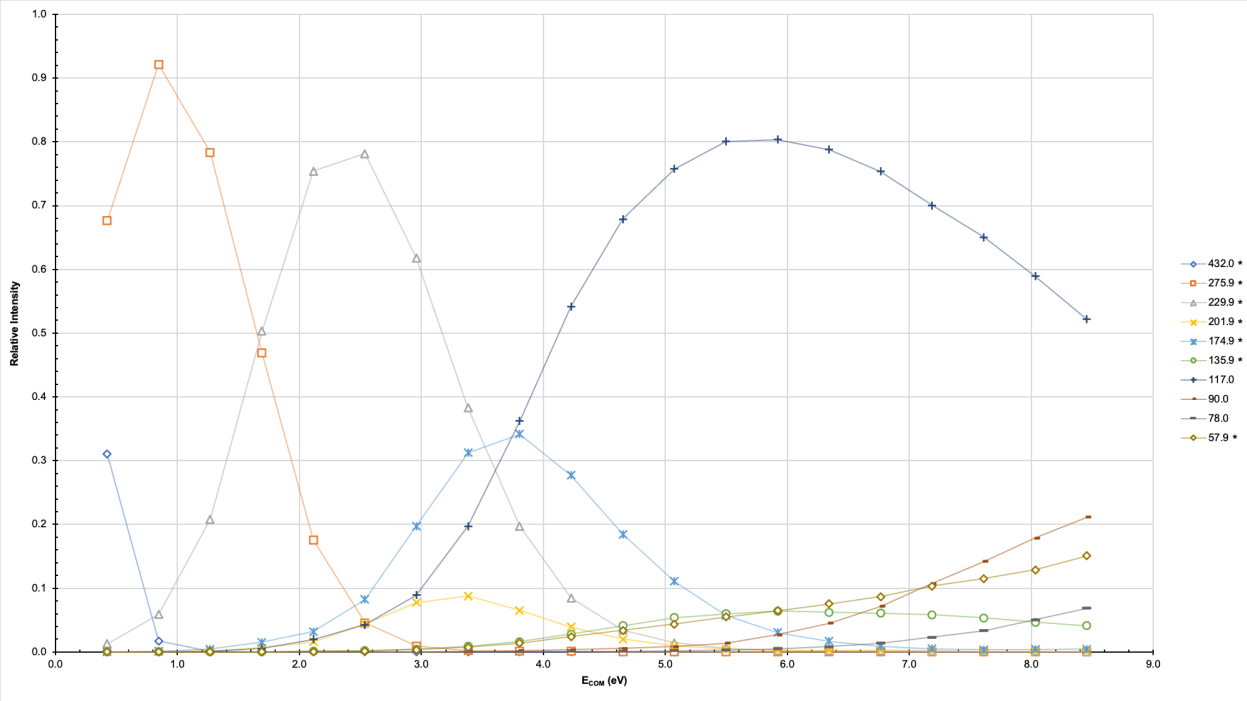

Figure 4.14 Breakdown diagram for the nitrated 1:2 complex of Nickel (II) Nitrate and 2,2'-Bipyridine ($NiC_{10}H_8N_2C_{10}H_8N_2NO_3^+$) at 432.0 *m/z* in the transfer from 0-100eV, single-spray.

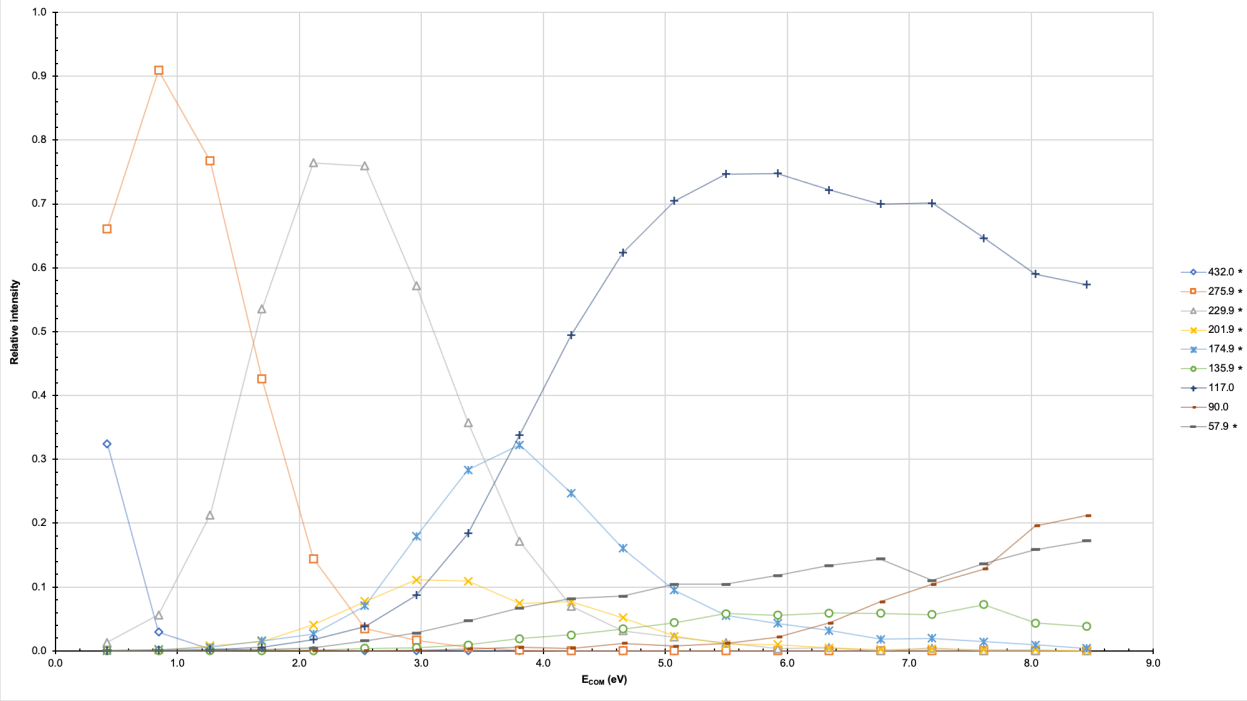

Figure 4.15 Breakdown diagram for the nitrated 1:2 complex of Nickel (II) Nitrate and 2,2'-Bipyridine ($NiC_{10}H_8N_2C_{10}H_8N_2NO_3^+$) at 432.1 *m/z* in the transfer from 0-100eV, dual-spray.

As with all previous results, many of the fragments created in the trap have coordinated with water while many of the others remain the same. The trends of all three graphs again follow similar patterns and very clearly depict the main pathways of the breakdown of this large fragment, for which the molecular structure can be found in Figure 4.16.

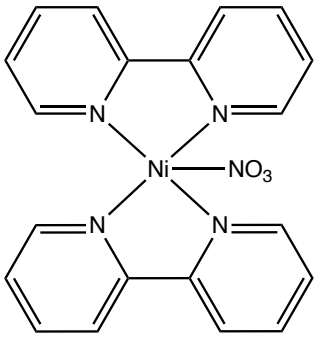

Chemical Formula: $C_{20}H_{16}N_5NiO_3^+$
Exact Mass: 432.0607

Figure 4.16 Possible skeletal ion made from the Nickel (II) Nitrate and 2,2'-Bipyridine analysis.

The same experiments were repeated, instead using Iron (III) Nitrate as the metal solution. This time, all experiments took place in the transfer cell to avoid water coordination as previously learned. Also, only one isotope of iron was used at 55.9 *m/z*. In both the single- and dual-spray experiments, the 1:1 metal: ligand complex, $FeC_{10}H_8N_2^+$, was observed at 211.9 *m/z*. The nitrated 1:1 complex, $FeC_{10}H_8N_2NO_3^+$, was observed at 274.0 *m/z*. The 1:2 complex, $FeC_{10}H_8N_2C_{10}H_8N_2^+$, was observed at 416.0 *m/z*. Finally, the nitrated 1:2 complex, $FeC_{10}H_8N_2C_{10}H_8N_2NO_3^+$, was observed at 478.0 *m/z*. All results can be found in the following figures.

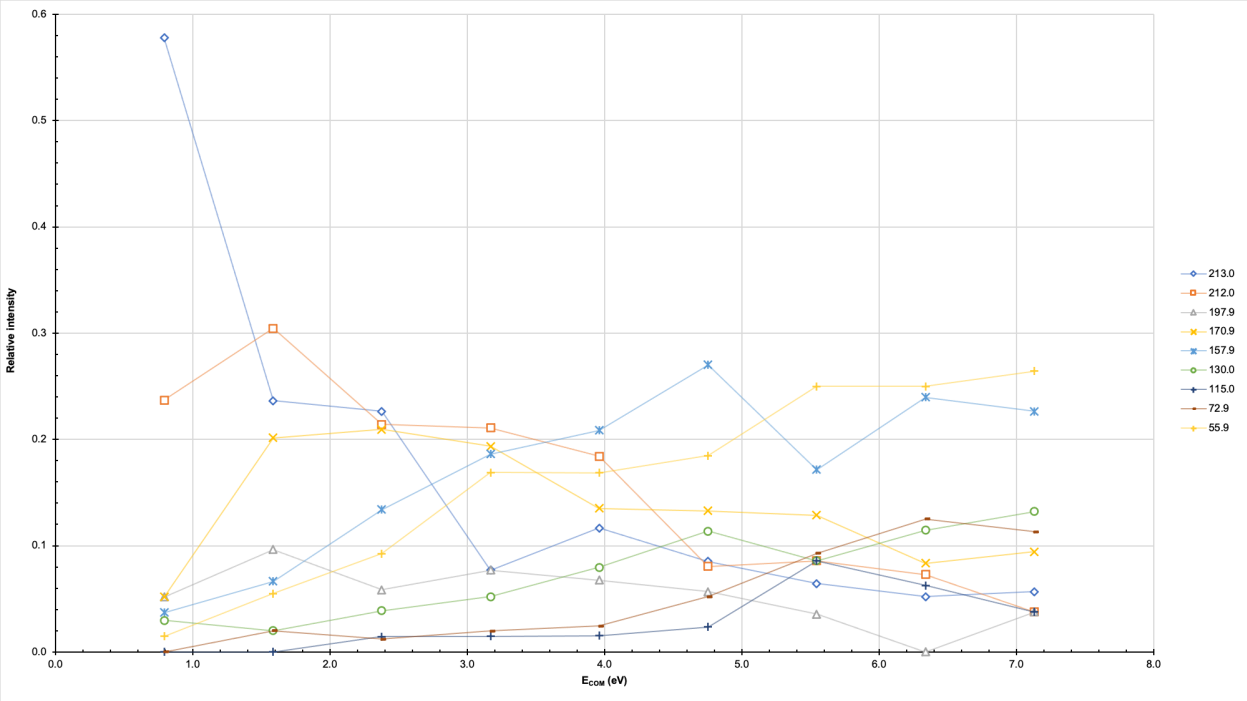

Figure 4.17 Breakdown diagram for the 1:1 complex of Iron (III) Nitrate and 2,2'-Bipyridine ($FeC_{10}H_8N_2^+$) at 211.9 *m/z* in the transfer from 0-50eV, single-spray.

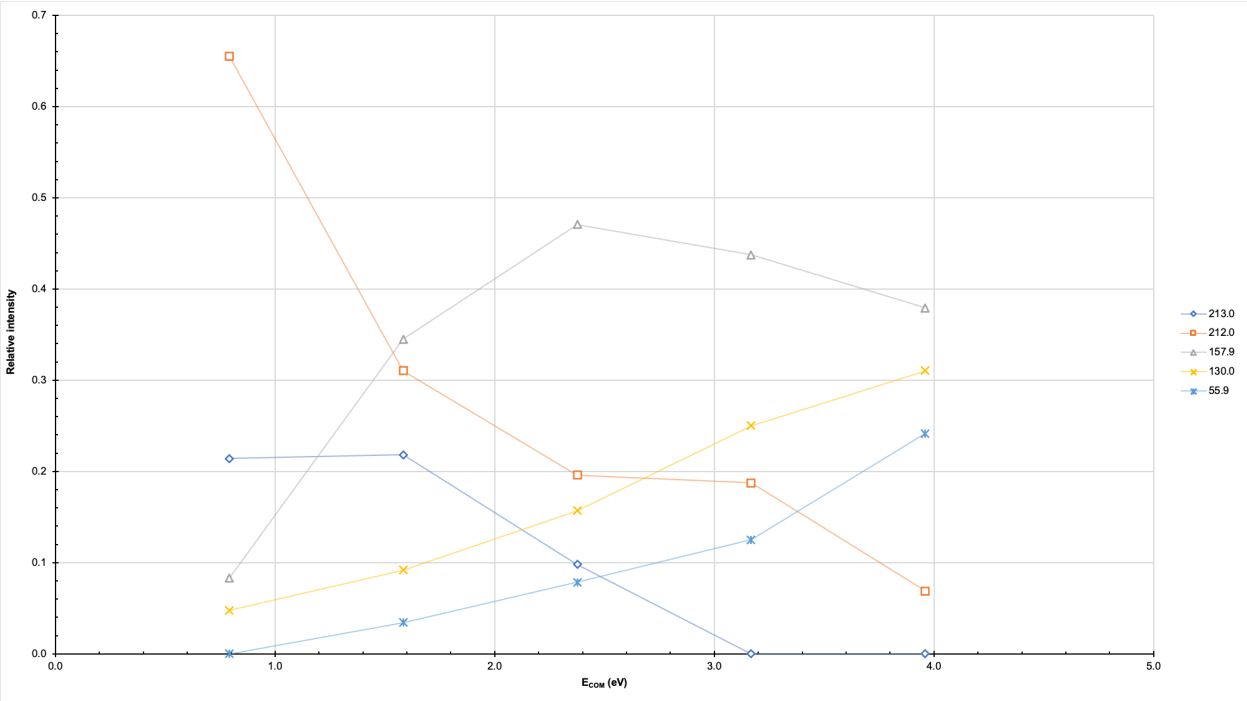

Figure 4.18 Breakdown diagram for the 1:1 complex of Iron (III) Nitrate and 2,2'-Bipyridine ($FeC_{10}H_8N_2^+$) at 212.0 *m/z* in the transfer from 0-25eV, dual-spray.

From Figures 4.17 and 4.18, it can be seen that both experiments provide little to no usable data for the breakdown pathways of the 1:1 complex. There are fragments of interest present within the graphs that confirm the breakdown of the ligand as seen in the Nickel (II) Nitrate experiments. However, with the combination of low relative intensities as well as low collision energies reached within the experiments, the information provided is extremely unreliable. As seen in Chapter 3, there was very little complex formed from each of the overall mass spectra making a collision-induced dissociation experiment very difficult to complete. Even so, fragments to note can be found in Table 4.3. Their potential structures can be found in Figure 4.19.

Table 4.3 Iron (III) Nitrate and 2,2'-Bipyridine fragment mass-to charge values and their possible molecular formulas.

Mass-to-Charge Value	*Possible Molecular Formula*
212.0	$FeC_{10}H_8N_2^+$
197.9	$FeC_{10}H_8N^+$
157.9	$FeC_7H_4N^+$
130.0	$C_9H_8N^+$
72.9	$FeNH_3^+$
55.9	Fe^+

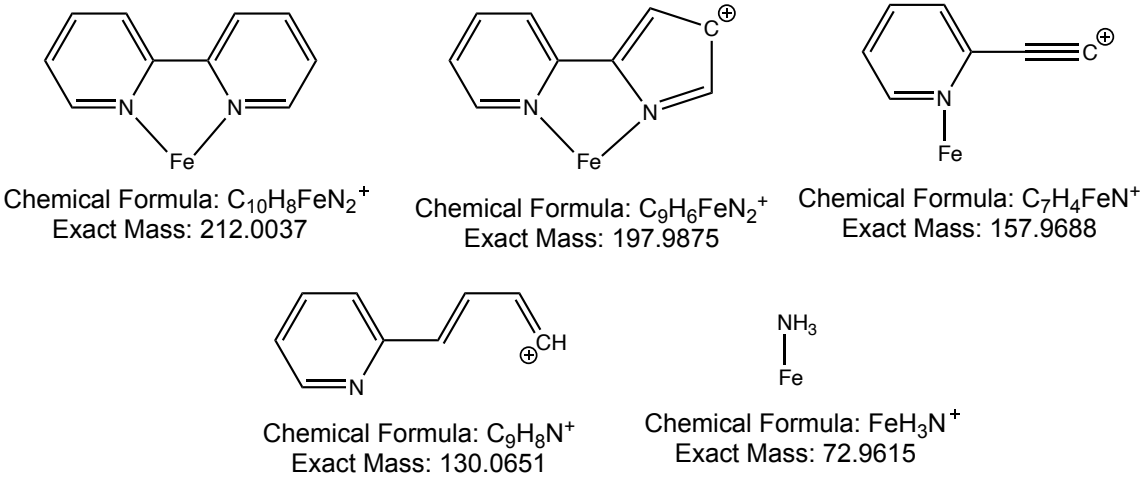

Figure 4.19 Possible skeletal ion fragments formed by collision induced dissociation of Iron (III) Nitrate and 2,2'-Bipyridine.

The following figures depict the single- and dual-spray experiments for the nitrated 1:1 complex.

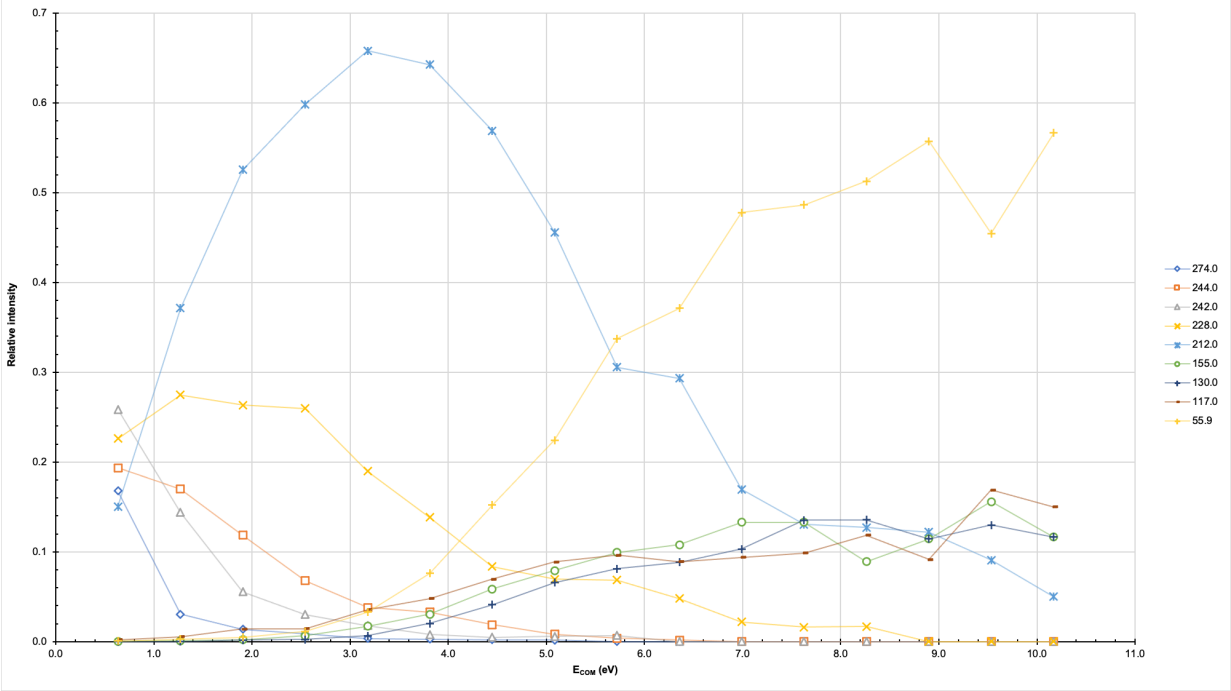

Figure 4.20 Breakdown diagram for the nitrated 1:1 complex of Iron (III) Nitrate and 2,2'-Bipyridine ($FeC_{10}H_8N_2NO_3^+$) at 274.0 *m/z* in the transfer from 0-80eV, single-spray.

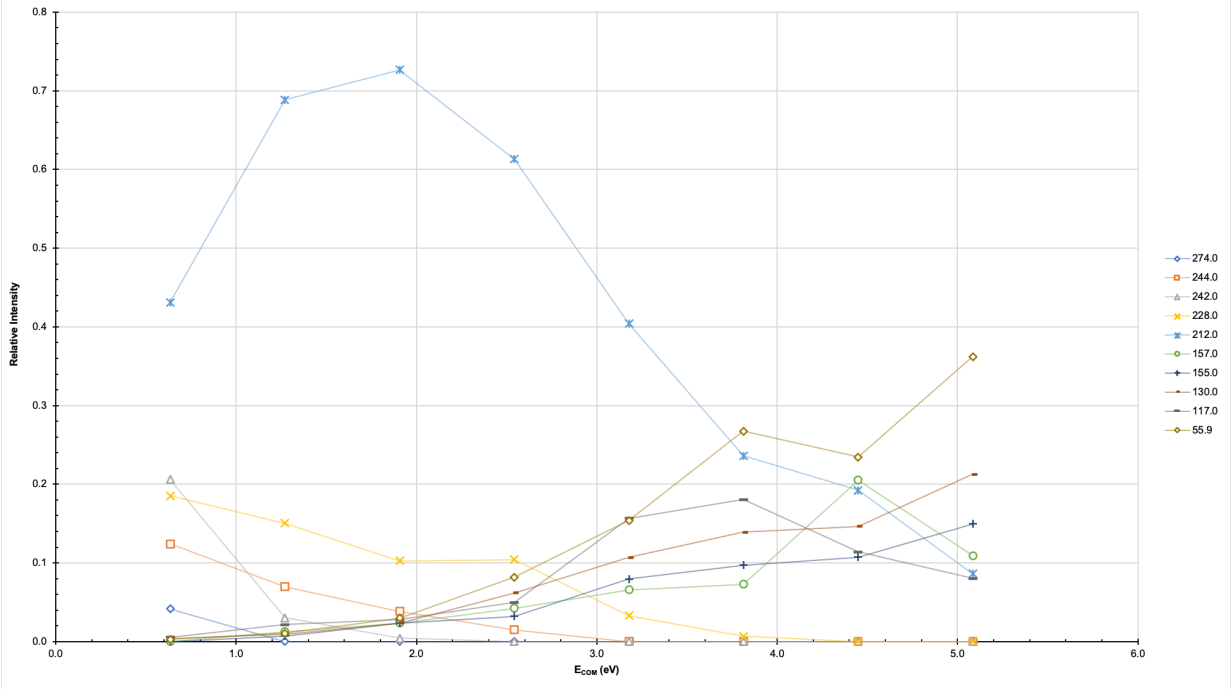

Figure 4.21 Breakdown diagram for the nitrated 1:1 complex of Iron (III) Nitrate and 2,2'-Bipyridine ($FeC_{10}H_8N_2NO_3^+$) at 274.0 *m/z* in the transfer from 0-40eV, dual-spray.

From Figures 4.20 and 4.21, it can be learned that the single-spray experiment was much more effective than the dual-spray although some valid results are observed. The fragments of each breakdown diagram are quite similar to each other as well as those observed in the Nickel (II) Nitrate experiments, attributing them to the breakdown of the ligand itself without the coordination of iron. In both instances, the overall complex at 274.0 *m/z*, the non-nitrated 1:1 complex at 212 *m/z*, as well as the Iron ion at 55.9 *m/z*, are all observed. Fragments to note can be found in Table 4.4. Their potential structures can be found in Figure 4.22.

Table 4.4 Iron (III) Nitrate and 2,2'-Bipyridine fragment mass-to charge values and their possible molecular formulas, continued.

Mass-to-Charge Value	*Possible Molecular Formula*
274.0	$FeC_{10}H_8N_2NO_3^+$
244.0	$FeC_{10}H_8N_2CH_3OH^+$
228.0	$FeC_{10}H_8N_2NH_2^+$
155.0	$C_{10}H_7N_2^+$
117.0	$C_8H_7N^+$

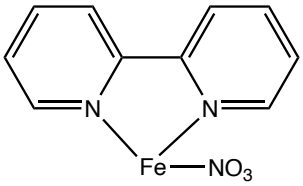

Chemical Formula: $C_{10}H_8FeN_3O_3^+$
Exact Mass: 273.9915

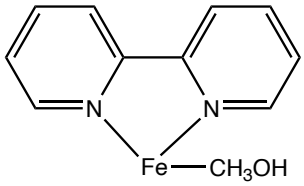

Chemical Formula: $C_{11}H_{12}FeN_2O^+$
Exact Mass: 244.0299

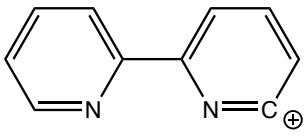

Chemical Formula: $C_{10}H_7N_2^{++}$
Exact Mass: 155.0604

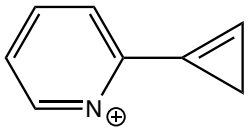

Chemical Formula: $C_8H_7N^+$
Exact Mass: 117.0573

Figure 4.22 Possible skeletal ion fragments formed by collision induced dissociation of Iron (III) Nitrate and 2,2'-Bipyridine, continued.

Next, the 1:2 complex experiment results are displayed in the following figures.

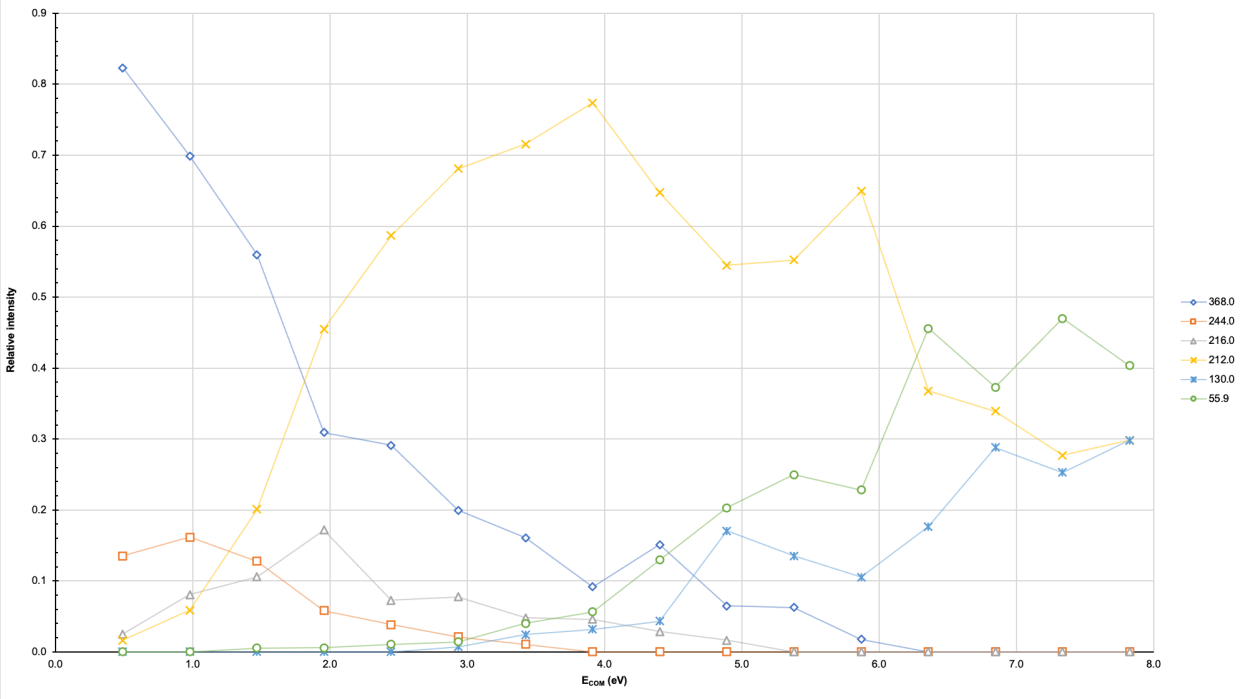

Figure 4.23 Breakdown diagram for the 1:2 complex of Iron (III) Nitrate and 2,2'-Bipyridine ($FeC_{10}H_8N_2C_{10}H_8N_2^+$) at 368.0 *m/z* in the transfer from 0-100eV, single-spray.

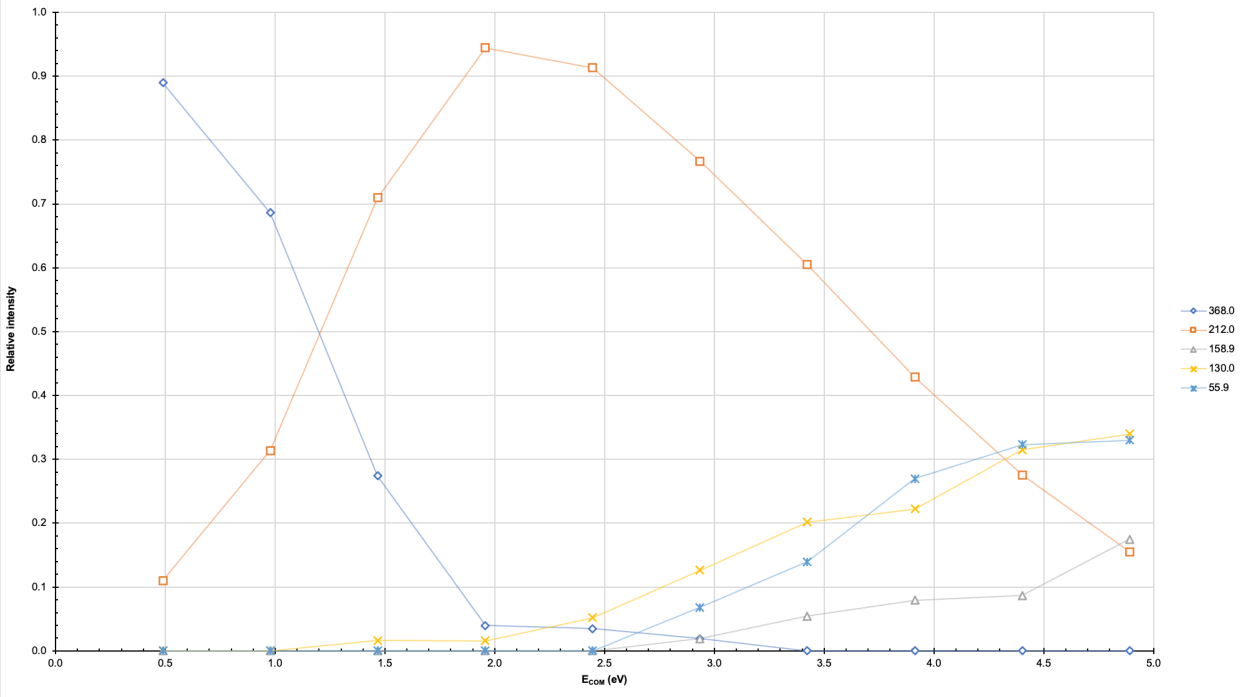

Figure 4.24 Breakdown diagram for the 1:2 complex of Iron (III) Nitrate and 2,2'-Bipyridine ($FeC_{10}H_8N_2C_{10}H_8N_2^+$) at 368.0 *m/z* in the transfer from 0-50eV, dual-spray.

When comparing the results from the single and dual-spray experiments, it is again seen the single-spray was more effective than the dual-spray since much high collision energies were reached. However, the data was not as clean as many of the other breakdown diagrams have been previously. Regardless, the graphs confirm the pathway from the 1:2 complex, to the 1:1 complex, to the iron ion alone. Other fragments of interest are noted in Table 4.5 and their possible structures can be found in Figure 4.25.

Table 4.5 Iron (III) Nitrate and 2,2'-Bipyridine fragment mass-to charge values and their possible molecular formulas, continued.

Mass-to-Charge Value	*Possible Molecular Formula*
368.0	$FeC_{10}H_8N_2C_{10}H_8N_2^+$
158.9	$FeC_7H_5N^+$

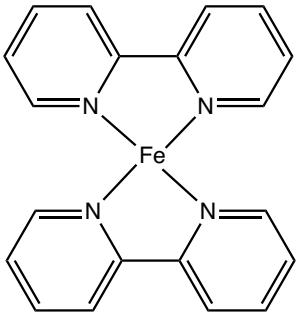

Chemical Formula: $C_{20}H_{16}FeN_4^+$
Exact Mass: 368.0724

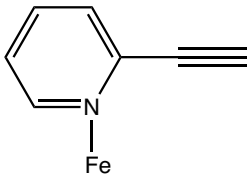

Chemical Formula: $C_7H_5FeN^+$
Exact Mass: 158.9771

Figure 4.25 Possible skeletal ion fragments formed by collision induced dissociation of Iron (III) Nitrate and 2,2'-Bipyridine, continued.

Finally, the following figures display the results of the nitrated 1:2 complex.

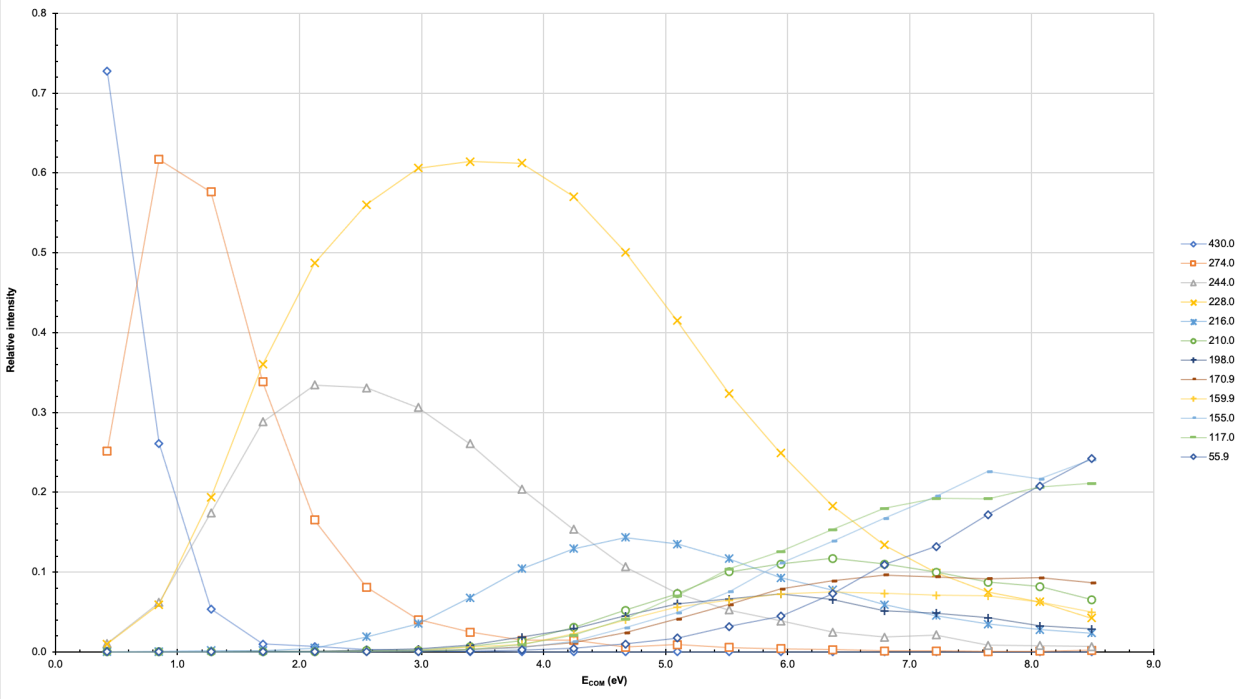

Figure 4.26 Breakdown diagram for the nitrated 1:2 complex of Iron (III) Nitrate and 2,2'-Bipyridine ($FeC_{10}H_8N_2C_{10}H_8N_2NO_3^+$) at 430.0 *m/z* in the transfer from 0-100eV, single-spray.

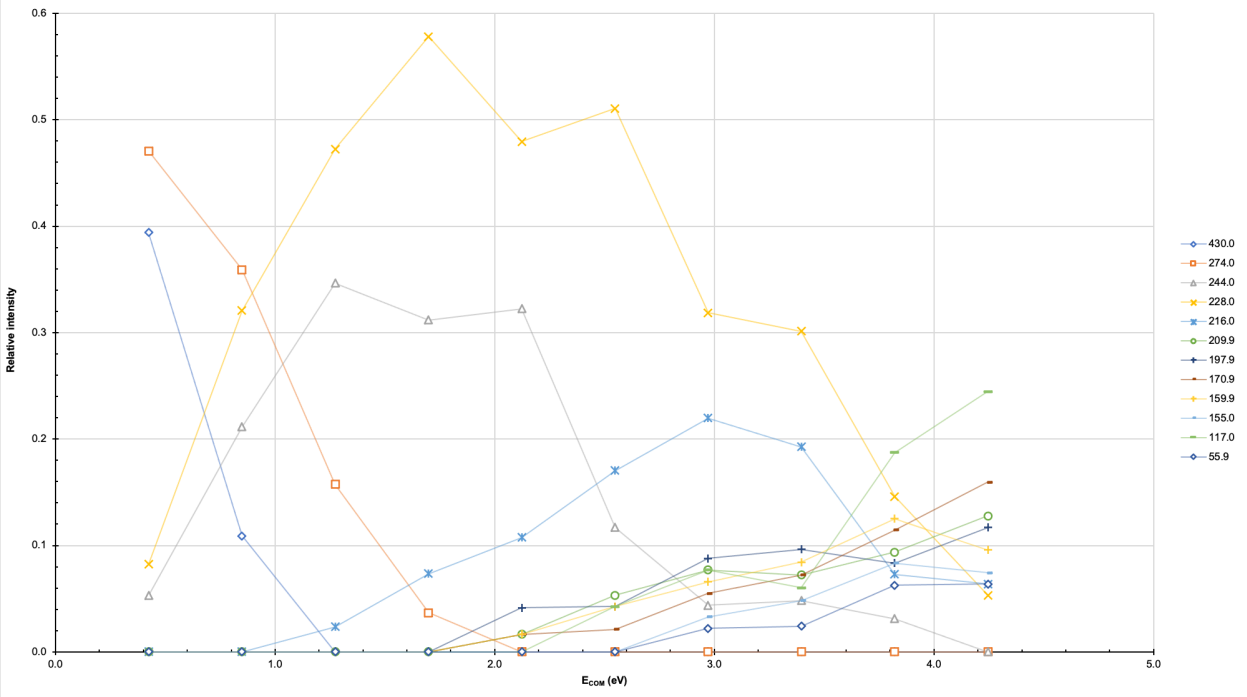

Figure 4.27 Breakdown diagram for the nitrated 1:2 complex of Iron (III) Nitrate and 2,2'-Bipyridine ($FeC_{10}H_8N_2C_{10}H_8N_2NO_3^+$) at 430.0 *m/z* in the transfer from 0-50eV, dual-spray.

It is made clear that the single-spray results are much more clear than that of the dual-spray. Fragments of both the other compounds of interest and many of the expected pieces of the ligand are visible in both breakdown diagrams, as well as the iron ion alone. The nitrated 1:2 complex at 430.0 *m/z* is quickly broken down into the nitrated 1:1 complex at 274.0 *m/z*, closely followed by the fragment at 128.0 *m/z* and then by several smaller ligand fragments and the iron ion at 55.9 *m/z*. The additional structures can be seen in Figure 4.28 below.

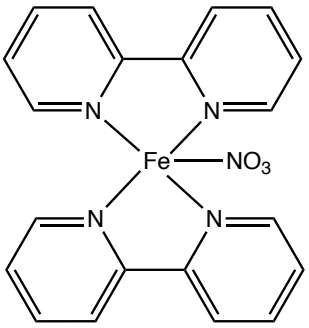

Chemical Formula: $C_{20}H_{16}FeN_5O_3^+$
Exact Mass: 430.0603

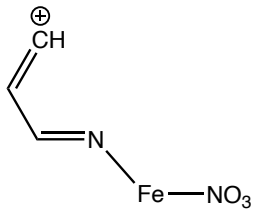

Chemical Formula: $C_3H_3FeN_2O_3^+$
Exact Mass: 170.9488

Figure 4.28 Possible skeletal ions made from the Iron (III) Nitrate and 2,2'-Bipyridine analysis.

In summary, when comparing the trap and transfer cells, experiments performed in the trap were less reliable overall as the fragments created coordinated with water before reaching the detector. When looking at the complexes created with Nickel (II) Nitrate as compared to those created with Iron (III) Nitrate, the nickel complexes were typically more consistent and could tolerate higher collision energies making for more accurate breakdown diagrams. More specifically, the iron complexes created via dual-spray did not withstand collision energies about 50 eV and therefore gave less information and less accuracy. Those created in single-spray created much better graphs as a whole.

This could be due to the fact that the iron complexes needed the full hour to complete their reaction, as established by the mixture, and the mixing in the gaseous phase was not enough time to create ions of interest to undergo further experimentation. However, both the single- and dual-spray experiments of the nickel complexes created very similar results. This establishes that the reaction time is significantly less than that of the iron complexes and the mixing of solutions in the gas phase as they enter the instrument does not negatively affect the outcome of the experiments performed.

4.2 4,4'-Bipyridine

In both the single- and dual-spray methods with the Nickel (II) Nitrate solution, each complex was observed at the same *m/z* ratios as was seen in the 2,2'-Bipyridine combination with the exception of the non-nitrated 1:2 complex that was seen at one mass unit less ($NiC_{10}H_8N_2C_{10}H_7N_2^+$) at 369.0 *m/z*, as previously stated. It is interesting to note that the collision induced dissociation experiment could not be performed on the non-nitrated 1:1 complex ($NiC_{10}H_8N_2^+$) only with the single-spray method. Many attempts to create these ions of interest were tried with unfortunately no success. The dual-spray method however was successful although to a relatively low collision energy.

All single-spray experiments were performed in both the trap and transfer while the dual-spray experiments were solely performed in the transfer for the issues previously discovered with the coordination of water. All results can be found in the following figures, as well as in the appendix. When looking at the fragment ions created from these experiments, most of them are also the same as those found in the previous experiments with the 2,2'-Bipyridine ligand. This is extremely interesting to note as the orientation of the 2,2'-Bipyridine ligand would result in bidentate ligands, having both nitrogen atoms coordinated to the metal. This is just not possible with the orientation of the 4,4'-Bipyridine ligand as it would result in monodentate coordination to the ligands to create ditopic complexes. These orientation results are not clear in the mass spectrum as the results are solely based on mass rather than on structural orientation.

The following table details the major fragments of interest and their likely chemical structures. Not listed are the ions that are likely created due to the addition of water at 18 mass units which include, 387.0, 293.9, 266.9, 232.0, 219.9 and 192.9 *m/z*.

Table 4.6 Nickel (II) Nitrate and 4,4'-Bipyridine fragment mass-to charge values and their possible molecular formulas.

Mass-to-Charge Value	*Possible Molecular Formula*
432.0*	$NiC_{10}H_8N_2C_{10}H_8N_2NO_3^+$
369.0*	$NiC_{10}H_8N_2C_{10}H_7N_2^+$
275.9*	$NiC_{10}H_8N_2NO_3^+$
229.9*	$NiC_6H_{10}N_2NO_3^+$
202.0*	$NiC_4H_6N_2NO_3^+$
214.0*	$NiC_{10}H_8N_2^+$
186.9*	$NiC_9H_7N_2^+$
174.9	$NiC_8H_7NNO_3^+$
155.0	$C_{10}H_7N_2^+$
144.0	$C_9H_8N_2^+$
130.0	$C_9H_8N^+$
117.0	$C_8H_7N_2^+$
89.0	$CHNNO_3^+$
77.9	$C_5H_4N^+$
57.9*	Ni^+

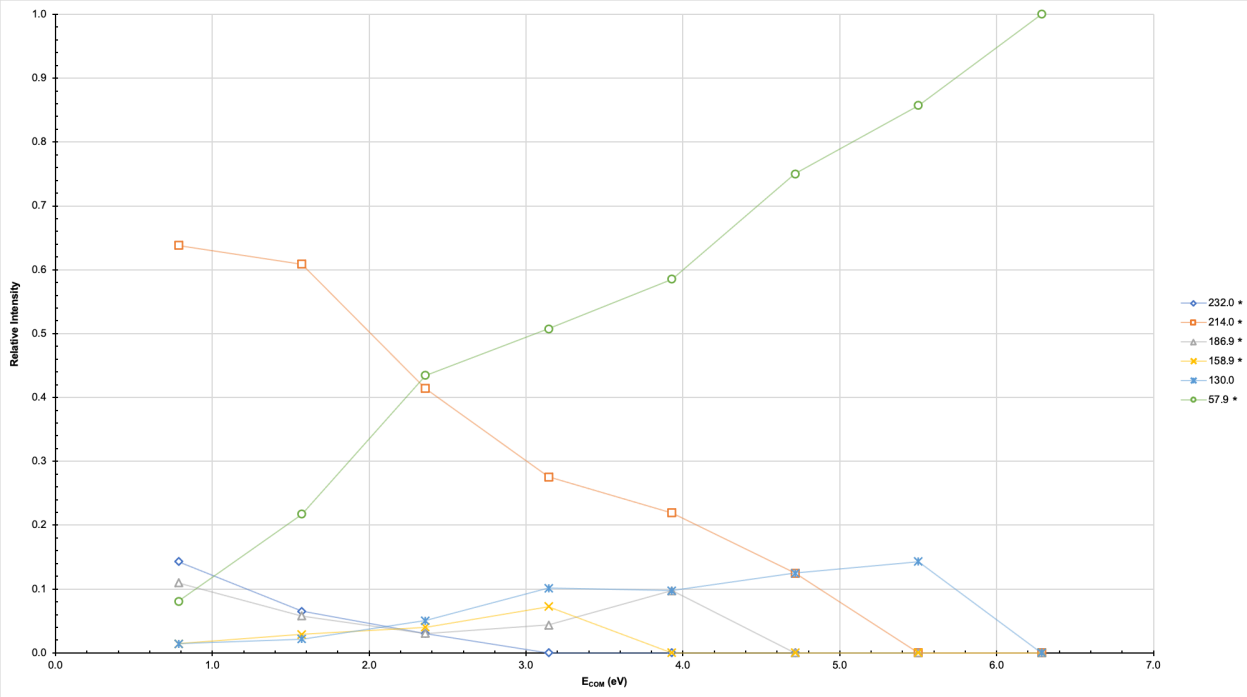

Figure 4.29 Breakdown diagram for the 1:1 complex of Nickel (II) Nitrate and 4,4'-Bipyridine ($NiC_{10}H_8N_2^+$) at 214.0 *m/z* in the transfer from 0-40eV, dual-spray.

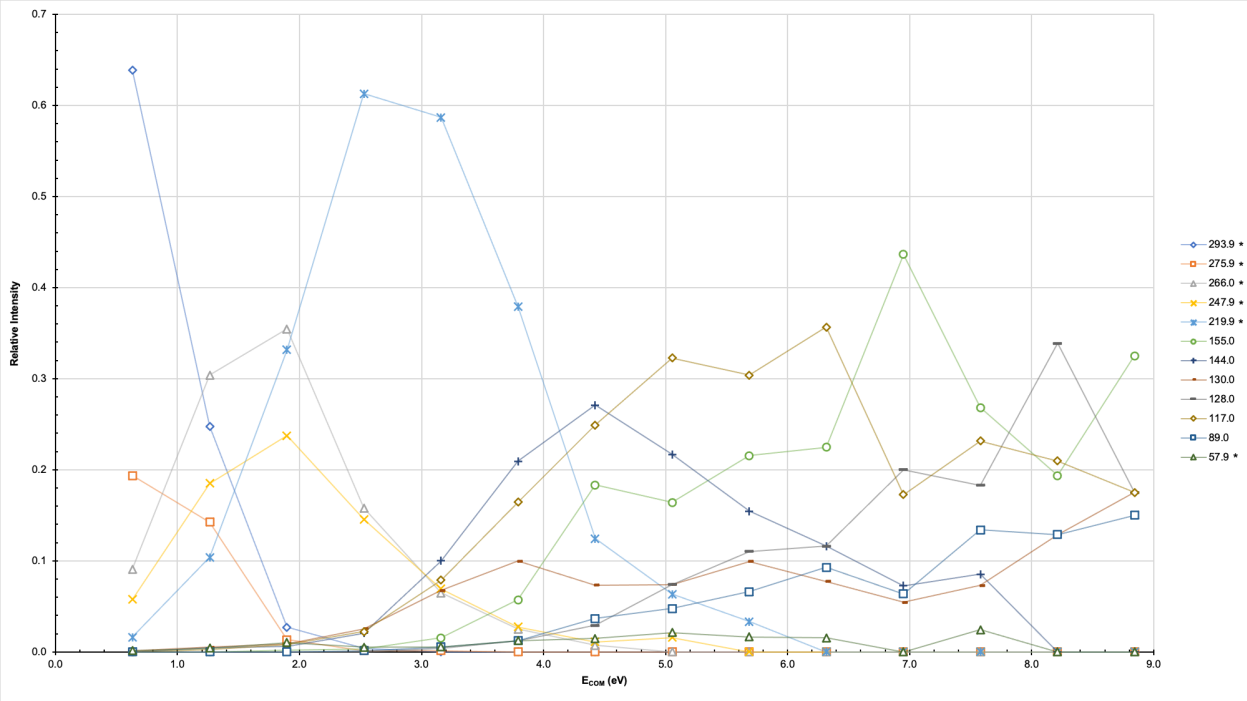

Figure 4.30 Breakdown diagram for the nitrated 1:1 complex of Nickel (II) Nitrate and 4,4'-Bipyridine ($NiC_{10}H_8N_2NO_3^+$) at 275.9 *m/z* in the trap from 0-70eV, single-spray.

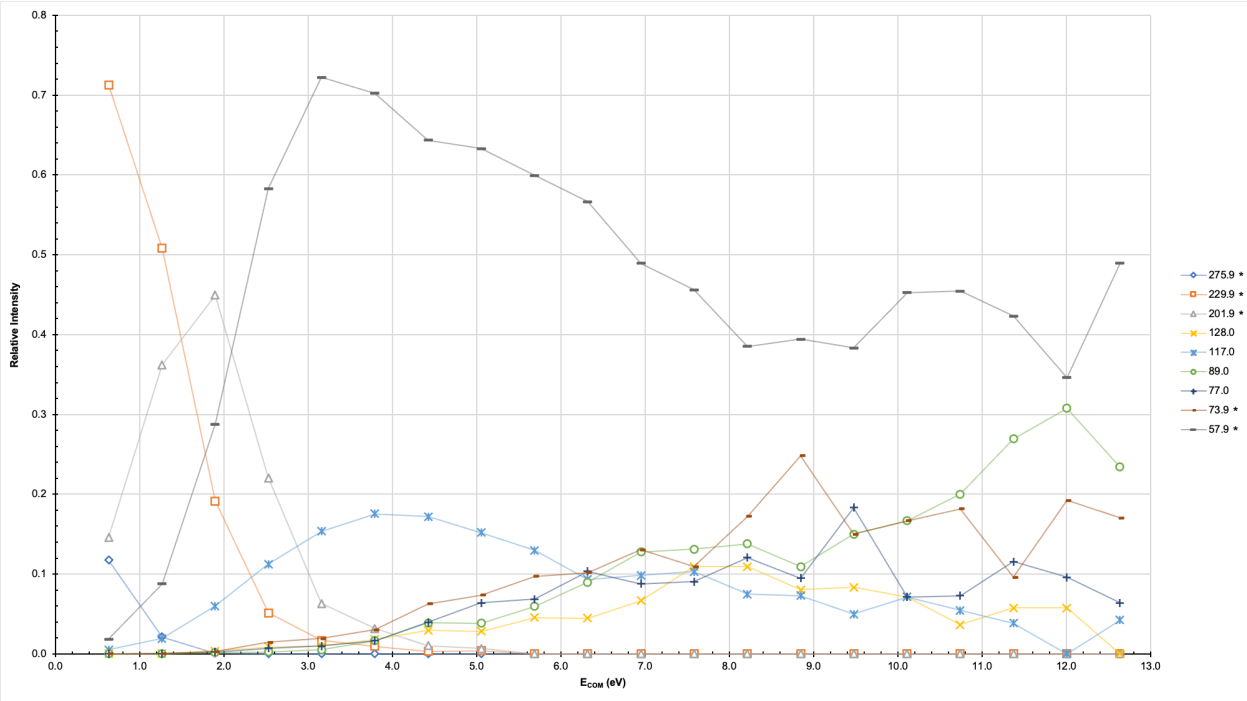

Figure 4.31 Breakdown diagram for the nitrated 1:1 complex of Nickel (II) Nitrate and 4,4'-Bipyridine ($NiC_{10}H_8N_2NO_3^+$) at 275.9 *m/z* in the transfer from 0-100eV, single-spray.

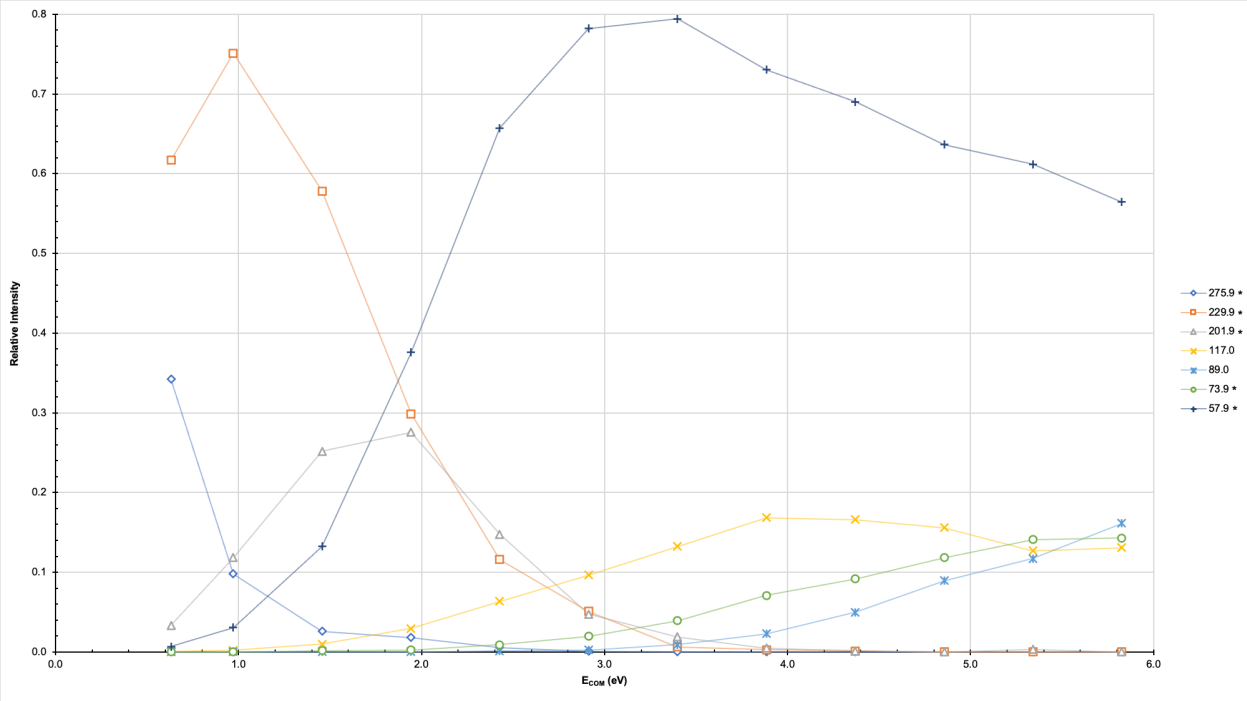

Figure 4.32 Breakdown diagram for the nitrated 1:1 complex of Nickel (II) Nitrate and 4,4'-Bipyridine ($NiC_{10}H_8N_2NO_3^+$) at 275.9 *m/z* in the transfer from 0-60eV, dual-spray.

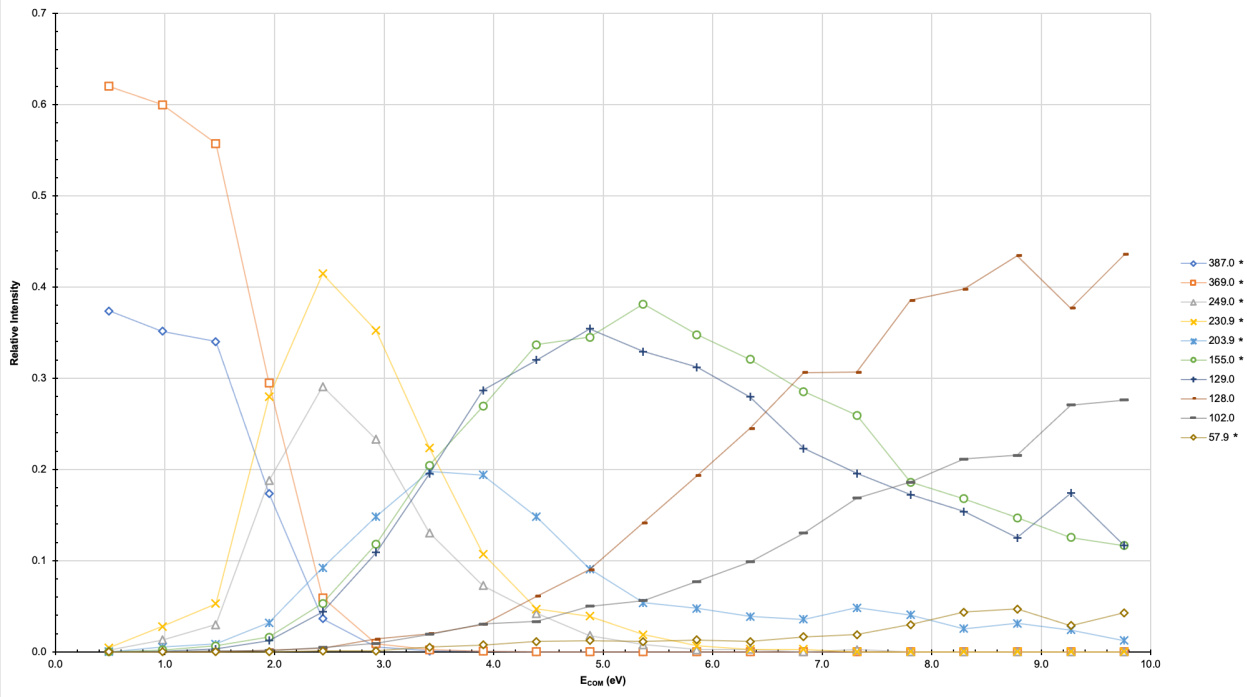

Figure 4.33 Breakdown diagram for the 1:2 complex of Nickel (II) Nitrate and 4,4'-Bipyridine ($NiC_{10}H_8N_2C_{10}H_7N_2^+$) at 369.0 *m/z* in the trap from 0-100eV, single-spray.

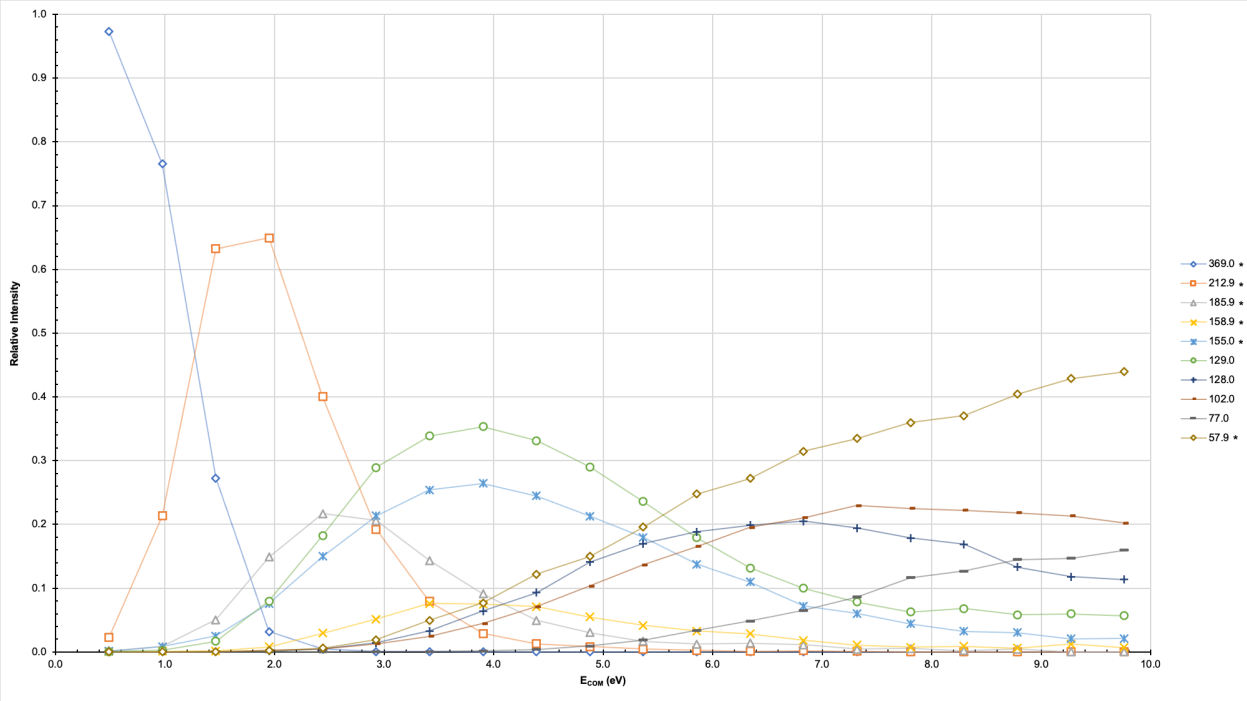

Figure 4.34 Breakdown diagram for the 1:2 complex of Nickel (II) Nitrate and 4,4'-Bipyridine ($NiC_{10}H_8N_2C_{10}H_7N_2^+$) at 369.0 *m/z* in the transfer from 0-100eV, single-spray.

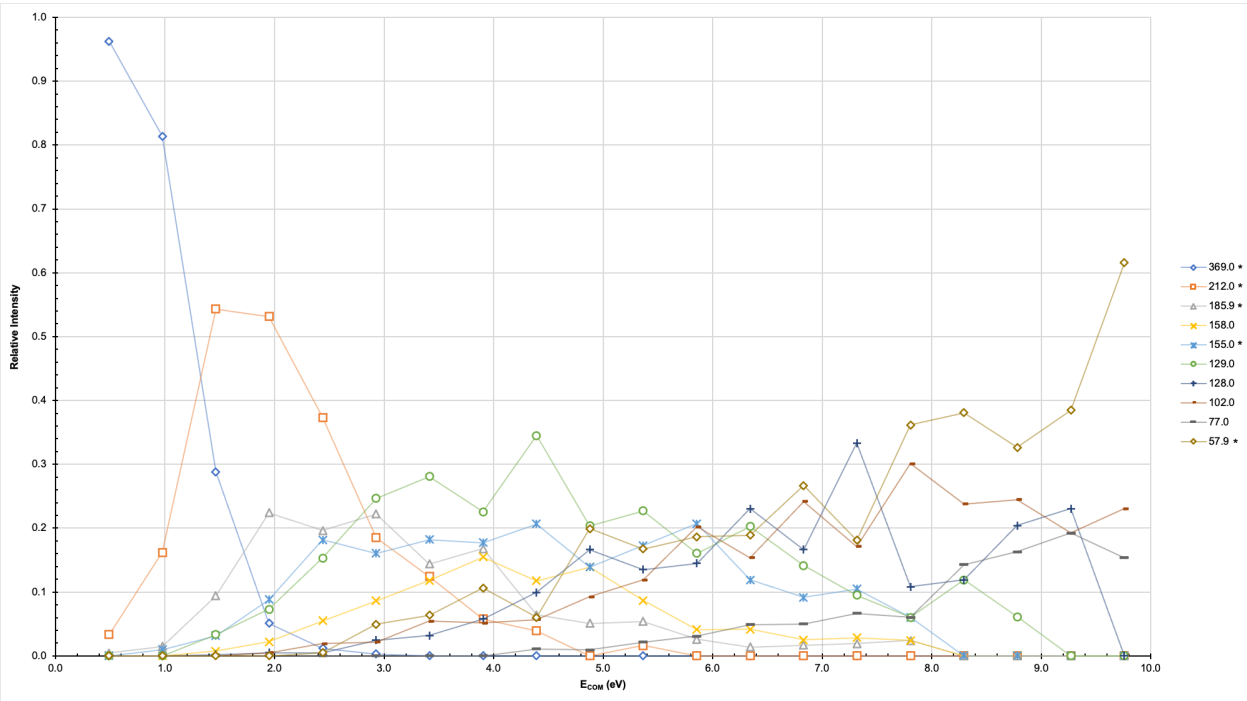

Figure 4.35 Breakdown diagram for the 1:2 complex of Nickel (II) Nitrate and 4,4'-Bipyridine ($NiC_{10}H_8N_2C_{10}H_7N_2^+$) at 369.0 *m/z* in the transfer from 0-100eV, dual-spray.

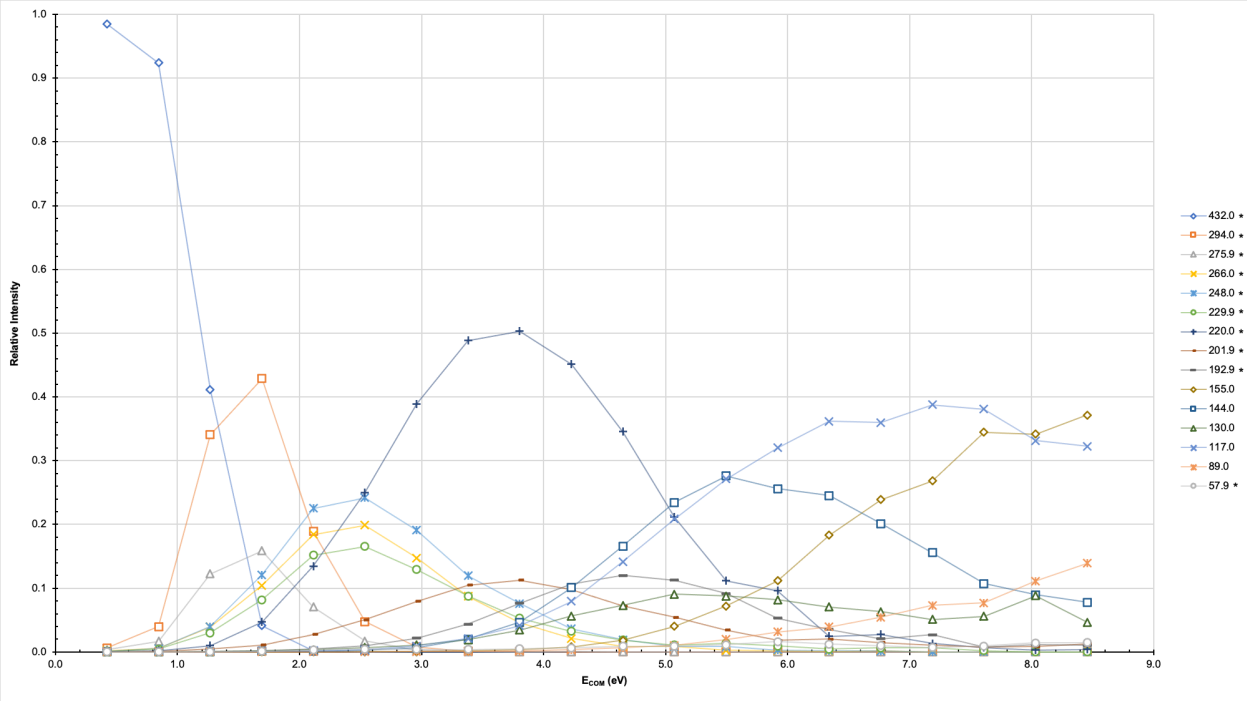

Figure 4.36 Breakdown diagram for the nitrated 1:2 complex of Nickel (II) Nitrate and 4,4'-Bipyridine ($NiC_{10}H_8N_2C_{10}H_8N_2NO_3^+$) at 432.0 *m/z* in the trap from 0-100eV, single-spray.

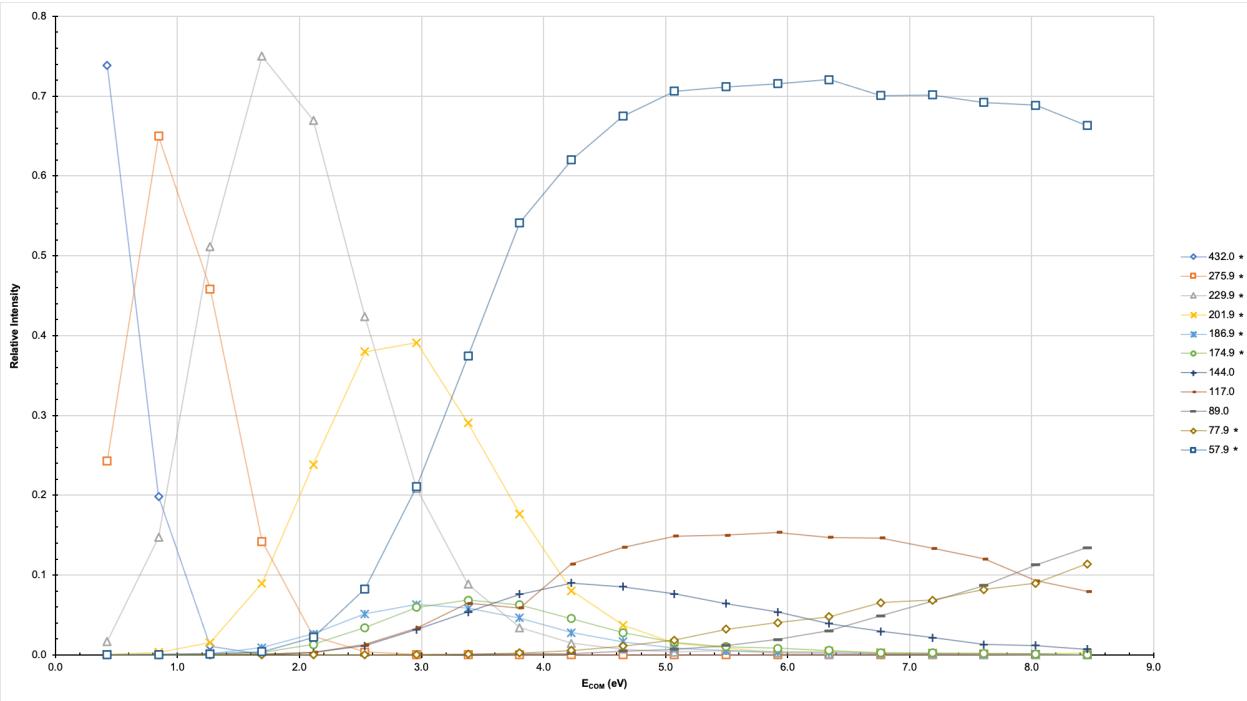

Figure 4.37 Breakdown diagram for the nitrated 1:2 complex of Nickel (II) Nitrate and 4,4'-Bipyridine ($NiC_{10}H_8N_2C_{10}H_8N_2NO_3^+$) at 432.0 *m/z* in the transfer from 0-100eV, single-spray.

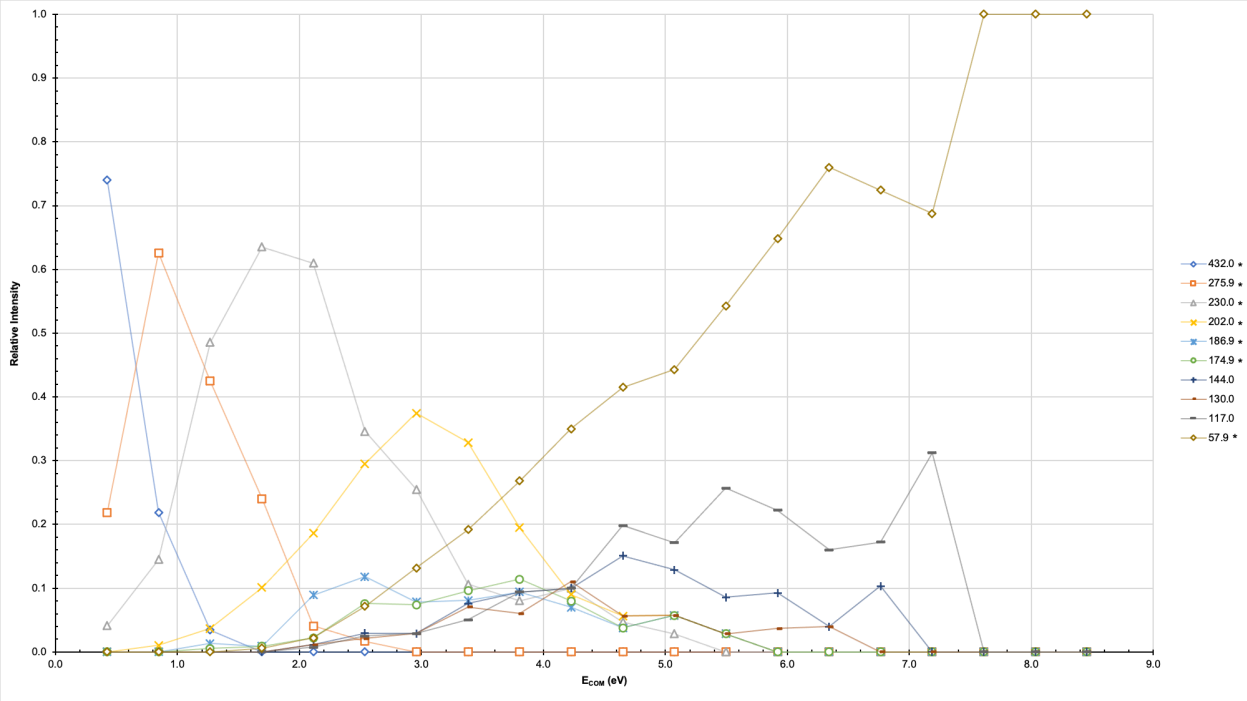

Figure 4.38 Breakdown diagram for the nitrated 1:2 complex of Nickel (II) Nitrate and 4,4'-Bipyridine ($NiC_{10}H_8N_2C_{10}H_8N_2NO_3^+$) at 432.0 *m/z* in the transfer from 0-100eV, dual-spray.

In both the single- and dual-spray methods with the Iron (III) Nitrate solution, each complex was observed at the same *m/z* ratios as was seen in the 2,2'-Bipyridine combination. Again, the collision induced dissociation experiment could not be performed on the non-nitrated 1:1 complex only with the single-spray method. However, some success to a relatively low collision energy was possible with the dual-spray method.

Most of the fragment ions were again similar to those found in the previous experiments with the 2,2'-Bipyridine ligand. All experiments were solely performed in both the transfer. All results can be found in the following figures, as well as in the appendix. The following table details the major fragments of interest and their likely chemical structures.

Table 4.7 Iron (III) Nitrate and 4,4'-Bipyridine fragment mass-to charge values and their possible molecular formulas.

Mass-to-Charge Value	*Possible Molecular Formula*
430.0	$FeC_{10}H_8N_2C_{10}H_8N_2NO_3^+$
368.0	$FeC_{10}H_8N_2C_{10}H_8N_2^+$
274.0	$FeC_{10}H_8N_2NO_3^+$
244.0	$FeC_{10}H_8N_2NO_3^+$
242.0	$FeC_{10}H_8N_2NO_3^+$
228.0	$FeC_{10}H_8N_2NH_2^+$
212.0	$FeC_{10}H_8N_2^+$
157.9	$FeC_7H_4N^+$
144.0	$C_9H_8N_2^+$
130.0	$C_9H_8N^+$
72.9	$FeNH_{3^+}$
55.9	Fe^+

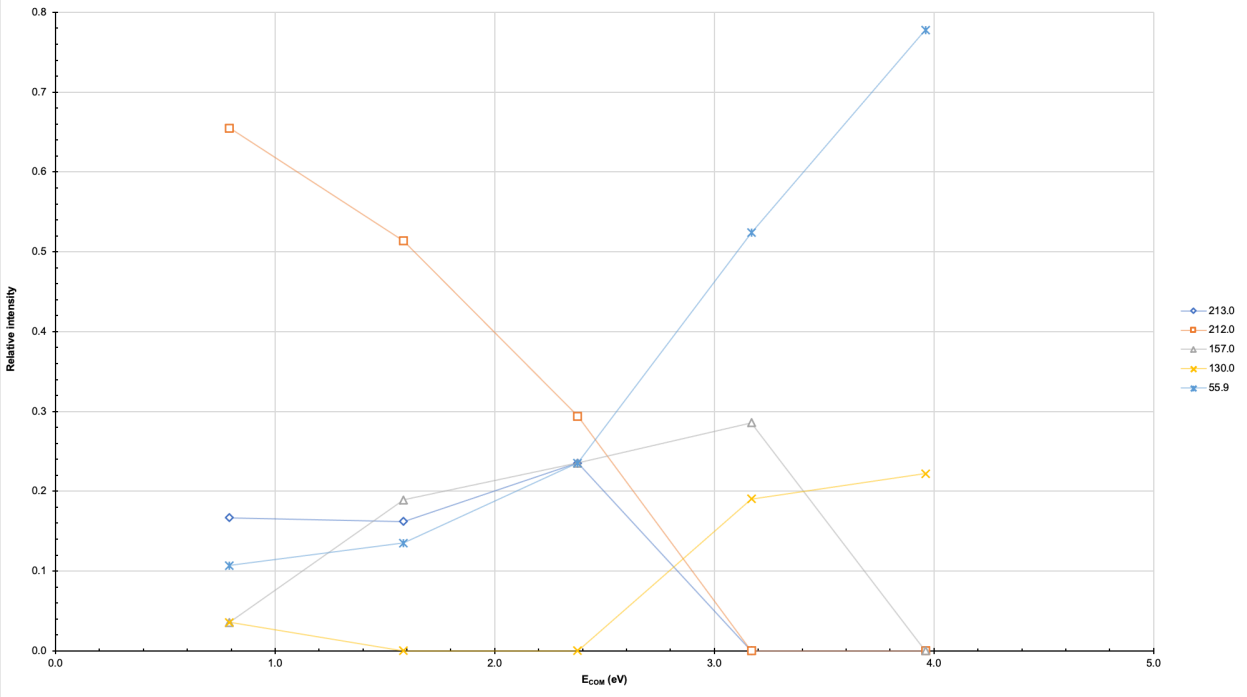

Figure 4.39 Breakdown diagram for the 1:1 complex of Iron (III) Nitrate and 4,4'-Bipyridine ($FeC_{10}H_8N_2^+$) at 211.9 *m/z* in the transfer from 0-25eV, dual-spray.

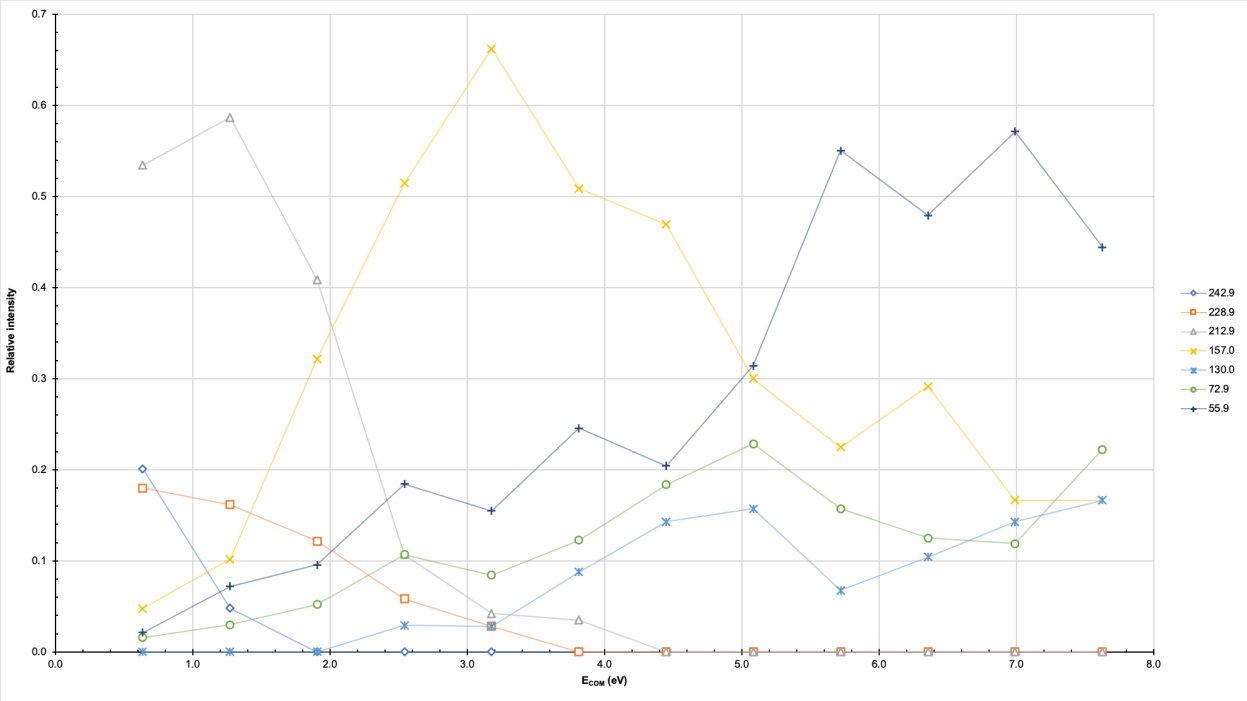

Figure 4.40 Breakdown diagram for the nitrated 1:1 complex of Iron (III) Nitrate and 4,4'-Bipyridine ($FeC_{10}H_8N_2NO_3^+$) at 274.0 *m/z* in the transfer from 0-60eV, single-spray.

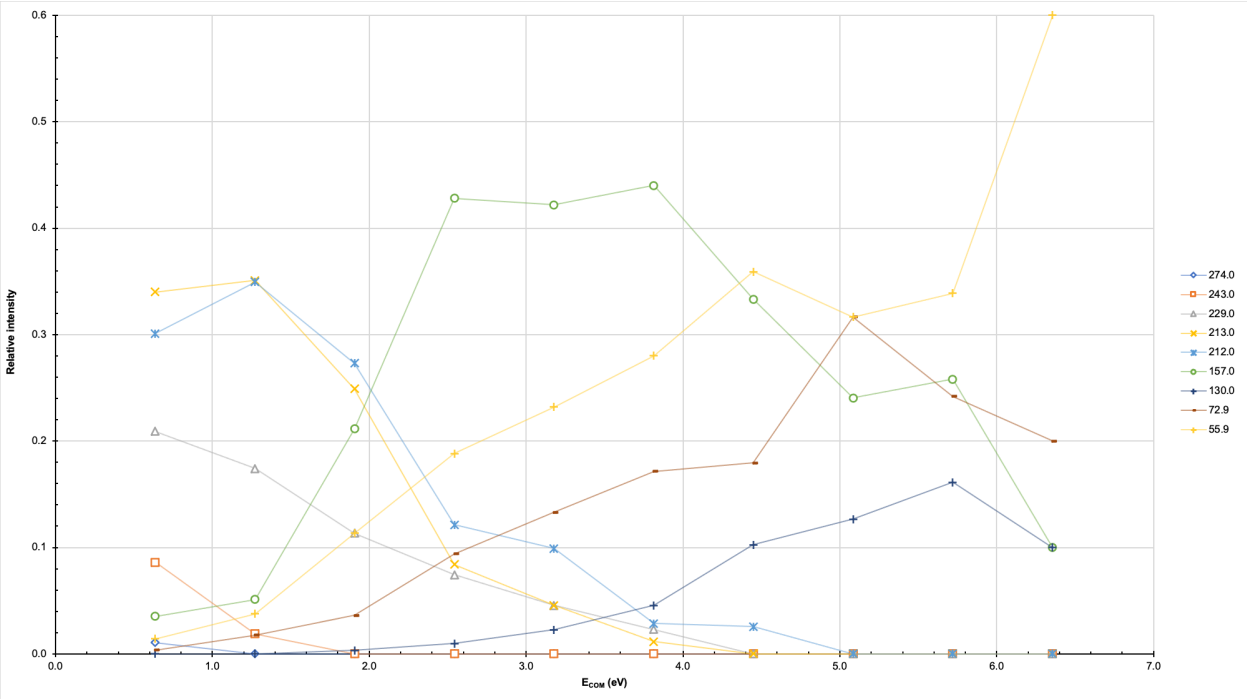

Figure 4.41 Breakdown diagram for the nitrated 1:1 complex of Iron (III) Nitrate and 4,4'-Bipyridine ($FeC_{10}H_8N_2NO_3^+$) at 274.0 *m/z* in the transfer from 0-50eV, dual-spray.

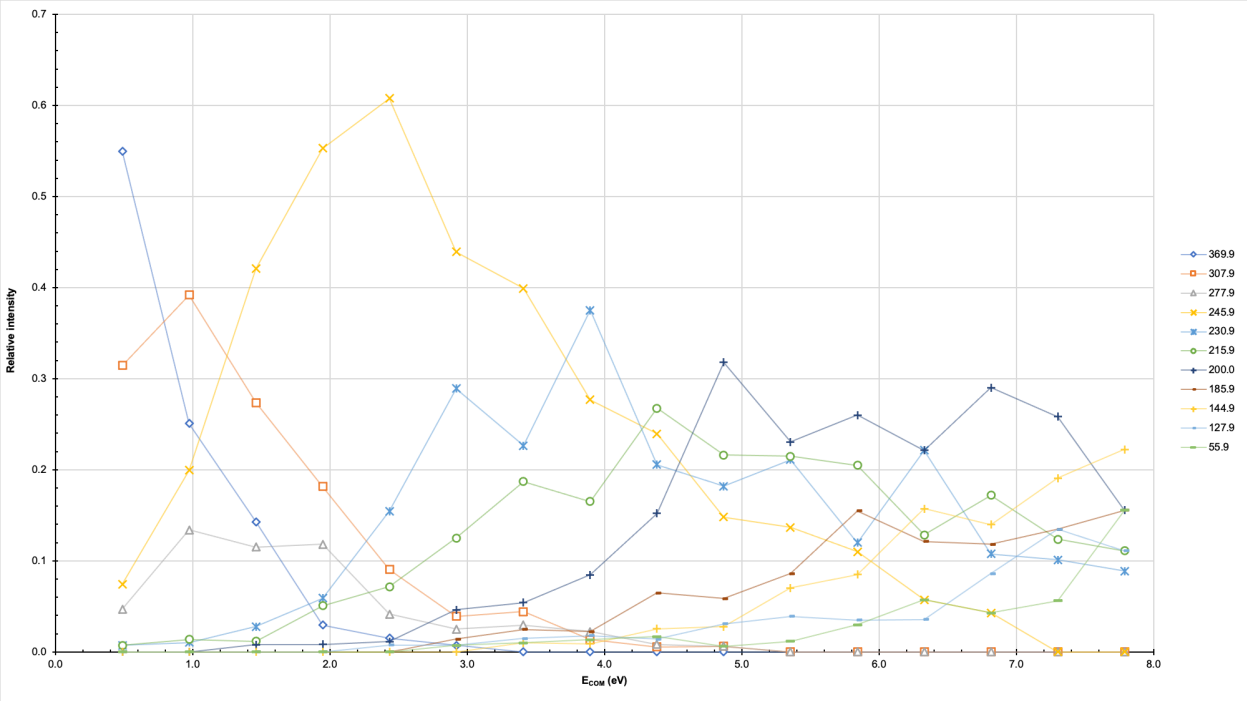

Figure 4.42 Breakdown diagram for the 1:2 complex of Iron (III) Nitrate and 4,4'-Bipyridine ($FeC_{10}H_8N_2C_{10}H_7N_2^+$) at 369.9 *m/z* in the transfer from 0-80eV, single-spray.

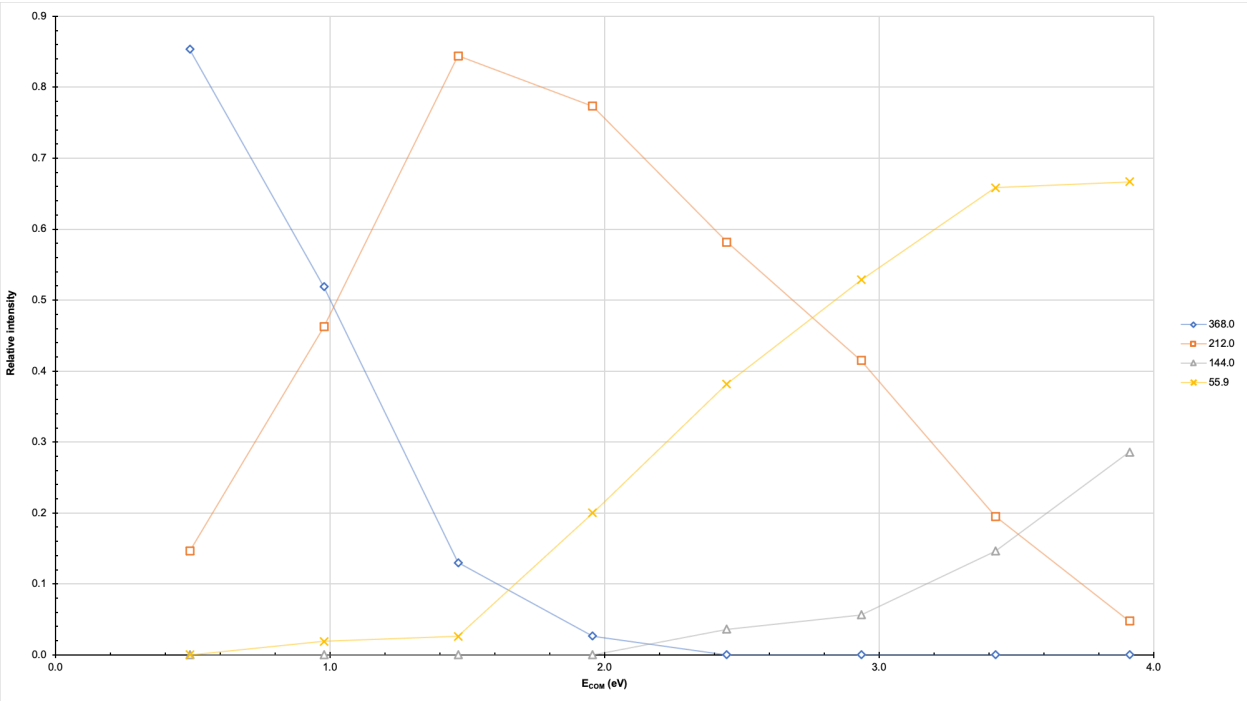

Figure 4.43 Breakdown diagram for the 1:2 complex of Iron (III) Nitrate and 4,4'-Bipyridine ($FeC_{10}H_8N_2C_{10}H_7N_2^+$) at 368.0 *m/z* in the transfer from 0-40eV, dual-spray.

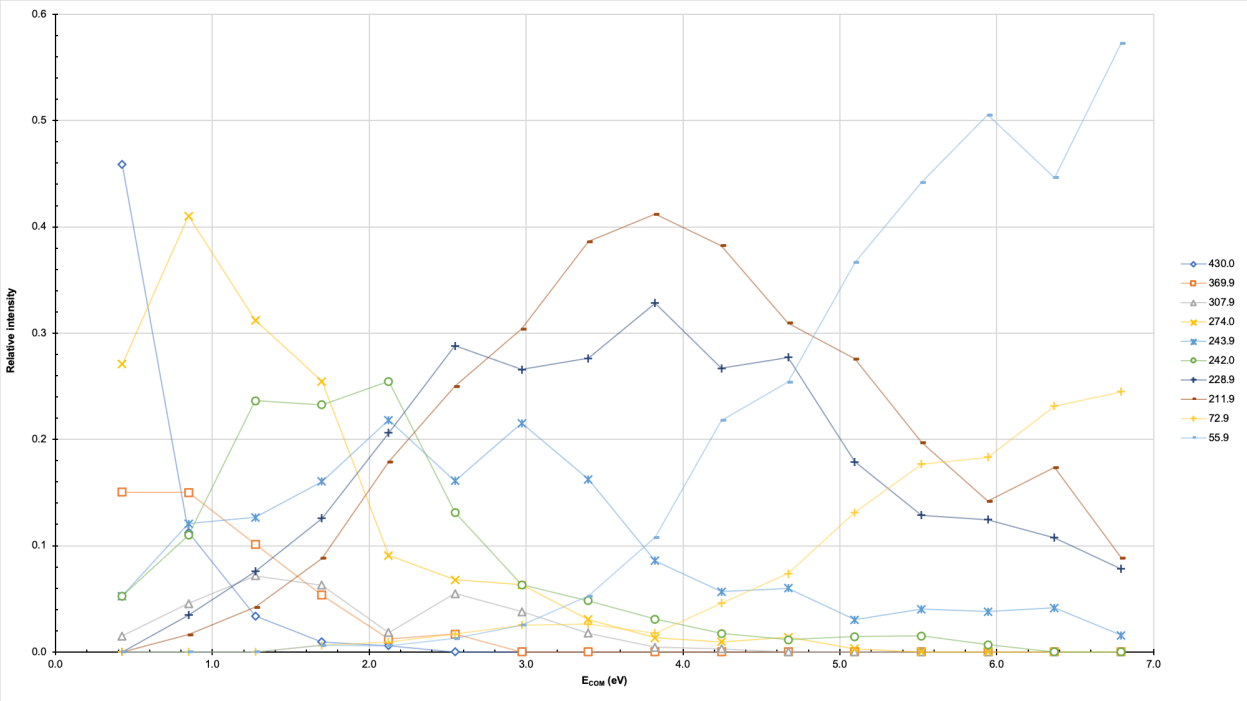

Figure 4.44 Breakdown diagram for the nitrated 1:2 complex of Iron (III) Nitrate and 4,4'-Bipyridine ($FeC_{10}H_8N_2C_{10}H_8N_2NO_3^+$) at 430.0 *m/z* in the transfer from 0-80eV, single-spray.

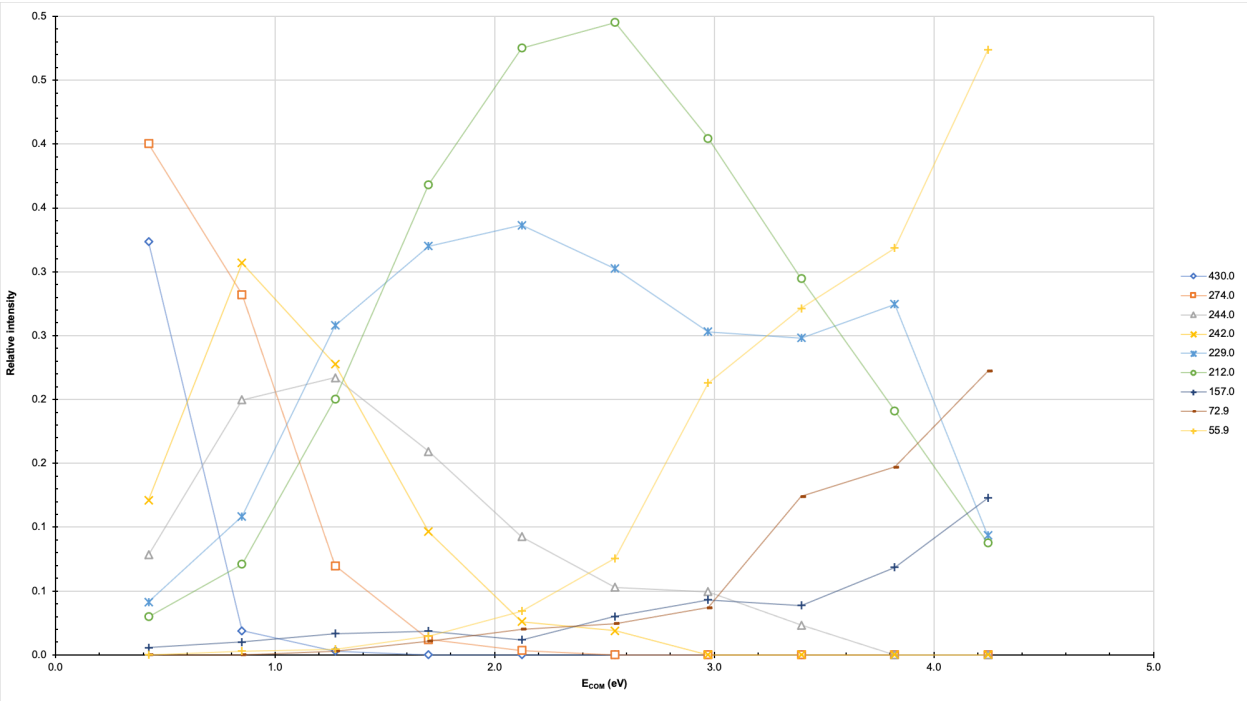

Figure 4.45 Breakdown diagram for the nitrated 1:2 complex of Iron (III) Nitrate and 4,4'-Bipyridine ($FeC_{10}H_8N_2C_{10}H_8N_2NO_3^+$) at 430.0 *m/z* in the transfer from 0-50eV, dual-spray.

In summary, as was the same with the 2,2'-Bipyridine ligand, experiments performed in the trap were less reliable due to the coordination with water before reaching the detector. Similarly, the level of collision energy reached in each experiment was significantly higher with Nickel (II) Nitrate combination over the Iron (III) Nitrate combinations. The data collected from the nickel experiments was also much clearer and more consistent than that of the iron. Again, the iron dual-spray experiments did not tolerate collision energies about 50 eV. The iron single-spray experiments were better but were still noisy and not very accurate. The inconstancies are likely related to the stability of the compound as well as its inability to react in the gas phase. The combination needed time to react but quickly deteriorated in solution. Therefore, the nickel solution was definitely a more successful and stable combination overall, specifically in the single-spray mixture as opposed to the dual-spray method.

4.3 2,2'-Bipyridine-4,4'-Dicarboxylic Acid

In the single-spray (mixture) method with the Nickel (II) Nitrate solution, the 1:1 metal: ligand complex, $NiC_{12}H_8N_2O_4^+$, was observed at 301.9 and 303.9 *m/z*. The nitrated 1:1 complex, $NiC_{12}H_8N_2O_4NO_3^+$, was observed at 363.9 and 365.9 *m/z*. The 1:2 complex, $NiC_{12}H_8N_2O_4C_{12}H_8N_2O_4^+$, was observed at 544.9 and 546.9 *m/z*. Finally, the nitrated 1:2 complex, $NiC_{12}H_8N_2O_4C_{12}H_8N_2O_4NO_3^+$, was observed at 607.9 and 609.9 *m/z*. All results can be found in the following figures. As learned from Chapter 3, the dual-spray method for this combination was unsuccessful. An attempt was made on the 1:1 complex but two mass units less than expected and can be seen in Figure 4.47.

Many of the fragment ions created were the same as those found in the other two bipyridine ligands. This is likely due to the fact that the carboxylic acid groups break from the main ligand fairly easily as seen in the spectrum of 2,2'-Bipyridine-4,4'-Dicarboxylic Acid alone. The following table details the major fragments of interest and their likely chemical structures. All results can be found in the following figures, as well as in the appendix.

Table 4.8 Nickel (II) Nitrate and 2,2'-Bipyridine-4,4'-Dicarboxylic Acid fragment mass-to charge values and their possible molecular formulas.

Mass-to-Charge Value	*Possible Molecular Formula*
607.9*	$NiC_{12}H_8N_2O_4C_{12}H_8N_2O_4NO_3^+$
544.9*	$NiC_{12}H_8N_2O_4C_{12}H_7N_2O_4^+$
501.0*	$NiC_{12}H_8N_2O_4C_{11}H_7N_2O_2^+$
363.9*	$NiC_{12}H_8N_2O_4NO_3^+$
333.9*	$NiC_{12}H_8N_2O_4CH_3OH^+$
319.9*	$NiC_{12}H_8N_2O_4H_2O^+$
301.9*	$NiC_{12}H_8N_2O_4^+$
201.0*	$NiC_4H_5N_2NO_3^+$
178.9*	$NiC_7H_5N_2H_2O^+$
144.0	$C_9H_8N_2^+$
128.0	$C_9H_6N^+$
116.0	$C_8H_6N_2^+$
95.9	$C_5H_8N_2^+$
78.0	$C_5H_4N^+$
57.9*	Ni^+

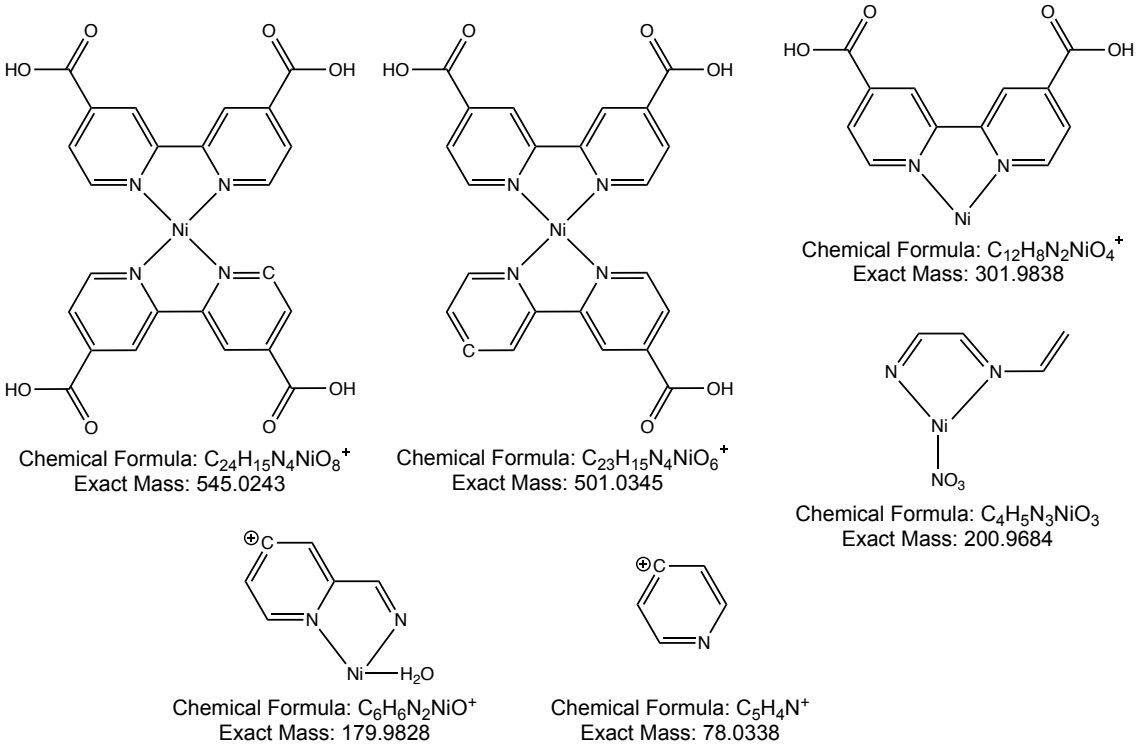

Figure 4.46 Some possible skeletal ion fragments made from the Nickel (II) Nitrate and 2,2'-Bipyridine-4,4'-Dicarboxylic Acid analysis.

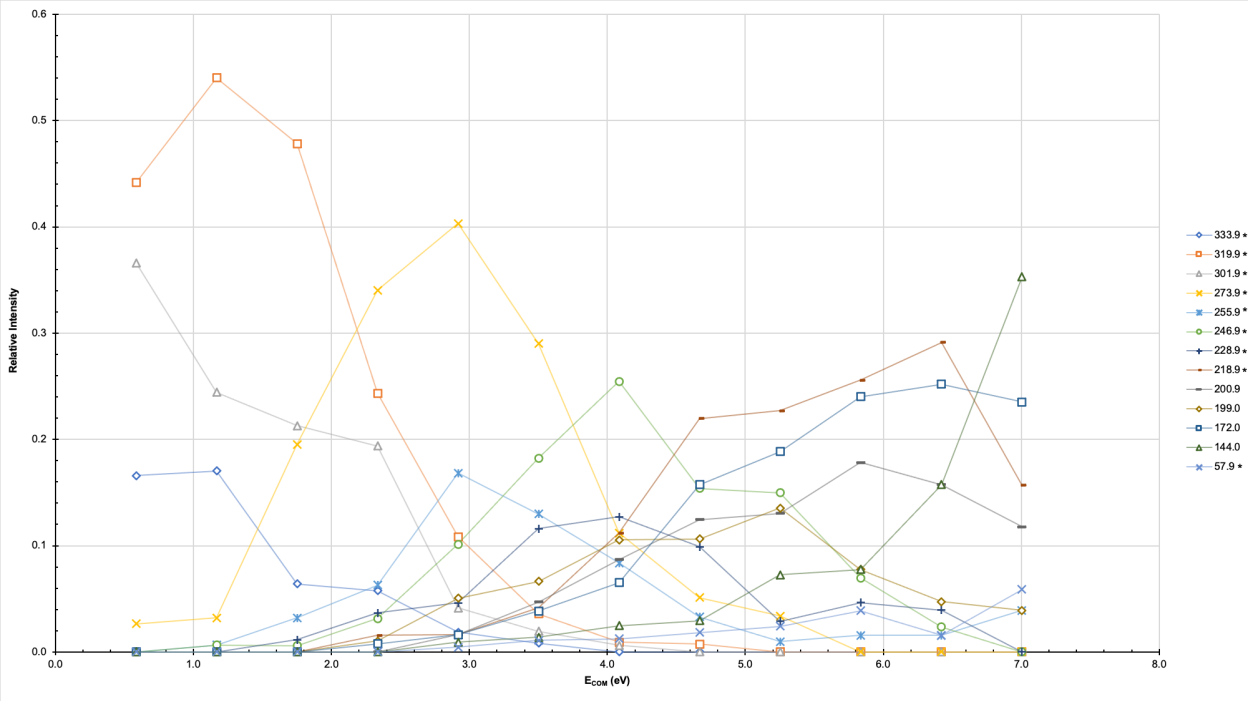

Figure 4.47 Breakdown diagram for the 1:1 complex of Nickel (II) Nitrate and 2,2'-Bipyridine-4,4'-Dicarboxylic Acid ($NiC_{12}H_8N_2O_4^+$) at 301.9 *m/z* in the trap from 0-60eV, single-spray.

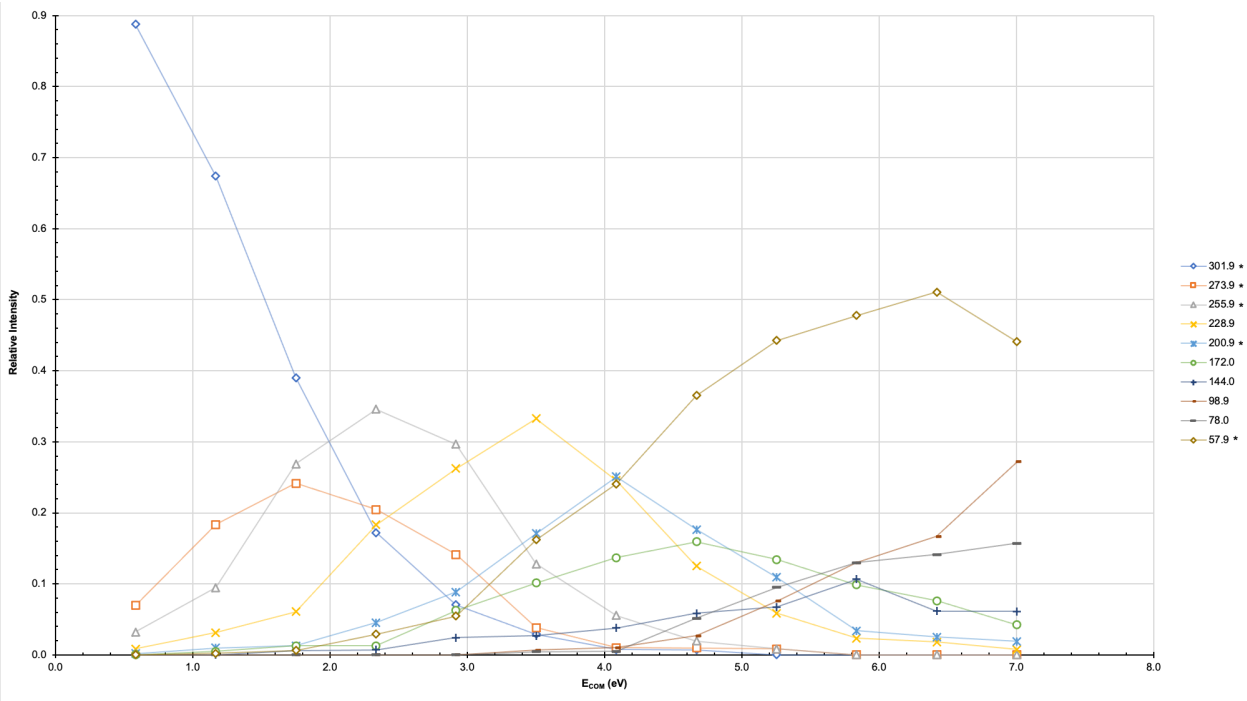

Figure 4.48 Breakdown diagram for the 1:1 complex of Nickel (II) Nitrate and 2,2'-Bipyridine-4,4'-Dicarboxylic Acid ($NiC_{12}H_8N_2O_4^+$) at 301.9 *m/z* in the transfer from 0-60eV, single-spray.

The figure below is the only collision induced dissociation performed on the dual-spray method of this combination. Very low collision energies were achieved on an ion that was two mass units less than the expected target ion. Many of the fragments formed also appear two mass units less than in other experiments. However, the Nickel ion is still visible at 57.9 *m/z*.

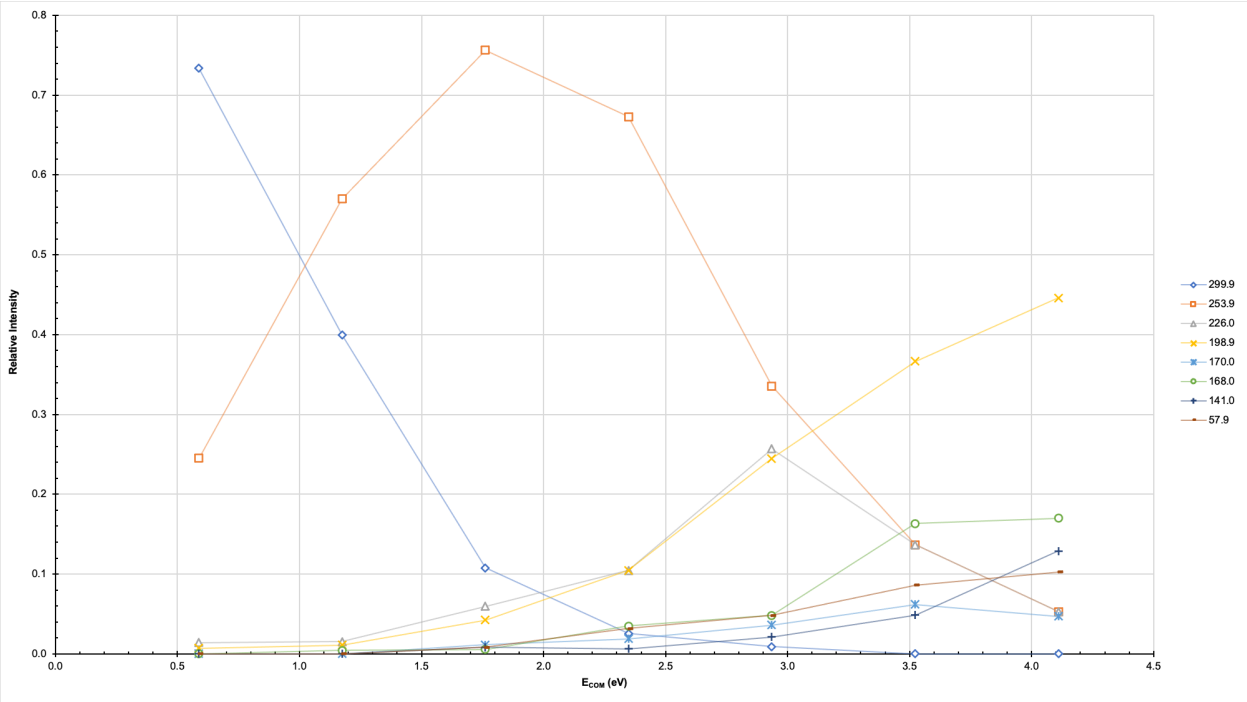

Figure 4.49 Breakdown diagram for the 1:1 complex of Nickel (II) Nitrate and 2,2'-Bipyridine-4,4'-Dicarboxylic Acid ($NiC_{12}H_6N_2O_4^+$) at 299.9 *m/z* in the transfer from 0-35eV, dual-spray.

Below are the rest of the breakdown diagrams for this combination.

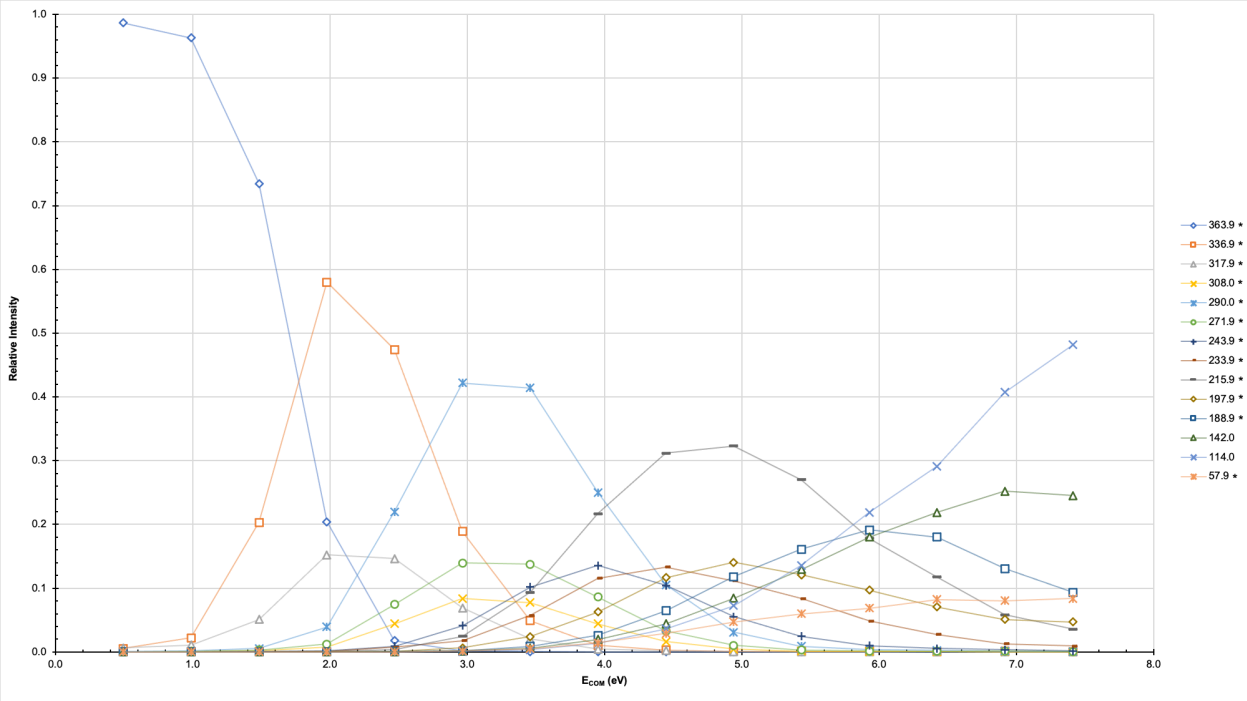

Figure 4.50 Breakdown diagram for the nitrated 1:1 complex of Nickel (II) Nitrate and 2,2'-Bipyridine-4,4'-Dicarboxylic Acid ($NiC_{12}H_8N_2O_4NO_3^+$) at 363.9 *m/z* in the trap from 0-75eV, single-spray.

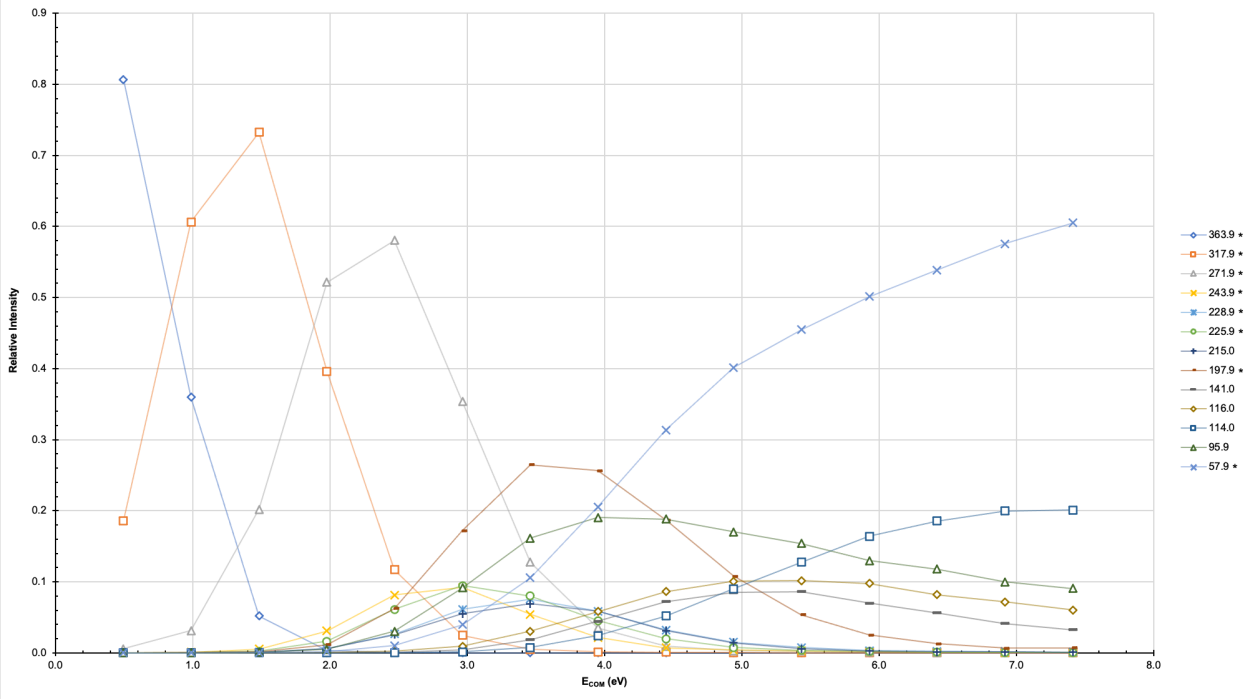

Figure 4.51 Breakdown diagram for the nitrated 1:1 complex of Nickel (II) Nitrate and 2,2'-Bipyridine-4,4'-Dicarboxylic Acid ($NiC_{12}H_8N_2O_4NO_3^+$) at 363.9 *m/z* in the transfer from 0-75eV, single-spray.

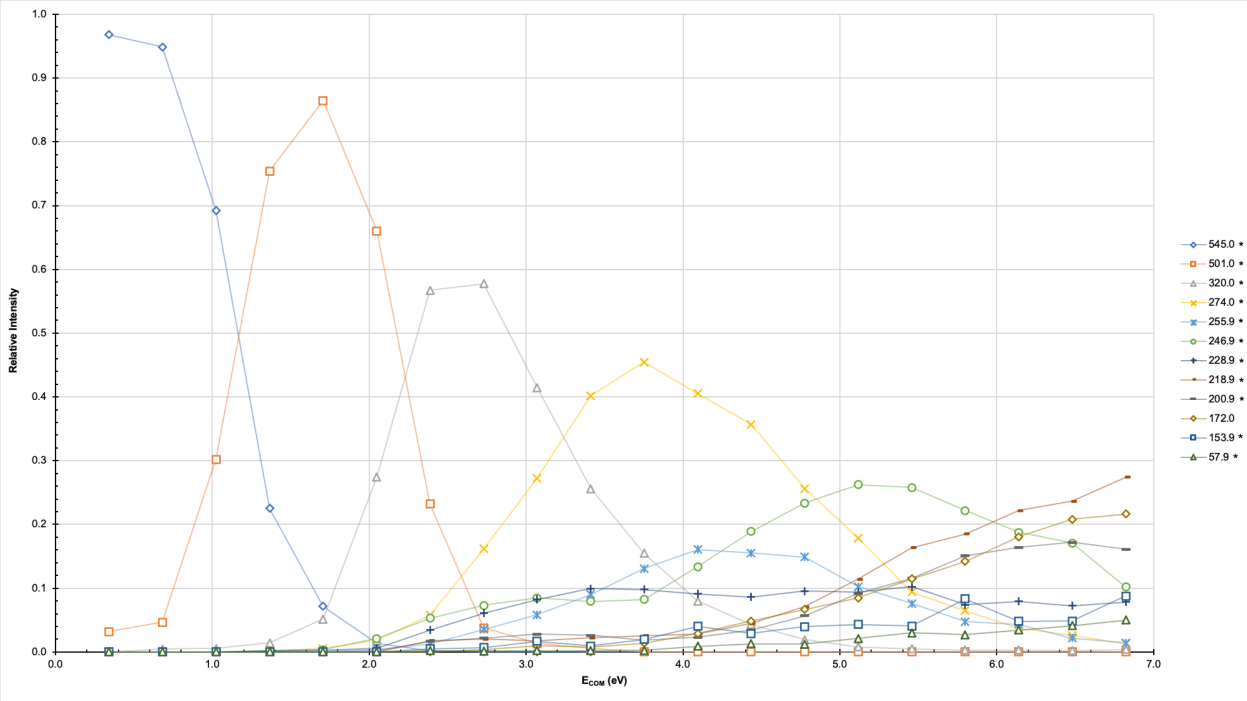

Figure 4.52 Breakdown diagram for the 1:2 complex of Nickel (II) Nitrate and 2,2'-Bipyridine-4,4'-Dicarboxylic Acid ($NiC_{12}H_8N_2O_4C_{12}H_8N_2O_4^+$) at 544.9 *m/z* in the trap from 0-100eV, single-spray.

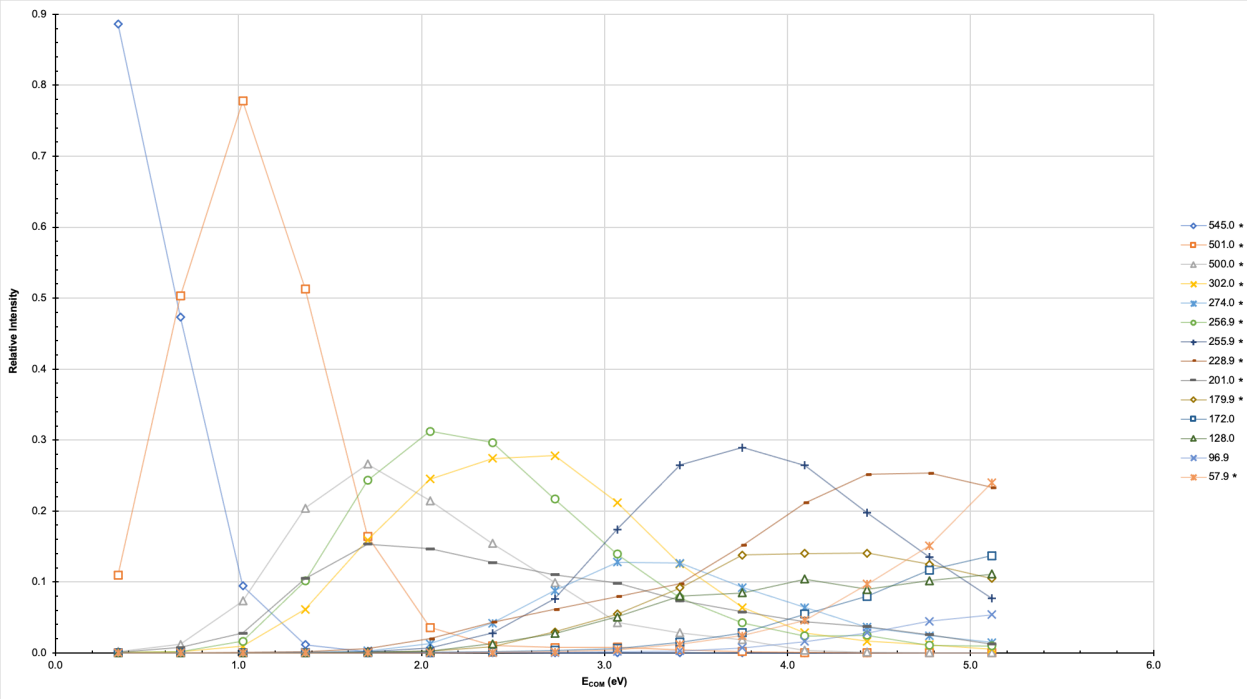

Figure 4.53 Breakdown diagram for the 1:2 complex of Nickel (II) Nitrate and 2,2'-Bipyridine-4,4'-Dicarboxylic Acid ($NiC_{12}H_8N_2O_4C_{12}H_8N_2O_4^+$) at 544.9 *m/z* in the transfer from 0-100eV, single-spray.

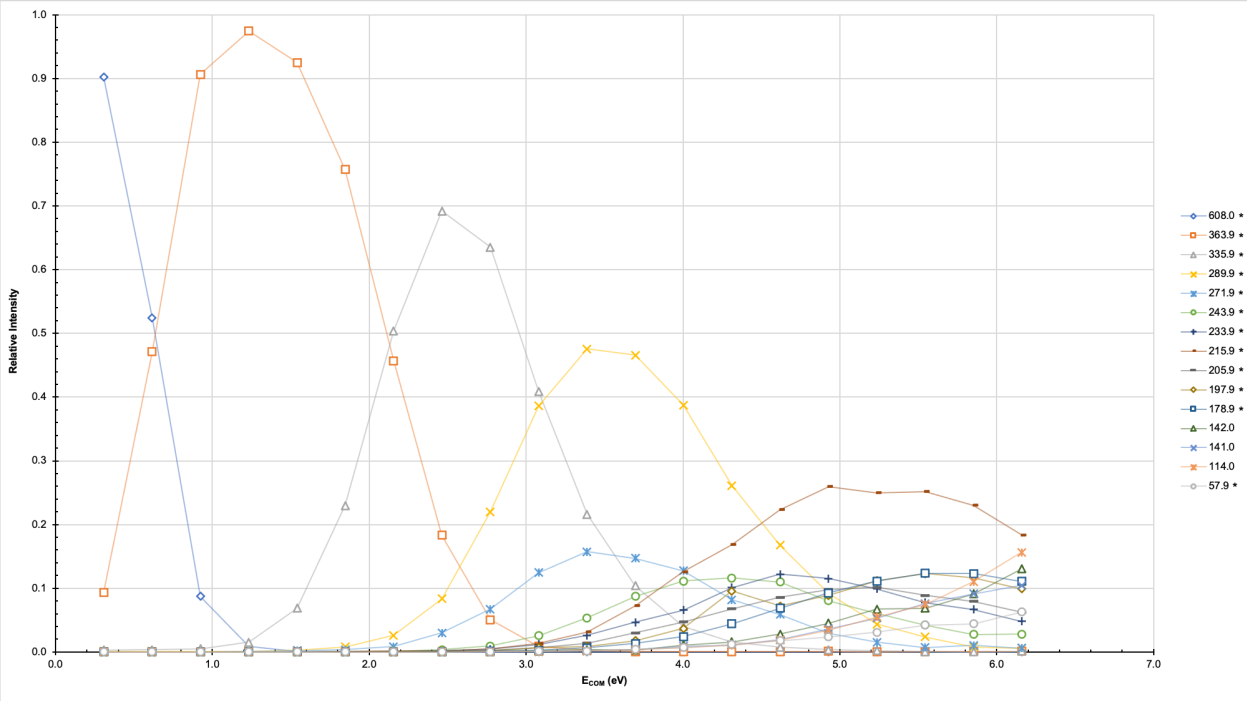

Figure 4.54 Breakdown diagram for the nitrated 1:2 complex of Nickel (II) Nitrate and 2,2'-Bipyridine-4,4'-Dicarboxylic Acid ($NiC_{12}H_8N_2O_4C_{12}H_8N_2O_4NO_3^+$) at 607.9 *m/z* in the trap from 0-100eV, single-spray.

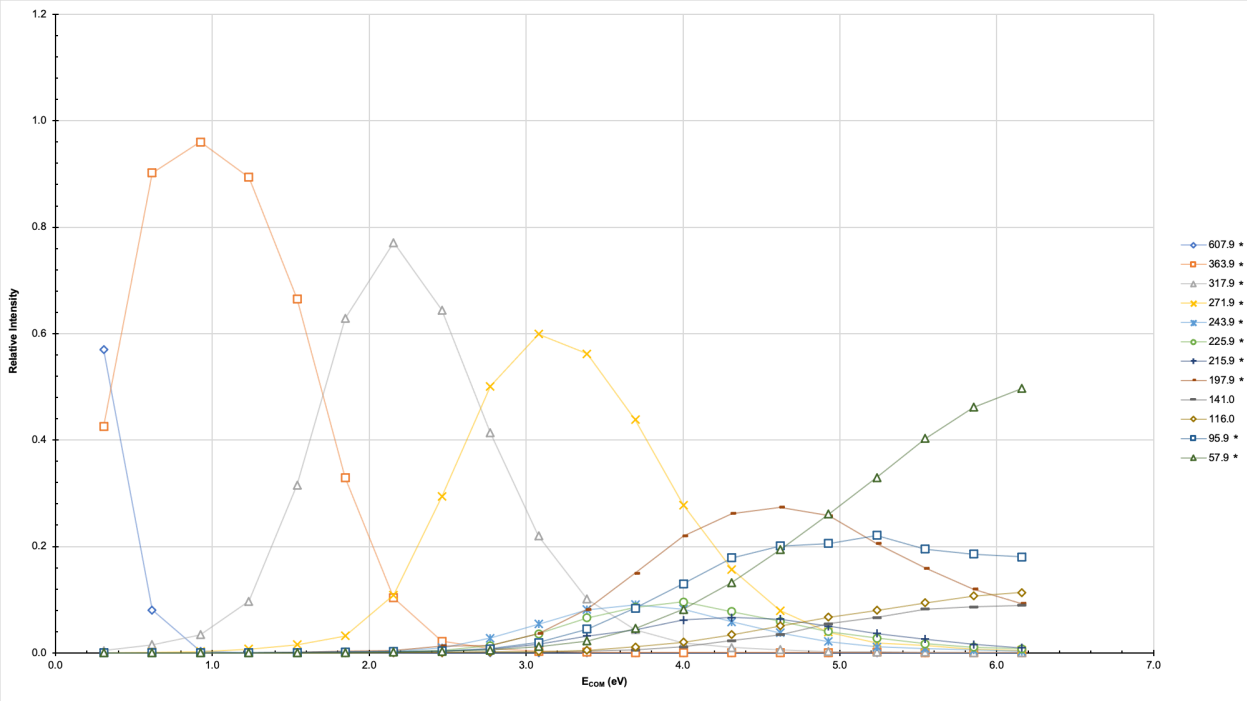

Figure 4.55 Breakdown diagram for the nitrated 1:2 complex of Nickel (II) Nitrate and 2,2'-Bipyridine-4,4'-Dicarboxylic Acid ($NiC_{12}H_8N_2O_4C_{12}H_8N_2O_4NO_3^+$) at 607.9 *m/z* in the transfer from 0-100eV, single-spray.

As in the Nickel (II) Nitrate combination, the dual-spray method was again unsuccessful with the Iron (III) Nitrate solution. Another attempt was made on 297.9 *m/z* as it as visible in the overall spectrum, but no usable data was collected. Interestingly, although visible in the overall spectrum, the 1:2 complexes of interest were unsuccessful at undergoing collision induced dissociation in the single-spray method.

Many of the fragment ions were again similar to those found in the previous experiments with the 2,2'-Bipyridine and 4,4'-Bipyridine ligands. All results can be found in the following figures, as well as in the appendix. The following table details the major fragments of interest and their likely chemical structures.

Table 4.9 Iron (III) Nitrate and 2,2'-Bipyridine-4,4'-Dicarboxylic Acid fragment mass-to charge values and their possible molecular formulas.

Mass-to-Charge Value	*Possible Molecular Formula*
360.9	$FeC_{12}H_7N_2O_4NO_3^+$
328.9	$FeC_{12}H_7N_2O_2NO_3^+$
298.9	$FeC_{12}H_7N_2O_4^+$
252.0	$FeC_{11}H_4N_2O_2^+$
236.0	$FeC_{11}H_4N_2O^+$
206.9	$FeC_7H_7N_2O_2^+$
190.9	$FeC_6H_3N_2CH_3OH^+$
158.9	$FeC_6H_3N_2^+$
144.9	$C_9H_9N_2^+$
130.0	$C_9H_8N^+$
127.9	$C_8H_4N_2^+$
111.9	$FeC_3H_6N^+$
86.9	$FeNNH_3^+$
72.9	$FeNH_3^+$
55.9	Fe^+

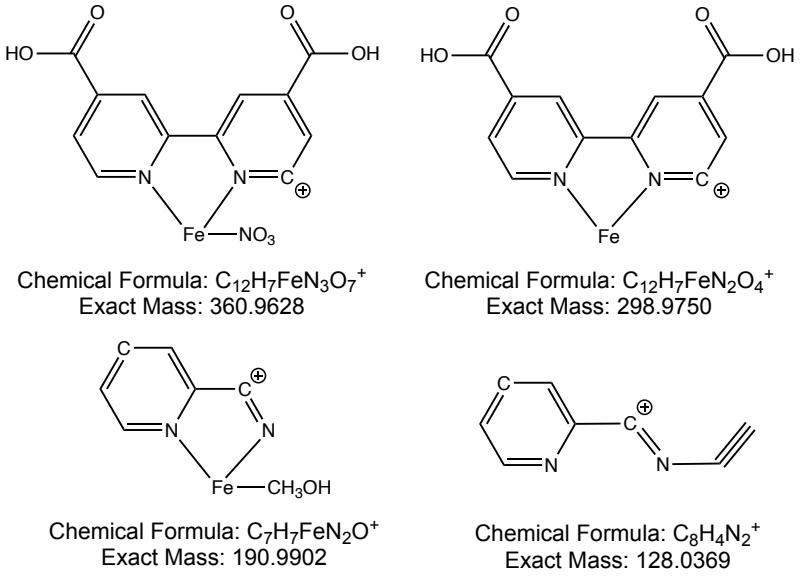

Figure 4.56 Some possible skeletal ion fragments made from the Iron (III) Nitrate and 2,2'-Bipyridine-4,4'-Dicarboxylic Acid analysis.

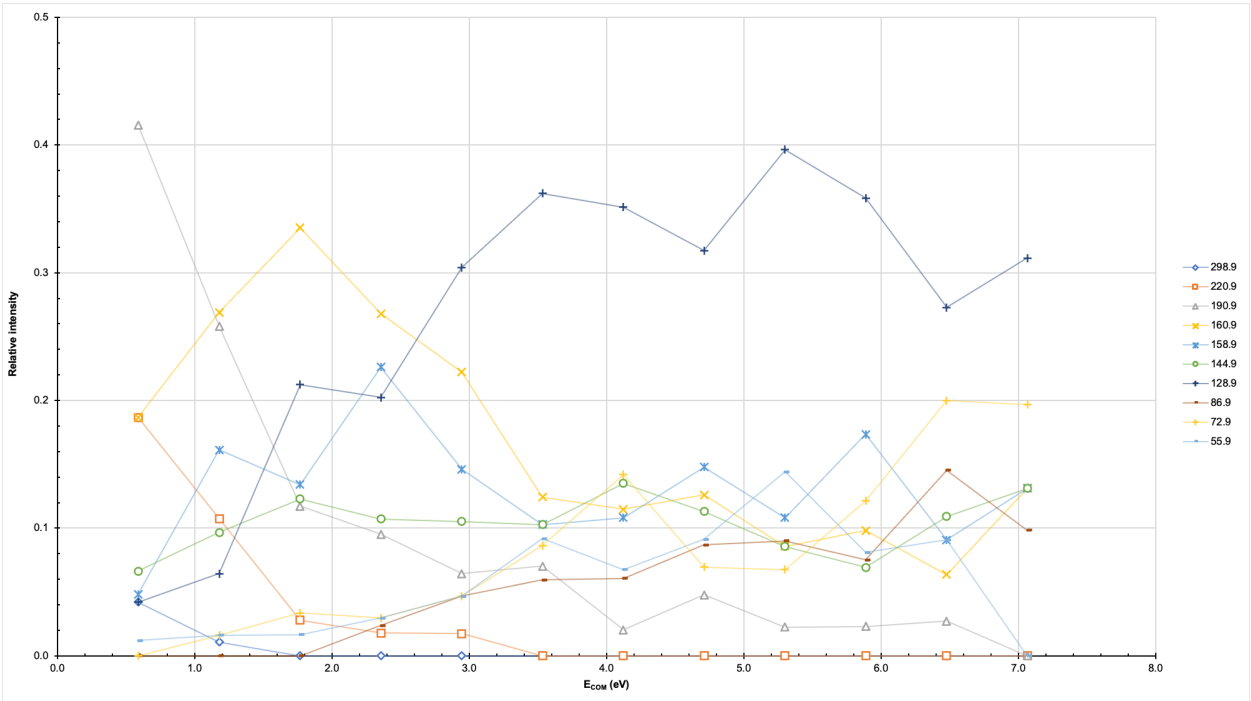

Figure 4.57 Breakdown diagram for the 1:1 complex of Iron (III) Nitrate and 2,2'-Bipyridine-4,4'-Dicarboxylic Acid ($FeC_{12}H_7N_2O_4^+$) at 298.9 *m/z* in the transfer from 0-60eV, single-spray.

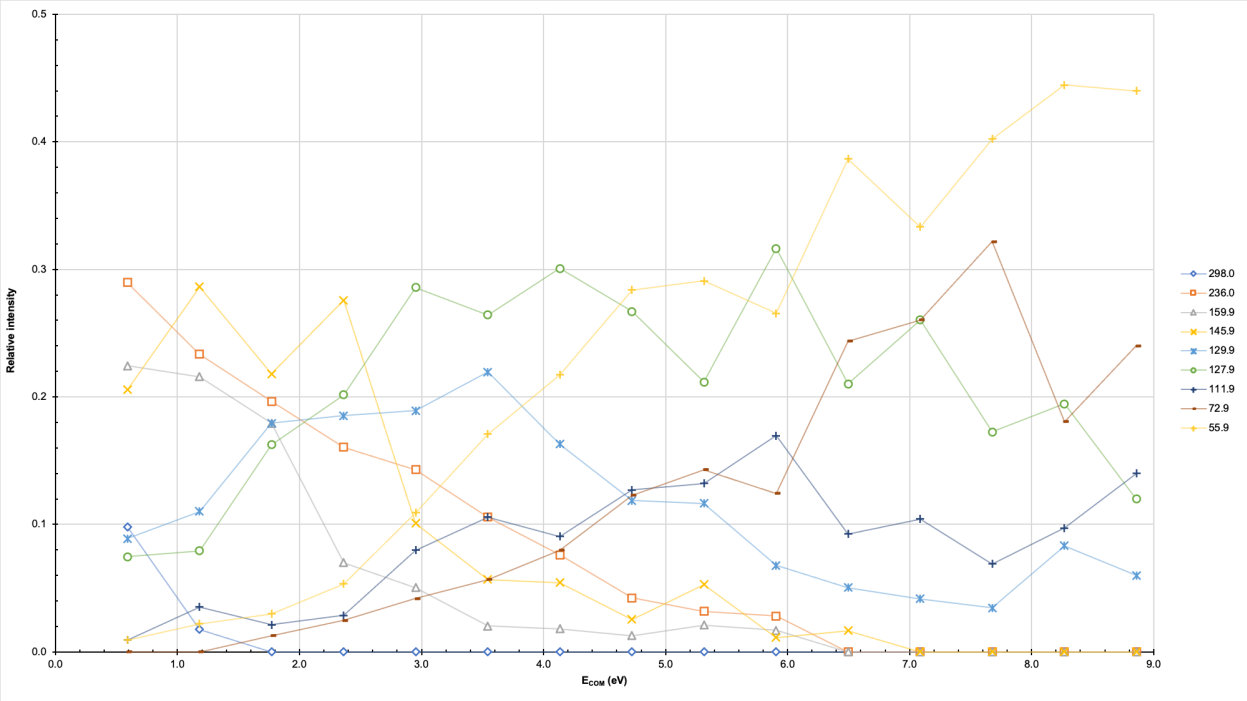

Figure 4.58 Breakdown diagram for the 1:1 complex of Iron (III) Nitrate and 2,2'-Bipyridine-4,4'-Dicarboxylic Acid ($NiC_{12}H_6N_2O_4^+$) at 297.9 *m/z* in the transfer from 0-75eV, dual-spray.

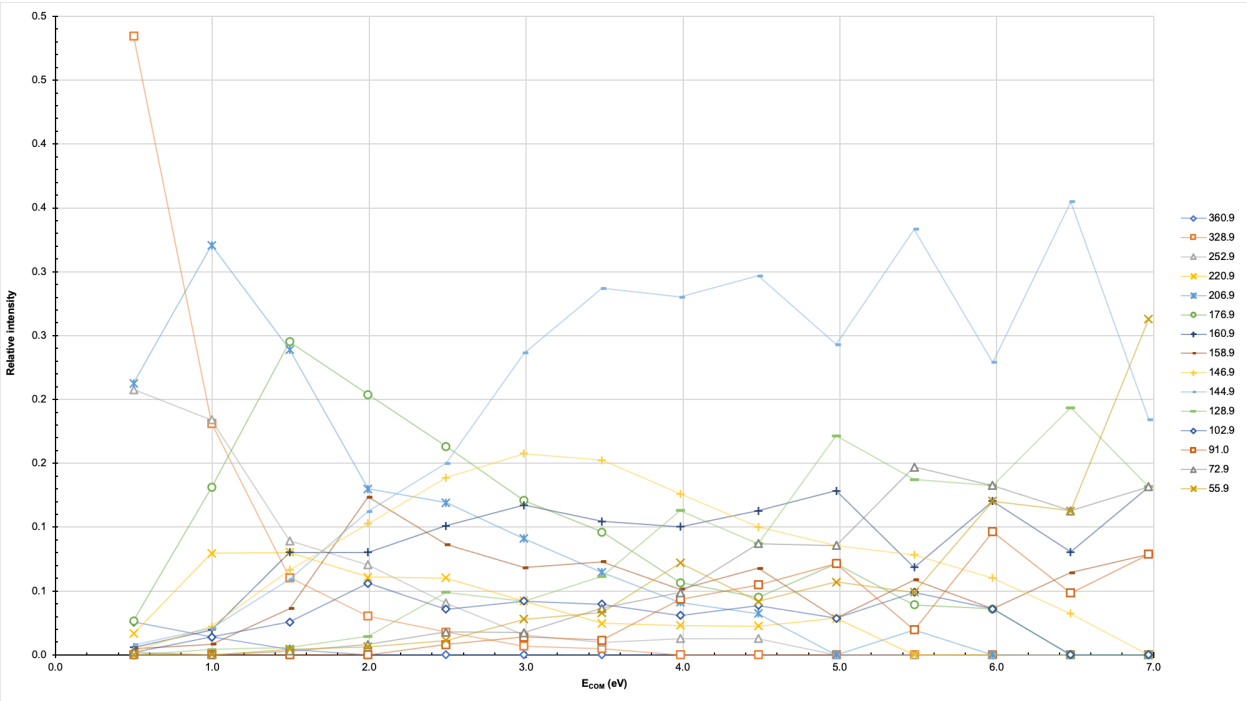

Figure 4.59 Breakdown diagram for the nitrated 1:1 complex of Iron (III) Nitrate and 2,2'-Bipyridine-4,4'-Dicarboxylic Acid ($FeC_{12}H_7N_2O_4NO_3^+$) at 360.9 *m/z* in the transfer from 0-70eV, single-spray.

In summary, the 2,2'-Bipyridine-4,4'-Dicarboxylic Acid combinations proved to be quite difficult to work with. With both Nickel (II) Nitrate and Iron (III) Nitrate solutions, they require a significant amount of reaction time making real-time mixing using the dual-spray method extremely ineffective. With the little data collected, the results still support the main breakdown pathways as the metal ion was always visible.

As seen in the previous figures, the iron combination was very ineffective in the performed experiments. The target ions were not found at the expected ion ratios and the breakdown diagrams were extremely messy. Therefore, this combination was not successful in reacting as was to be expected.

Looking at the nickel combination, when comparing the trap and transfer cells there was very little difference in the appearance of the breakdown diagrams. Of course, the coordination of water made for a more complex data analysis as previously learned. In addition, the coordination of methanol was observed. However, there was much less coordination with water than with the other bipyridine ligands. This can likely be attributed to the extra complexity within the carboxylic acid ligand and the addition of many free-floating ions within the instrument during these collision induced dissociation experiments. Moreover, all CID experiments were successful at least until 50 eV which is higher than either of the other two bipyridine combinations were able to achieve, specifically with the iron solution. Having the pre-mixed solution react for a minimum of 24 hours, increased the number of ions formed in solution, making the experimentation and fragment of the target complexes much easier.

4.4 Summary of Results

Below is a table summarizing the results of Chapter 4. It details the expected and analysed mass-to charge ratio of the target complexes and which were successful at undergoing collision induced dissociation.

Table 4.10 Summary of bipyridine ligand collision induced dissociation results.

Nickel (II) Nitrate				
Ligand	*Metal to Ligand Ratio*	*Expected m/z*	*Analysed m/z*	
			Single-Spray	*Dual-Spray*
2,2'-Bipyridine	M:1L	213.9	213.9	214.0
	M_{NO_3}:1L	275.9	275.9	276.0
	M:2L	370.0	370.0	369.0
	M_{NO_3}:2L	432.0	432.0	432.0
4.4'-Bipyridine	M:1L	213.9	✗	214.0
	M_{NO_3}:1L	275.9	275.9	275.9
	M:2L	370.0	369.0	369.0
	M_{NO_3}:2L	432.0	432.0	432.0
2,2'-Bipyridine-4,4'-Dicarboxylic Acid	M:1L	301.9	301.9	299.9
	M_{NO_3}:1L	363.9	363.9	✗
	M:2L	544.9	544.9	✗
	M_{NO_3}:2L	607.9	607.9	✗

Iron (III) Nitrate				
Ligand	*Metal to Ligand Ratio*	*Expected m/z*	*Analysed m/z*	
			Single-Spray	*Dual-Spray*
2,2'-Bipyridine	M:1L	211.9	211.9	212.0
	M_{NO_3}:1L	274.0	274.0	274.0
	M:2L	368.0	368.0	368.0
	M_{NO_3}:2L	430.0	430.0	430.0
4.4'-Bipyridine	M:1L	211.9	✗	211.9
	M_{NO_3}:1L	274.0	274.0	274.0
	M:2L	368.0	369.0	368.0
	M_{NO_3}:2L	430.0	430.0	430.0
2,2'-Bipyridine-4,4'-Dicarboxylic Acid	M:1L	299.9	298.9	297.9
	M_{NO_3}:1L	361.9	360.9	✗
	M:2L	542.9	✗	✗
	M_{NO_3}:2L	605.9	✗	✗

CHAPTER 5 – GAS PHASE REACTIVITY OF METAL COMPLEXES: PHENANTHROLINE LIGAND

5.1 Data and Results

Collision Induced Dissociation (CID) experiments were again performed within both the single- and dual-spray methods on each of the four target complexes. In the case of the Nickel (II) Nitrate combination, complexes marked with an asterisk (*) confirm the presence of Nickel by the breakdown diagram of the second isotope containing complex (see appendix).

In the single-spray (mixture) method with the Nickel (II) Nitrate solution, the 1:1 metal: ligand complex, $NiC_{12}H_8N_2^+$, was observed at 237.9 and 239.9 *m/z*. The nitrated 1:1 complex, $NiC_{12}H_8N_2NO_3^+$, was observed at 299.9 and 301.9 *m/z*. The 1:2 complex, $NiC_{12}H_8N_2C_{12}H_8N_2^+$, was observed at 418.0 and 420.0 *m/z*. Finally, the nitrated 1:2 complex, $NiC_{12}H_8N_2C_{12}H_8N_2NO_3^+$, was observed at 480.0 and 482.0 *m/z*. All results can be found in the following figures, as well as in the appendix.

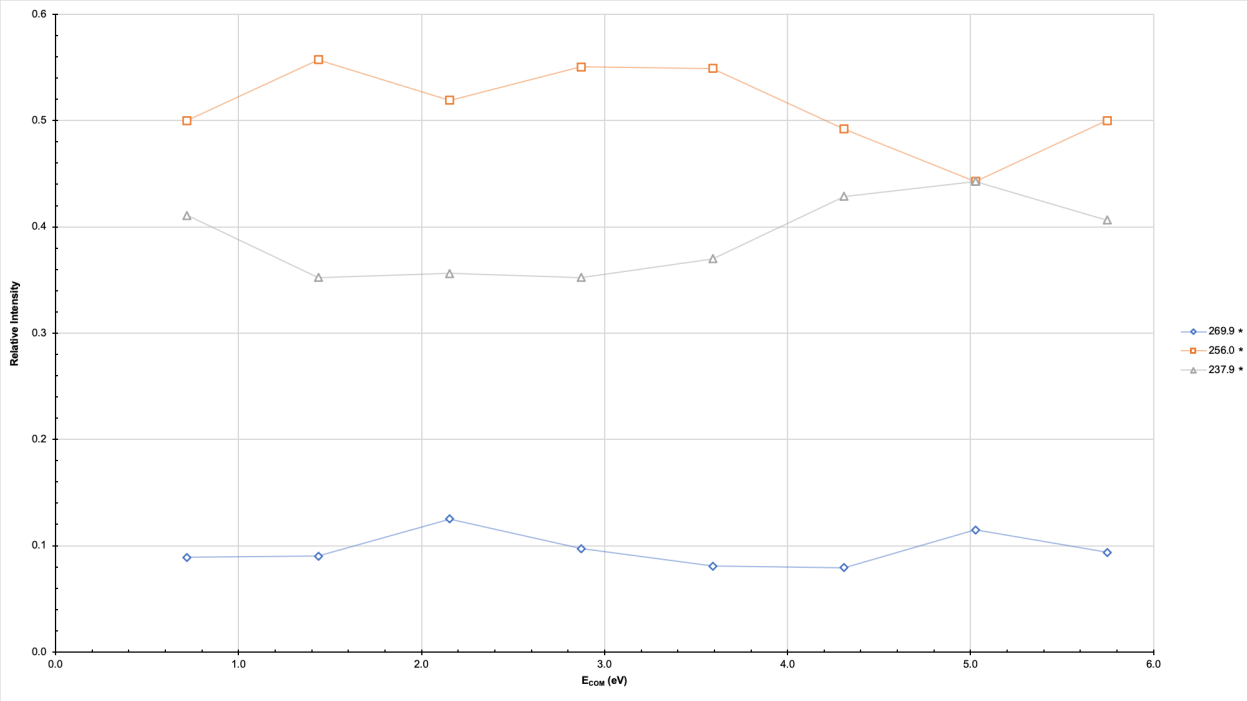

Figure 5.1 Breakdown diagram for the 1:1 complex of Nickel (II) Nitrate and 1,10-Phenanthroline ($NiC_{12}H_8N_2^+$) at 237.9 *m/z* in the trap from 0-40eV, single-spray.

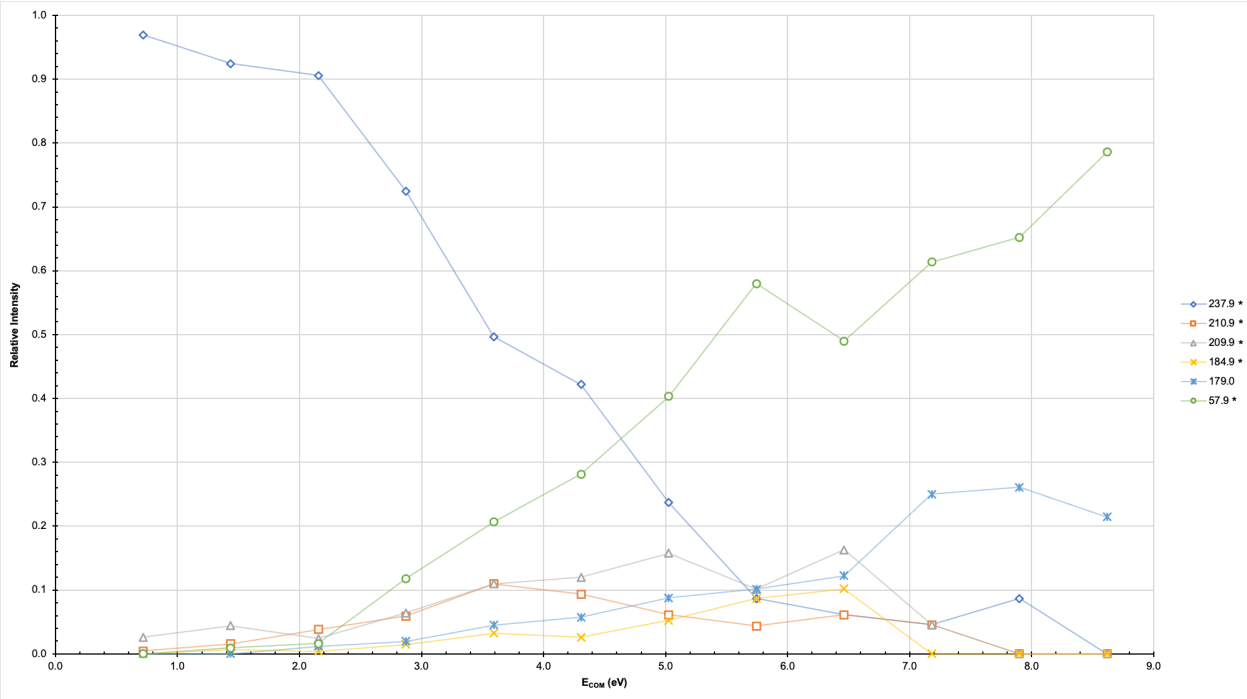

Figure 5.2 Breakdown diagram for the 1:1 complex of Nickel (II) Nitrate and 1,10-Phenanthroline ($NiC_{12}H_8N_2^+$) at 237.9 *m/z* in the transfer from 0-40eV, single-spray.

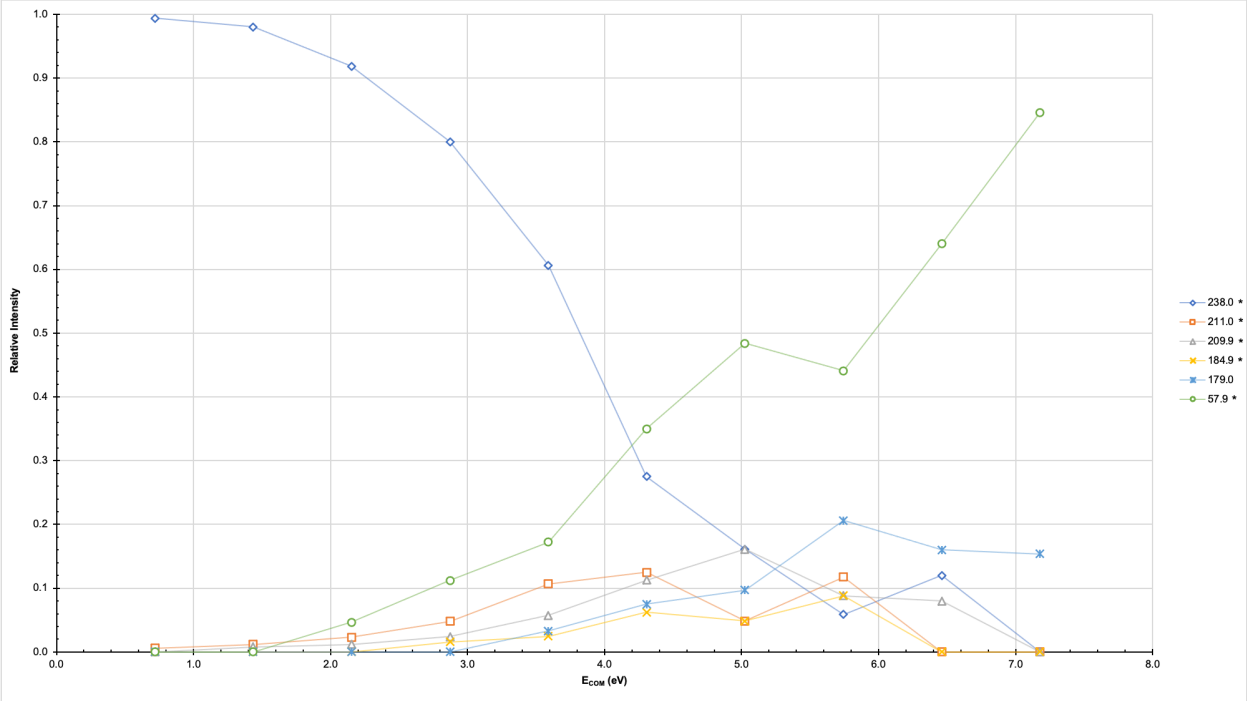

Figure 5.3 Breakdown diagram for the 1:1 complex of Nickel (II) Nitrate and 1,10-Phenanthroline ($NiC_{12}H_8N_2^+$) at 238.0 *m/z* in the transfer from 0-50eV, dual-spray.

The single-spray experiment in the trap was seen to have little success with the 1,10-Phenanthroline ligand. However, both single- and dual-spray in the transfer give very similar results. Fragments to note can be found in Table 5.1. Some of the potential structures of these fragments can be found in Figure 5.4.

Table 5.1 Nickel (II) Nitrate and 1,10-Phenanthroline fragment mass-to charge values and their possible molecular formulas.

Mass-to-Charge Value	*Possible Molecular Formula*
269.9*	$NiC_{12}H_8N_2CH_3OH^+$
256.0*	$NiC_{12}H_8N_2H_2O^+$
237.9*	$NiC_{12}H_8N_2^+$
210.9*	$NiC_{10}H_5N_2^+$
184.9*	$NiC_9H_5N^+$
179.0	$C_{12}H_7N_2^+$
57.9*	Ni^+

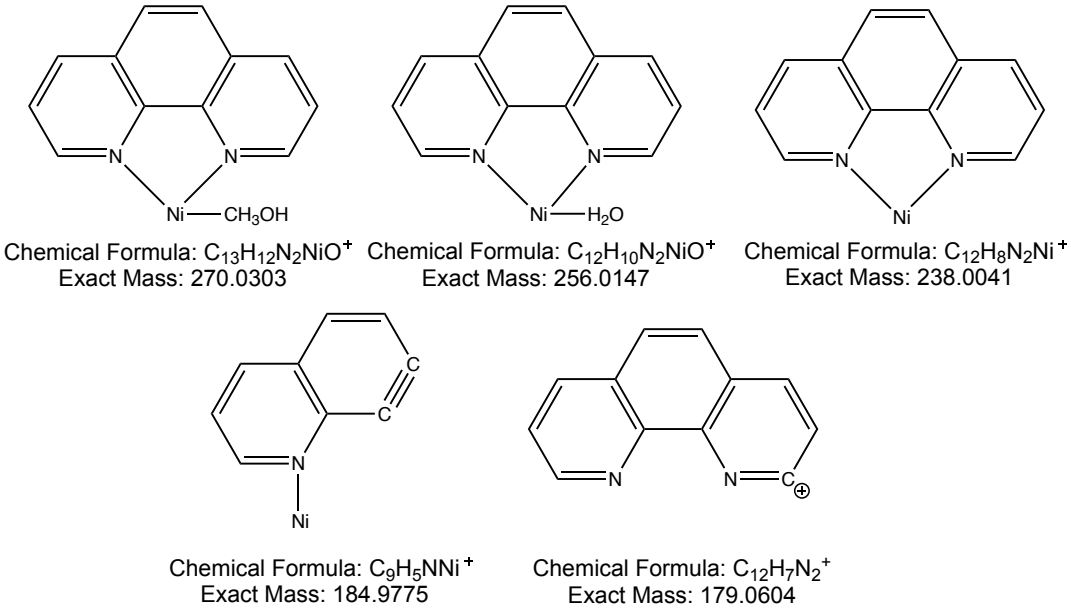

Figure 5.4 Possible structures of fragments formed by collision induced dissociation of Nickel (II) Nitrate and 1,10-Phenanthroline.

The following figures depict the single- and dual-spray experiments for the nitrated 1:1 complex.

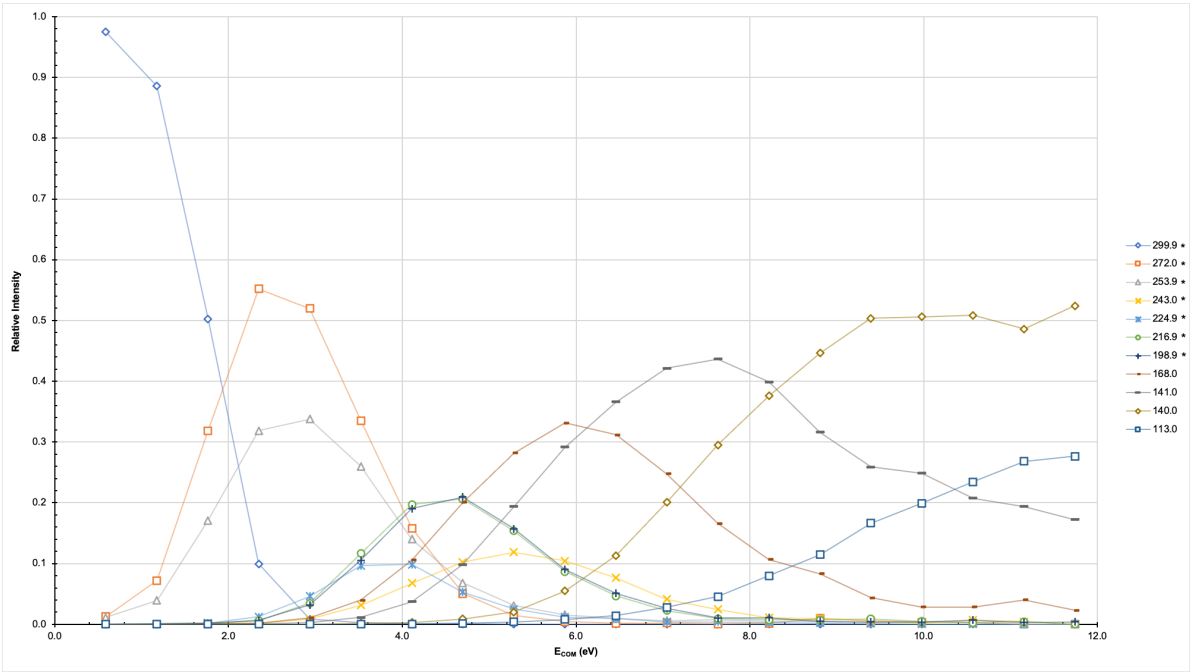

Figure 5.5 Breakdown diagram for the nitrated 1:1 complex of Nickel (II) Nitrate and 1,10-Phenanthroline ($NiC_{12}H_8N_2NO_3^+$) at 299.9 *m/z* in the trap from 0-100eV, single-spray.

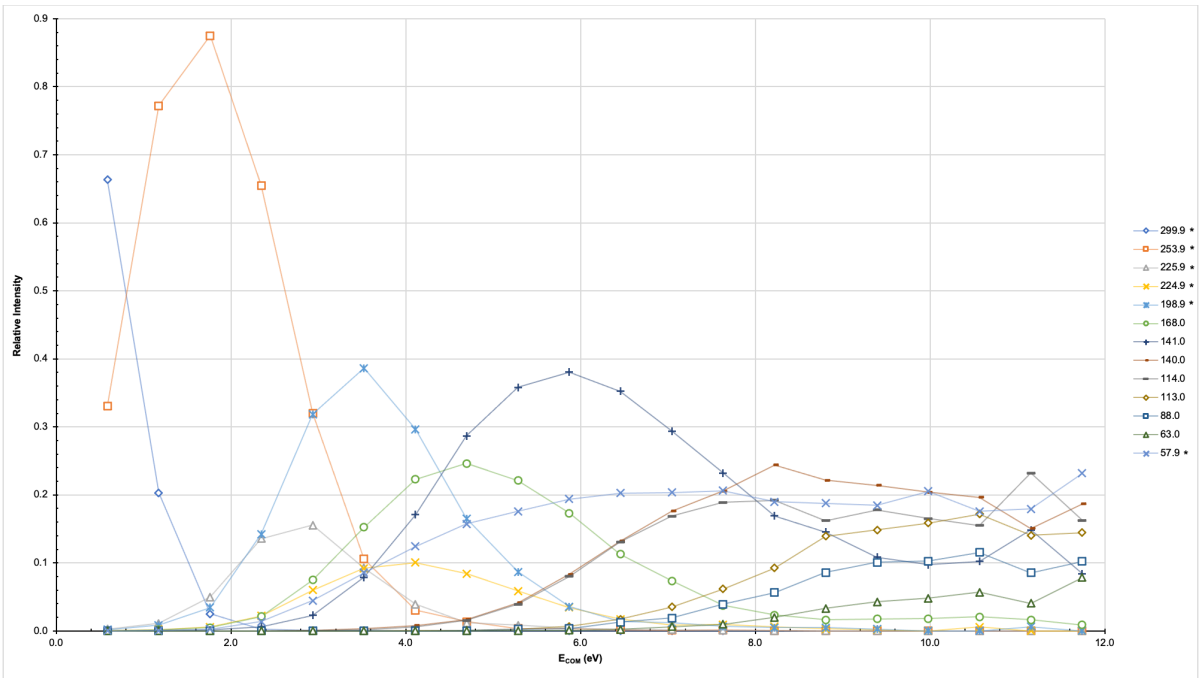

Figure 5.6 Breakdown diagram for the nitrated 1:1 complex of Nickel (II) Nitrate and 1,10-Phenanthroline ($NiC_{12}H_8N_2NO_3^+$) at 299.9 *m/z* in the transfer from 0-100eV, single-spray.

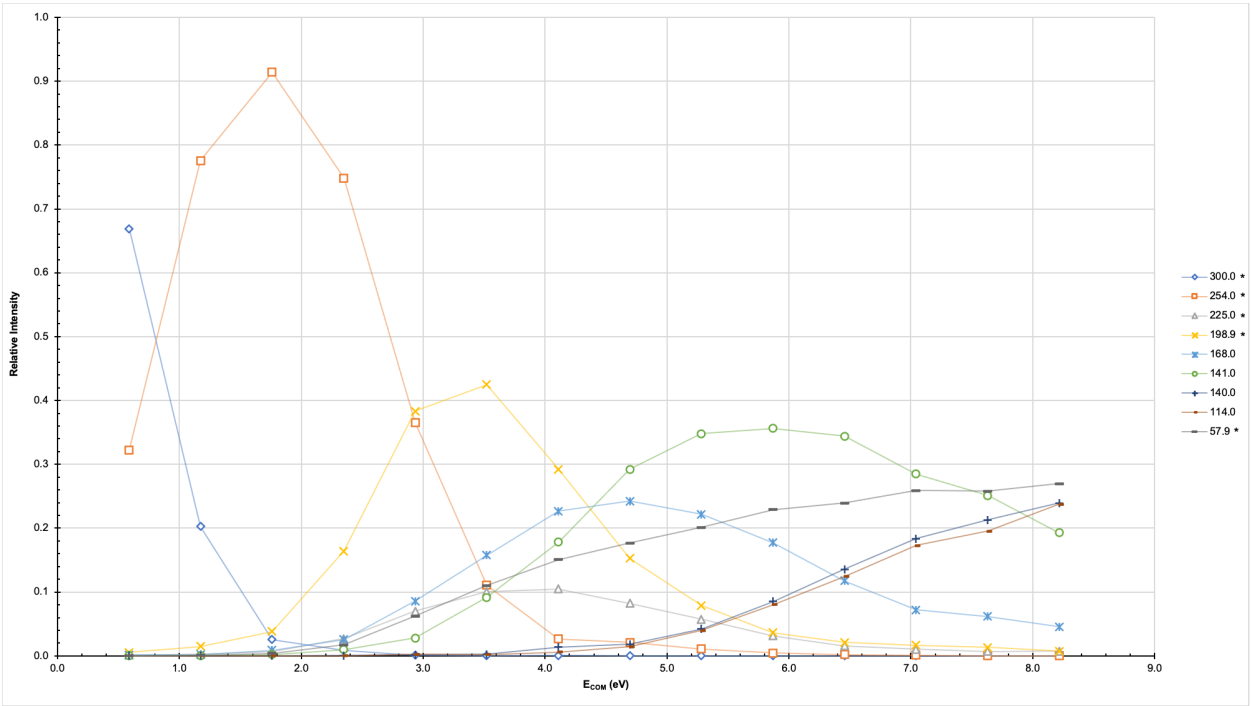

Figure 5.7 Breakdown diagram for the nitrated 1:1 complex of Nickel (II) Nitrate and 1,10-Phenanthroline ($NiC_{12}H_8N_2NO_3^+$) at 300.0 *m/z* in the transfer from 0-70eV, dual-spray.

As has been the trend, all three of breakdown diagrams looks fairly similar with many of the same fragments. Again, water appears coordinated in the trap experiment. In the others, the target ion is quickly destroyed with the 141.0 m/z ion dominating a large portion of remainder. As usual, the nickel ion is present and makes up a large percentage of the relative intensities by the end of the experiments.

The results of the 1:2 complex and the nitrated 1:2 complex are as follows.

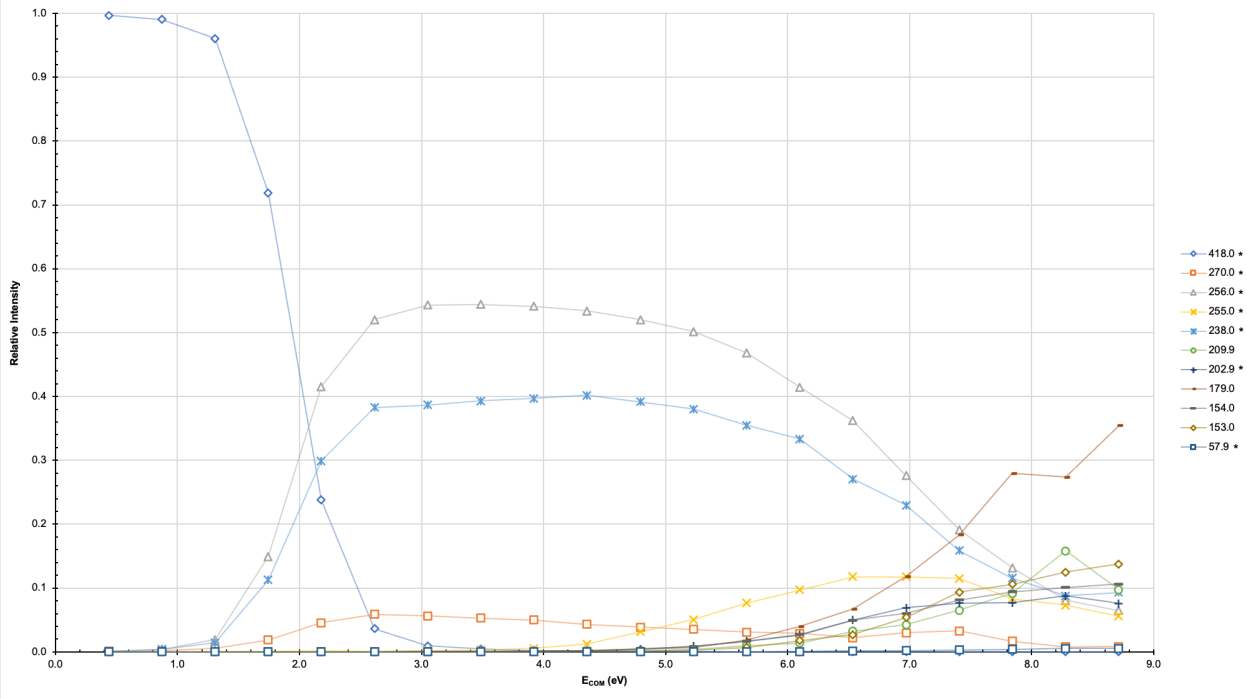

Figure 5.8 Breakdown diagram for the 1:2 complex of Nickel (II) Nitrate and 1,10-Phenanthroline ($NiC_{12}H_8N_2C_{12}H_8N_2^+$) at 418.0 *m/z* in the trap from 0-100eV, single-spray.

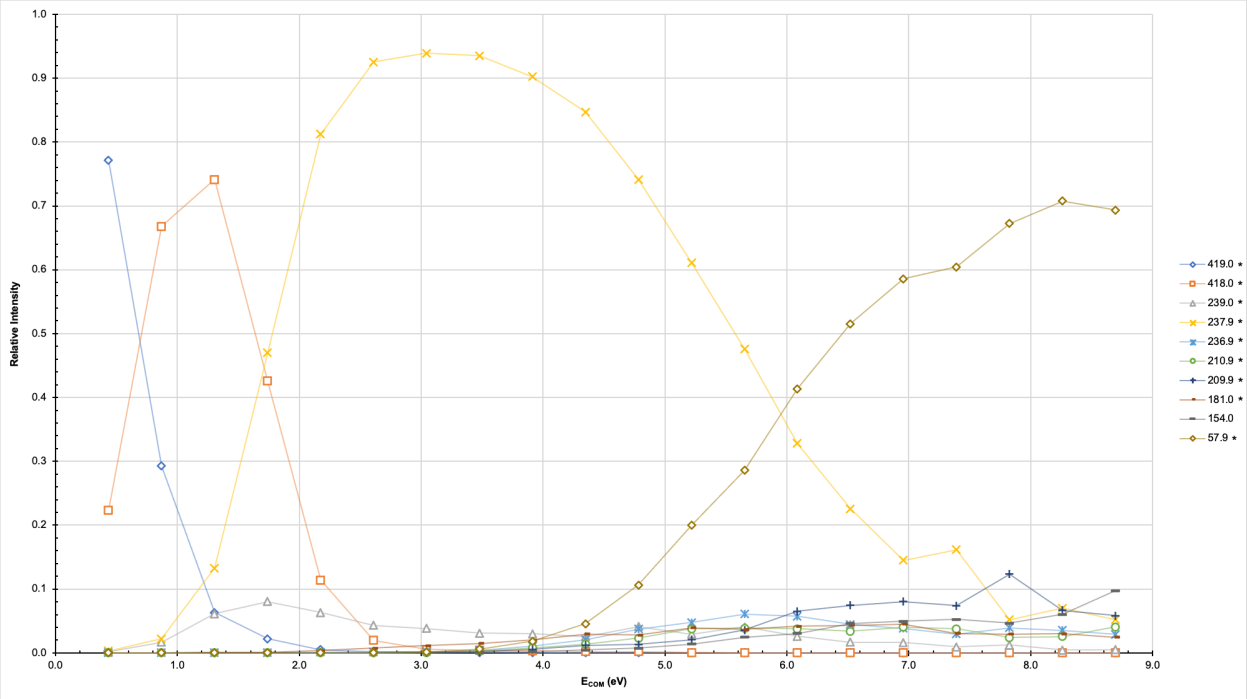

Figure 5.9 Breakdown diagram for the 1:2 complex of Nickel (II) Nitrate and 1,10-Phenanthroline ($NiC_{12}H_8N_2C_{12}H_8N_2^+$) at 419.0 *m/z* in the transfer from 0-100eV, single-spray.

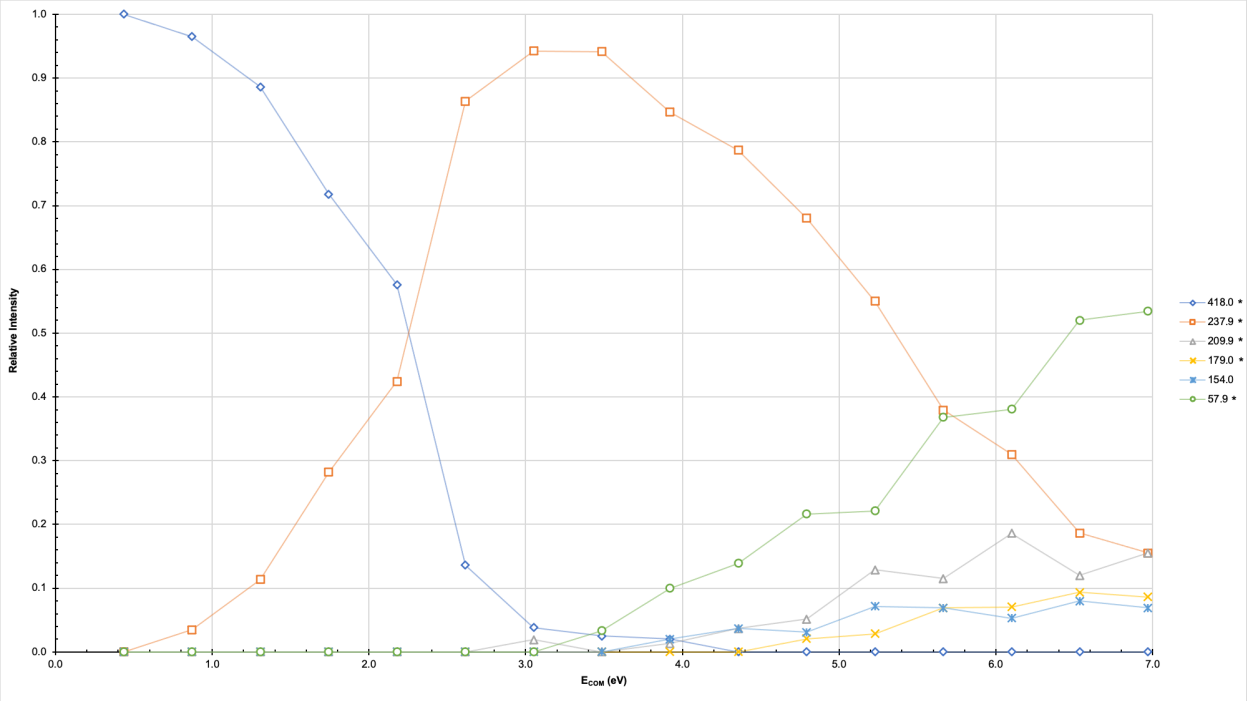

Figure 5.10 Breakdown diagram for the 1:2 complex of Nickel (II) Nitrate and 1,10-Phenanthroline ($NiC_{10}H_8N_2C_{10}H_8N_2^+$) at 418.0 *m/z* in the transfer from 0-80eV, dual-spray.

In the single-spray experiments, it is interesting to note that the 418.0 and 420.0 *m/z* ($NiC_{10}H_8N_2C_{10}H_8N_2^+$) were visible in the trap while the 419.0 and 421.0 *m/z* ($NiC_{10}H_8N_2C_{10}H_8N_2H^+$) were visible in the transfer. All four ions were visible in the dual-spray experiment in the transfer. These experiments were performed on different days making lab conditions a possible factor in their differences. However, it is highly unusual that this discrepancy occurred as an overall mass spectrum was taken each day before experimenting confirming the difference in expected ion masses. The other breakdown diagrams are visible in the appendix. Nonetheless, the fragments of each diagram are all fairly similar and reflect the same overall pathways of the breakdown on the 1:2 complex.

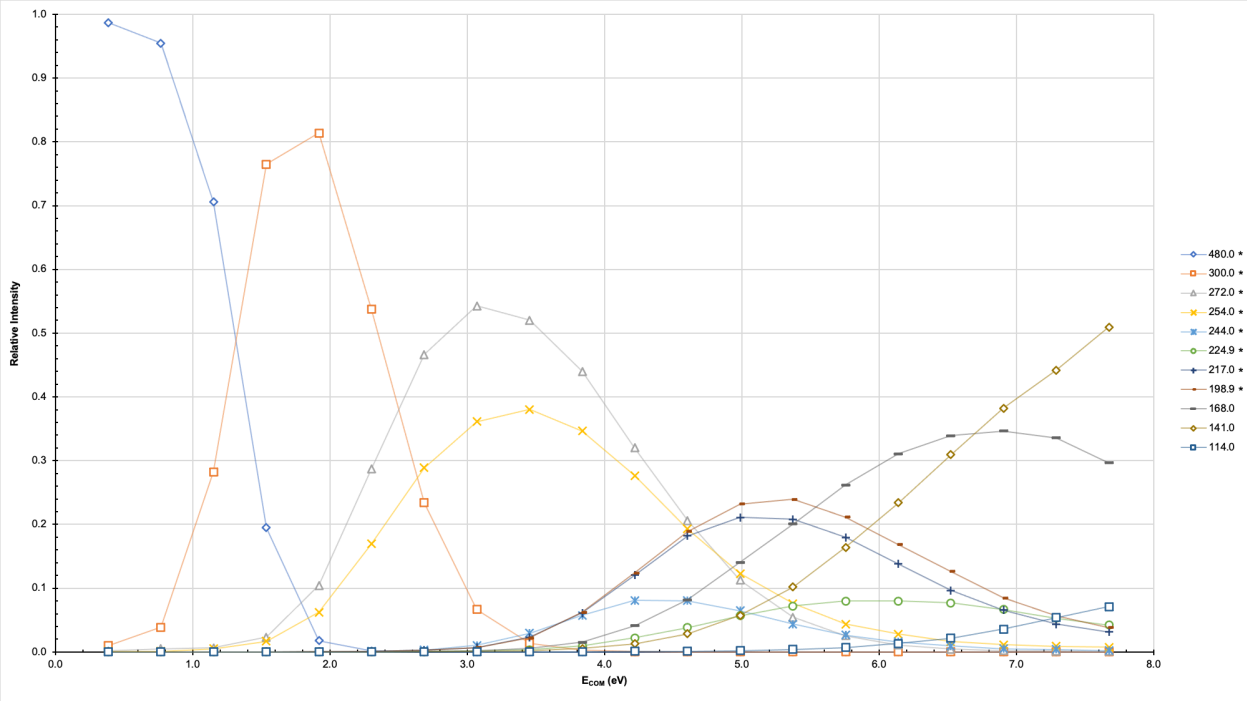

Figure 5.11 Breakdown diagram for the nitrated 1:2 complex of Nickel (II) Nitrate and 1,10-Phenanthroline ($NiC_{12}H_8N_2C_{12}H_8N_2NO_3^+$) at 480.0 *m/z* in the trap from 0-100eV, single-spray.

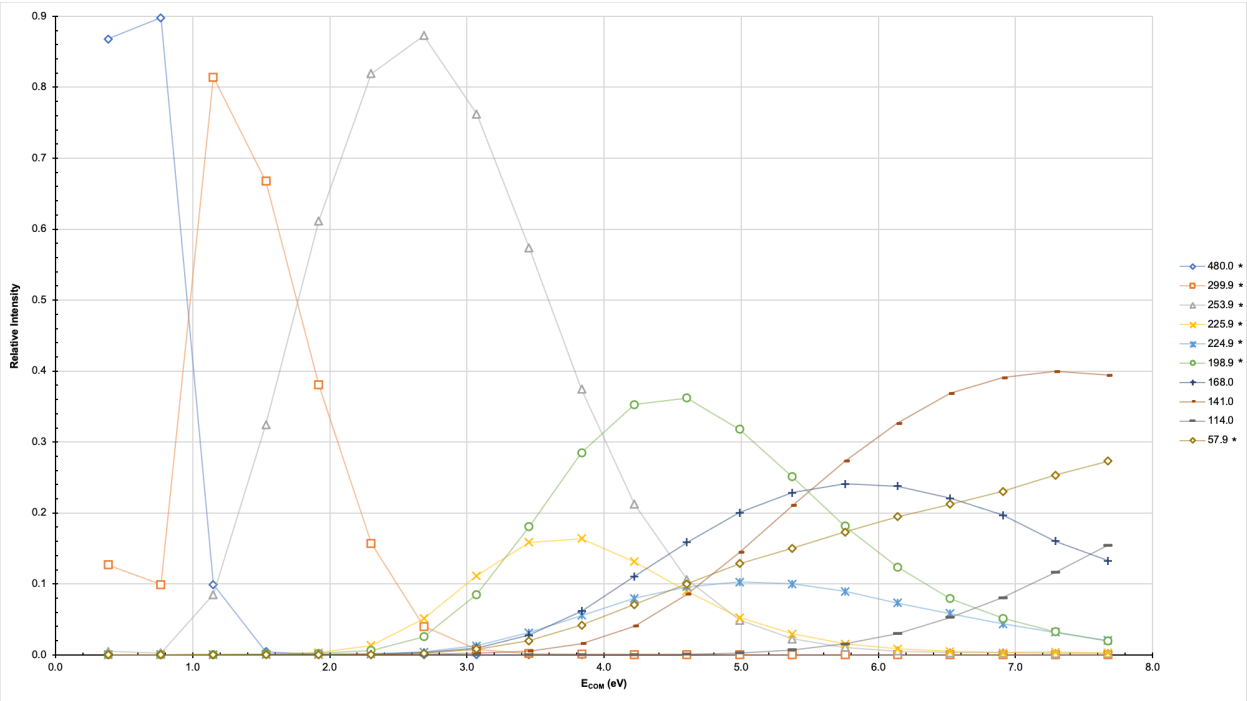

Figure 5.12 Breakdown diagram for the nitrated 1:2 complex of Nickel (II) Nitrate and 1,10-Phenanthroline ($NiC_{12}H_8N_2C_{12}H_8N_2NO_3^+$) at 480.0 *m/z* in the transfer from 0-100eV, single-spray.

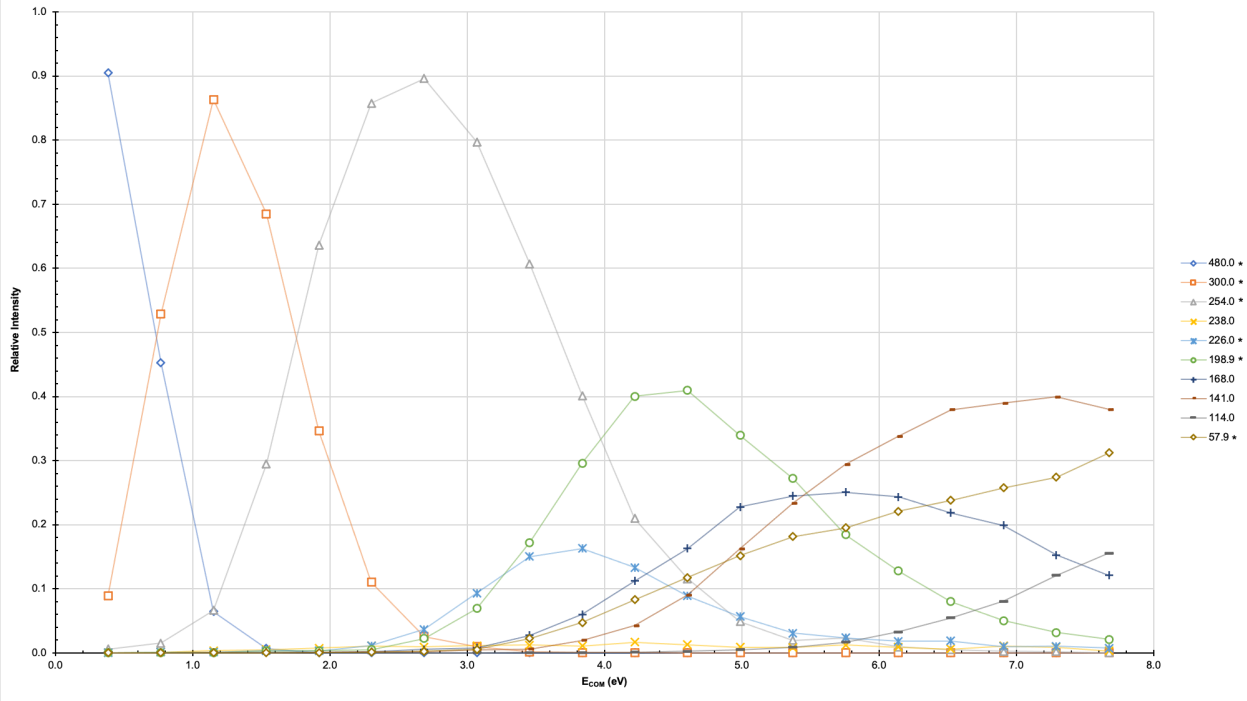

Figure 5.13 Breakdown diagram for the nitrated 1:2 complex of Nickel (II) Nitrate and 1,10-Phenanthroline ($NiC_{12}H_8N_2C_{12}H_8N_2NO_3^+$) at 480.0 *m/z* in the transfer from 0-100eV, dual-spray.

A very similar pattern is present in the trends of all three graphs once again. The main breakdown pathways are confirmed by the repetition in experiments. The potential fragments and their molecular structures can be found in Table 5.2 and Figure 5.14.

Table 5.2 Nickel (II) Nitrate and 1,10-Phenanthroline fragment mass-to charge values and their possible molecular formulas.

Mass-to-Charge Value	*Possible Molecular Formula*
480.0*	$NiC_{12}H_8N_2C_{12}H_8N_2NO_3^+$
418.0*	$NiC_{12}H_8N_2C_{12}H_8N_2^+$
300.0*	$NiC_{12}H_8N_2NO_3^+$
254.0*	$NiC_{12}H_8N_2NH_2^+$
238.0*	$NiC_{12}H_8N_2^+$
224.9*	$NiC_{12}H_9N^+$
217.0*	$NiC_{11}H_6NH_2O^+$
209.9*	$NiC_{11}H_6N^+$
202.9*	$NiC_{10}H_{11}N^+$
198.9*	$NiC_{10}H_7N^+$
168.0	$C_{11}H_8N_2^+$
154.0	$C_{10}H_6N_2^+$
141.0	$C_{10}H_7N^+$
114.9	$C_{18}H_5N^+$
89.0	$C_6H_3N^+$

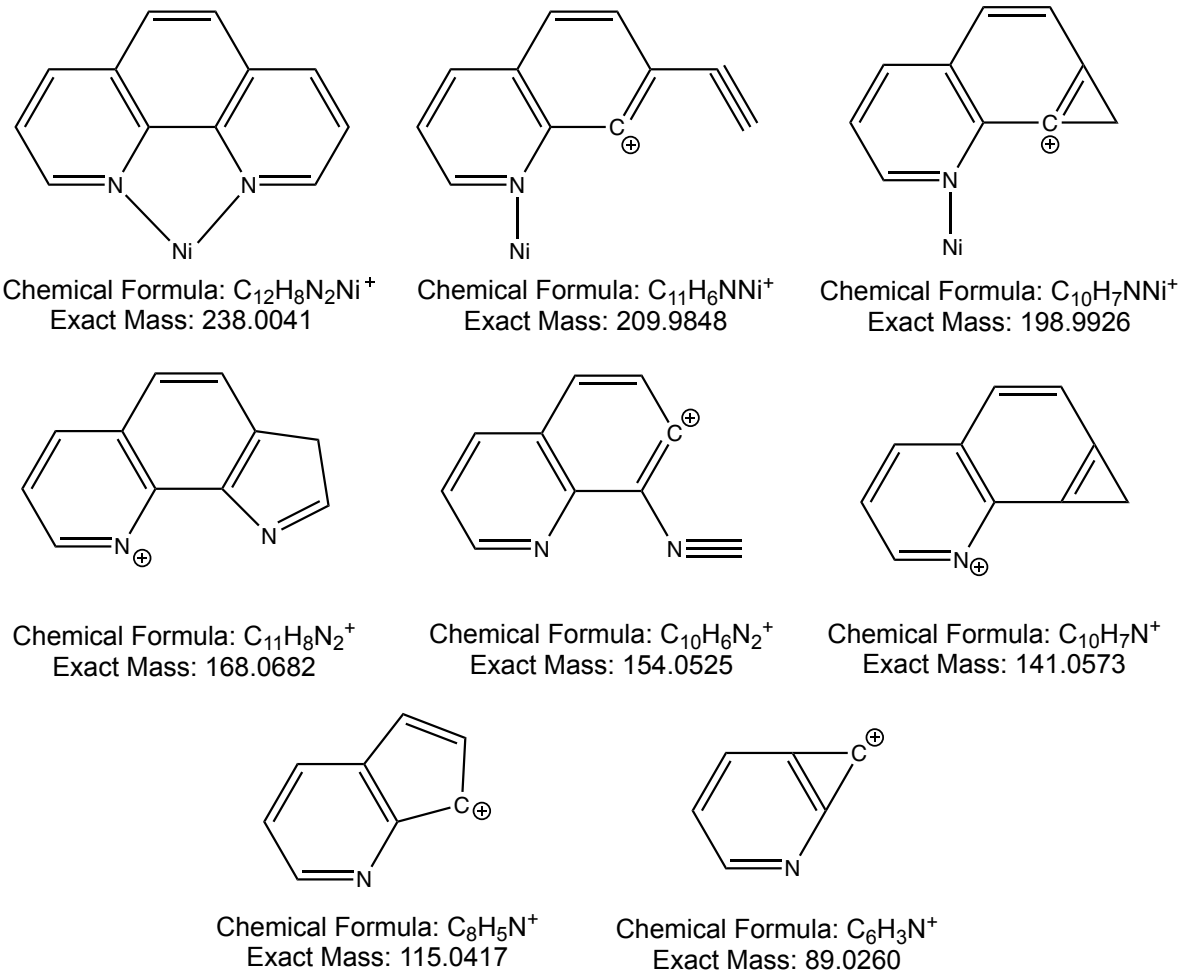

Figure 5.14 Possible skeletal ion fragments made from the Nickel (II) Nitrate and 1,10-Phenanthroline.

Iron (III) Nitrate was used as the metal solution to repeat this experiment, only taking place in the transfer cell to avoid water coordination. In both the single- and dual-spray experiments, the 1:1 metal: ligand complex, $FeC_{12}H_8N_2^+$, was observed at 235.9 *m/z*. The nitrated 1:1 complex, $FeC_{12}H_8N_2NO_3^+$, was observed at 297.9 *m/z*. The 1:2 complex, $FeC_{12}H_8N_2C_{12}H_8N_2^+$, was observed at 416.0 *m/z*. Finally, the nitrated 1:2 complex, $FeC_{12}H_8N_2C_{12}H_8N_2NO_3^+$, was observed at 478.0 *m/z*. All results can be found in the following tables and figures.

Table 5.3 Iron (III) Nitrate and 1,10-Phenanthroline fragment mass-to charge values and their possible molecular formulas.

Mass-to-Charge Value	*Possible Molecular Formula*
478.0	$FeC_{12}H_8N_2C_{12}H_8N_2NO_3^+$
416.0	$FeC_{12}H_8N_2C_{12}H_8N_2^+$
353.9	$FeC_{12}H_8N_2C_7H_5N_2^+$
291.9	$FeC_{12}H_8N_2C_3H_6N^+$
297.9	$FeC_{12}H_8N_2NO_3^+$
267.9	$FeC_{12}H_8N_2CH_3OH^+$
252.0	$FeC_{12}H_7N_2OH^+$
235.9	$FeC_{12}H_8N_2^+$
221.9	$FeC_{11}H_6N_2^+$
208.9	$FeC_{10}H_5N_2^+$
182.9	$FeC_9H_5N^+$
179.0	$C_{12}H_7N_2^+$
154.0	$C_{10}H_6N_2^+$
127.0	$C_9H_5N^+$
101.0	$C_7H_3N^+$
77.0	$C_5H_3N^+$
55.9	Fe^+

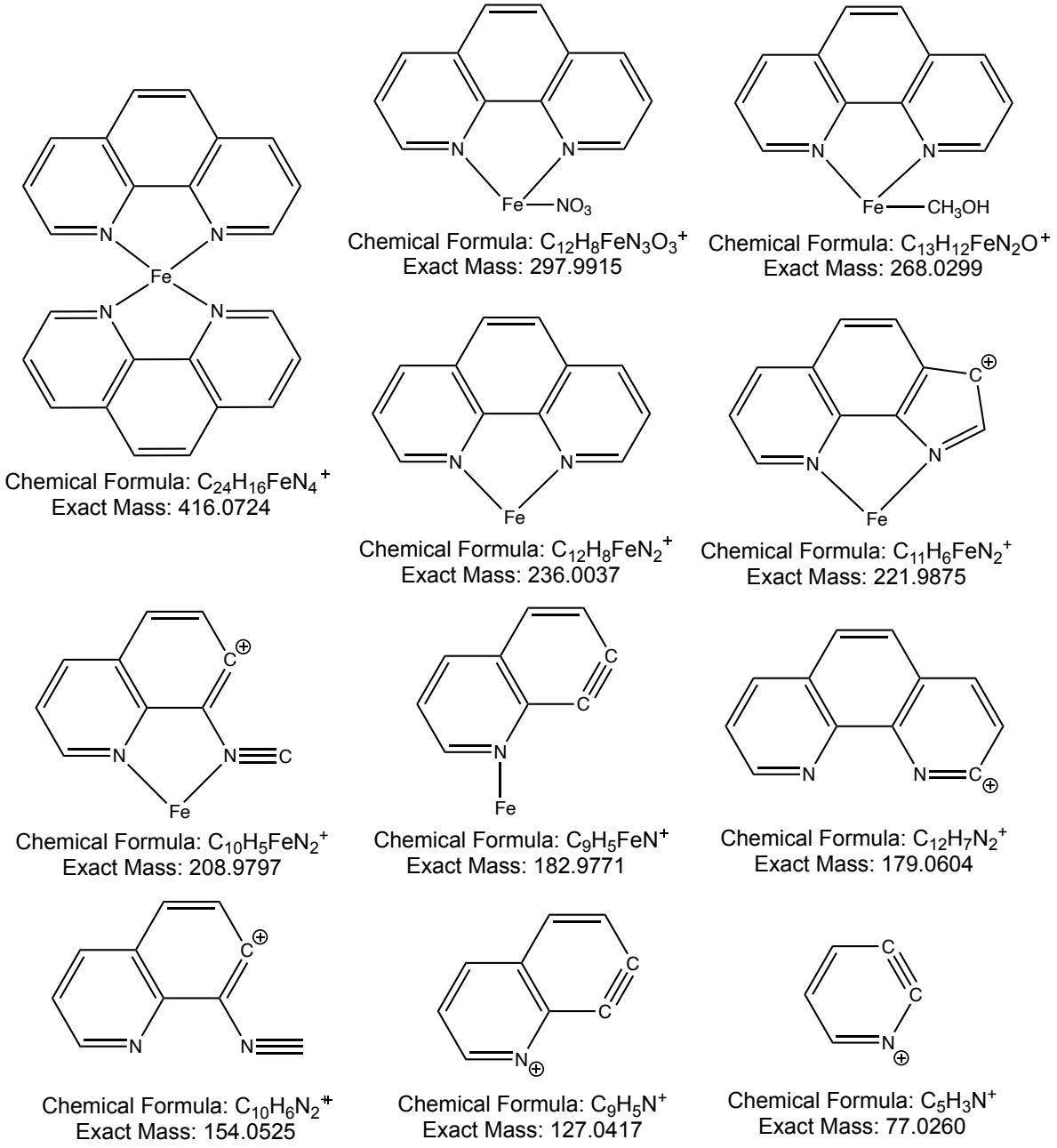

Figure 5.15 Possible skeletal ion fragments formed by collision induced dissociation of Iron (III) Nitrate and 1,10-Phenanthroline.

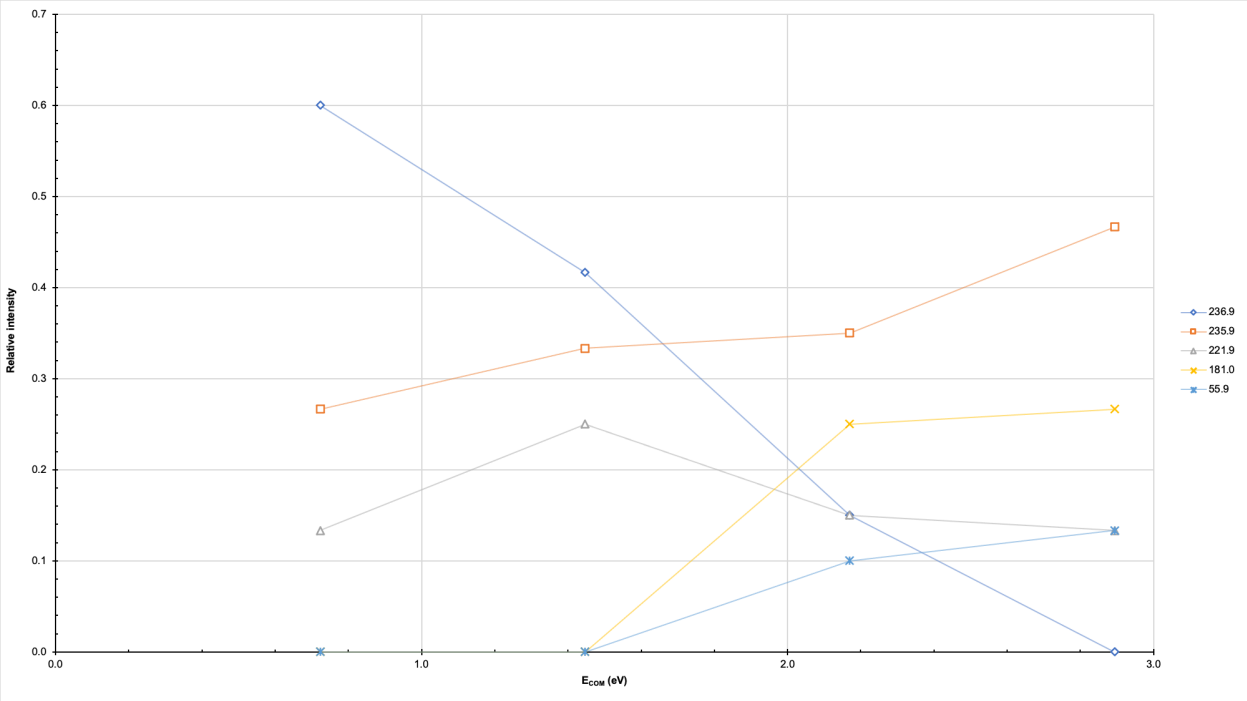

Figure 5.16 Breakdown diagram for the 1:1 complex of Iron (III) Nitrate and 1,10-Phenanthroline ($FeC_{12}H_8N_2^+$) at 235.9 m/z in the transfer from 0-20eV, single-spray.

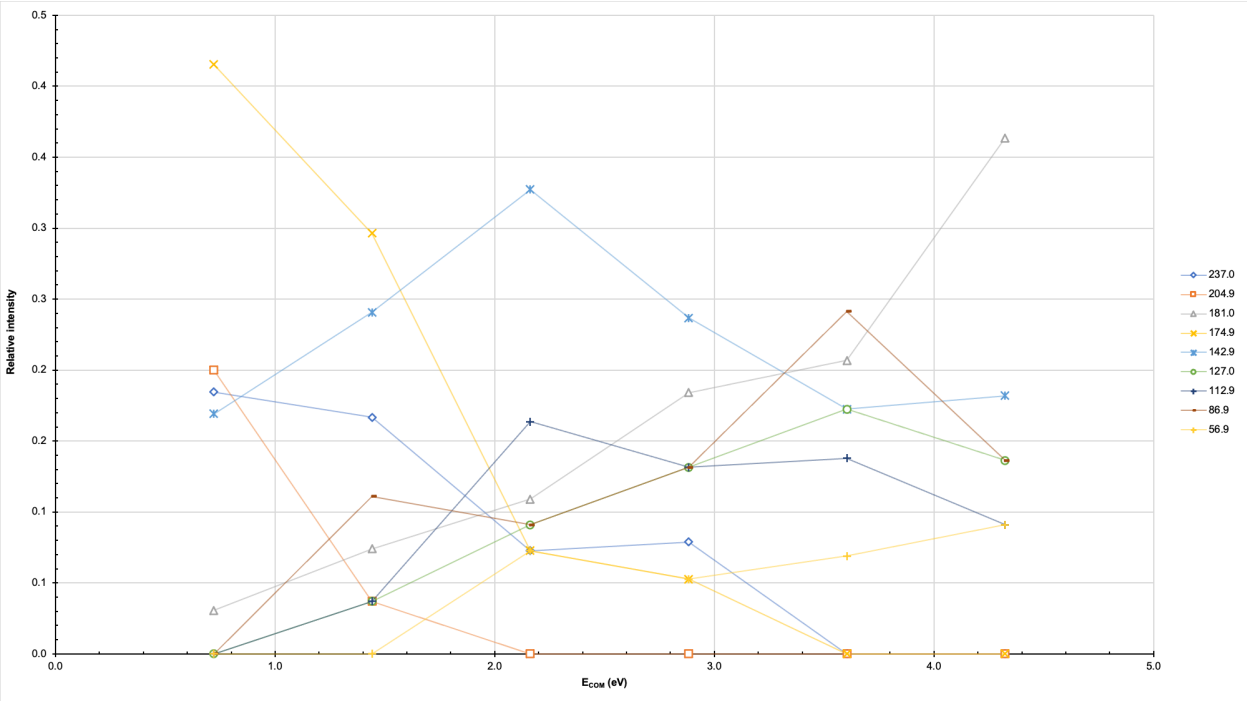

Figure 5.17 Breakdown diagram for the 1:1 complex of Iron (III) Nitrate and 1,10-Phenanthroline ($FeC_{12}H_9N_2^+$) at 236.9 *m/z* in the transfer from 0-30eV, dual-spray.

It is interesting to note that the target ion in dual-spray was found one mass unit above expected 236.9 m/z ($FeC_{12}H_9N_2^+$). Neither breakdown diagram in Figures 5.16 and 5.17 are very clear, as well as quite noisy and are therefore unreliable data. However, many of the same fragments appear in the other figures for both single- and dual-spray methods for this combination.

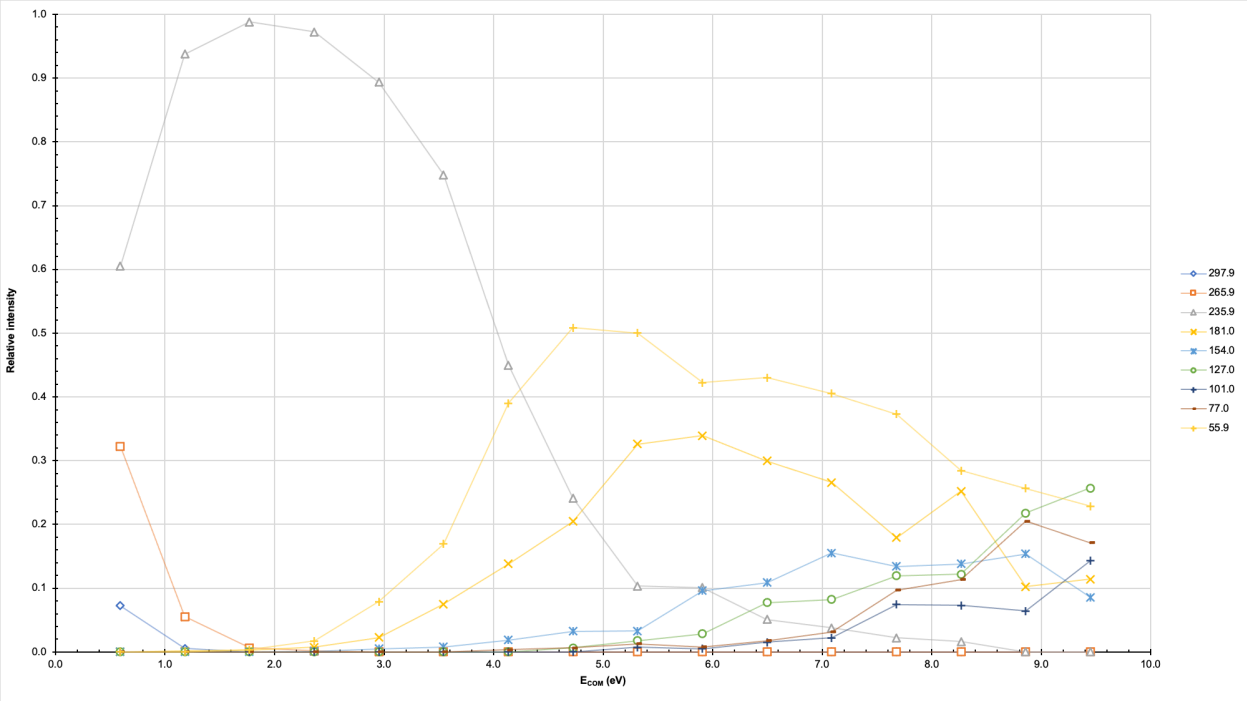

Figure 5.18 Breakdown diagram for the nitrated 1:1 complex of Iron (III) Nitrate and 1,10-Phenanthroline ($FeC_{10}H_8N_2NO_3^+$) at 297.9 *m/z* in the transfer from 0-80eV, single-spray.

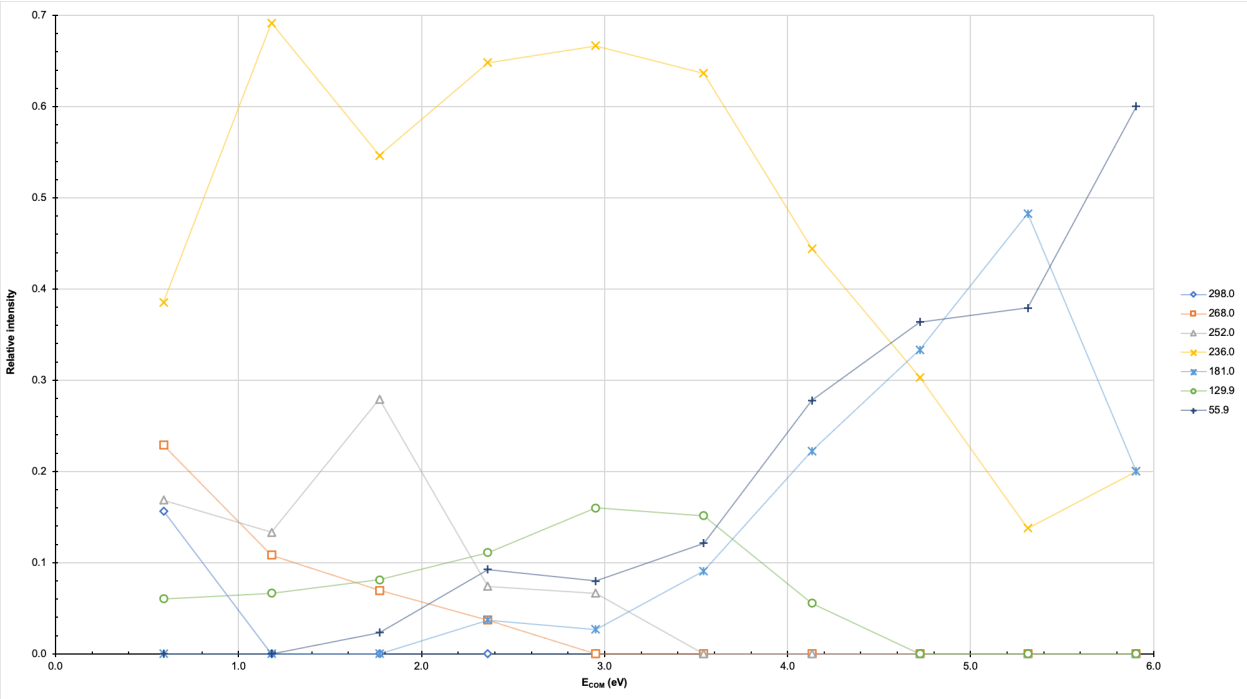

Figure 5.19 Breakdown diagram for the nitrated 1:1 complex of Iron (III) Nitrate and 1,10-Phenanthroline ($FeC_{10}H_8N_2NO_3^+$) at 298.0 *m/z* in the transfer from 0-50eV, dual-spray.

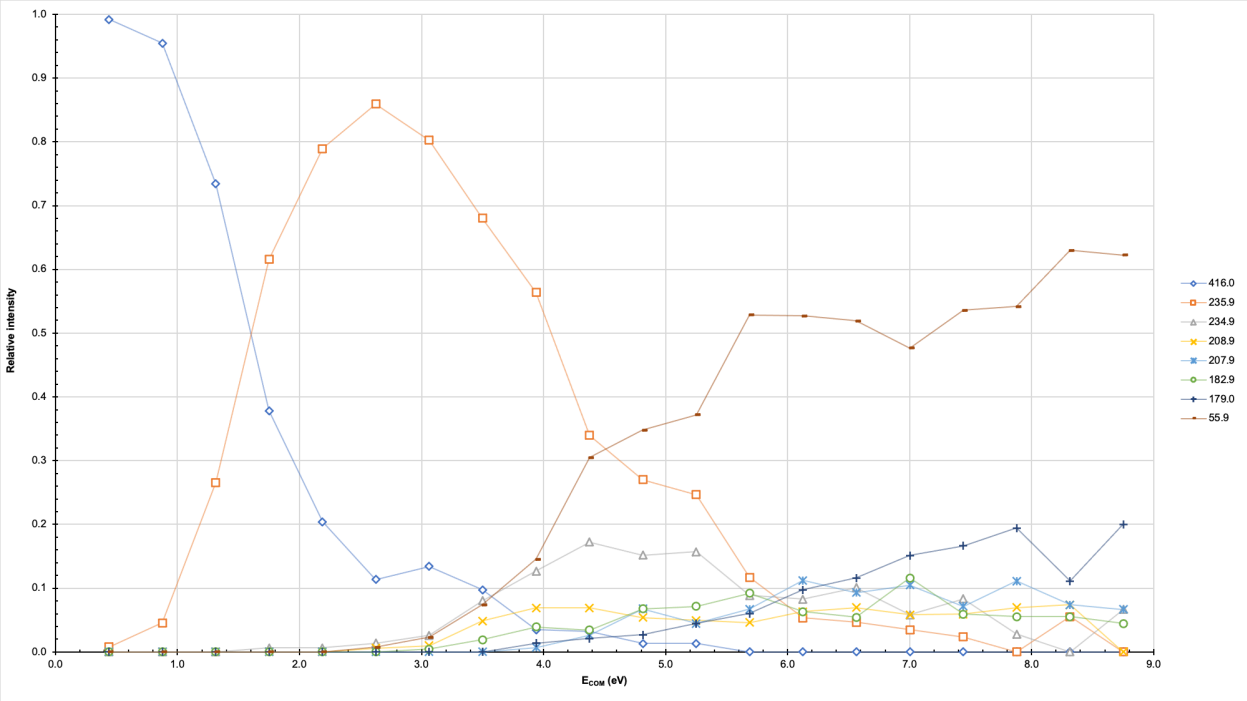

Figure 5.20 Breakdown diagram for the 1:2 complex of Iron (III) Nitrate and 2,2'-Bipyridine ($FeC_{10}H_8N_2C_{10}H_8N_2^+$) at 416.0 *m/z* in the transfer from 0-100eV, single-spray.

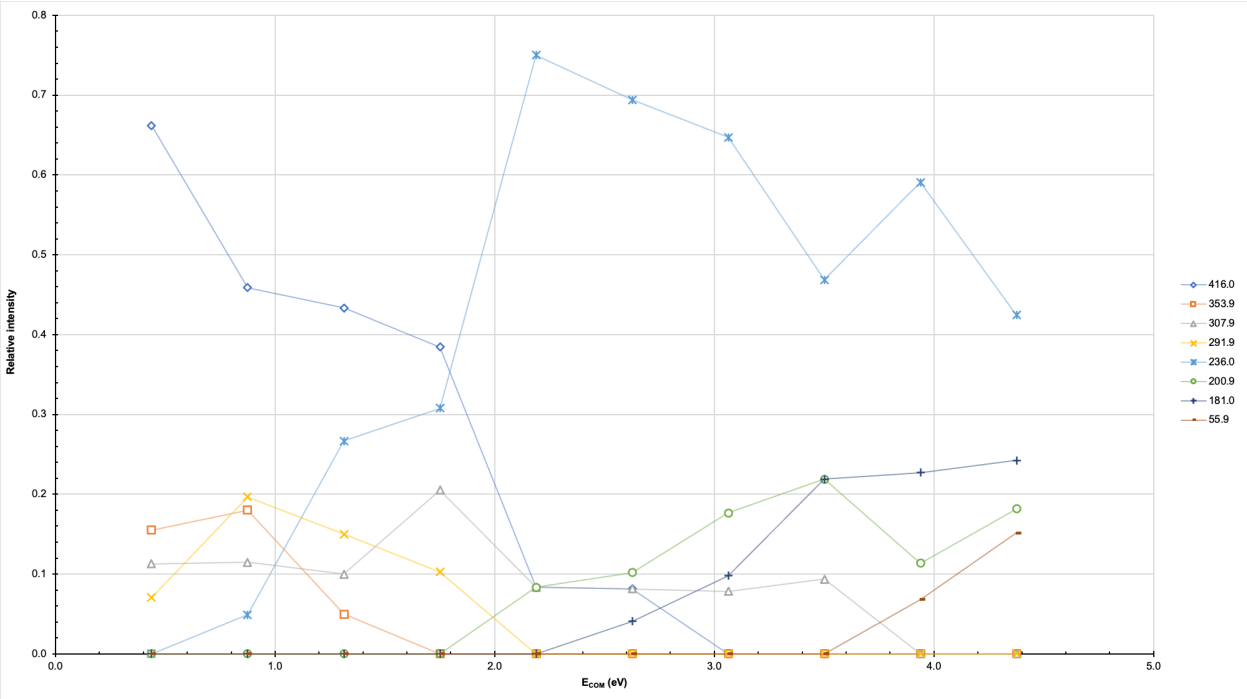

Figure 5.21 Breakdown diagram for the 1:2 complex of Iron (III) Nitrate and 2,2'-Bipyridine ($FeC_{10}H_8N_2C_{10}H_8N_2^+$) at 416.0 *m/z* in the transfer from 0-50eV, dual-spray.

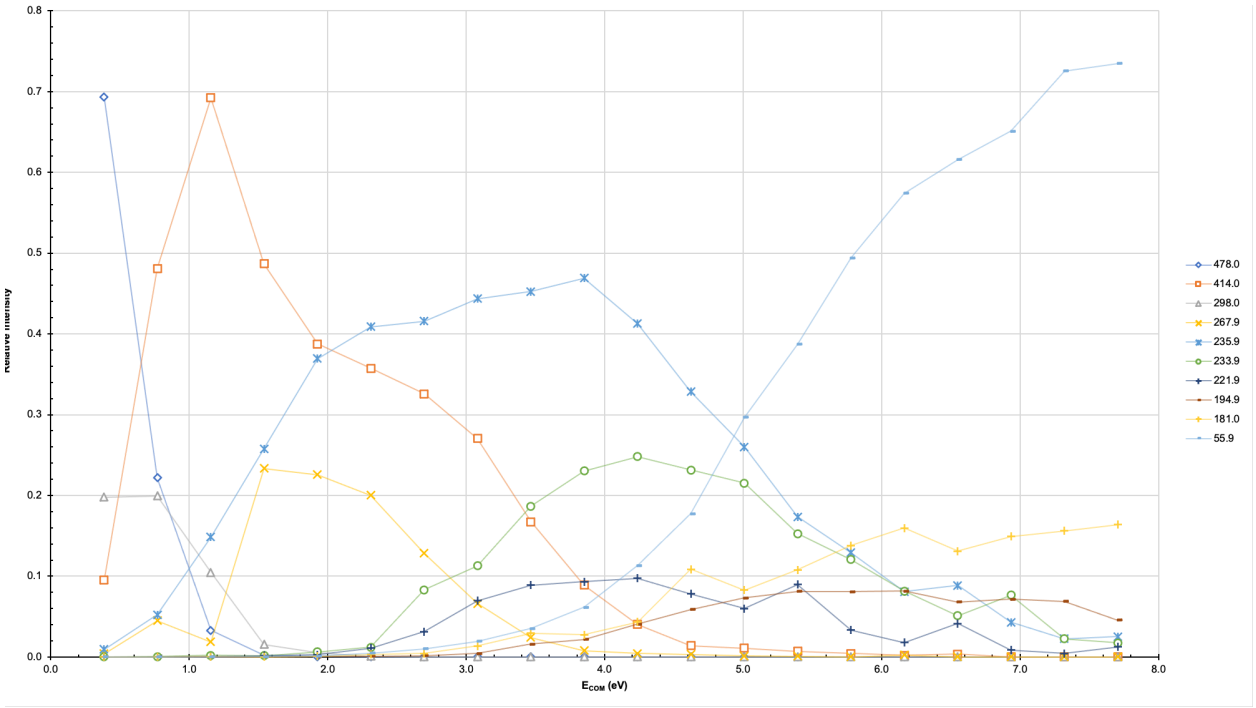

Figure 5.22 Breakdown diagram for the nitrated 1:2 complex of Iron (III) Nitrate and 2,2'-Bipyridine ($FeC_{10}H_8N_2C_{10}H_8N_2NO_3^+$) at 478.0 *m/z* in the transfer from 0-100eV, single-spray.

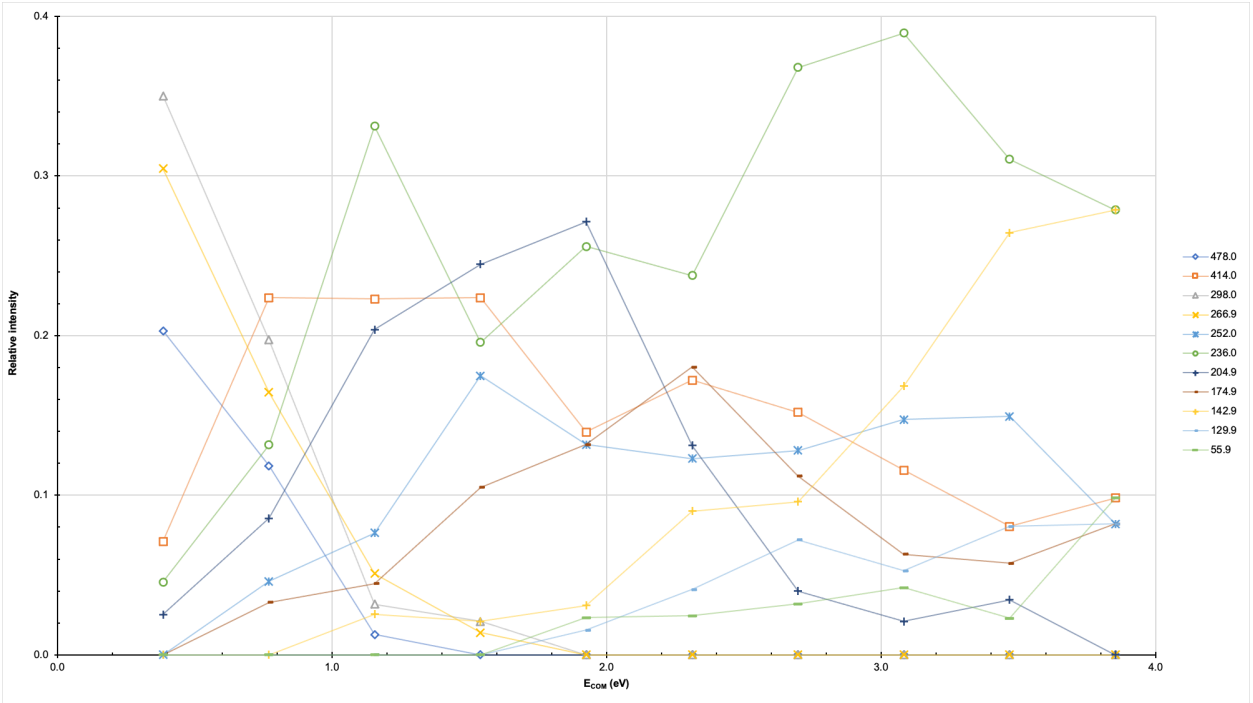

Figure 5.23 Breakdown diagram for the nitrated 1:2 complex of Iron (III) Nitrate and 2,2'-Bipyridine ($FeC_{10}H_8N_2C_{10}H_8N_2NO_3^+$) at 477.9 *m/z* in the transfer from 0-50eV, dual-spray.

In summary, both the Nickel (II) Nitrate and Iron (III) Nitrate combinations with 1,10-Phenanthroline overall were successful at creating their target complexes. The exception to this is the 1:1 metal: ligand compound for each of the combinations as the intensity in the breakdown diagram is not as clear as the rest and very low collision energies were reached. The nickel combination gave clear and consistent results across all breakdown diagrams, regardless of trap or transfer experiments. Also, although the iron combination created a constant pattern in the breakdown diagrams formed from the collected data, the dual-spray method was much less effective at giving clear and accurate data. Therefore, the nickel combination was more reactive in both the gas and liquid phases of mixing whereas the iron preferred the liquid phase with ample time to react.

5.2 Summary of Results

Table 5.4 Summary of results for the phenanthroline ligand.

1,10-Phenanthroline				
Metal Solution	*Metal to Ligand Ratio*	*Expected m/z*	*Analysed m/z*	
			Single-Spray	*Dual-Spray*
Nickel (II) Nitrate	M:1L	237.9	237.9	238.0
	M_{NO_3}:1L	299.9	299.9	300.0
	M:2L	418.0	418.0	418.0
	M_{NO_3}:2L	480.0	480.0	480.0
Iron (III) Nitrate	M:1L	235.9	✗	✗
	M_{NO_3}:1L	297.9	297.9	297.9
	M:2L	416.0	416.0	416.0
	M_{NO_3}:2L	478.0	478.0	478.0

CHAPTER 6 – GAS PHASE REACTIVITY OF METAL COMPLEXES: SNS LIGAND

6.1 Data and Results

In the single-spray (mixture) method with the Nickel (II) Nitrate solution, the 1:1 metal: ligand complex less one hydrogen, $NiC_{14}H_{12}NS_2^+$, was observed at 315.9 and 317.9 *m/z*. The nitrated 1:1 complex less two hydrogens, $NiC_{14}H_{11}NS_2NO_3^+$, was observed at 376.9 and 378.9 *m/z*. The 1:2 complex less one hydrogen, $NiC_{14}H_{13}NS_2C_{14}H_{12}NS_2^+$, was observed at 575.0 and 577.0 *m/z* but only in the single-spray method. Finally, the nitrated 1:2 complex less four hydrogens, $NiC_{14}H_{13}NS_2C_{14}H_9NS_2NO_3^+$, was observed at 633.9 and 635.9 *m/z* but again only in the single-spray method. Complexes marked with an asterisk (*) confirm the presence of Nickel by the breakdown diagram of the second isotope containing complex. All results can be found in the following figures, as well as in the appendix.

Table 6.1 Nickel (II) Nitrate and SNS ligand fragment mass-to charge values and their possible molecular formulas.

Mass-to-Charge Value	*Possible Molecular Formula*
633.9*	$NiC_{14}H_{13}NS_2C_{14}H_9NS_2NO_3^+$
619.0*	$NiC_{14}H_{13}NS_2C_{13}H_6NS_2NO_3^+$
604.0*	$NiC_{14}H_{13}NS_2C_{14}H_{11}NSNO_3^+$
575.0*	$NiC_{14}H_{13}NS_2C_{14}H_{13}NS_2^+$
392.9*	$NiC_{14}H_{13}NC_{10}H_6N^+$
376.9*	$NiC_{14}H_{11}NS_2NO_3^+$
330.9*	$NiC_{13}H_9NSNO_3^+$
315.9*	$NiC_{14}H_{12}NS_2^+$
281.9*	$NiC_{14}H_{10}NS^+$
267.9*	$NiC_{13}H_8NS^+$
240.9*	$NiC_{13}H_{13}N^+$
224.0	$C_{14}H_{10}NS^+$
212.0	$C_{13}H_{10}NS^+$
181.9*	$NiC_6H_6NS^+$
152.0	$C_{11}H_6N^+$
135.0	$C_7H_5NS^+$
122.9*	$NiC_4H_3N^+$
109.0	$C_6H_5S^+$
77.0	$C_6H_5^+$
57.9	Ni^+

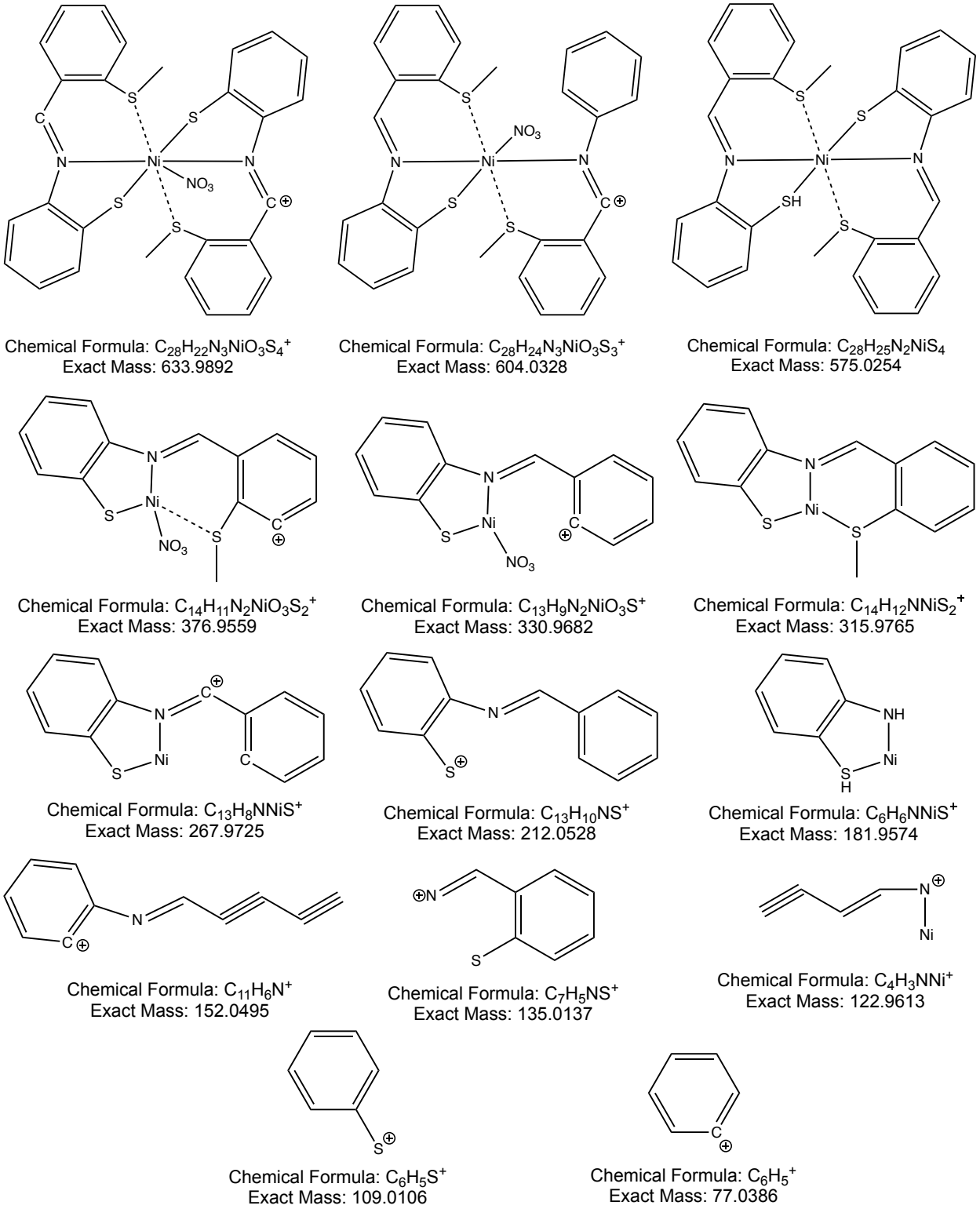

Figure 6.1 Possible skeleton ion fragments formed by collision induced dissociation of Nickel (II) Nitrate and SNS ligand.

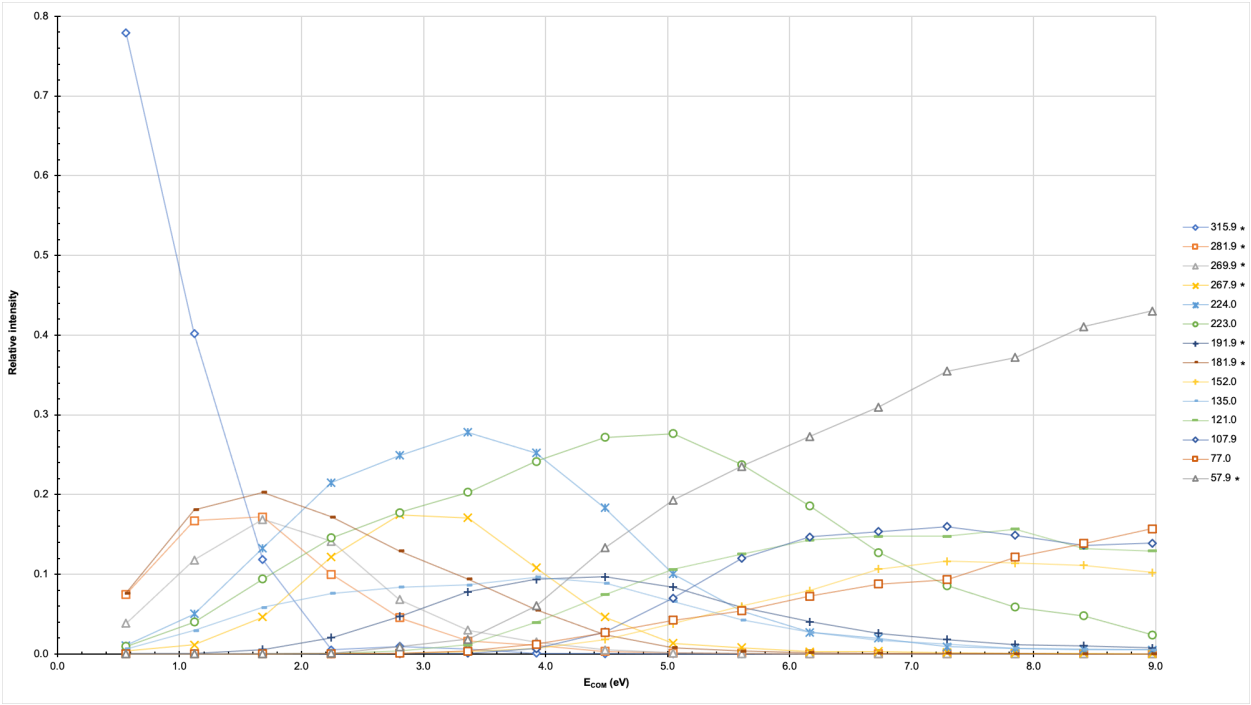

Figure 6.2 Breakdown diagram for the 1:1 complex of Nickel (II) Nitrate and SNS ligand ($NiC_{14}H_{12}NS_2^+$) at 315.9 *m/z* in the transfer from 0-80eV, single-spray.

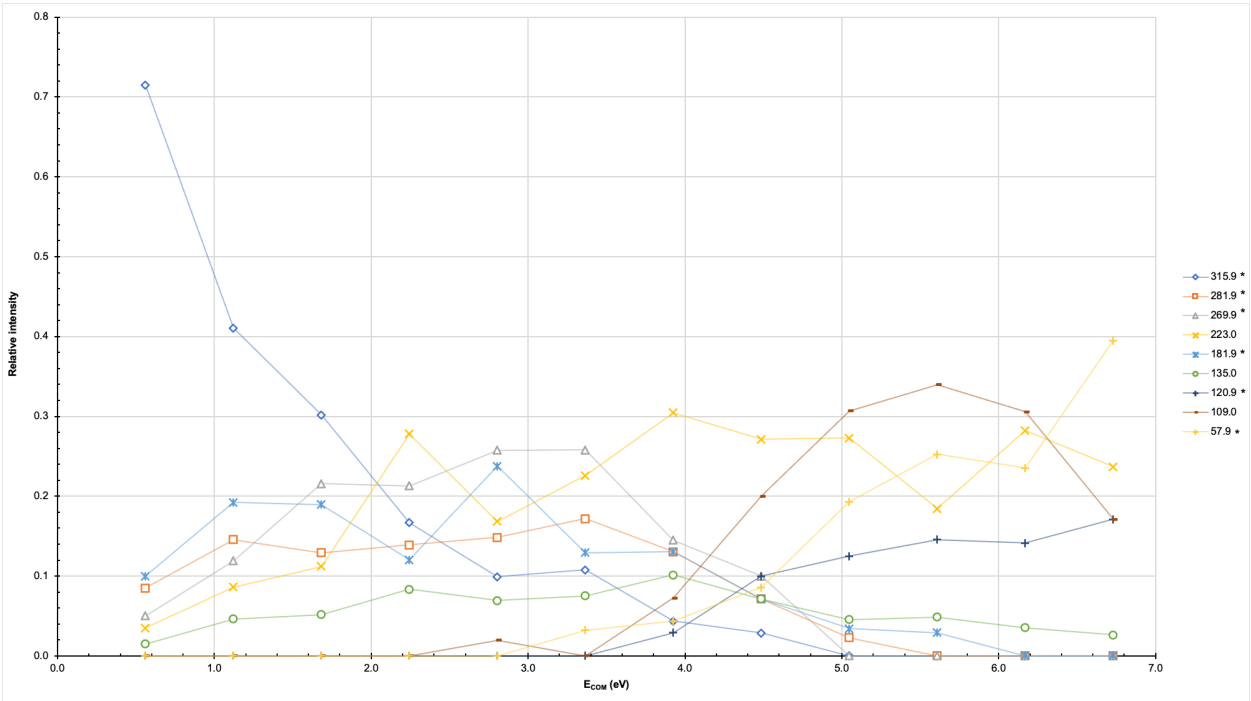

Figure 6.3 Breakdown diagram for the 1:1 complex of Nickel (II) Nitrate and SNS ligand ($NiC_{14}H_{12}NS_2^+$) at 315.9 *m/z* in the transfer from 0-60eV, dual-spray.

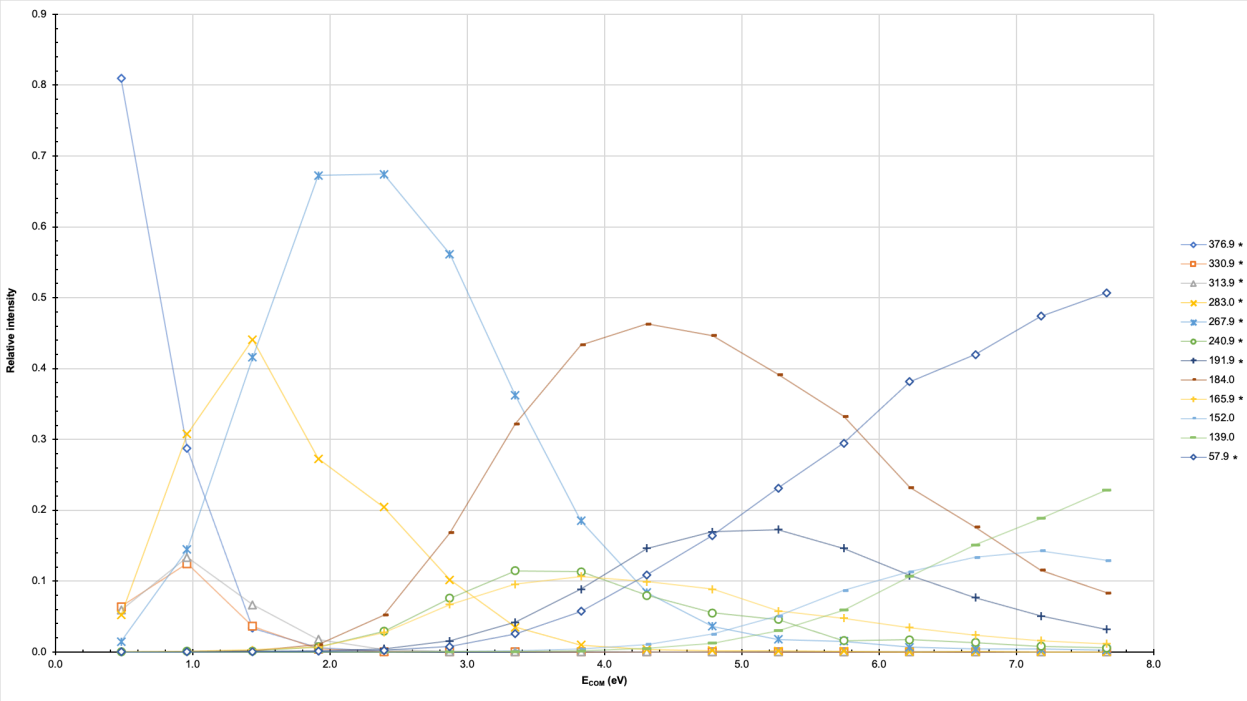

Figure 6.4 Breakdown diagram for the nitrated 1:1 complex of Nickel (II) Nitrate and SNS ligand ($NiC_{14}H_{11}NS_2NO_3^+$) at 376.9 *m/z* in the transfer from 0-80eV, single-spray.

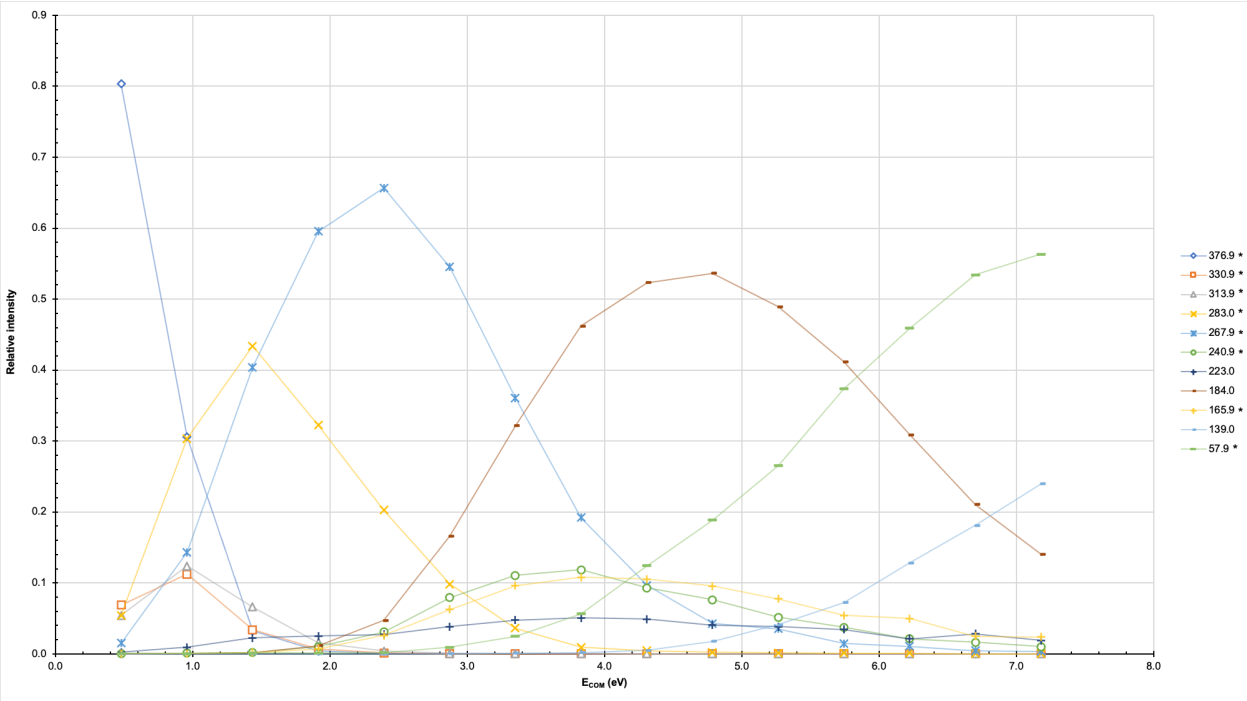

Figure 6.5 Breakdown diagram for the nitrated 1:1 complex of Nickel (II) Nitrate and SNS ligand ($NiC_{14}H_{11}NS_2NO_3^+$) at 376.9 *m/z* in the transfer from 0-75eV, dual-spray.

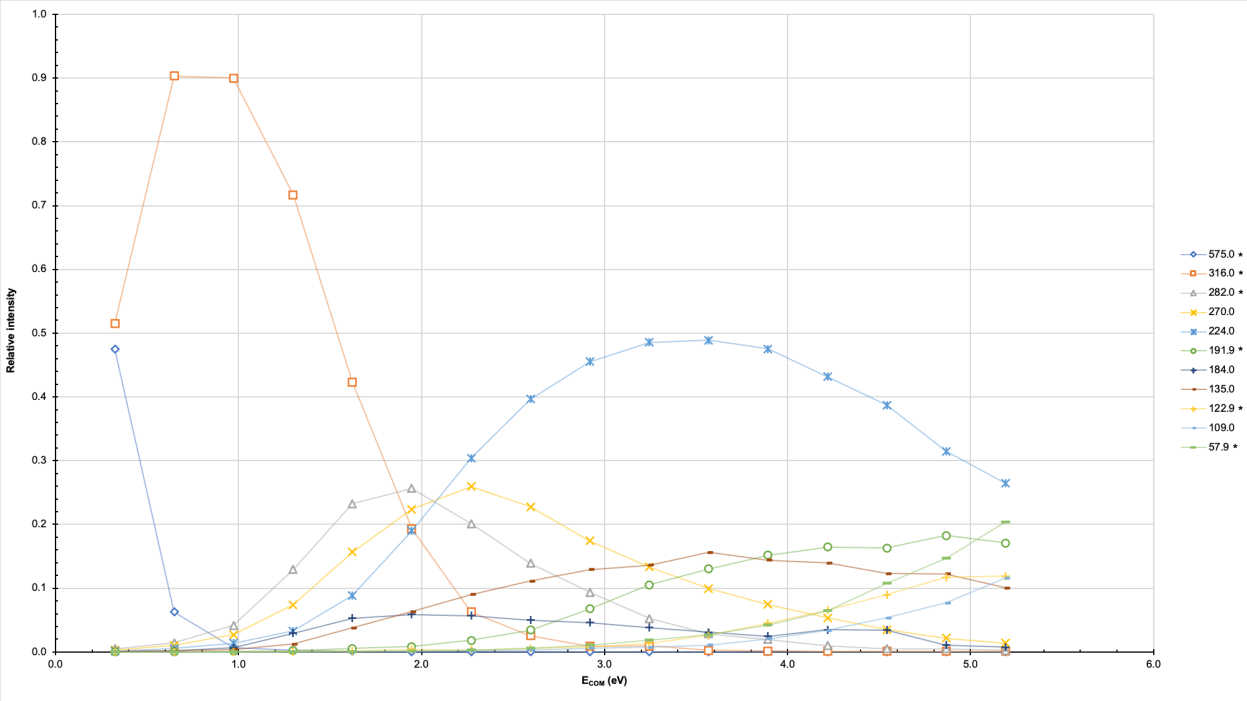

Figure 6.6 Breakdown diagram for the 1:2 complex of Nickel (II) Nitrate and SNS ligand ($NiC_{14}H_{13}NS_2C_{14}H_{12}NS_2^+$) at 575.0 *m/z* in the transfer from 0-80eV, single-spray.

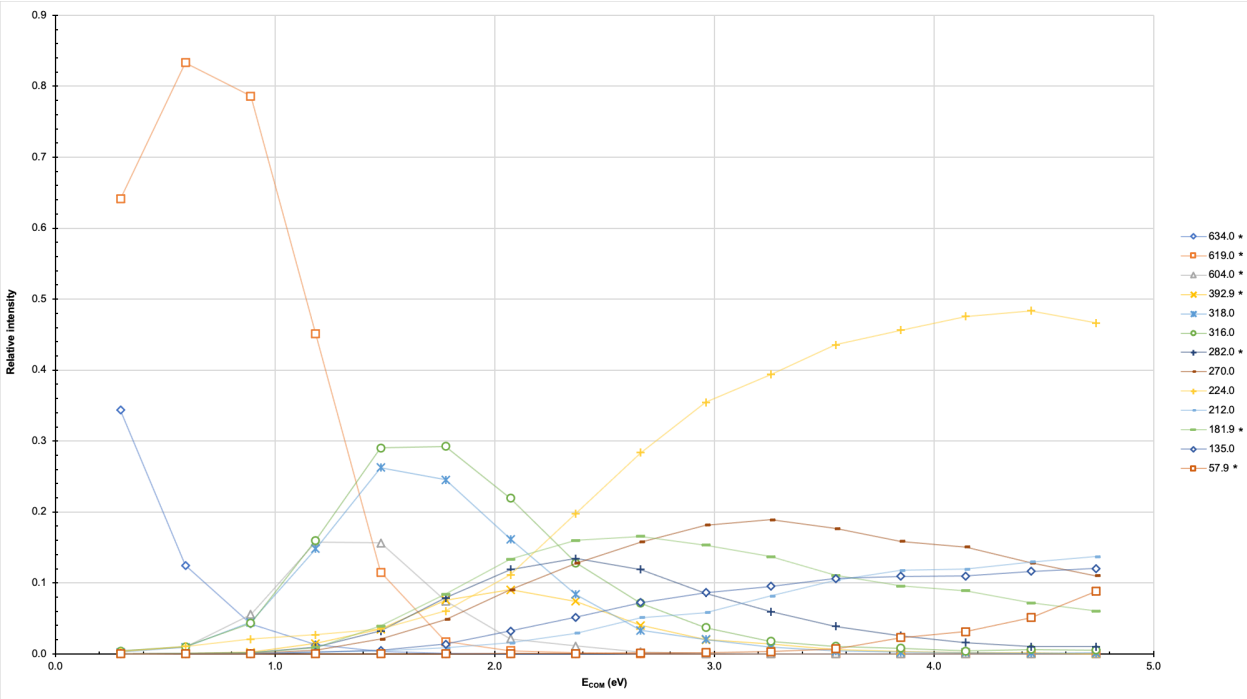

Figure 6.7 Breakdown diagram for the 1:2 complex of Nickel (II) Nitrate and SNS ligand ($NiC_{14}H_{13}NS_2C_{14}H_9NS_2NO_3^+$) at 633.9 *m/z* in the transfer from 0-80eV, single-spray.

Using only one isotope of iron, the experiments were repeated using Iron (III) Nitrate as the metal solution. In both the single- and dual-spray experiments, the 1:1 metal: ligand complex less two hydrogens $FeC_{14}H_{11}NS_2^+$, was observed at 312.9 *m/z*. The nitrated 1:1 complex less two hydrogens, $FeC_{14}H_{11}NS_2NO_3^+$, was observed at 374.9 *m/z*. The 1:2 complex plus three hydrogens, $FeC_{14}H_{13}NS_2C_{14}H_{16}NS_2^+$, was observed at 577.0 *m/z* but for single-spray only. Finally, the nitrated 1:2 complex less four hydrogens, $FeC_{14}H_{13}NS_2C_{14}H_9NS_2NO_3^+$, was observed at 631.9 *m/z* but for single-spray only. All results can be found in the following figures.

Table 6.2 Iron (III) Nitrate and SNS fragment mass-to charge values and their possible molecular formulas.

Mass-to-Charge Value	*Possible Molecular Formula*
632.0	$FeC_{14}H_{13}NS_2C_{14}H_9NS_2NO_3^+$
375.0	$FeC_{14}H_{11}NS_2NO_3^+$
345.0	$FeC_{14}H_{13}NSNO_3^+$
326.9	$FeC_{13}H_7NSNO_3^+$
312.9	$FeC_{14}H_{11}NS_2^+$
298.9	$FeC_{13}H_9NS_2^+$
283.0	$FeC_{14}H_{13}NS^+$
266.0	$FeC_{13}H_8NS^+$
189.9	$FeC_{11}H_{12}NS^+$
173.9	$C_{10}H_8NS^+$
163.9	$C_9H_{10}NS^+$
157.9	$FeC_7H_4N^+$
107.9	$C_6H_4S^+$
55.9	Fe^+

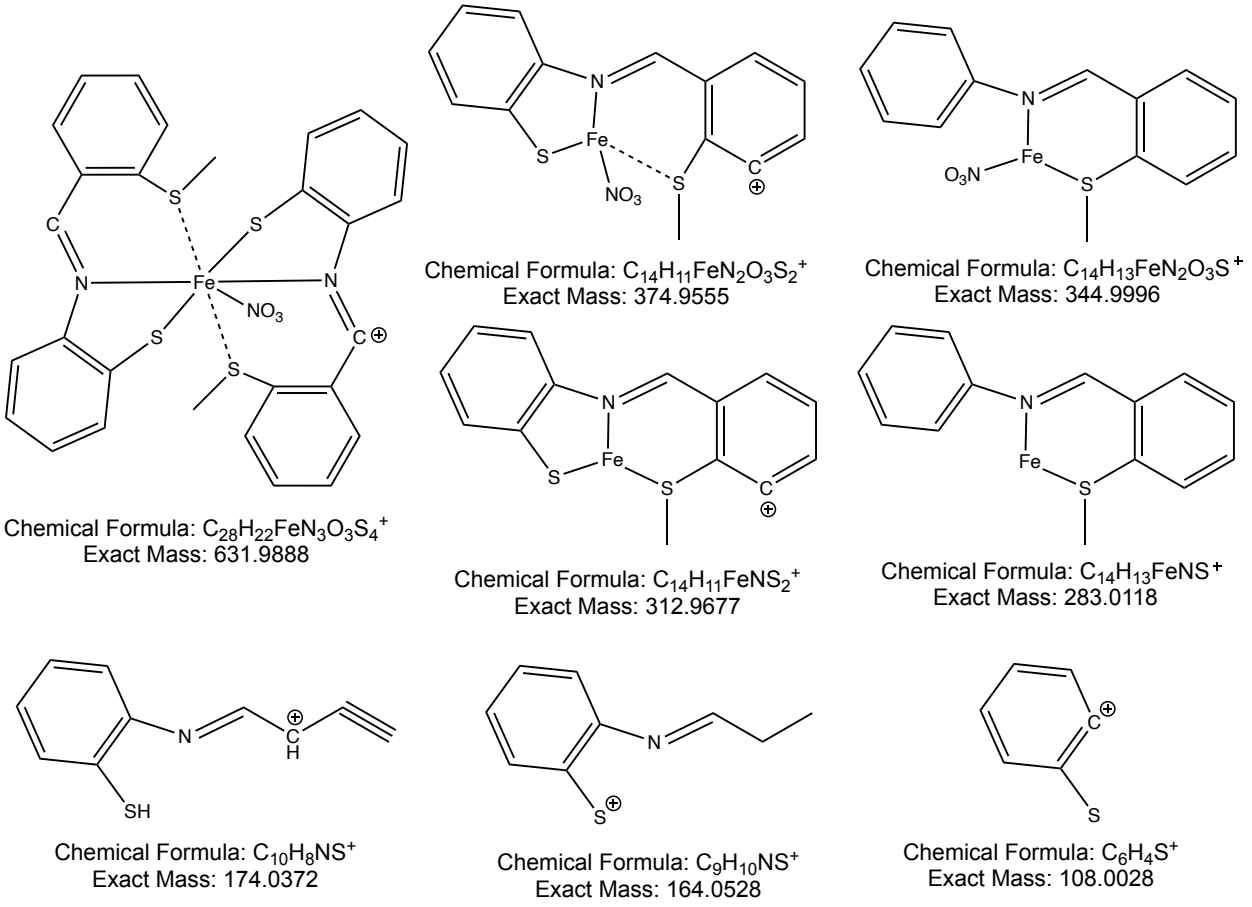

Figure 6.8 Possible skeletal ion fragments formed by collision induced dissociation of Iron (III) Nitrate and SNS Ligand.

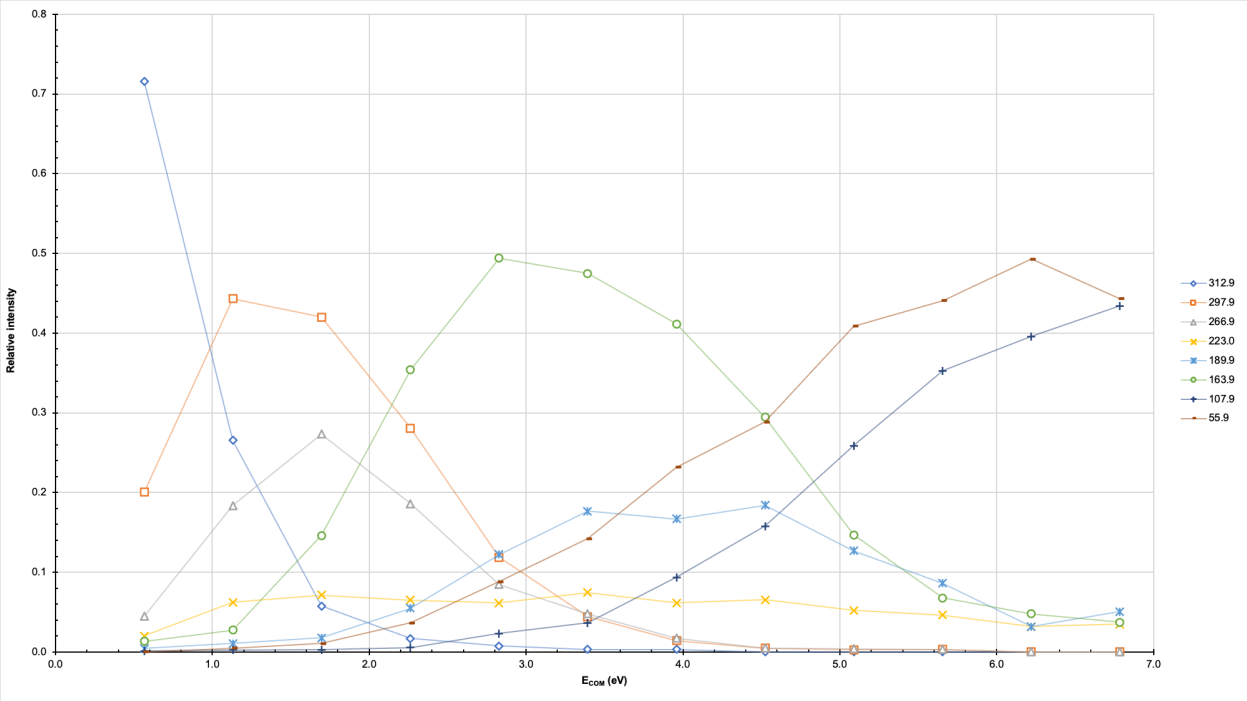

Figure 6.9 Breakdown diagram for the 1:1 complex of Iron (III) Nitrate and SNS ($FeC_{14}H_{11}NS_2^+$) at 312.9 *m/z* in the transfer from 0-60eV, single-spray.

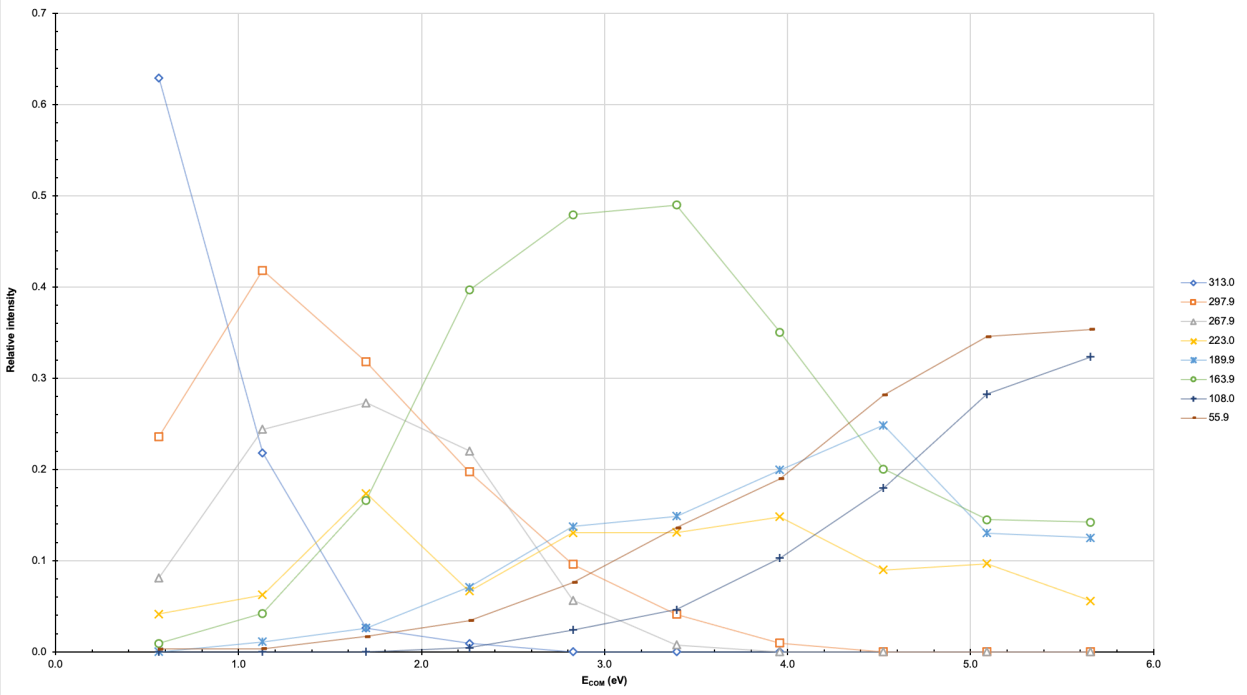

Figure 6.10 Breakdown diagram for the 1:1 complex of Iron (III) Nitrate and SNS ($FeC_{14}H_{11}NS_2^+$) at 312.9 *m/z* in the transfer from 0-55eV, dual-spray.

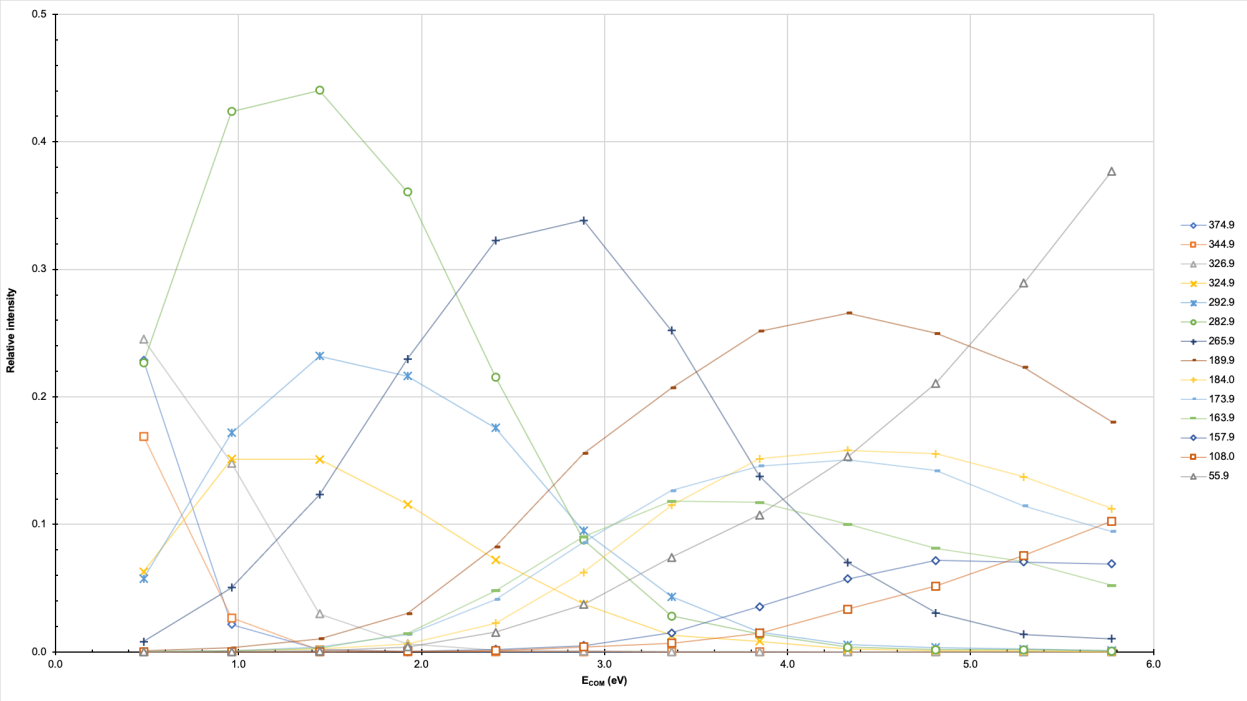

Figure 6.11 Breakdown diagram for the nitrated 1:1 complex of Iron (III) Nitrate and SNS ($FeC_{14}H_{11}NS_2NO_3^+$) at 374.9 *m/z* in the transfer from 0-60eV, single-spray.

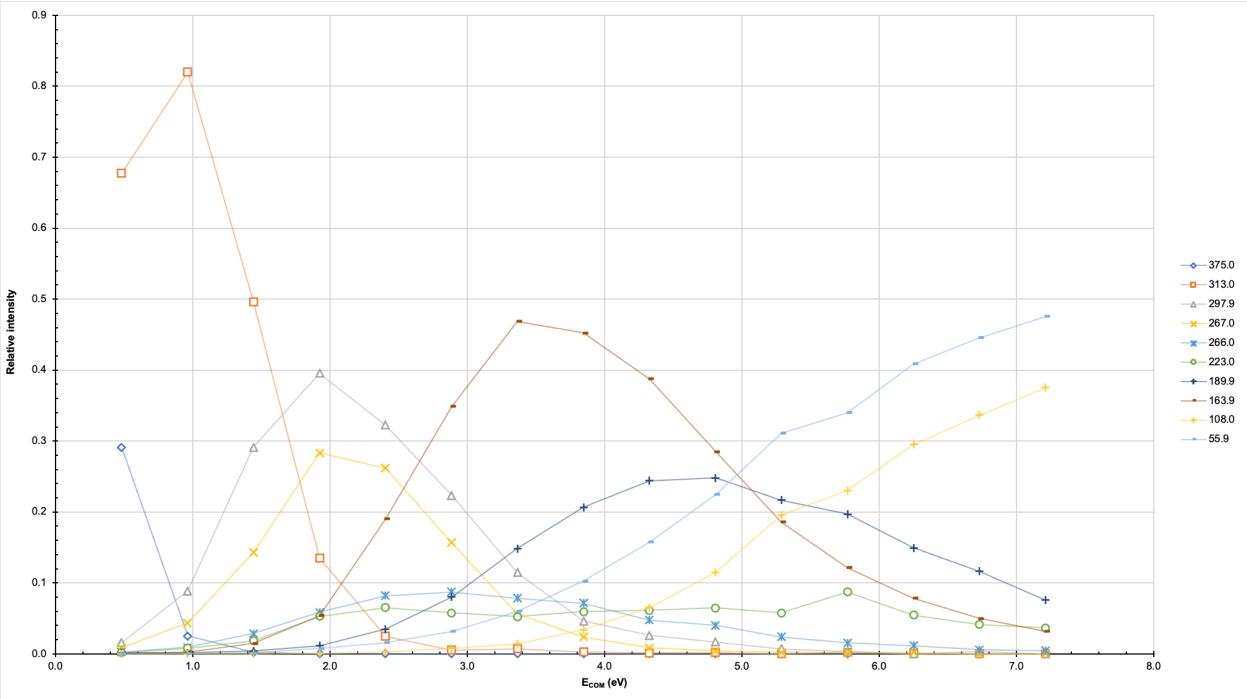

Figure 6.13 Breakdown diagram for the nitrated 1:1 complex of Iron (III) Nitrate and SNS ($FeC_{14}H_{11}NS_2NO_3^+$) at 375.0 *m/z* in the transfer from 0-75eV, dual-spray.

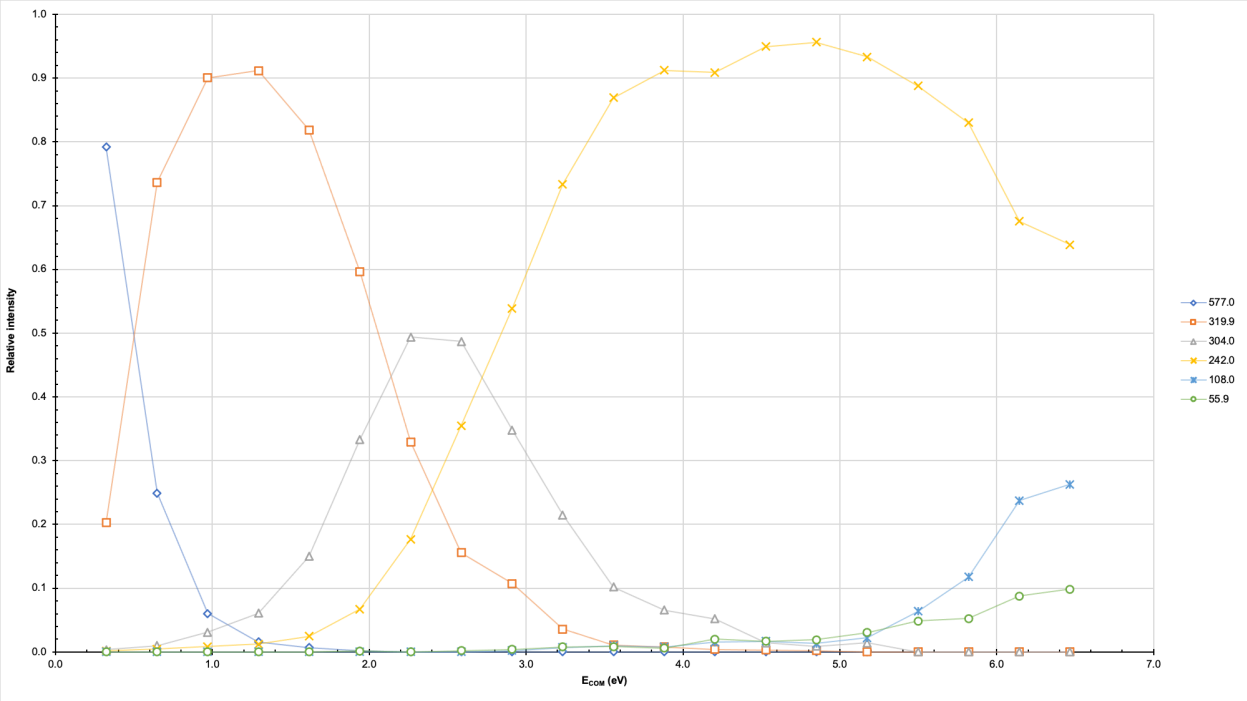

Figure 6.14 Breakdown diagram for the 1:2 complex of Iron (III) Nitrate and SNS ($FeC_{14}H_{13}NS_2C_{14}H_{16}NS_2^+$) at 577.0 *m/z* in the transfer from 0-100eV, single-spray.

Although Figure 6.14 displays some expected patterns and similar fragments, the target ion complex is not at all like the rest of the ions analyzed and therefore is not reliable data to compare to the other results.

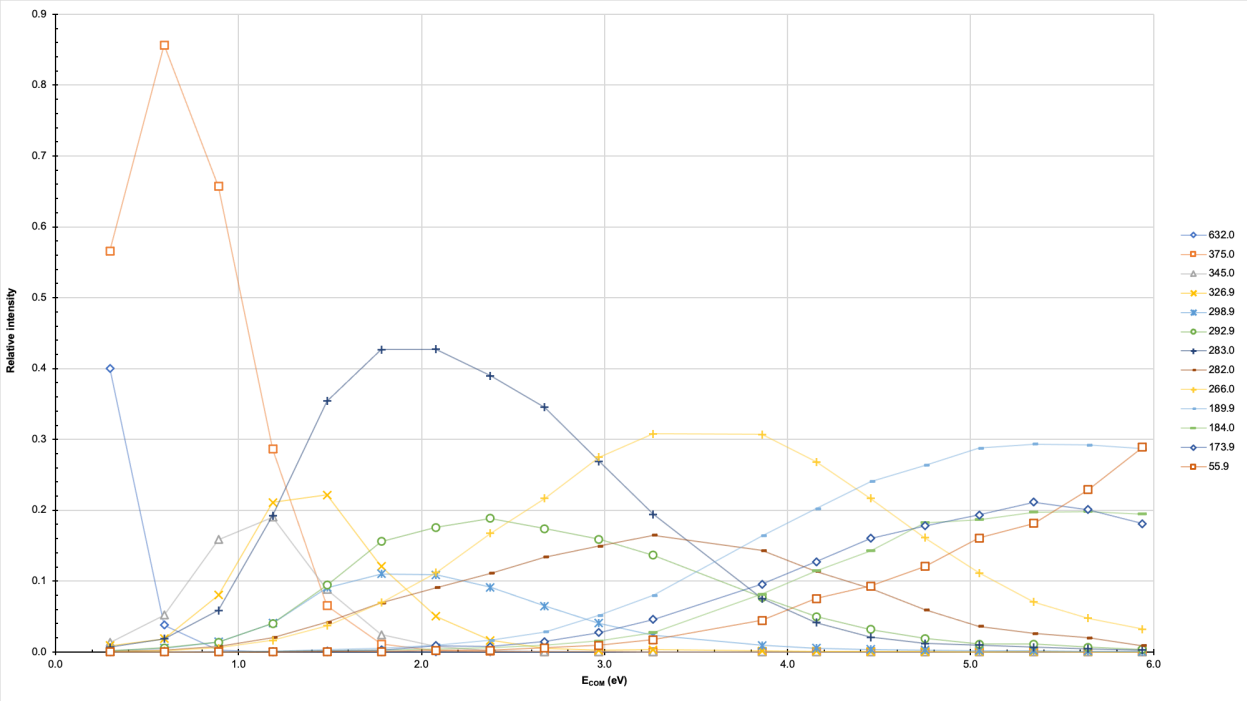

Figure 6.15 Breakdown diagram for the nitrated 1:2 complex of Iron (III) Nitrate and SNS ($FeC_{14}H_{13}NS_2C_{14}H_9NS_2NO_3^+$) at 632.0 *m/z* in the transfer from 0-100eV, single-spray.

In summary, both the Nickel (II) Nitrate and Iron (III) Nitrate combinations with the Baker Group SNS ligand were overall successful at creating their target complexes when looking at the single-spray method. On the other hand, the dual-spray method was only successful for the 1:1 metal: ligand compounds for each combination. It was evident in the breakdown diagrams that the dual-spray method was much less effective and created much noisier results even with the compounds it was successful with. It is made clear that these compounds do not react as effectively in the gas phase as they do in the liquid phase, particularly with time to go to completion.

6.2 Summary of Results

Table 6.3 Summary of results for the SNS ligand.

SNS				
Metal Solution	*Metal to Ligand Ratio*	*Expected m/z*	*Analysed m/z*	
			Single-Spray	*Dual-Spray*
Nickel (II) Nitrate	M:1L	316.9	315.9	315.9
	M_{NO_3}:1L	378.9	376.9	376.9
	M:2L	576.0	575.0	✗
	M_{NO_3}:2L	638.0	633.9	✗
Iron (III) Nitrate	M:1L	314.9	312.9	312.9
	M_{NO_3}:1L	376.9	374.9	375.0
	M:2L	574.0	577.0	✗
	M_{NO_3}:2L	636.0	632.0	✗

CHAPTER 7 – CONCLUSIONS AND FUTURE DIRECTIONS

Electrospray Ionization paired with Quadrupole Time-of-Flight mass spectrometry has proven to be a valuable method of analysing coordination complexes with Nickel and Iron Nitrate solutions. Dual-spray and TRESI techniques deliver unique data and allow comparisons between gas- and liquid-phase real-time mixing of solutions. However, these techniques are not always successful as they require relatively fast reaction times for the compounds being analysed. TRESI has the distinctive ability to adjust mixing volumes in order to prolong the reaction time before the solution enters the instrument, however, small adjustments do not generally impact the results. The dual-spray method proved to give very similar results as compared to the single-spray mixture solutions. It was found that the compounds of choice do not largely differ in their breakdown pathways when subjected to these techniques.

Overall, smaller ligands such as the 2,2'-Bipyridine, 4,4'-Bipyridine and 1,10-Phenanthroline were more successful in all three techniques as compared to the larger or more complex ligands such as 2,2'-Bipyridine-4,4'-Dicarboxylic Acid and the Baker Group's SNS ligand. The ligand combinations with the Iron (III) Nitrate solution typically posed more problems and less results than the Nickel (II) Nitrate solution combinations. The SNS ligand was unable to undergo dual-spray analysis as was the case with the 2,2'-Bipyridine-4,4'-Dicarboxylic Acid ligand. The SNS ligand also proved difficult to analyze using the proposed methods due to its "open" form anionic properties. The 2,2'-Bipyridine-4,4'-Dicarboxylic Acid ligand gave the most resistance to analysis overall and was only successful with the Nickel (II) Nitrate solution in the single-spray method. This is likely

due to the size and solubility of the molecule itself. It needed the most time to react and did not flow through the instrument as easily as the other solutions used in this research. It was proven that the functional groups do indeed play a role in the coordination of such complexes. It is likely that acidic functional groups interfere with these interactions making the complex less successful in these techniques.

Additionally, the TRESI technique provided an excellent comparison method between the single- and dual-spray techniques. However, little to no change was seen across the spectra (see appendix) for each combination. More work should be done to investigate this technique further in regard to coordination complexes as it may prove to be an invaluable resource. Perhaps more length should be added to the inner capillary, or use a wider capillary entirely, to provide a larger capacity for mixing and extend the reaction time of a solution before it undergoes analysis. It was learned that many reactions are complete within the first hours of mixing but only 60 seconds of reaction time is provided with a capillary length of 10 cm. This technique should also be applied to other combinations of metals and ligands known to react quickly in solution.

When performing collision induced dissociation experiments, only the transfer cell should be used so as to avoid the coordination of water to the complexes of interest. Other free-floating molecules such as methanol, hydrogen and nitrogen atoms were observed to coordinate as well but could not be avoided. Many fragments across breakdown diagrams appeared to differ by one or more hydrogen atoms. This is likely due to the excess of ions within the instrument. However, the isotopic patterns of each of the skeletal ions also play a role in this difference.

In the future, more analysis could be conducted into these unexplained coordination problems. It is currently unclear why certain ions coordinate to the fragments after they have dissociated from the precursor ion of interest and not others. It was established that the water fragment came from somewhere in the trap cell, but it is unknown as to why. Additionally, the methanol fragments are explained by the compounds being dissolved in this solution. However, there is no pattern as to which fragments become coordinated.

It would also be helpful to further analyse the differences in fragmentation patterns between the 2,2'-Bipyridine and 4,4'-Bipypridine orientations. The similar results of these two complexes proved to be an interesting discovery as one typically chelates a single metal while the other bridges two metals. Since mass spectrometry can only analyze the molecular weight of these compounds, other techniques would need to be used in order to discern the differences expected between these two combinations.

Moreover, it would be interesting to see this experiment replicated with other metal solutions, including those not containing nitrate molecules. The target complexes of interest in this research included the nitrated versions of the monovalent and divalent complexes. It can be hypothesized that using another solution such as an oxalate would create different target complexes and quite possibly very interesting results. It would also be interesting to use ligands that do not contain nitrogen with the nitrate metal solution. As mentioned previously, those compounds that contain nitrogen tend to create monocations with the coordinated monovalent counterion $[M(L)_mX]^+$.[7] This was proven throughout the duration of this research and would be interesting to investigate further.

In conclusion, this research only begins to explore some of the possible combinations of metal-ligand coordination complexes observed in electrospray mass spectrometry. There are many studies that came before this and many that will come after. As previously discussed, many studies have only focused on the coordination of these complexes in solution, or they used mass spectrometry as a confirmation technique rather than an experimental method. The key is to combine these areas of research to develop a more multifaceted understanding of the behaviours of these coordination complexes in the gas phase. Mass spectrometry is a highly valuable tool in the analysis of coordination chemistry and will only continue to develop in the future.

REFERENCES

1. Vollhardt, K.P.C & Schore, N.E. *Organic Chemistry: Structure and Function*. (W. H. Freeman and Company, 2007).

2. Premier Biosoft. Mass Spectrometry. (2021).

3. Department of Chemistry. Mass Spectrometry Introduction. *University of Pittsburgh*.

4. Atkins, P. W. *et al. Shriver and Atkins' Inorganic Chemistry*. (Oxford University Press, 2010).

5. Traeger, J.C. Electrospray mass spectrometry of organometallic compounds. *International Journal of Mass Spectrometry* 200, 387–401 (2000).

6. McIndoe, J.S. & Vikse, K.L. Assigning the ESI mass spectra of organometallic and coordination compounds. *Journal of Mass Spectrometry* 54, 466–479 (2019).

7. Glasovac, Z. *et al.* Coordination chemistry of nickel(II) nitrate with superbasic guanidines as studied by electrospray mass spectrometry. *International Journal of Mass Spectrometry* 290, 22–31 (2010).

8. History of Coordination Compounds. *LibreTexts* (2017).

9. Schilt, A.A. *Analytical Applications of 1,10-phenanthroline and Related Compounds*. (Elsevier, 1969).

10. Kauffman, G.B. Alfred Werner's Research on Geometrically Isomeric Coordination Compounds. *Coordination Chemistry Reviews* 15, 1–92 (1975).

11. Heinz, B. 'Counting ions' in Alfred Werner's coordination chemistry using electrical conductivity measurements. *Educación Química* 25, 267–275 (2014).

12. Martinez-Bulit, P. *et al.* 2,6-Bis(2,6-diethylphenyliminomethyl)pyridine coordination compounds with cobalt(II), nickel(II), copper(II), and zinc(II): synthesis, spectroscopic characterization, X-ray study and in vitro cytotoxicity. *Journal of Inorganic Biochemistry* 142, 1–7 (2015).

13. Wang, Y.N. *et al.* Novel nickel(II) coordination polymer based on a semi-rigid tricarboxylate acid ligand: synthesis, structure, and fluorescence recognition of acetylacetone in aqueous media. *Journal of Molecular Structure* 1247, 131317 (2022).

14. Sivaev, I.B. & Bregadze, V.I. Chemistry of nickel and iron bis(dicarbollides). A review. *Journal of Organometallic Chemistry* 614–615, 27–36 (2000).

15. Selmi, W., Abdelhak, J., Marchivie, M., Chastanet, G. & Zid, M. F. An investigation by DFT of the electronic structure and magnetic properties of a novel μ-oxo-iron(III) complex with the 1,10-phenathroline ligand. *Polyhedron* 123, 441–452 (2017).

16. Stevenson, B.C. *et al.* An investigation of inter-ligand coordination and flexibility: IRMPD spectroscopic and theoretical evaluation of calcium and nickel histidine dimers. *Journal of Molecular Spectroscopy* 381, 111532 (2021).

17. García-España, E., Díaz, P., Llinares, J.M. & Bianchi, A. Anion coordination chemistry in aqueous solution of polyammonium receptors. *Coordination Chemistry Reviews* 250, 2952–2986 (2006).

18. Szymczak, N.K. & Tyler, D.R. Aspects of dihydrogen coordination chemistry relevant to reactivity in aqueous solution. *Coordination Chemistry Reviews* 252, 212–230 (2008).

19. Rajput, A. & Mukherjee, R. Coordination chemistry with pyridine/pyrazine amide ligands. Some noteworthy results. *Coordination Chemistry Reviews* 257, 350–368 (2013).

20. Eya'ane Meva, F., Prior, T.J., Evans, D.J., Shah, S. & Cespedes, O. Iron(III), cobalt(II) and zinc(II) coordination compounds with a carboximidamide ligand: Synthesis, structures and properties. *Inorganic Chemistry Communications* 121, 108196 (2020).

21. Vacheta, R.W., Hartman, J.R., Gertner, J.W. & Callahan, J.H. Investigation of metal complex coordination structure using collision-induced dissociation and ion–molecule reactions in a quadrupole ion trap mass spectrometer. *International Journal of Mass Spectrometry* 204, 101–112 (2001).

22. Combariza, M.Y., Fahey, A.M., Milshteyn, A. & Vachet, R.W. Gas-phase ion-molecule reactions of divalent metal complex ions: Toward coordination structure analysis by mass spectrometry and some intrinsic coordination chemistry along the way. *International Journal of Mass Spectrometry* 244, 109–124 (2005).

23. Rashid, S. & Mayer, P.M. Dual-electrospray synthesis: A method of studying unique coordination complexes in the gas phase. *International Journal of Mass Spectrometry* 429, 107–114 (2018).

24. Nath, H. *et al.* Phenanthroline-based Ni(II) coordination compounds involving unconventional discrete fumarate-water-nitrate clusters and energetically significant cooperative ternary π-stacked assemblies: Antiproliferative evaluation and theoretical studies. *Journal of Molecular Structure* 1248, 131424 (2022).

25. Kumari, P., Lobana, T.S., Butcher, R.J., Castineiras, A. & Zeller, M. The effect of substituents at C2/N1 atoms of salicyladehyde and 2-hydroxyacetophenone based thiosemicarbazones on the nature of nickel(II) complexes with 1,10-phenathroline and terpyridine as co-ligands. *Inorganica Chimica Acta* 482, 268–274 (2018).

26. Zhu, S., Brennessel, W.W., Harrison, R.G. & Que, L. Iron coordination chemistry of N-(bis(2-pyridyl)methyl)pyridine-2-carboxamide. *Inorganica Chimica Acta* 337, 32–38 (2002).

27. Travis, J.Z., Pumford, S.R., Martinez, B.L. & LaDuca, R.L. Nickel adamantanedicarboxylate and adamantanediacetate 2D and 3D coordination polymers with hydrogen-bonding capable dipyridyl ligands. *Polyhedron* 142, 25–37 (2018).

28. Seitz, M., Milius, W. & Alt, H.G. Iron(II) coordination compounds with ω-alkenyl substituted bis(imino)pyridine ligands: Self-immobilizing catalysts for the polymerization of ethylene. *Journal of Molecular Catalysis A: Chemical* 261, 246–253 (2007).

29. Breci, L. Mass Spec. *LibreTexts* (2020).

30. American Physical Society News. April 1946: First Concept of Time-of-Flight Mass Spectrometer. *American Physical Society* 10, (2001).

31. Griffiths, J. A Brief History of Mass Spectrometry. *Journal of Analytical Chemistry.* 80, 6 (2008).

32. McIndoe, S.J. Mass spectrometry in organometallic chemistry. *Spectroscopic Properties of Inorganic and Organometallic Compounds*. 41, 288–309 (Royal Society of Chemistry, 2010).

33. Eelman, M.D., Blacquiere, J.M., Moriarty, M.M. & Fogg, D.E. Shining New Light on an Old Problem: Retooling MALDI Mass Spectrometry for Organotransition-Metal Catalysis. *Angewandte Chemie International Edition.* 47, 303–306 (2008).

34. Jennifer Murphy. Electrospray Ionization Mass Spectrometry. *LibreTexts* (2020).

35. Steckel, A. & Schlosser, G. An Organic Chemist's Guide to Electrospray Mass Spectrometric Structure Elucidation. *Molecules* 24, 611 (2019).

36. Waters. What Types of Instruments Are Used? (2021).

37. Miller, P. E. & Denton, M. B. The quadrupole mass filter: Basic operating concepts. *Journal of Chemical Education* 63, 617 (1986).

38. Khan, O. Mass Analyzers (Mass Spectrometry). *LibreTexts* (2021).

39. TOFWERK. Advantages of Time-of-Flight Mass Spectrometry Over Quadrupole MS. (2021).

40. Mass Analyzer - Time of Flight. *LibreTexts* (2021).

41. Liuni, P., Deng, B. & Wilson, D. J. Comparing equilibrium and kinetic protein unfolding using time-resolved electrospray-coupled ion mobility mass spectrometry. *Analyst* 140, 6973–6979 (2015).

42. Wilson, D. J. & Konermann, L. A Capillary Mixer with Adjustable Reaction Chamber Volume for Millisecond Time-Resolved Studies by Electrospray Mass Spectrometry. *Journal of Analytical Chemistry* 75, 6408–6414 (2003).

43. Sleno, L. & Volmer, D. A. Ion activation methods for tandem mass spectrometry. *Journal of Mass Spectrometry* 39, 1091–1112 (2004).

44. Johnson, A. R. & Carlson, E. E. Collision-Induced Dissociation Mass Spectrometry: A Powerful Tool for Natural Product Structure Elucidation. *Journal of Analytical Chemistry* 87, 10668–10678 (2015).

45. Mohler, F. L., Bloom, E. G., Wells, E. J., Lengel, J. H. & Wise, C. E. Doubly charged ion spectra in mass spectra of hydrocarbons. *Journal of Research of the National Bureau of Standards* 42, 369 (1949).

46. Das, U. K. *et al.* Mononuclear, Dinuclear and Trinuclear Iron Complexes Featuring a new Monoanionic SNS Thiolate Ligand. *Inorganic Chemistry* 987–997 (2016).

47. PubChem. Nickel Nitrate (compound).

48. Sigma-Aldrich. Nickel (II) Nitrate Hexahydrate.

49. PubChem. Iron (III) Nitrate Nonahydrate (compound).

50. PubChem. Ferric Nitrate (compound).

51. Sigma-Aldrich. Iron (III) Nitrate Nonahydrate.

52. PubChem. 2,2’-Bipyridine (compound).

53. PubChem. 4,4’-Bipyridine (compound).

54. Sigma-Aldrich. 4,4’-Dipridyl.

55. Fisher Scientific. Alfa Aesar 2,2’-Bipyridine-4,4’-dicarboxylic acid, 98%.

56. PubChem. 2,2’-Bipyridine-4,4’-dicarboxylic acid (compound).

57. Sigma-Aldrich. 2,2’-Bipyridine-4,4’-dicarboxylic acid.

58. PubChem. 1,10-Phenanthroline (compound).

59. Sigma-Aldrich. 1,10-Phenanthroline.

60. Waters. Synapt High Definition MS System. (2008).

APPENDICES

Appendix I. TRESI mass spectra for Nickel (II) Nitrate.

A1.1 TRESI mass spectra for 2,2'-Bipyridine for 0 cm (top) to 7 cm (bottom).

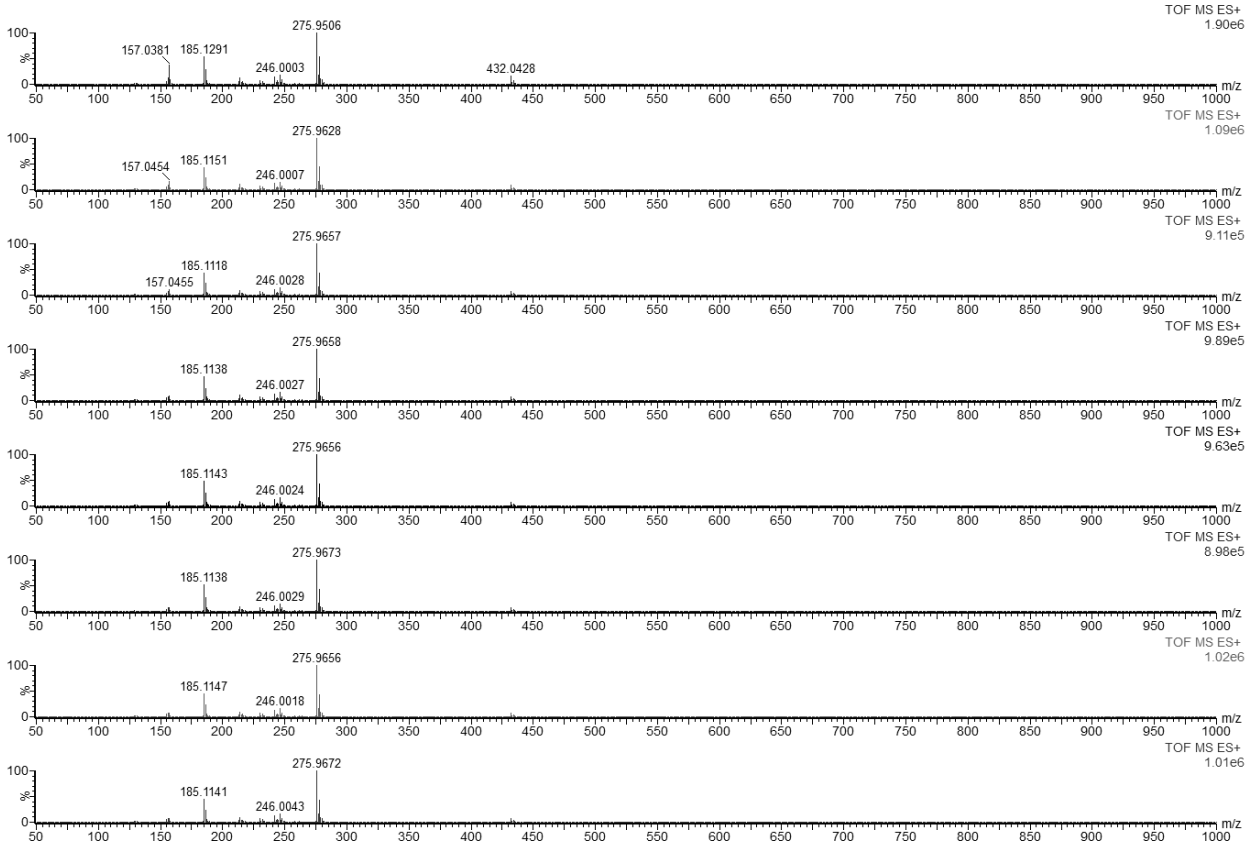

A1.2 TRESI mass spectra for 4,4'-Bipyridine for 0 cm (top) to 7 cm (bottom).

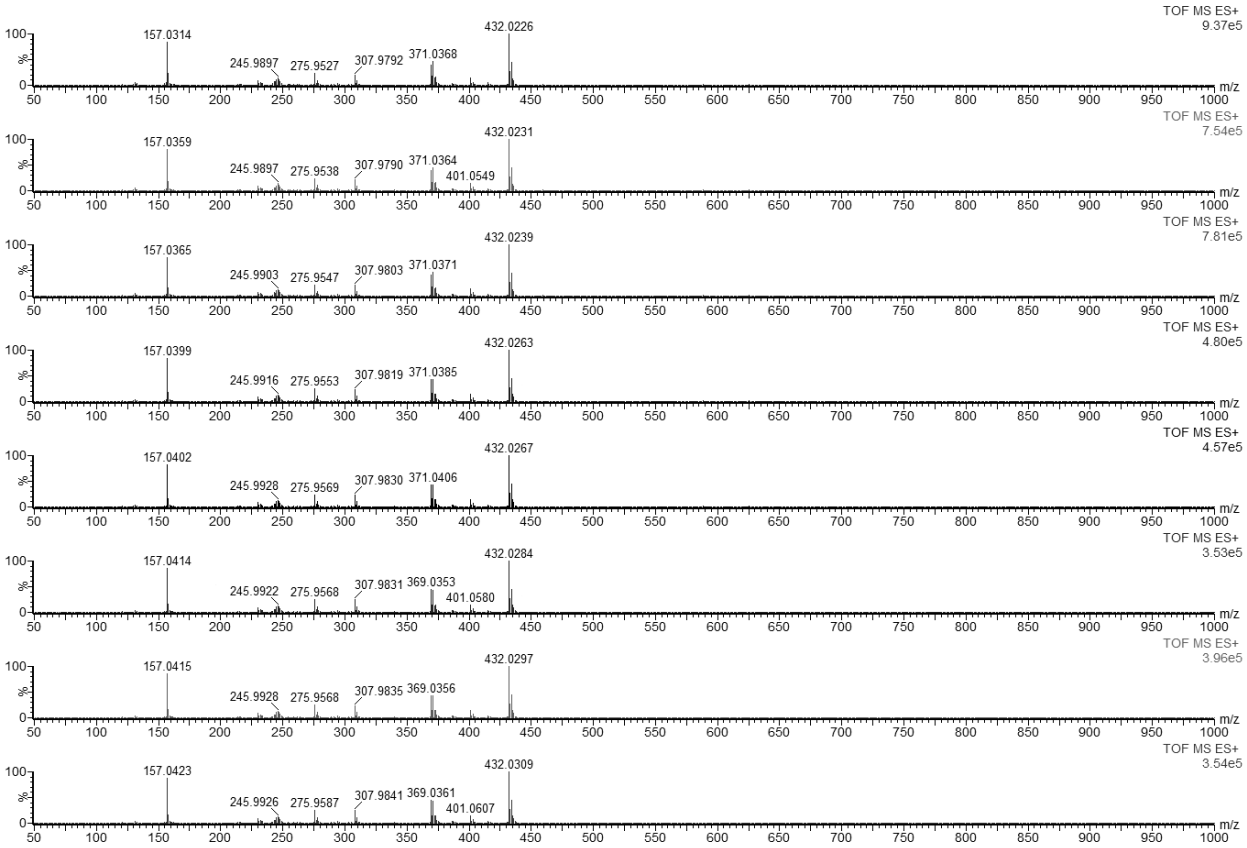

A1.3 TRESI mass spectra for 2,2'-Bipyridine-4,4'-Dicarboxylic Acid for 0 cm (top) to 7 cm (bottom).

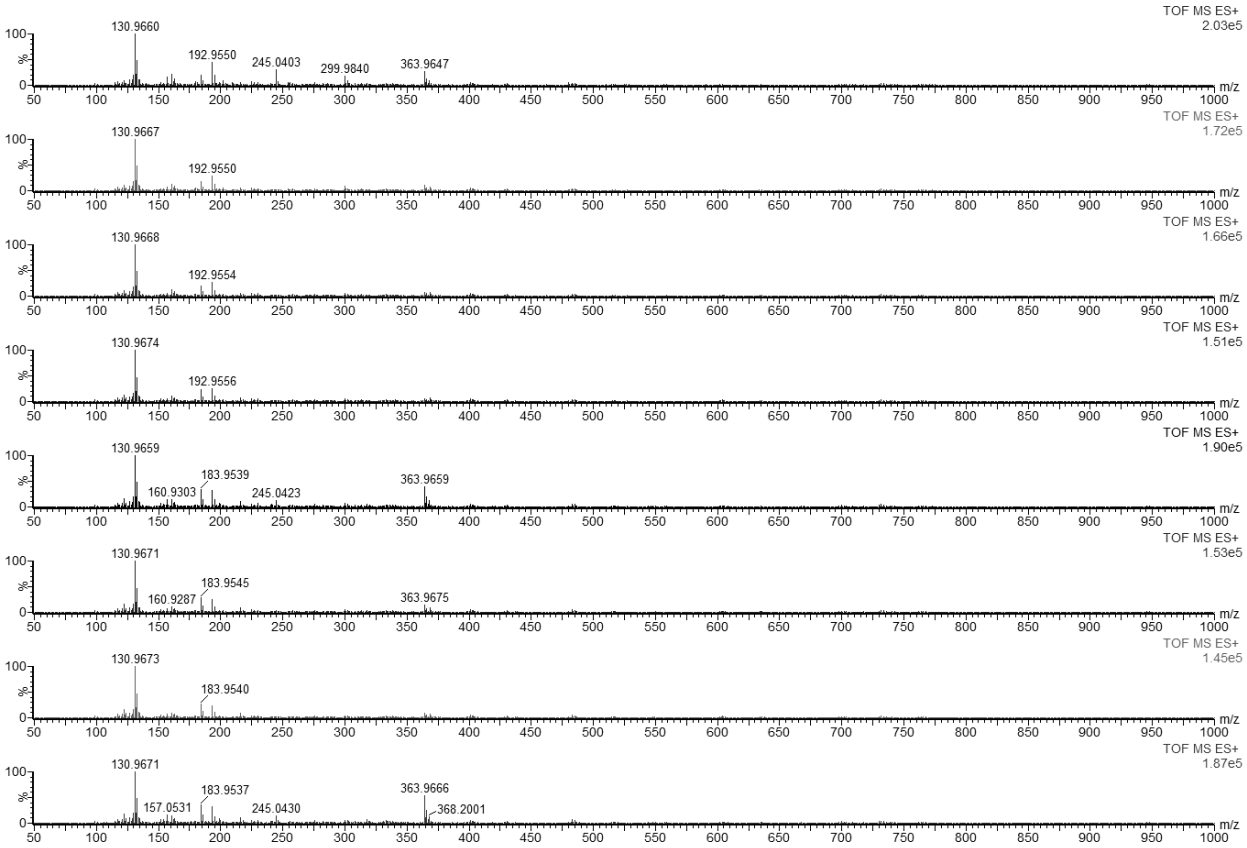

A1.4 TRESI mass spectra for 1,10-Phenanthroline for 0 cm (top) to 7 cm (bottom).

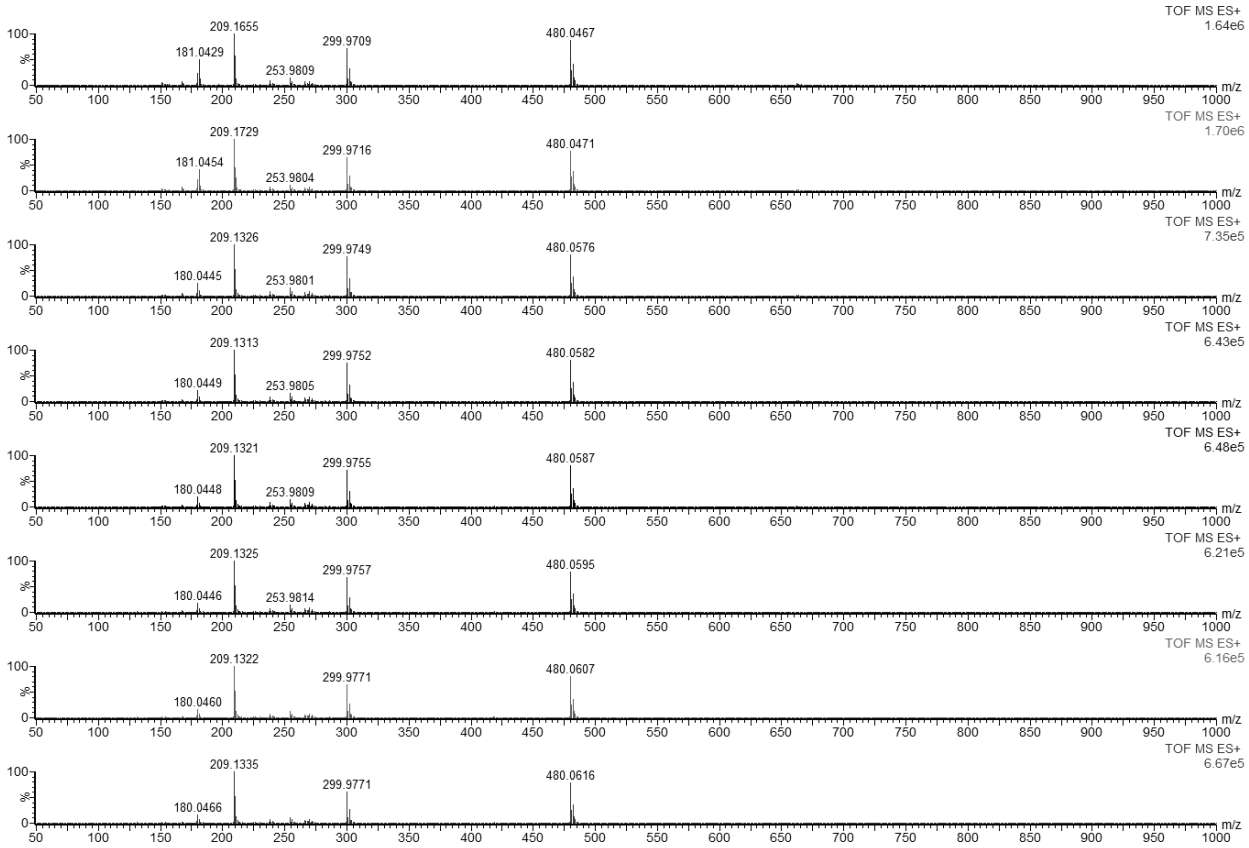

A1.5 TRESI mass spectra for SNS for 0 cm (top) to 8 cm (bottom).

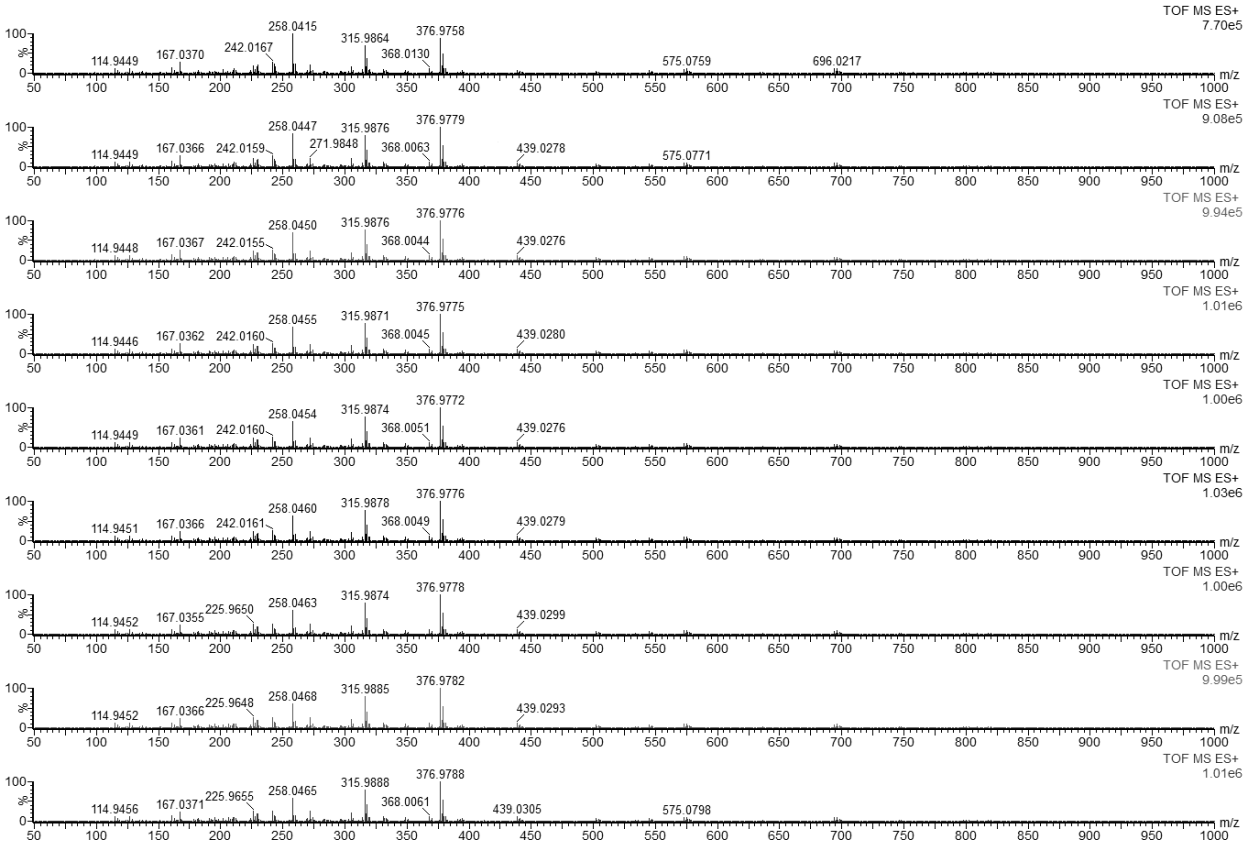

Appendix II. TRESI mass spectra for Iron (III) Nitrate.

A2.1 TRESI mass spectra for 2,2'-Bipyridine for 0 cm (top) to 9 cm (bottom).

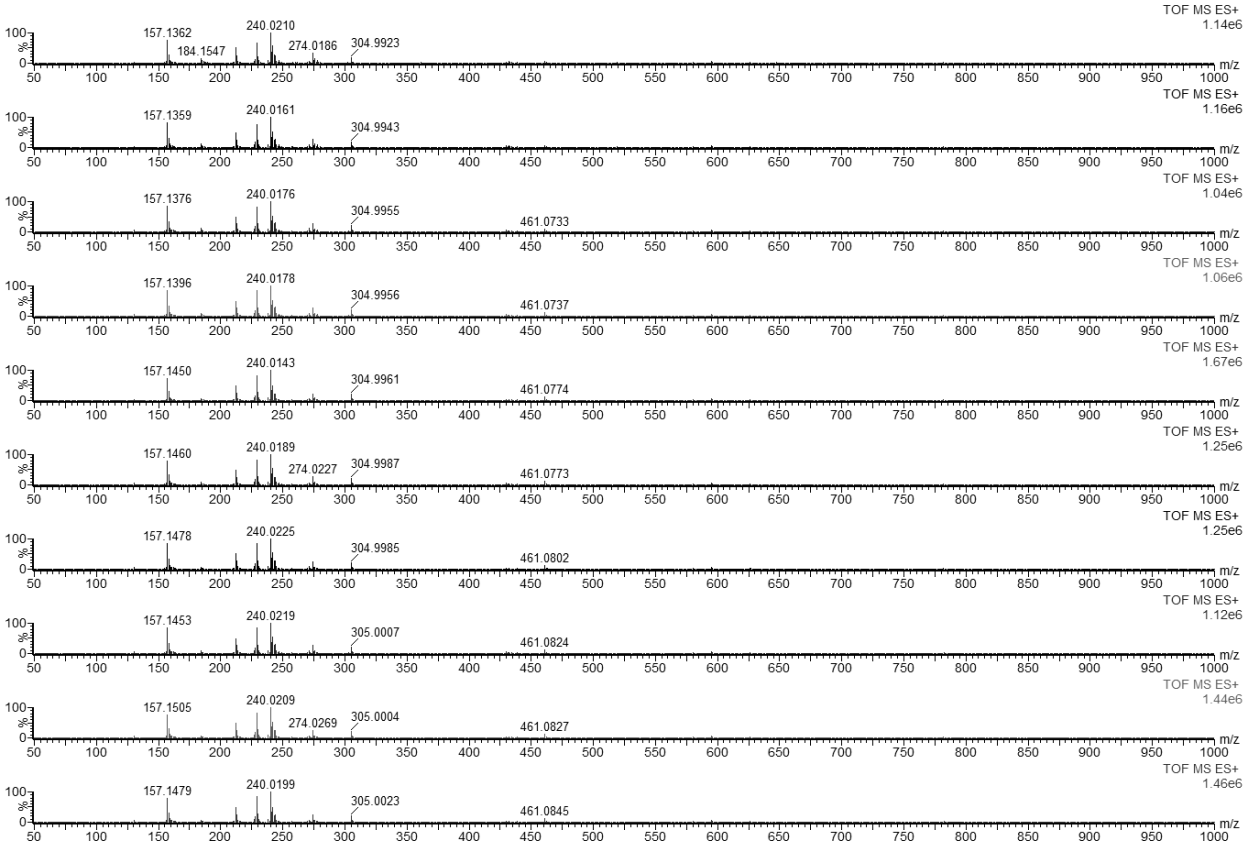

A2.2 TRESI mass spectra for 4,4'-Bipyridine for 0 cm (top) to 8 cm (bottom).

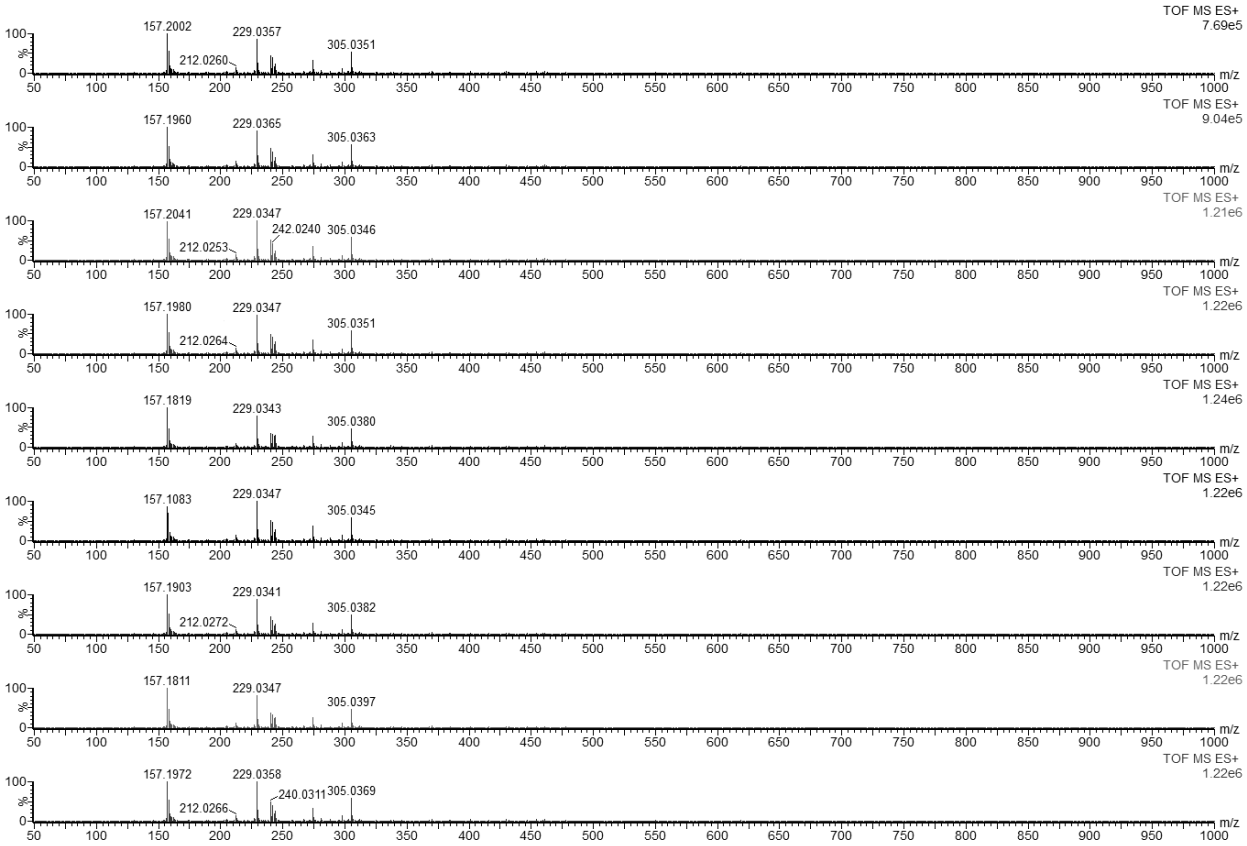

A2.3 TRESI mass spectra for 2,2'-Bipyridine-4,4'-Dicarboxylic Acid for 0 cm (top) to 7 cm (bottom).

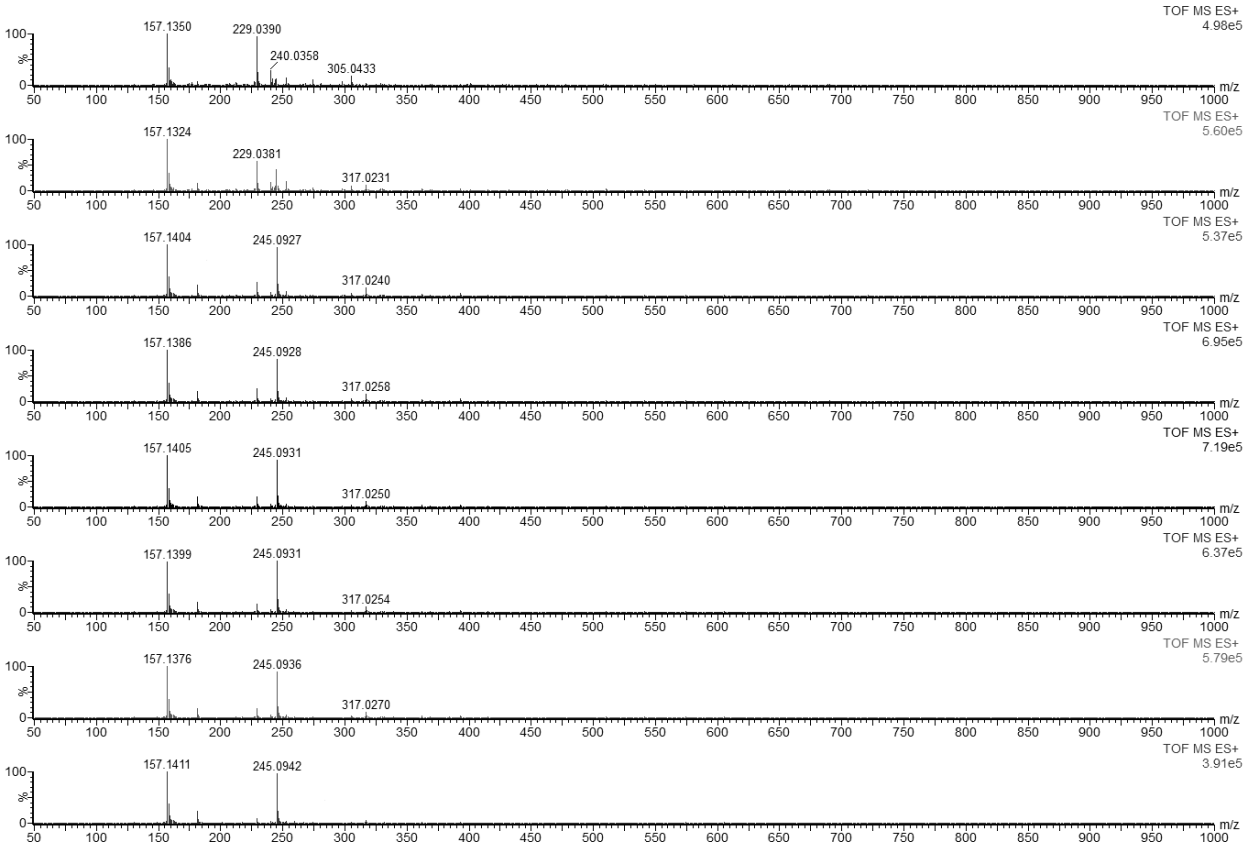

A2.4 TRESI mass spectra for 1,10-Phenanthroline for 0 cm (top) to 9 cm (bottom).

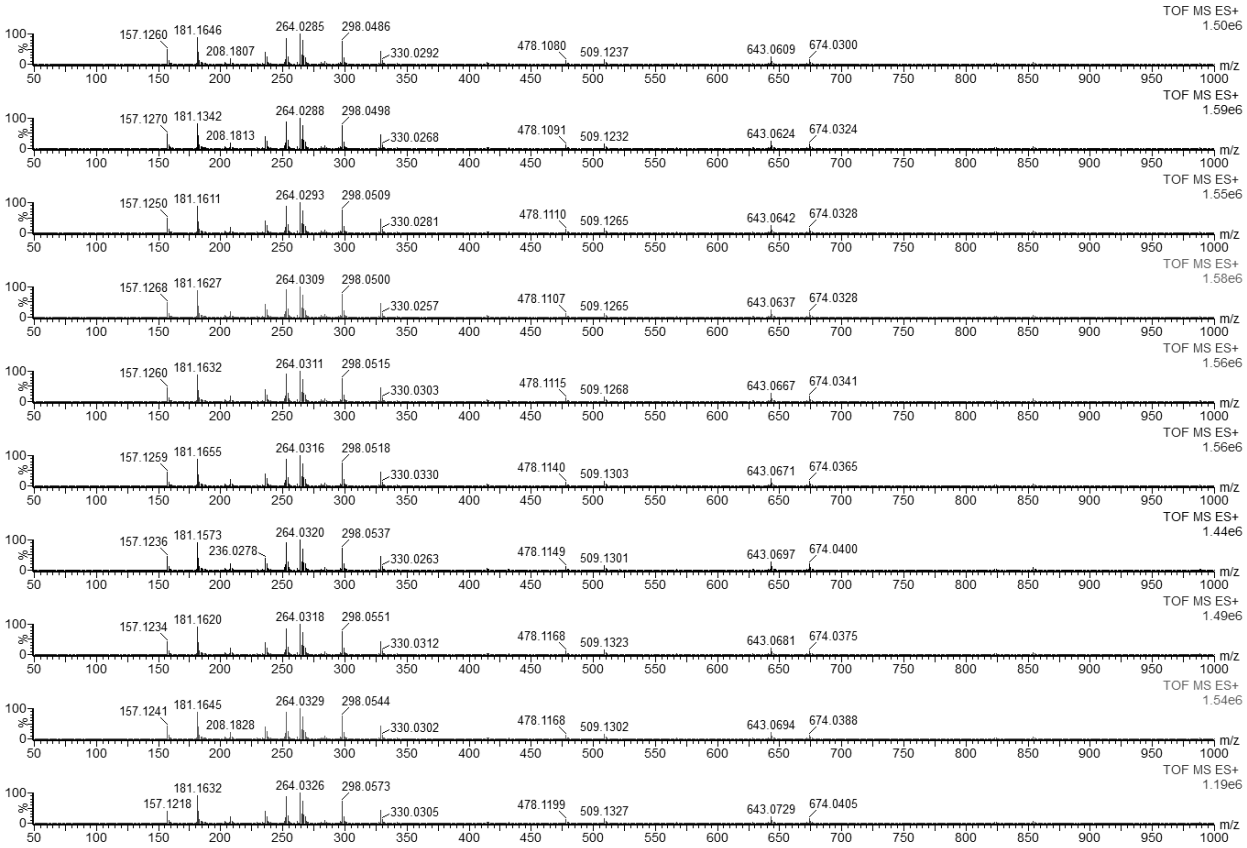

A2.5 TRESI mass spectra for SNS for 0 cm (top) to 8 cm (bottom).

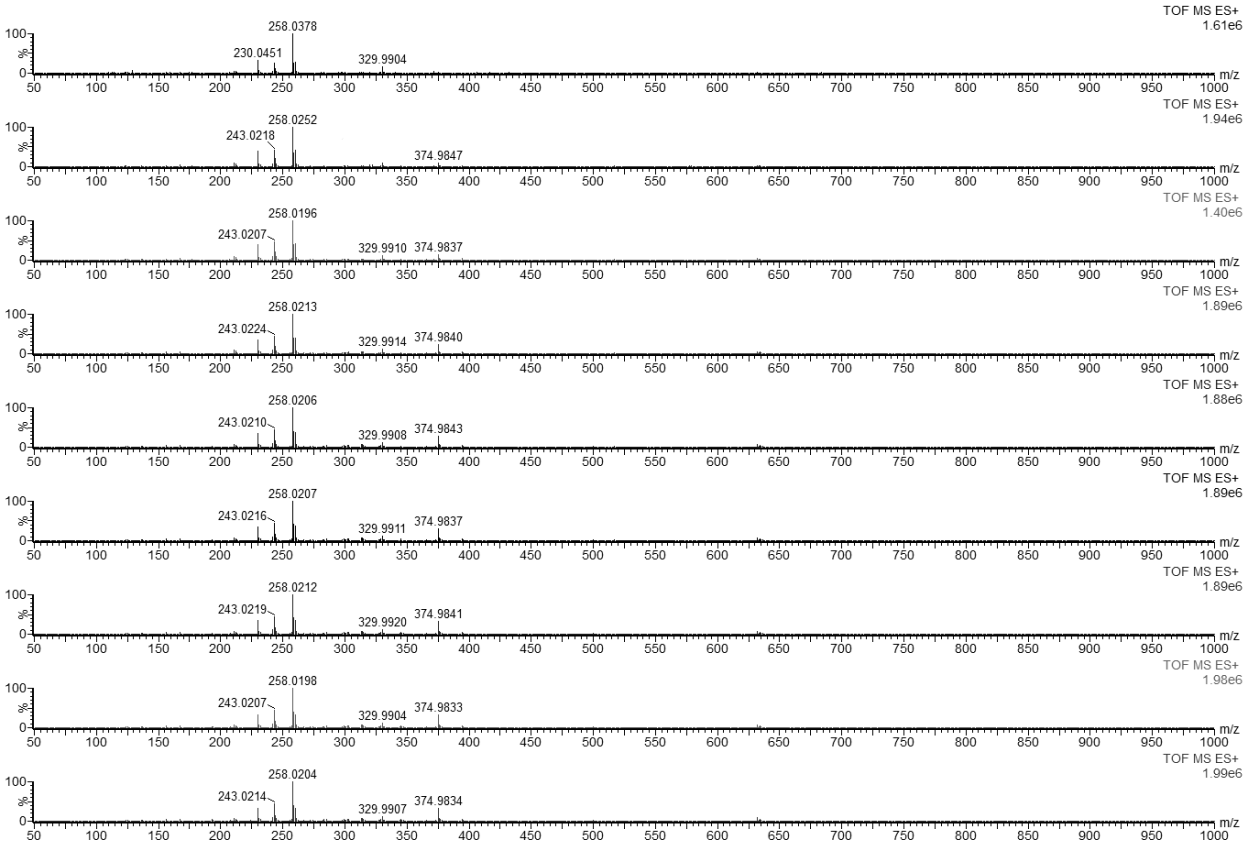

Appendix III. Breakdown diagrams for Nickel (II) Nitrate and 2,2'-Bipyridine, single-spray.

A3.1 Breakdown diagram for the 1:1 complex ($NiC_{10}H_8N_2^+$) at 215.9 *m/z* in the trap from 0-55eV.

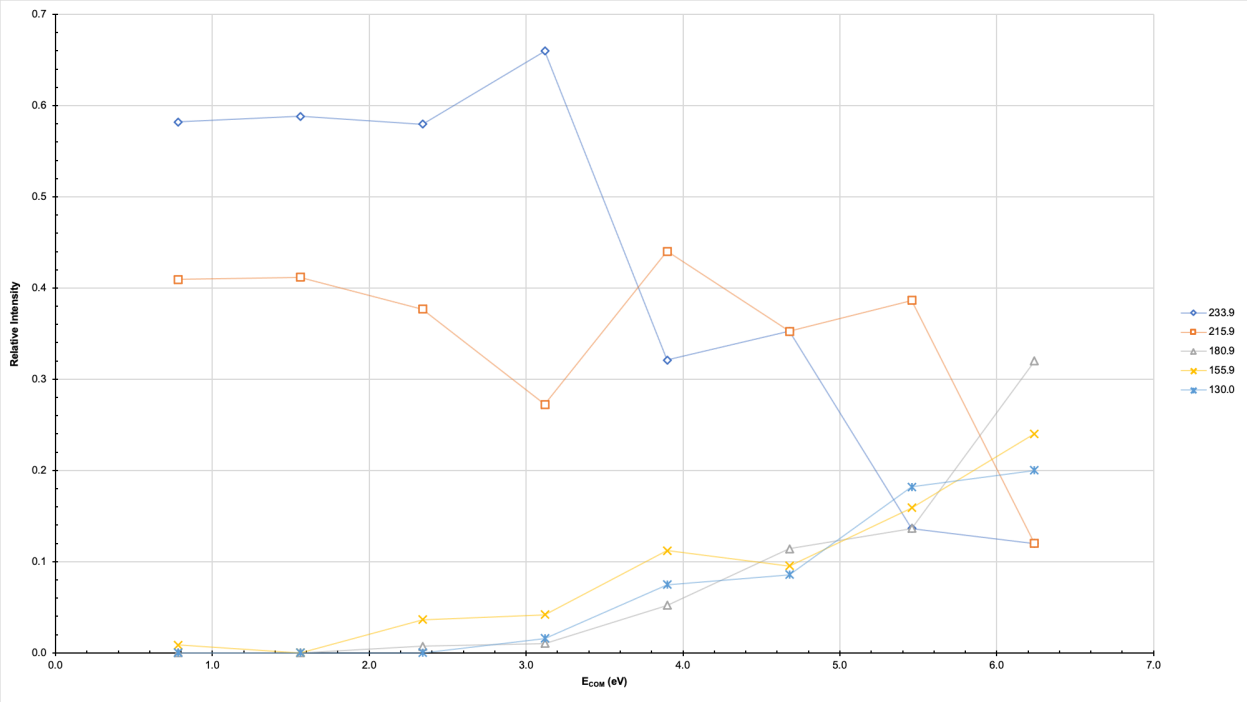

A3.2 Breakdown diagram for the 1:1 complex ($NiC_{10}H_8N_2^+$) at 215.9 *m/z* in the transfer from 0-45eV.

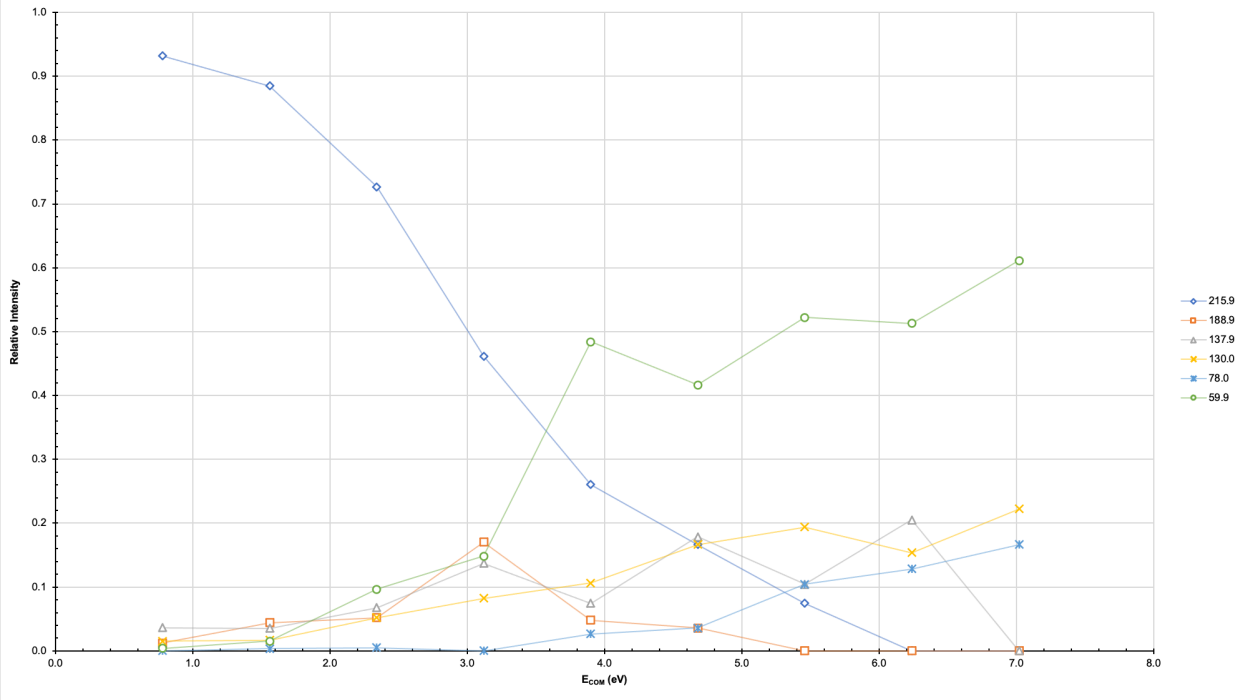

A3.3 Breakdown diagram for the nitrated 1:1 complex ($NiC_{10}H_8N_2NO_3^+$) at 277.9 *m/z* in the trap from 0-100eV.

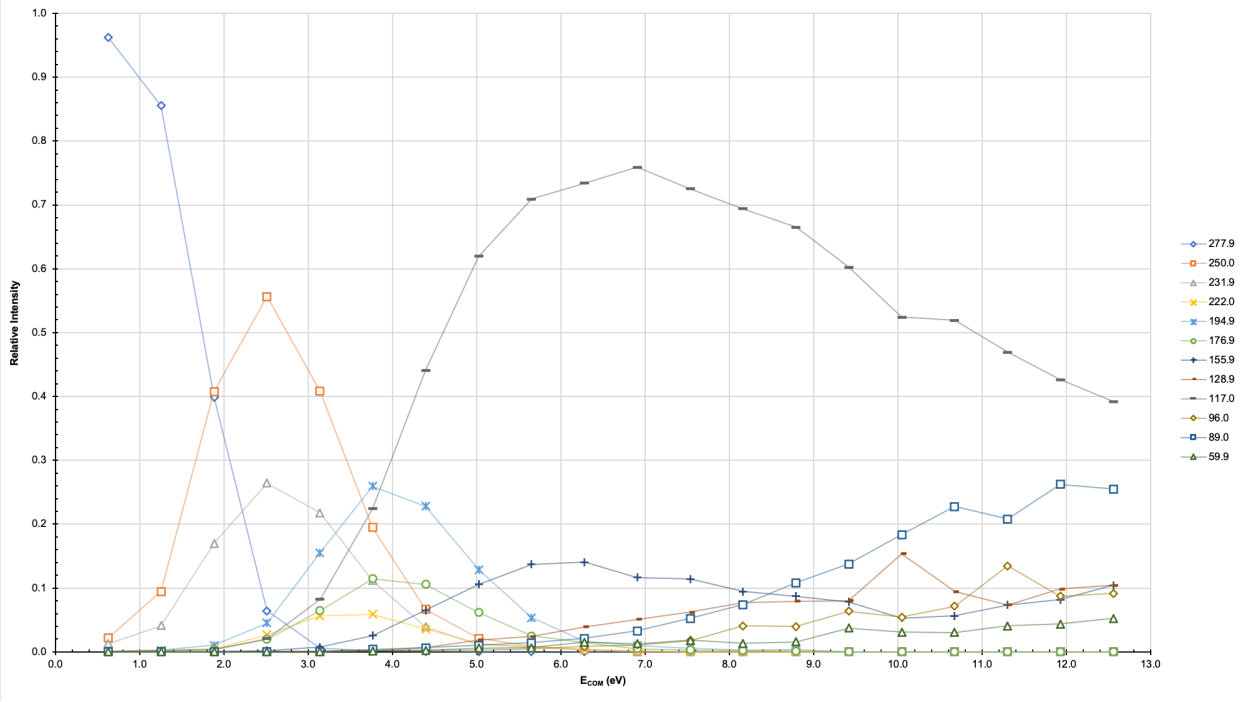

A3.4. Breakdown diagram for the nitrated 1:1 complex ($NiC_{10}H_8N_2NO_3^+$) at 277.9 *m/z* in the transfer from 0-100eV.

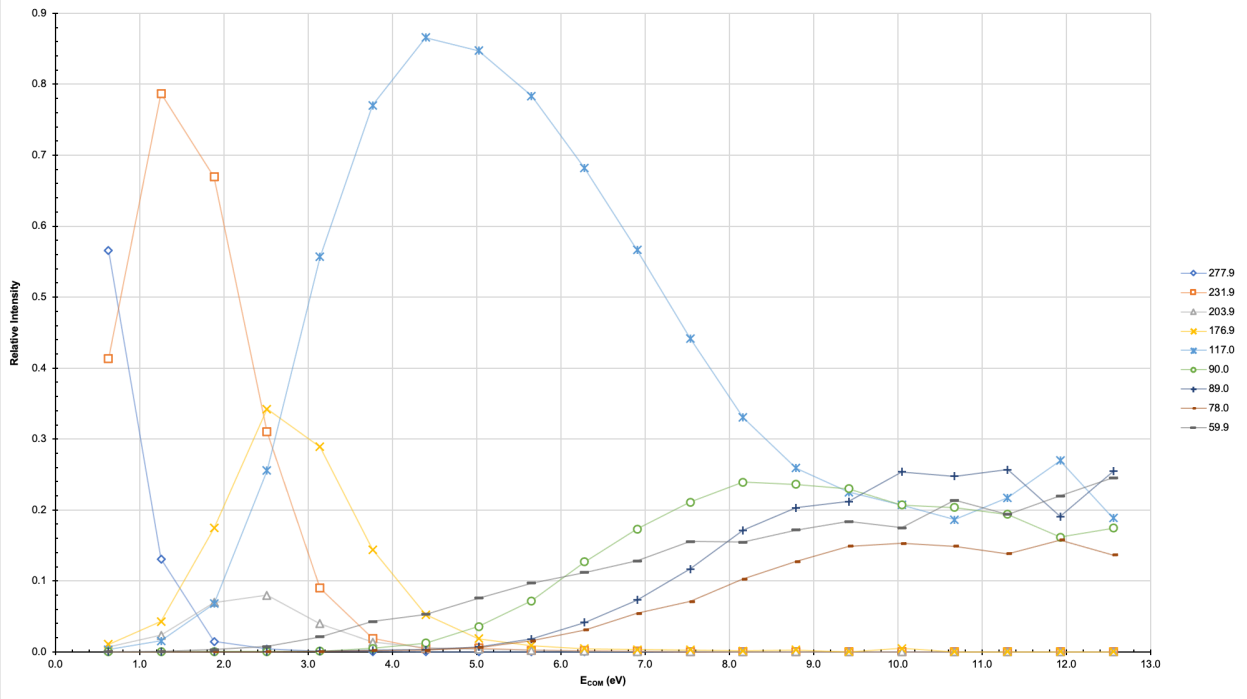

A3.5. Breakdown diagram for the 1:2 complex ($NiC_{10}H_8N_2C_{10}H_8N_2^+$) at 372.0 *m/z* in the trap from 0-100eV.

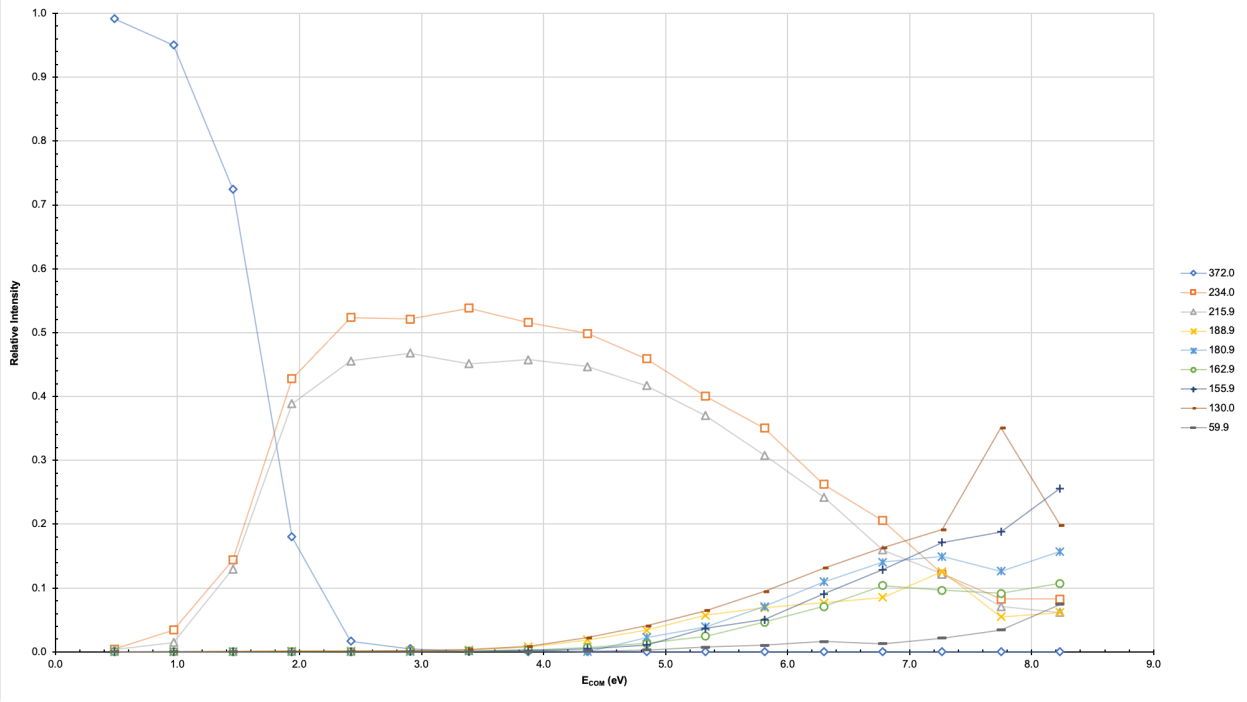

A3.6. Breakdown diagram for the 1:2 complex ($NiC_{10}H_8N_2C_{10}H_8N_2^+$) at 372.0 *m/z* in the transfer from 0-100eV.

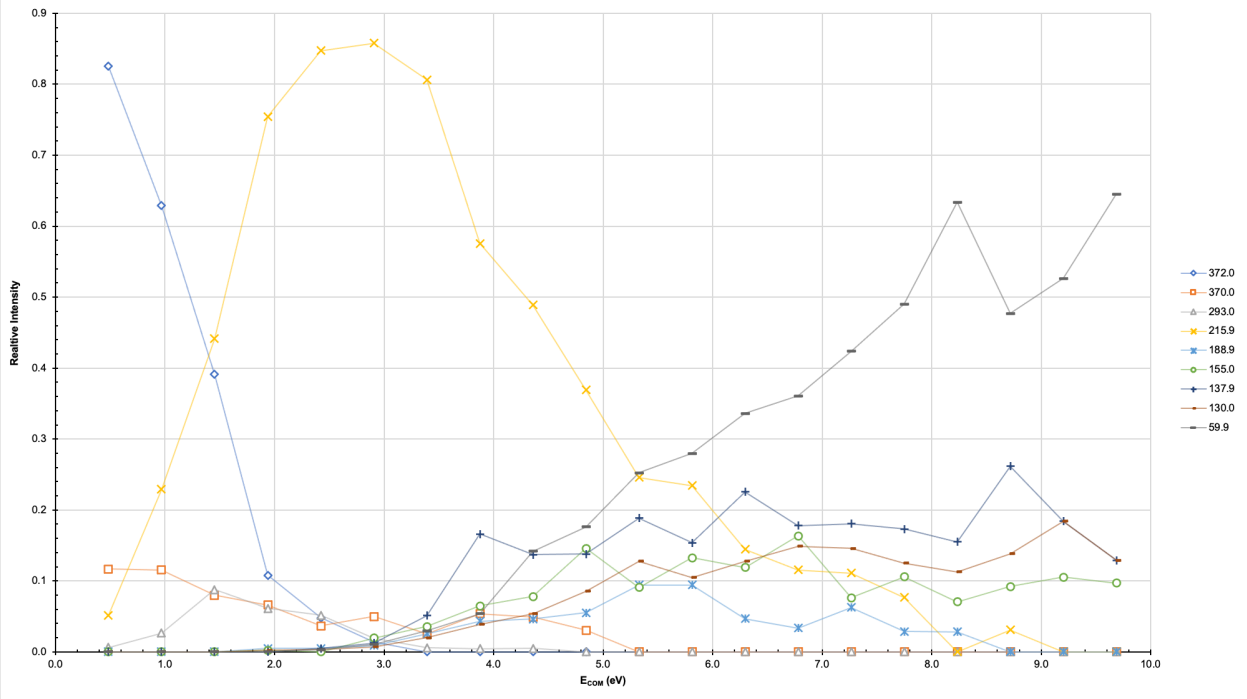

A3.7. Breakdown diagram for the nitrated 1:2 complex ($NiC_{10}H_8N_2C_{10}H_8N_2NO_3^+$) at 434.0 *m/z* in the trap from 0-100eV.

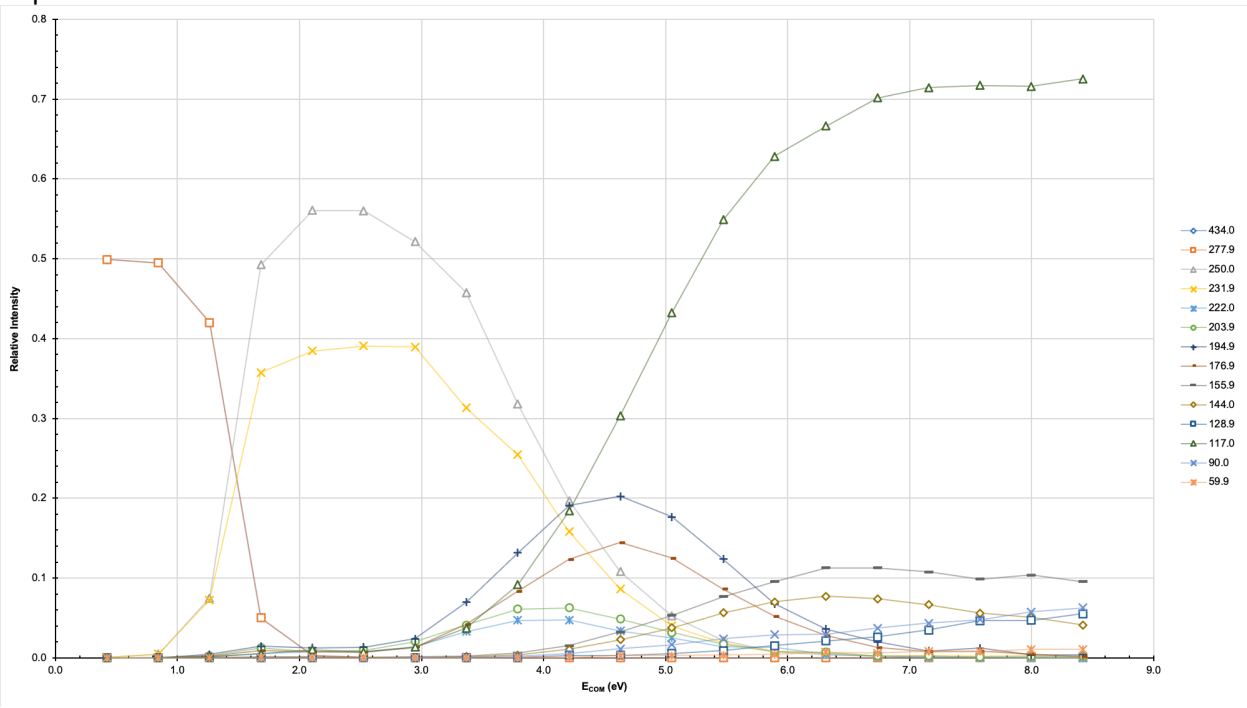

A3.8. Breakdown diagram for the nitrated 1:2 complex ($NiC_{10}H_8N_2C_{10}H_8N_2NO_3^+$) at 434.0 *m/z* in the transfer from 0-100eV.

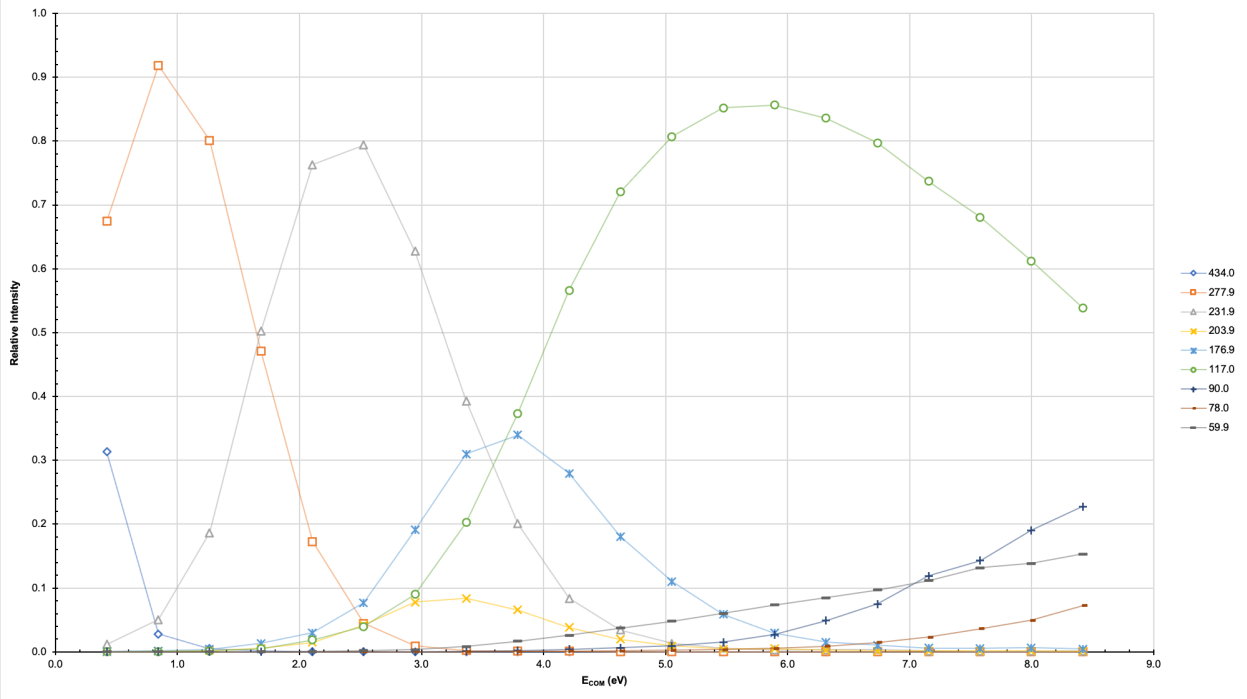

Appendix IV. Breakdown diagrams for Nickel (II) Nitrate and 2,2'-Bipyridine, dual-spray.

A4.1. Breakdown diagram for the 1:1 complex ($NiC_{10}H_8N_2^+$) at 216.0 *m/z* in the transfer from 0-35eV.

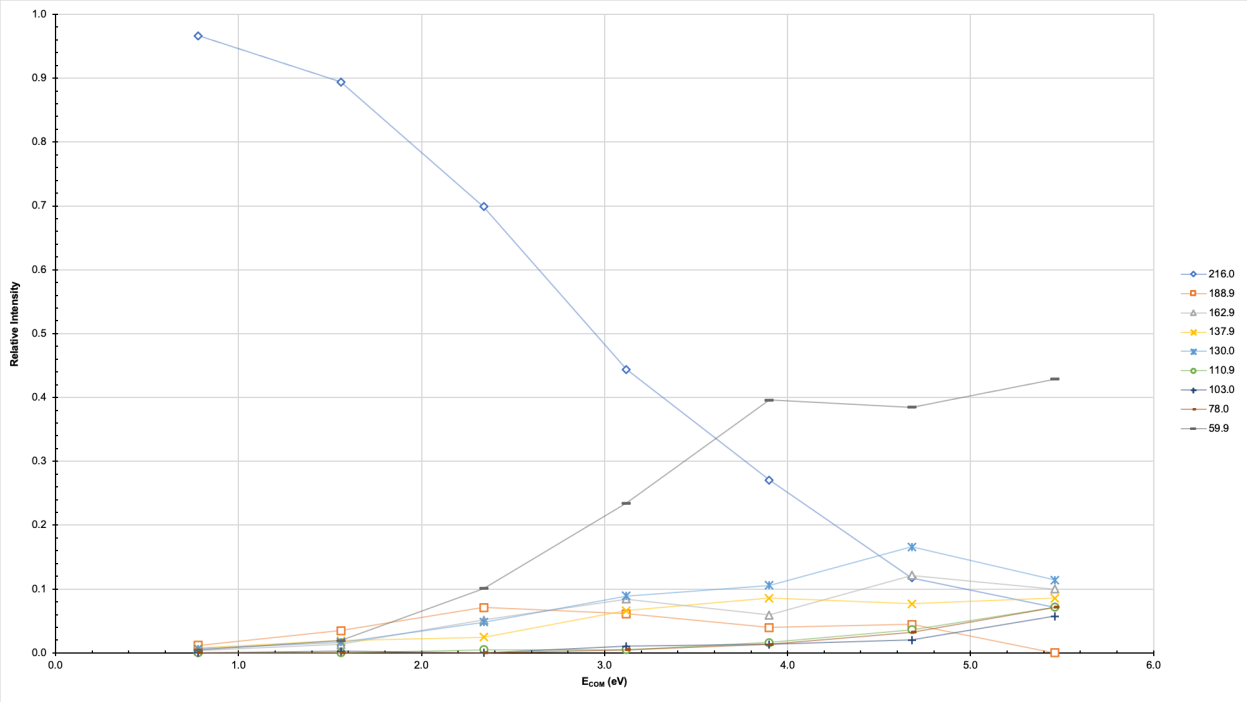

A4.2. Breakdown diagram for the nitrated 1:1 complex ($NiC_{10}H_8N_2NO_3^+$) at 277.9 *m/z* in the transfer from 0-100eV.

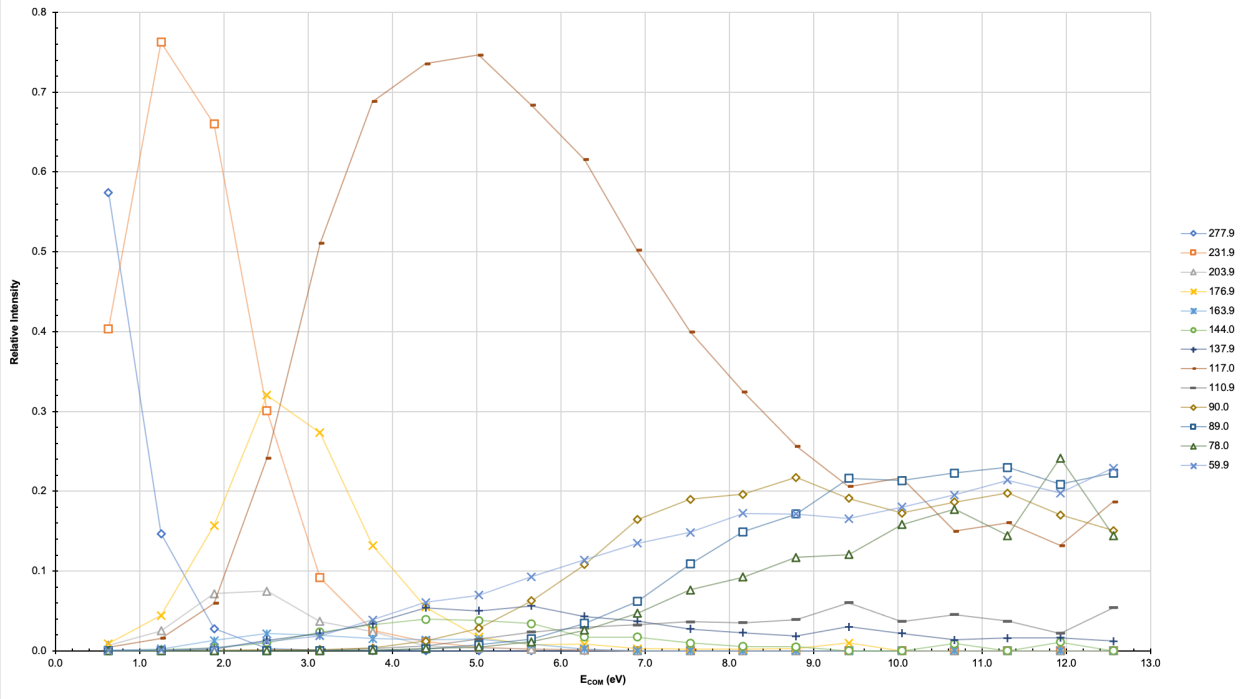

A4.3. Breakdown diagram for the 1:2 complex ($NiC_{10}H_8N_2C_{10}H_7N_2^+$) at 371.1 *m/z* in the transfer from 0-80eV.

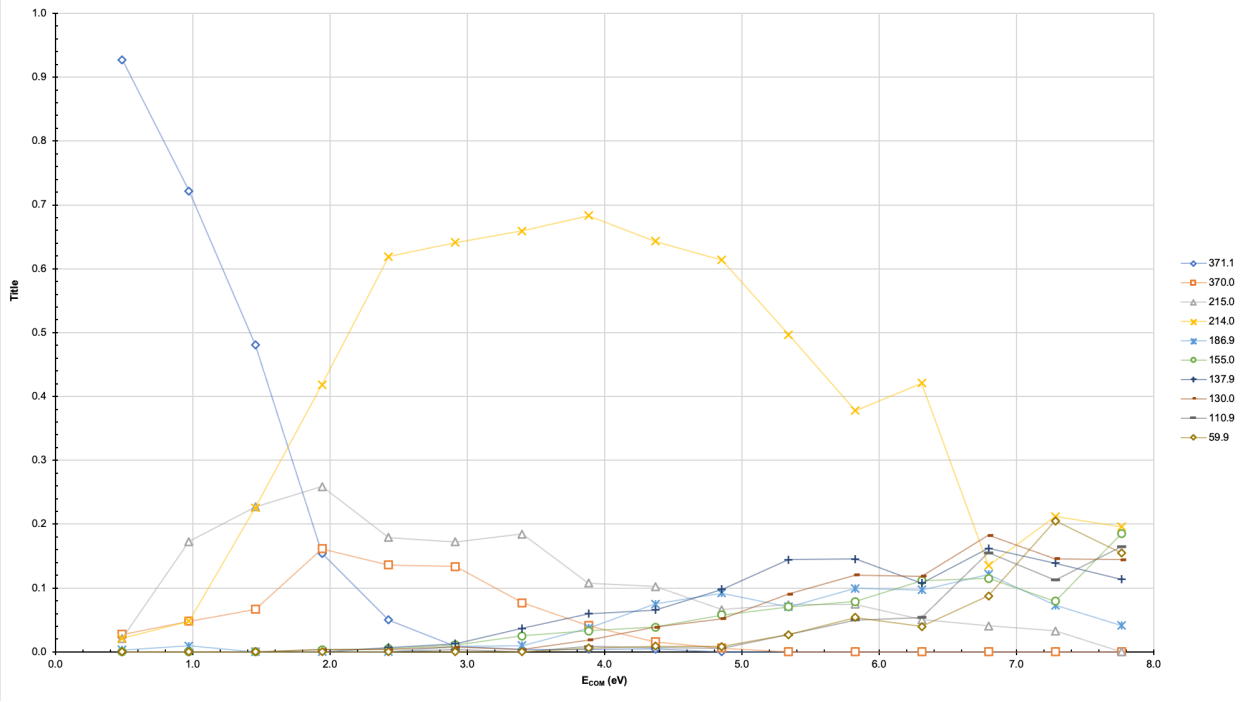

A4.4. Breakdown diagram for the nitrated 1:2 complex ($NiC_{10}H_8N_2C_{10}H_8N_2NO_3^+$) at 434.0 *m/z* in the transfer from 0-100eV.

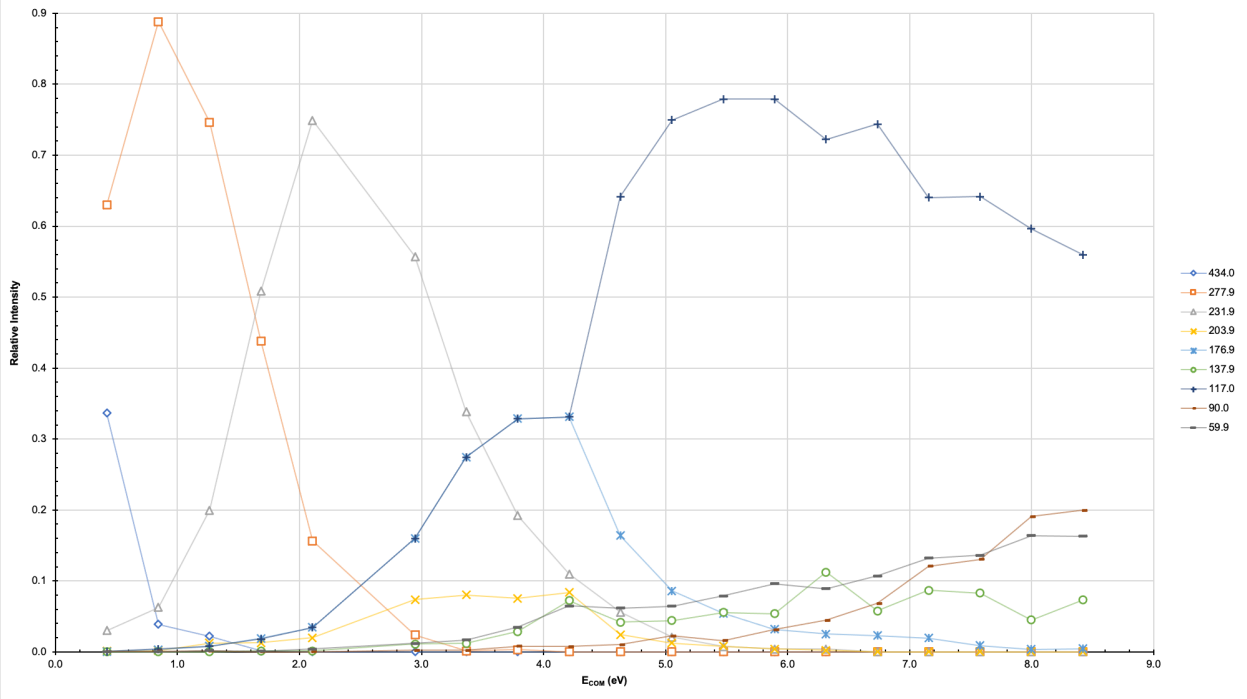

Appendix V. Breakdown diagrams for Nickel (II) Nitrate and 4,4'-Bipyridine, single-spray.

A5.1 Breakdown diagram for the nitrated 1:1 complex ($NiC_{10}H_8N_2NO_3^+$) at 277.9 *m/z* in the trap from 0-90eV.

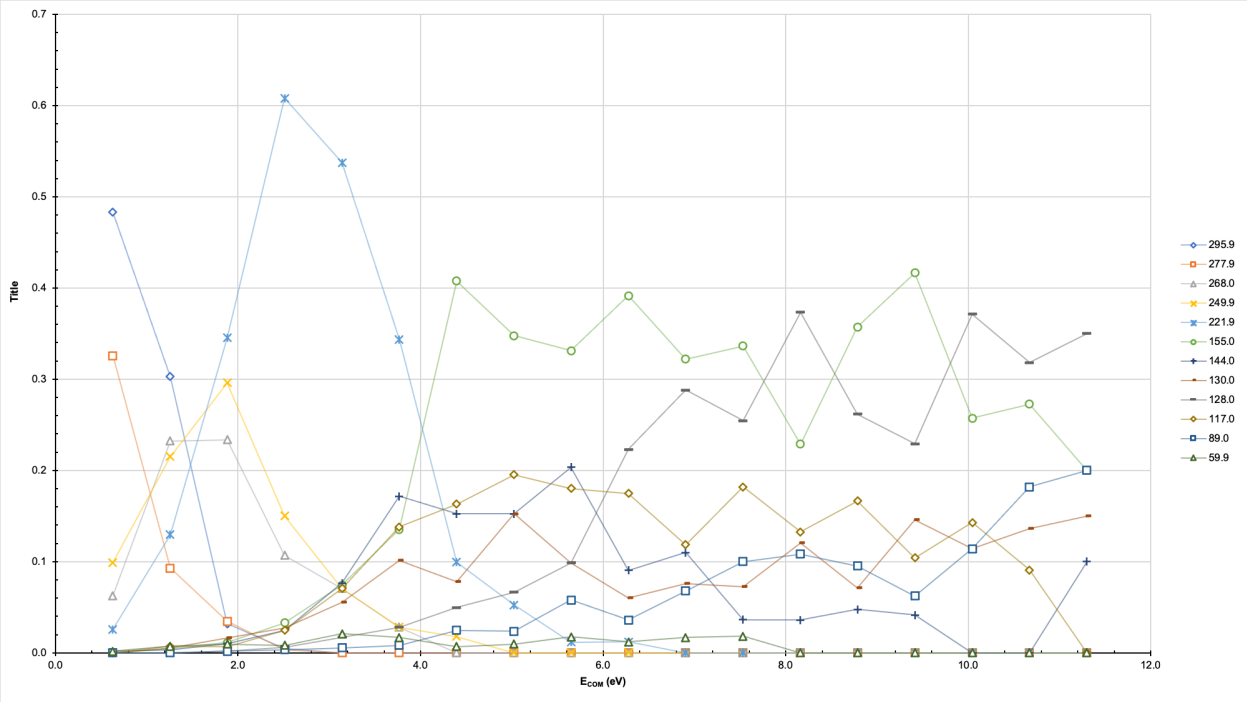

A5.2. Breakdown diagram for the nitrated 1:1 complex ($NiC_{10}H_8N_2NO_3^+$) at 277.9 *m/z* in the transfer from 0-75eV.

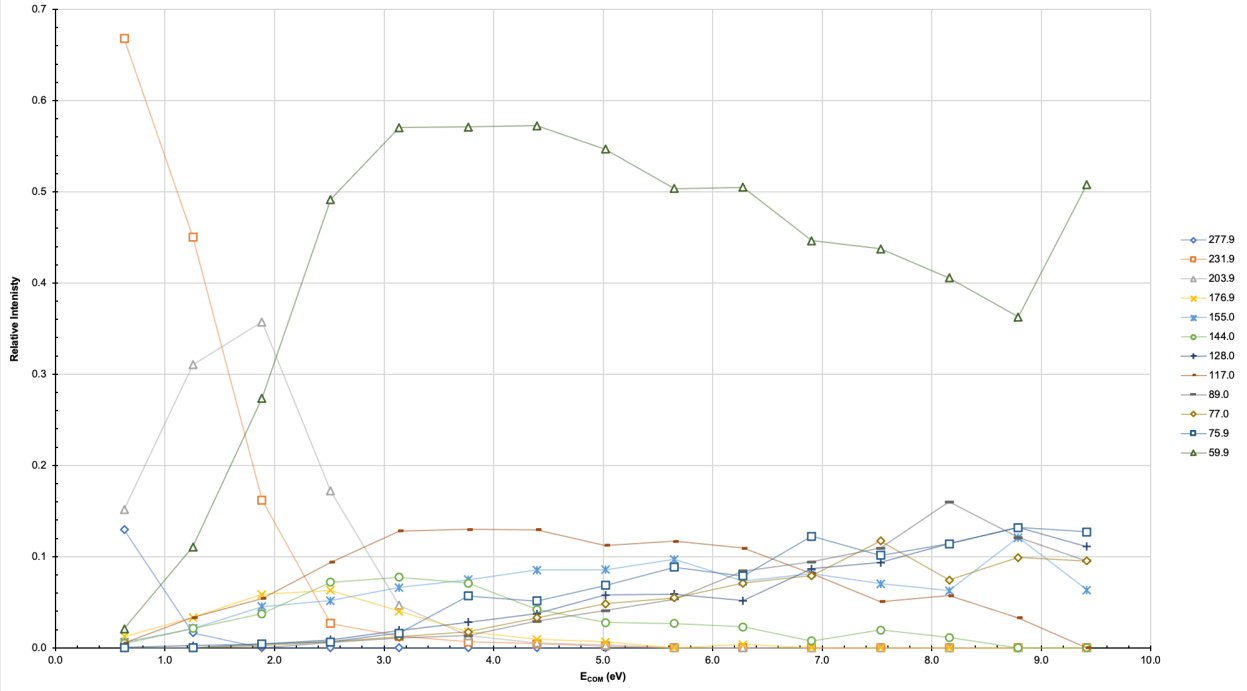

A5.3. Breakdown diagram for the 1:2 complex ($NiC_{10}H_8N_2C_{10}H_7N_2^+$) at 371.0 *m/z* in the trap from 0-100eV.

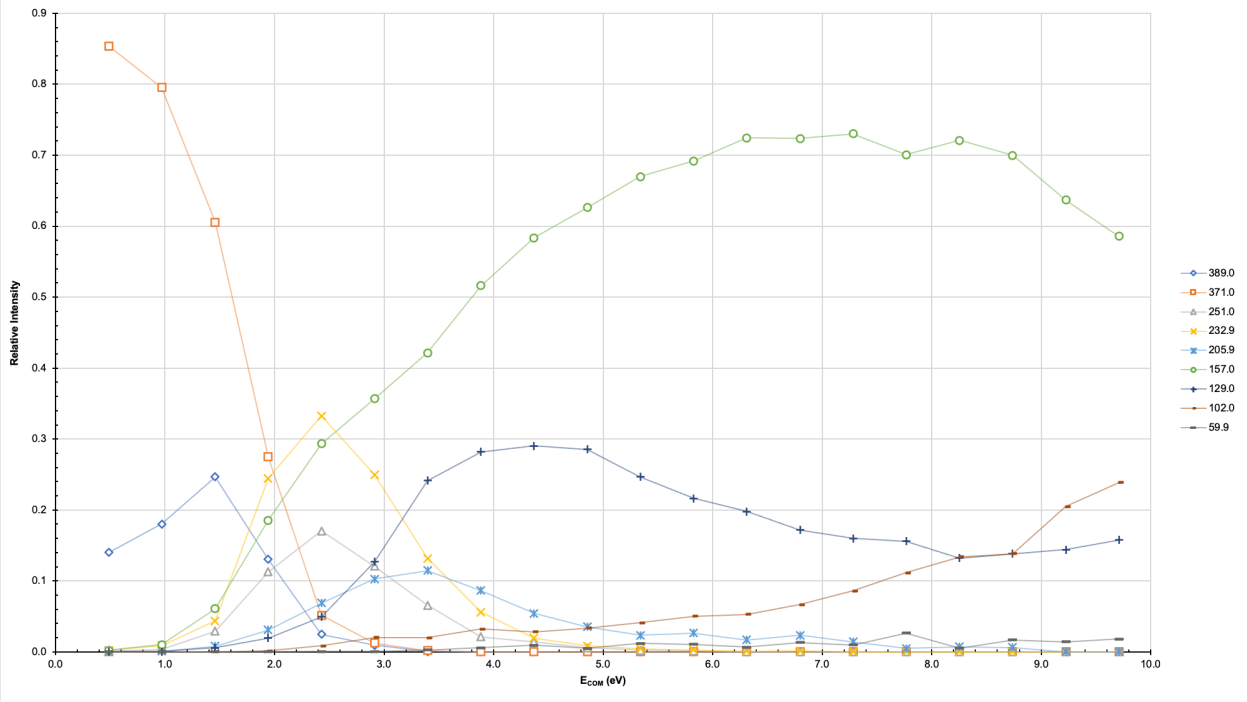

A5.4. Breakdown diagram for the 1:2 complex ($NiC_{10}H_8N_2C_{10}H_7N_2^+$) at 371.0 *m/z* in the transfer from 0-100eV.

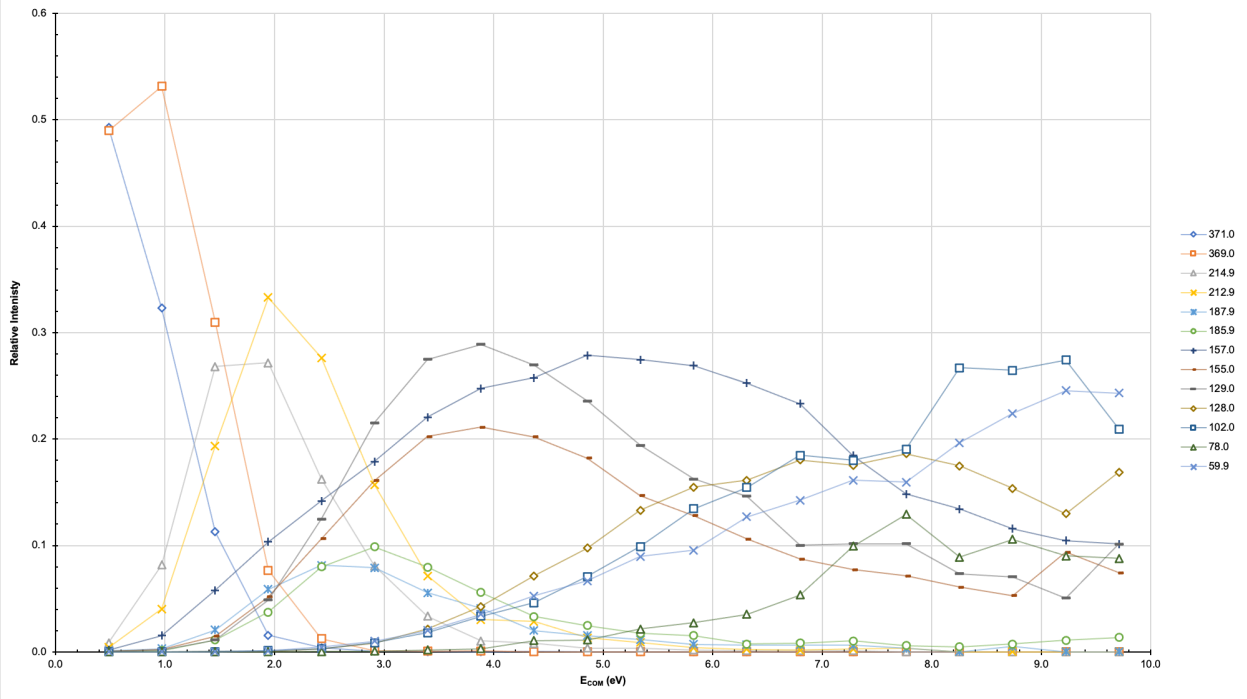

A5.5. Breakdown diagram for the nitrated 1:2 complex ($NiC_{10}H_8N_2C_{10}H_8N_2NO_3^+$) at 434.0 *m/z* in the trap from 0-100eV.

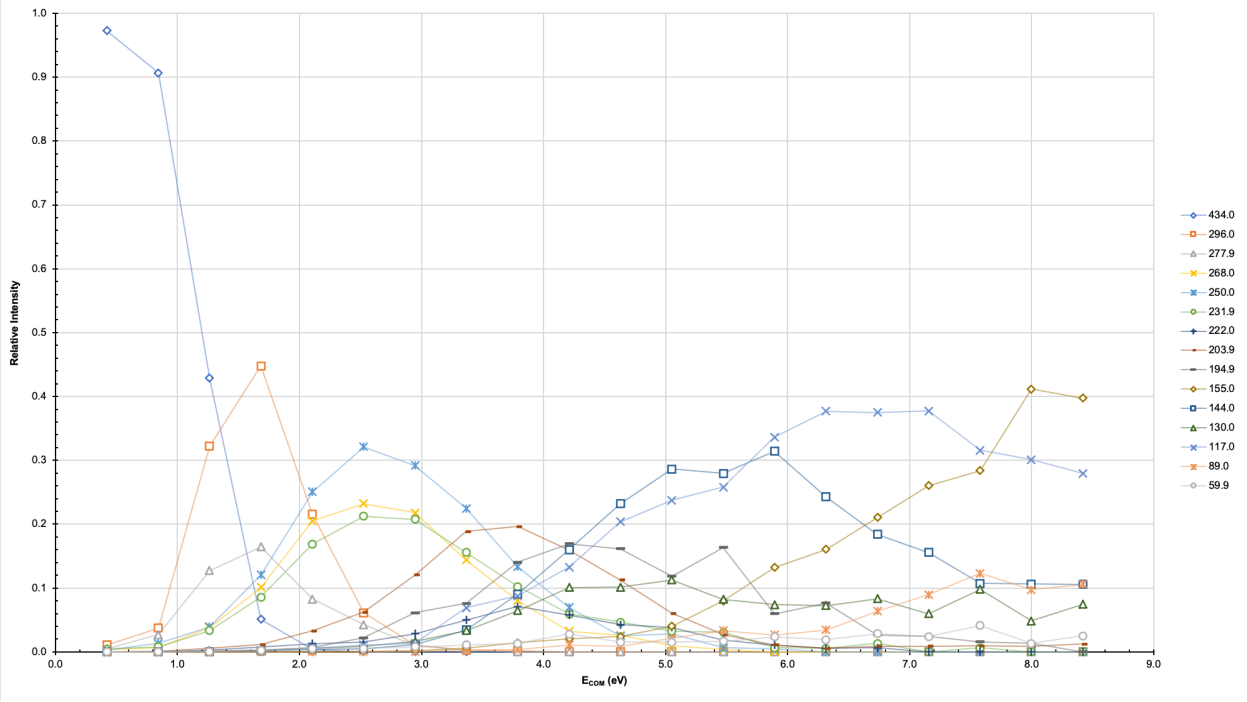

A5.6. Breakdown diagram for the nitrated 1:2 complex ($NiC_{10}H_8N_2C_{10}H_8N_2NO_3^+$) at 434.0 *m/z* in the transfer from 0-100eV.

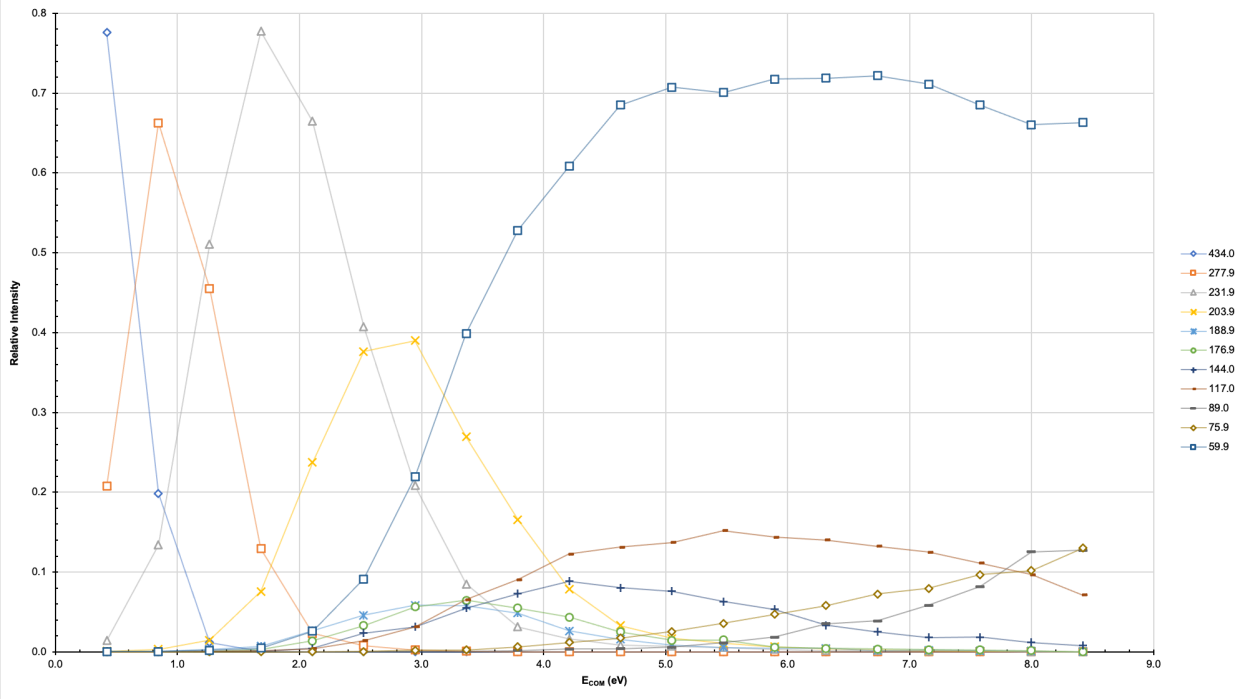

Appendix VI. Breakdown diagrams for Nickel (II) Nitrate and 4,4'-Bipyridine, dual-spray.

A6.1. Breakdown diagram for the 1:1 complex ($NiC_{10}H_8N_2^+$) at 216.0 *m/z* in the transfer from 0-30eV.

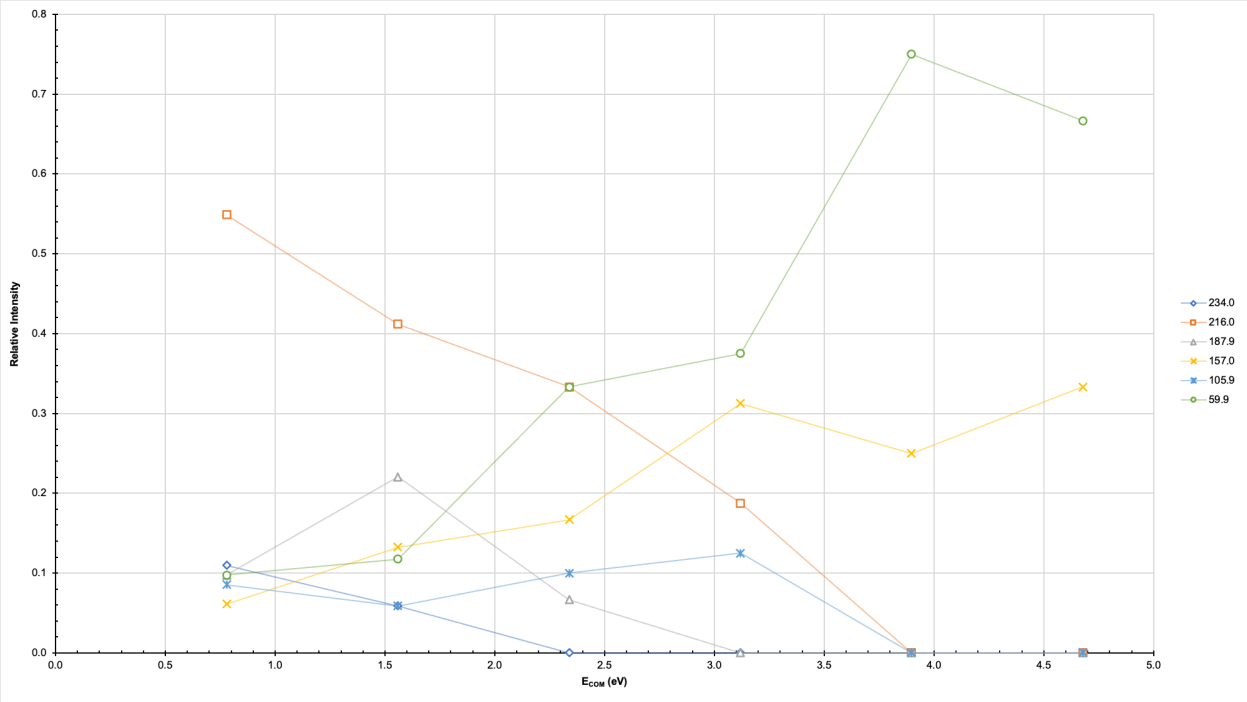

A6.2. Breakdown diagram for the nitrated 1:1 complex ($NiC_{10}H_8N_2NO_3^+$) at 277.9 *m/z* in the transfer from 0-60eV.

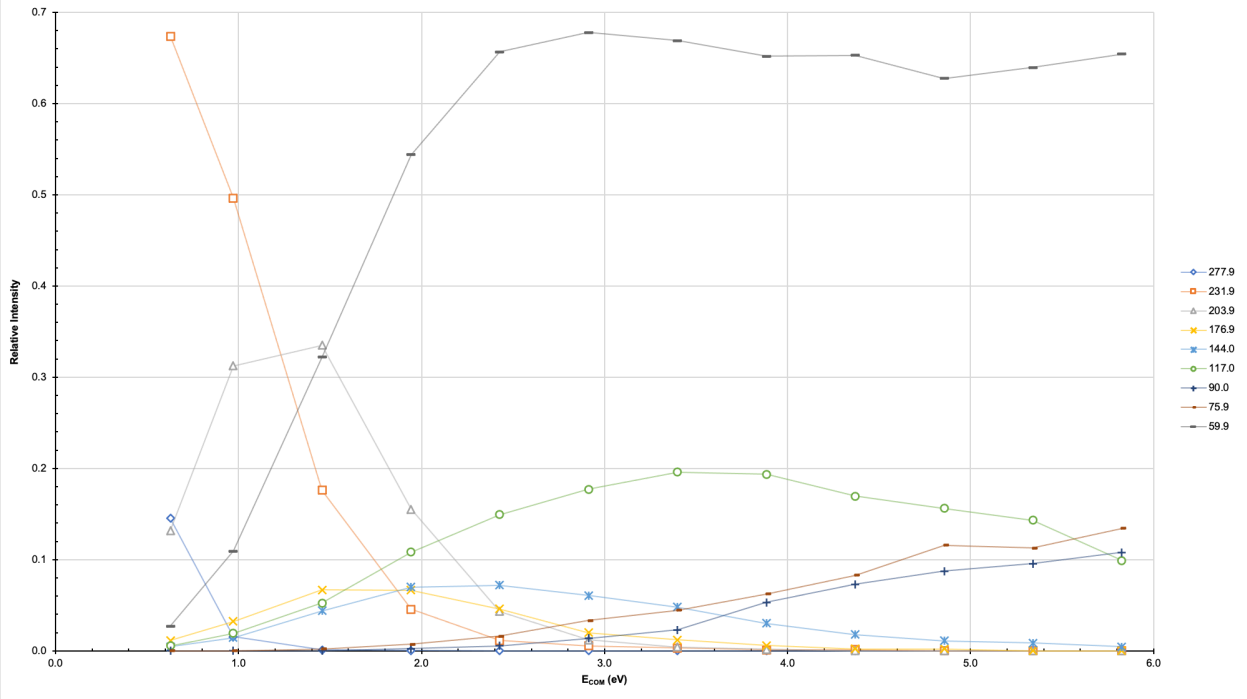

A6.3. Breakdown diagram for the 1:2 complex ($NiC_{10}H_8N_2C_{10}H_7N_2^+$) at 371.0 *m/z* in the transfer from 0-100eV.

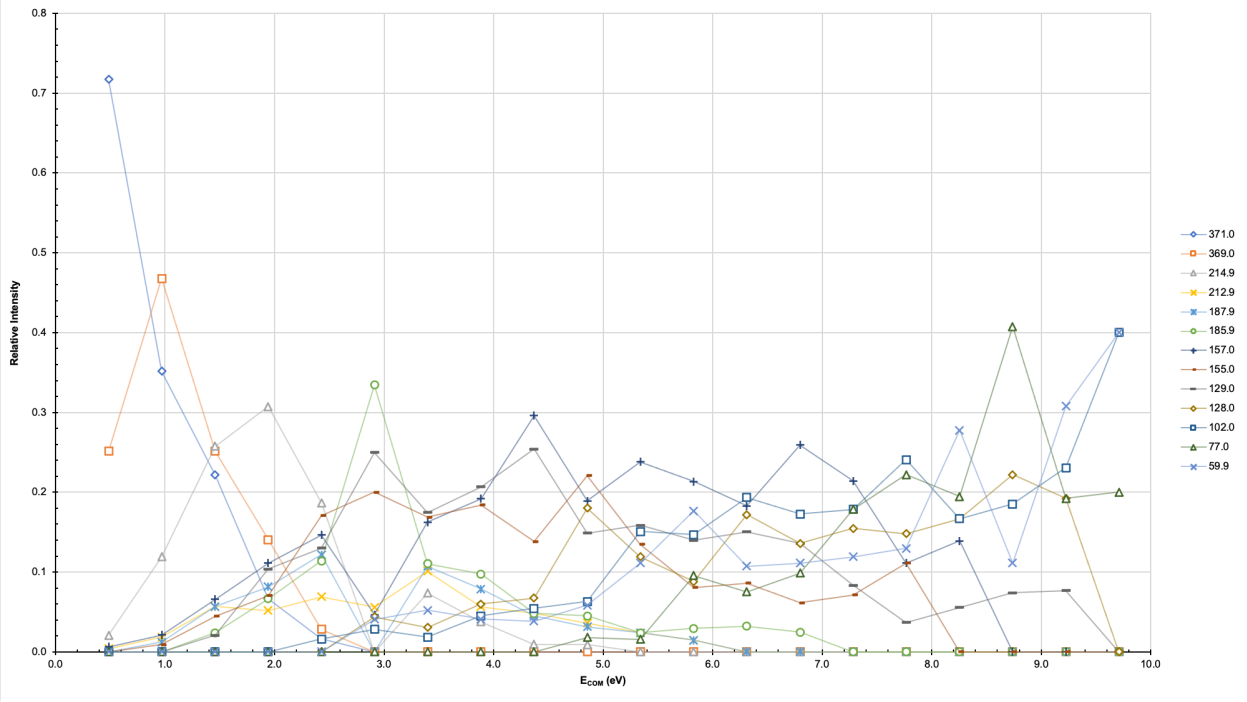

A6.4. Breakdown diagram for the nitrated 1:2 complex ($NiC_{10}H_8N_2C_{10}H_8N_2NO_3^+$) at 434.0 *m/z* in the transfer from 0-100eV.

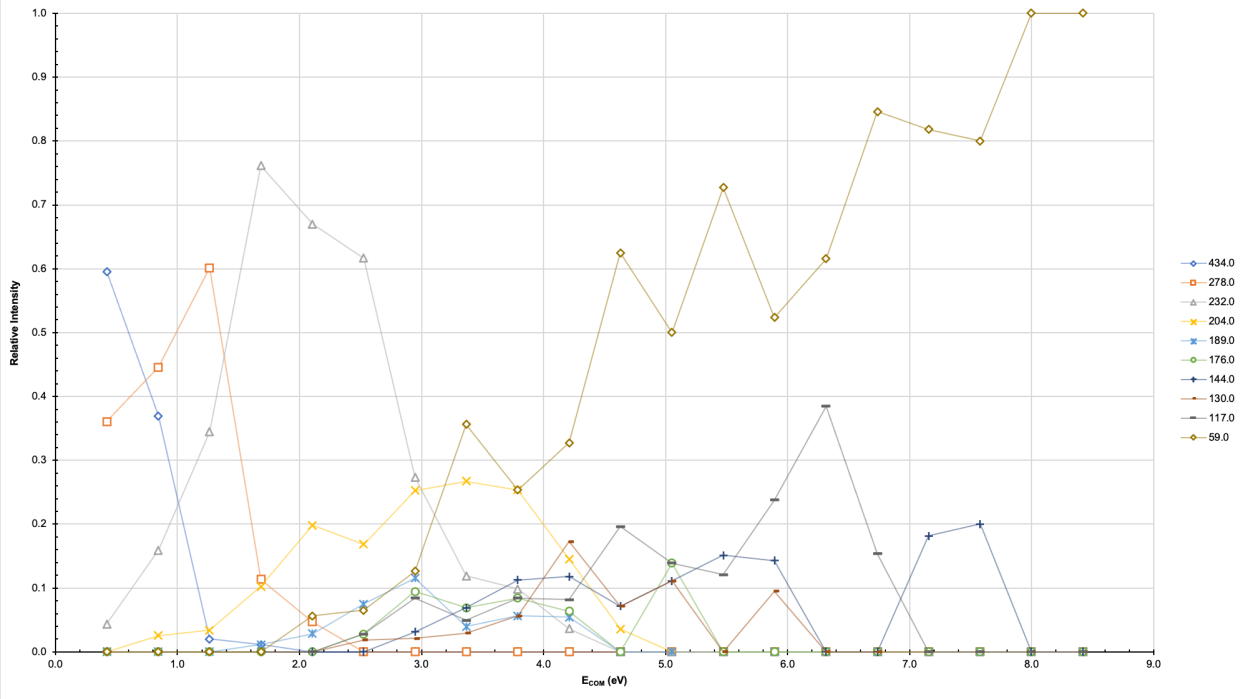

Appendix VII. Breakdown diagrams for Nickel (II) Nitrate and 2,2'-Bipyridine-4,4'-Dicarboxylic Acid, single-spray.

A7.1. Breakdown diagram for the 1:1 complex ($NiC_{12}H_8N_2O_4^+$) at 303.9 *m/z* in the trap from 0-60eV.

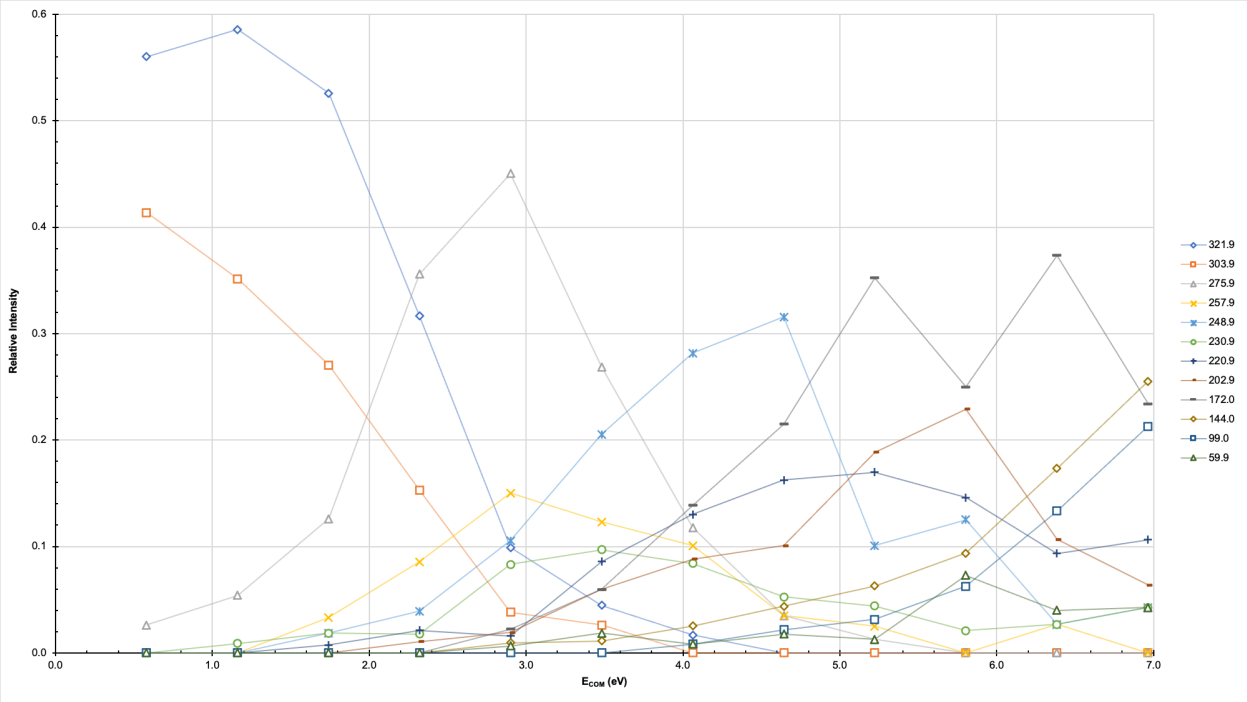

A7.2. Breakdown diagram for the 1:1 complex ($NiC_{12}H_8N_2O_4^+$) at 303.9 *m/z* in the transfer from 0-60eV.

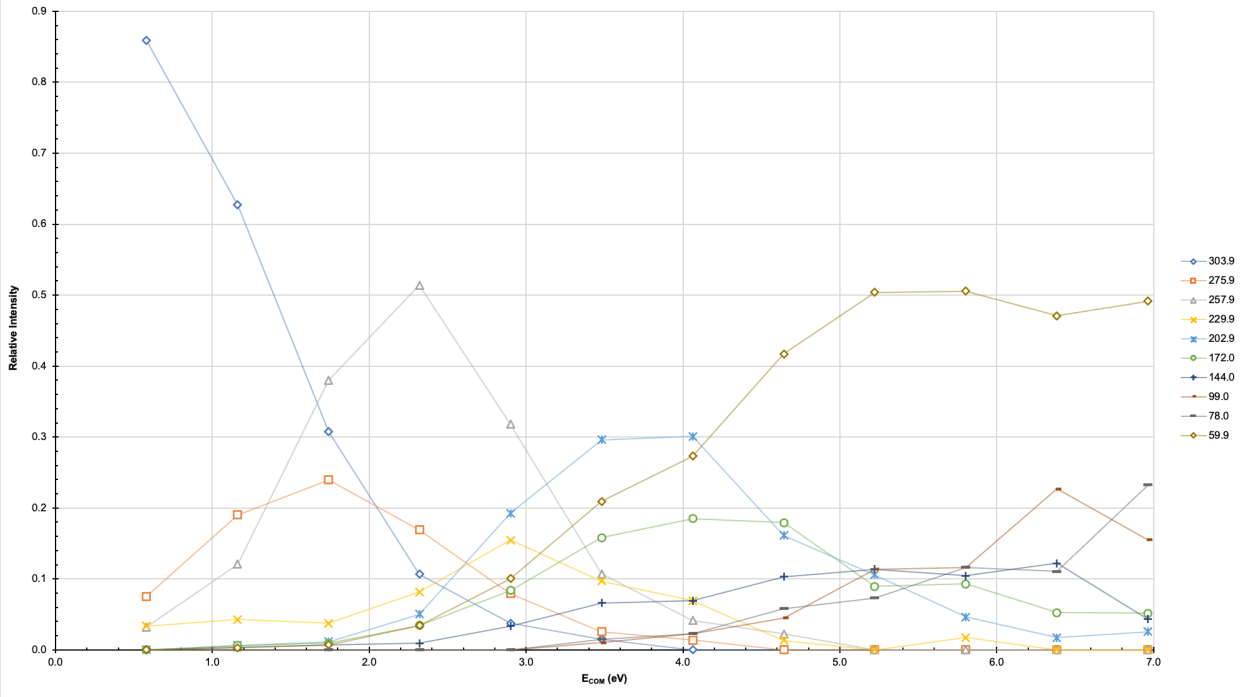

A7.3. Breakdown diagram for the nitrated 1:1 complex ($NiC_{12}H_8N_2O_4NO_3^+$) at 365.9 *m/z* in the trap from 0-75eV.

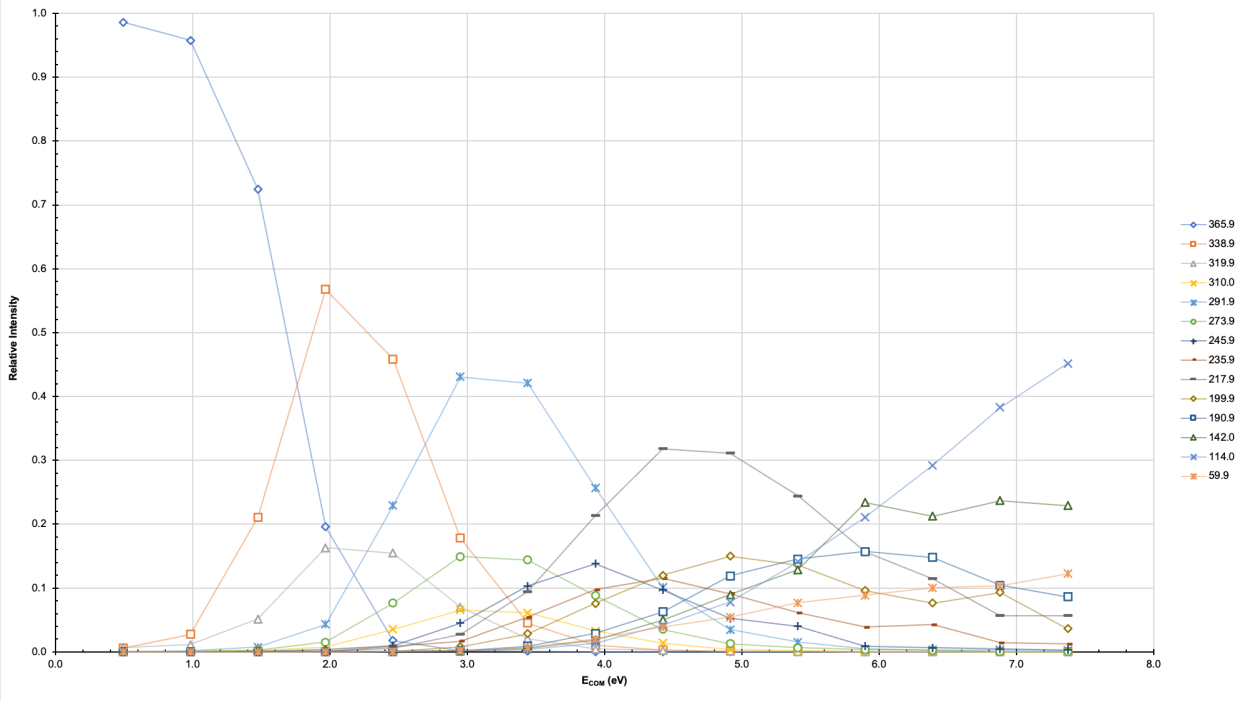

A7.4. Breakdown diagram for the nitrated 1:1 complex ($NiC_{12}H_8N_2O_4NO_3^+$) at 365.9 *m/z* in the transfer from 0-75eV.

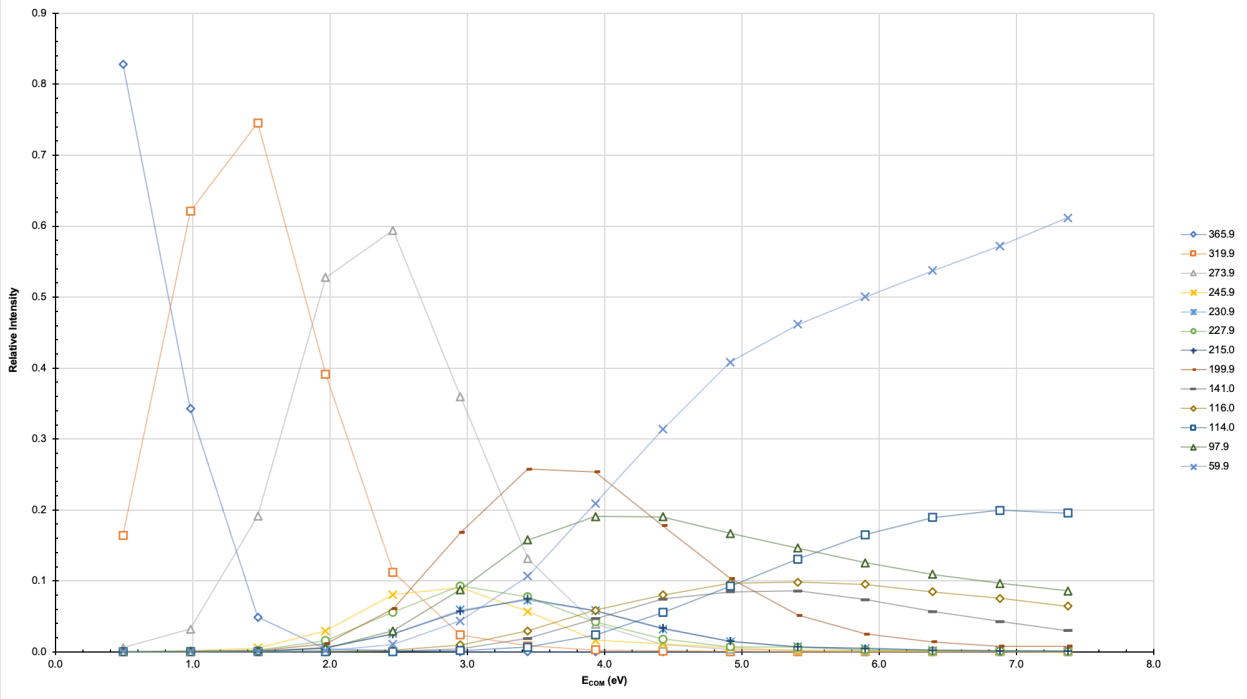

A7.5. Breakdown diagram for the 1:2 complex ($NiC_{12}H_8N_2O_4C_{12}H_8N_2O_4^+$) at 546.9 *m/z* in the trap from 0-100eV.

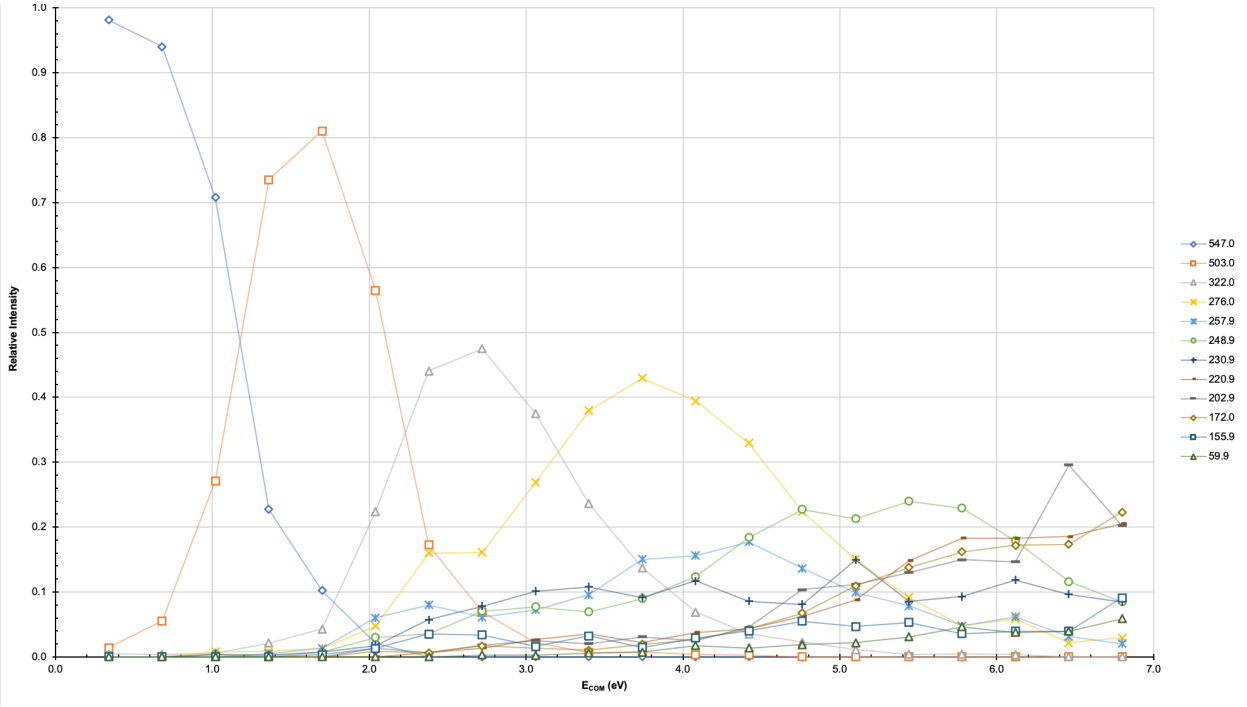

A7.6. Breakdown diagram for the 1:2 complex ($NiC_{12}H_8N_2O_4C_{12}H_8N_2O_4^+$) at 546.9 *m/z* in the transfer from 0-75eV.

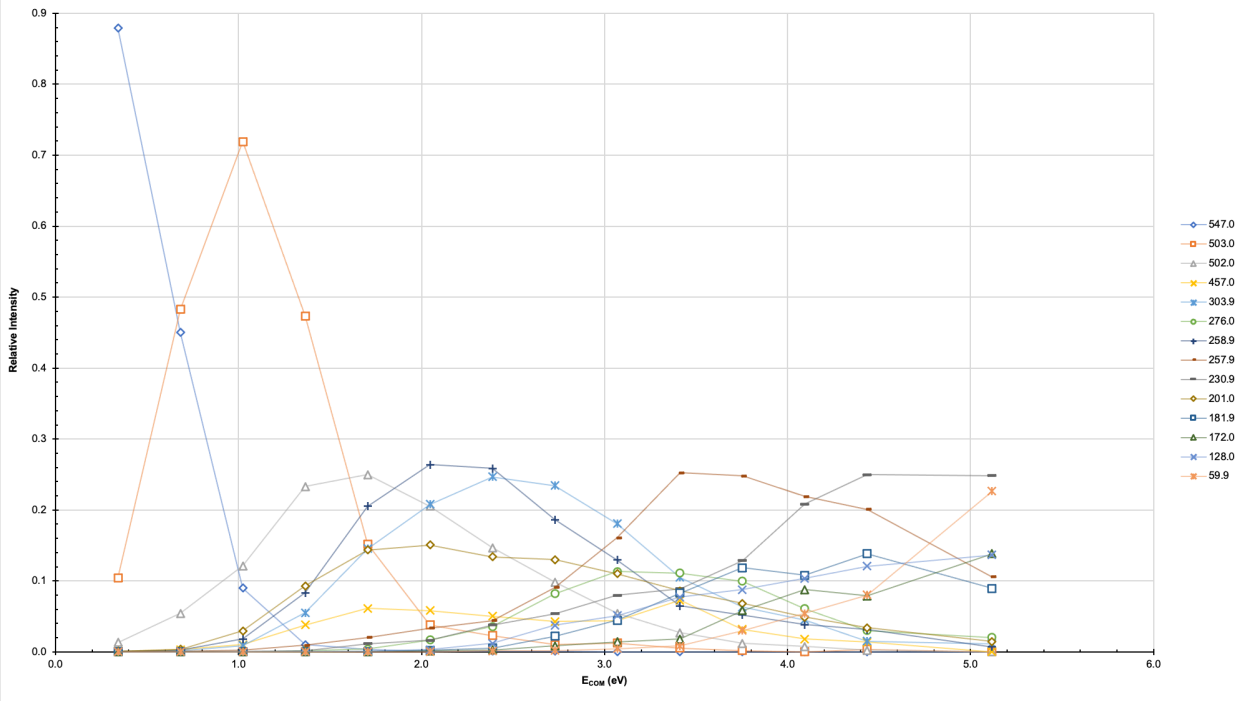

A7.7. Breakdown diagram for the nitrated 1:2 complex ($NiC_{12}H_8N_2O_4NiC_{12}H_8N_2O_4NO_3^+$) at 609.9 *m/z* in the trap from 0-100eV.

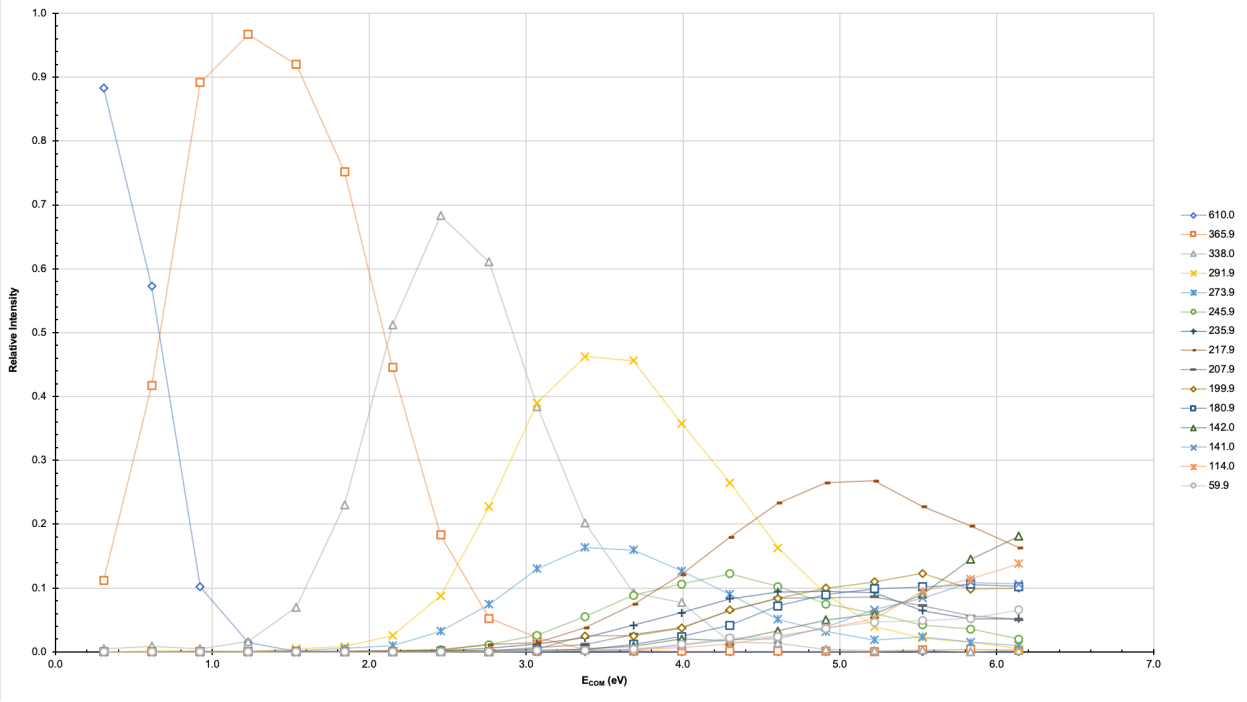

A7.8. Breakdown diagram for the nitrated 1:2 complex ($NiC_{12}H_8N_2O_4NiC_{12}H_8N_2O_4NO_3^+$) at 609.9 *m/z* in the transfer from 0-100eV.

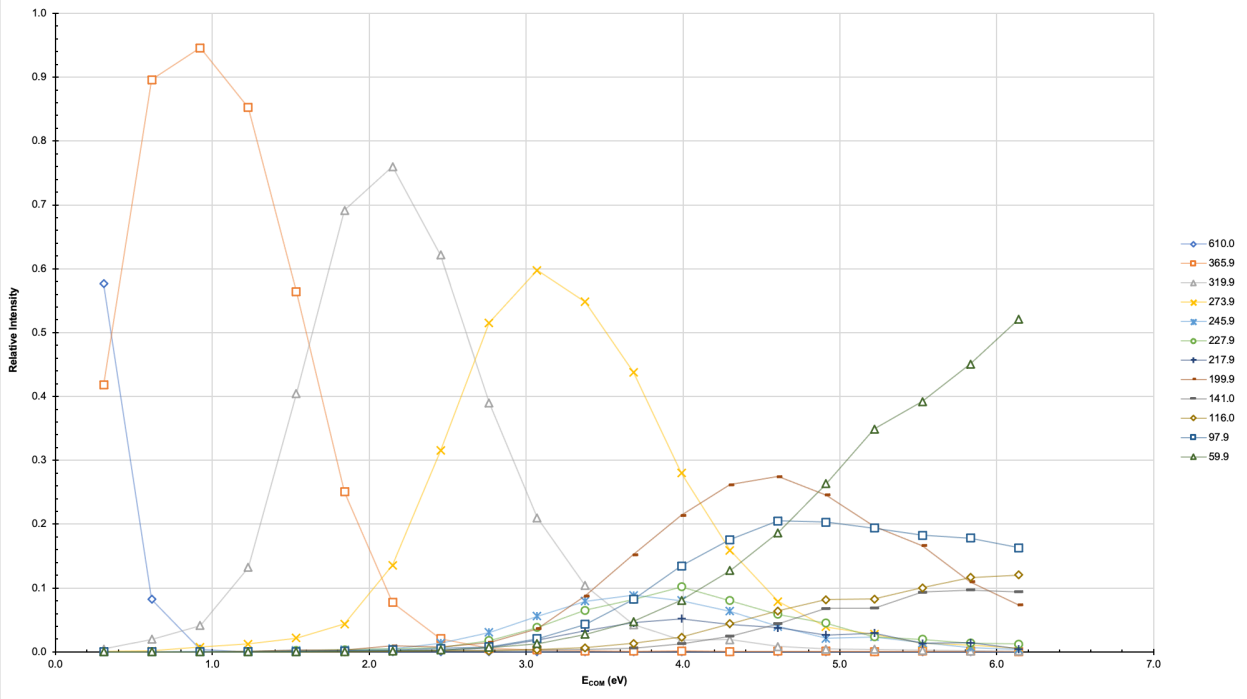

Appendix VIII. Breakdown diagrams for Nickel (II) Nitrate and 1,10-Phenanthroline, single-spray.

A8.1 Breakdown diagram for the 1:1 complex ($NiC_{12}H_8N_2^+$) at 239.9 *m/z* in the trap from 0-40eV.

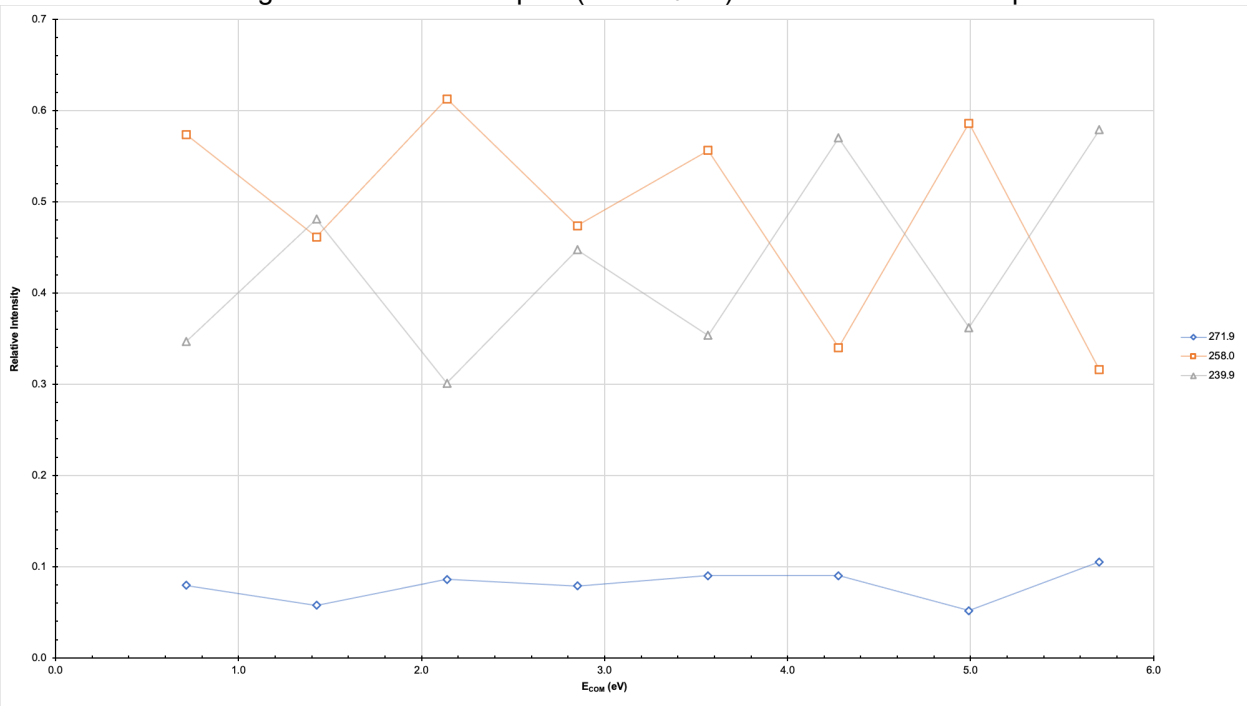

A8.2 Breakdown diagram for the 1:1 complex ($NiC_{12}H_8N_2^+$) at 239.9 *m/z* in the transfer from 0-60eV.

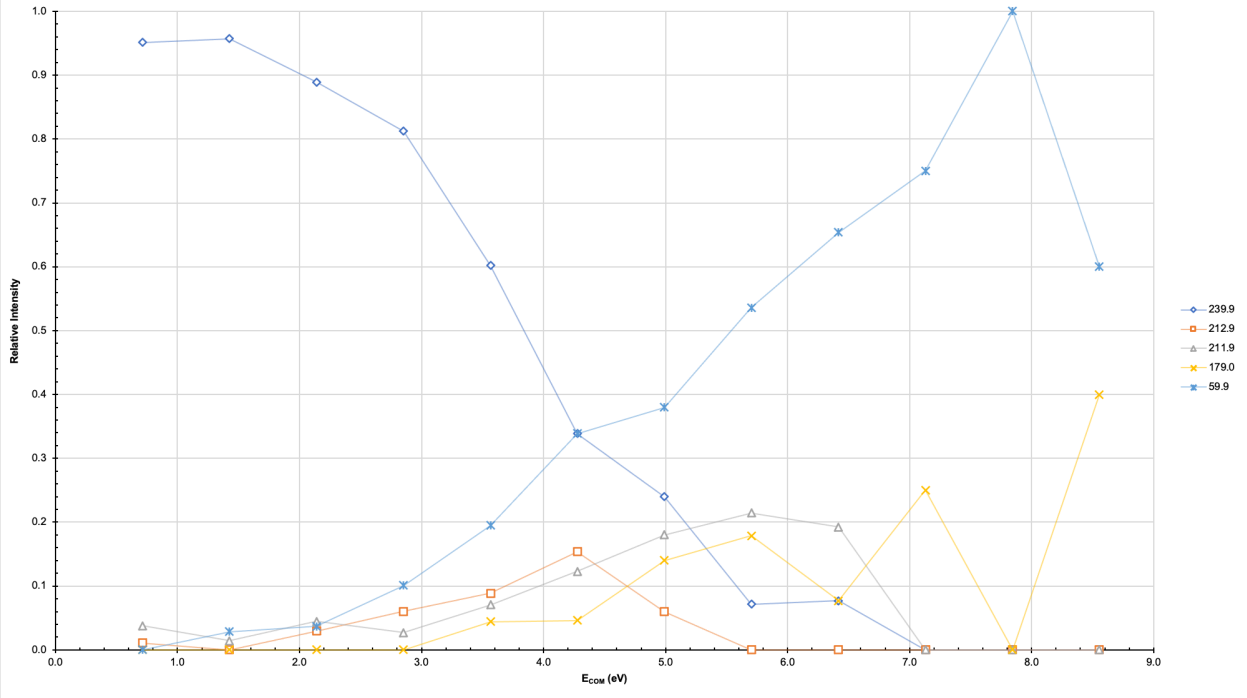

A8.3 Breakdown diagram for the nitrated 1:1 complex ($NiC_{12}H_8N_2NO_3^+$) at 301.9 *m/z* in the trap from 0-100eV.

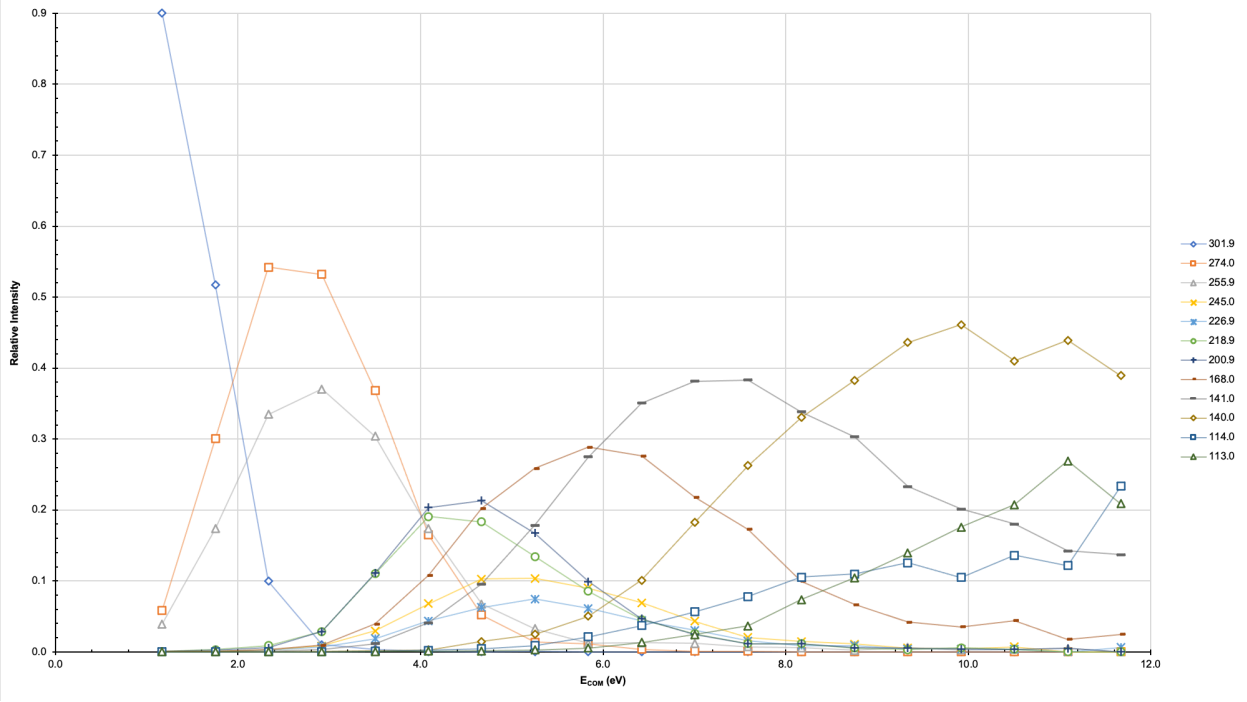

A8.4. Breakdown diagram for the nitrated 1:1 complex ($NiC_{12}H_8N_2NO_3^+$) at 301.9 *m/z* in the transfer from 0-100eV.

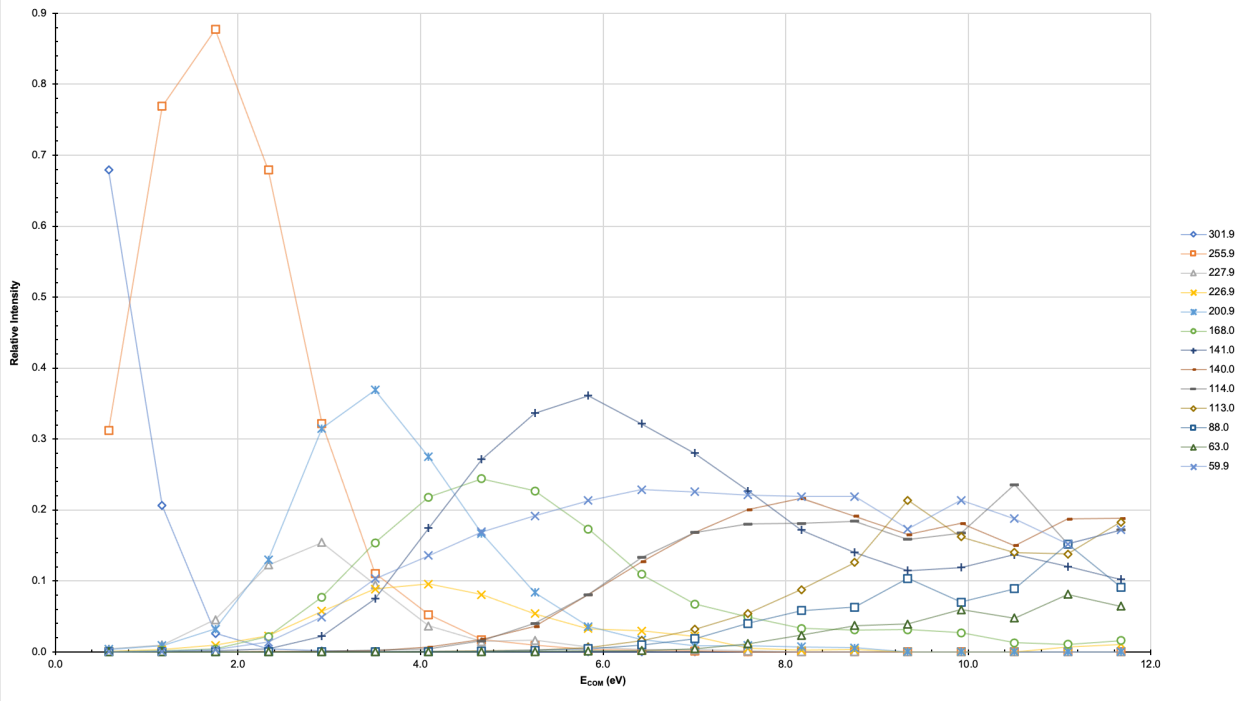

A8.5. Breakdown diagram for the 1:2 complex ($NiC_{12}H_8N_2C_{12}H_8N_2^+$) at 420.0 *m/z* in the trap from 0-100eV.

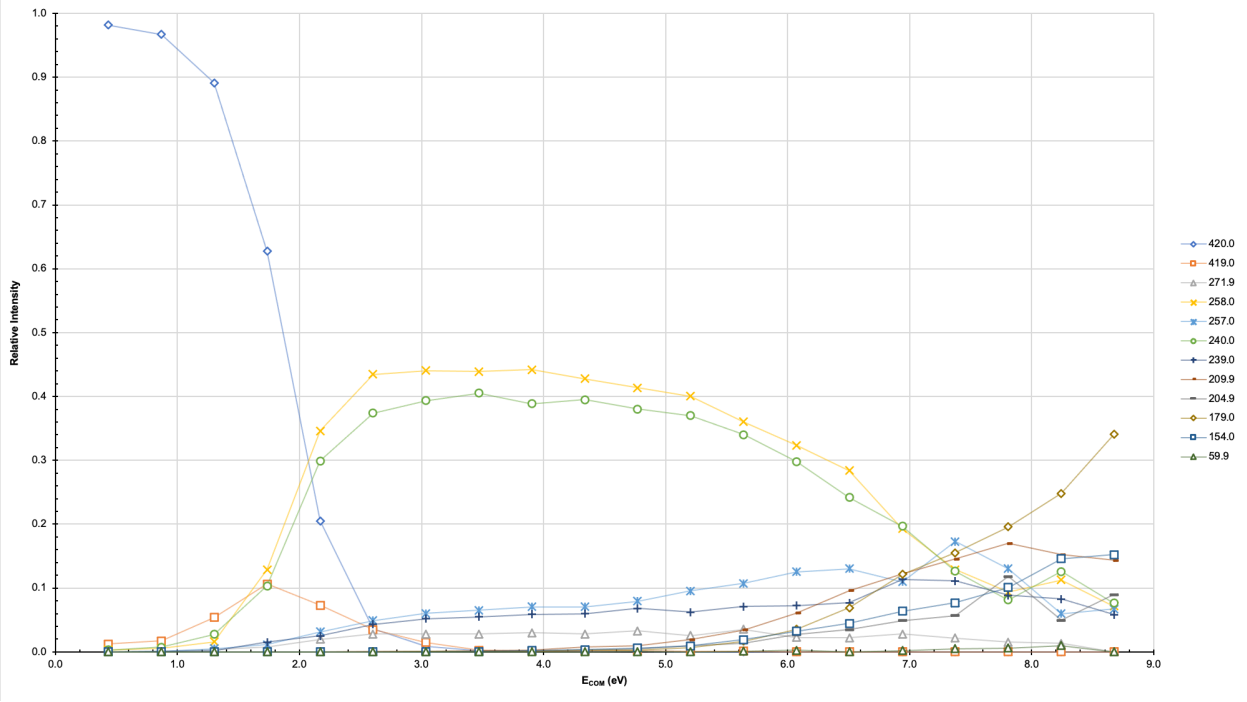

A8.6. Breakdown diagram for the 1:2 complex ($NiC_{12}H_8N_2C_{12}H_9N_2^+$) at 421.0 *m/z* in the transfer from 0-100eV.

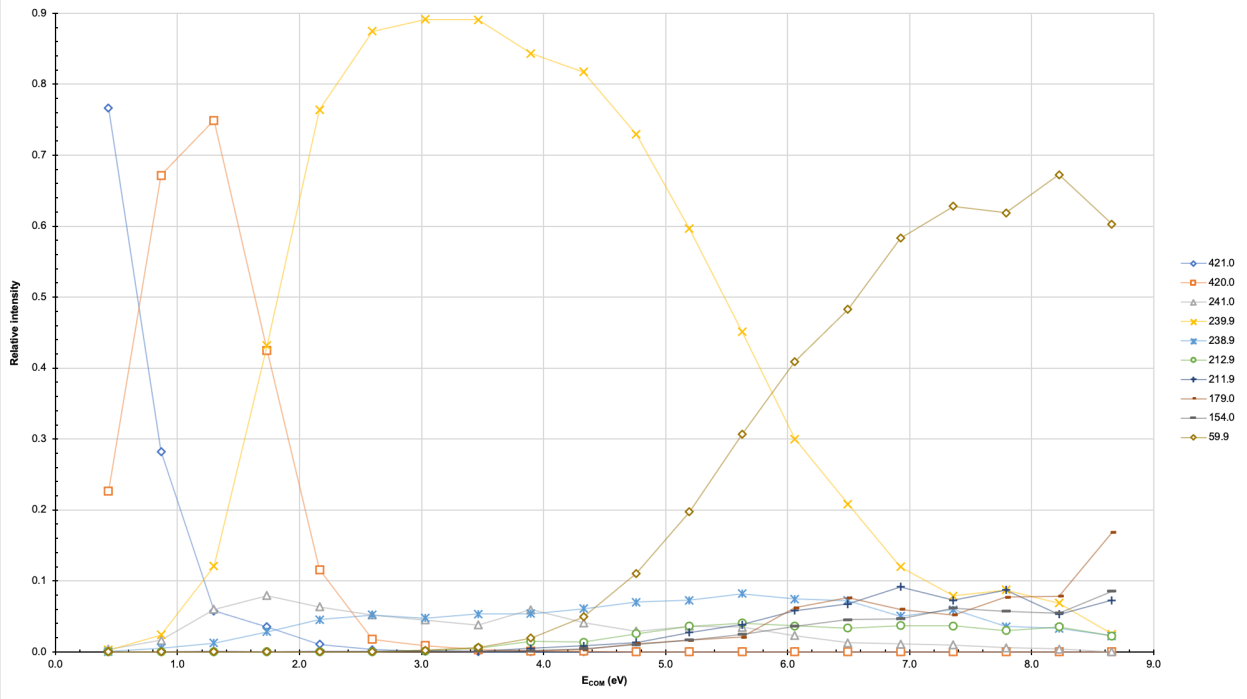

A8.7. Breakdown diagram for the nitrated 1:2 complex ($NiC_{12}H_8N_2C_{12}H_8N_2NO_3^+$) at 482.0 *m/z* in the trap from 0-100eV.

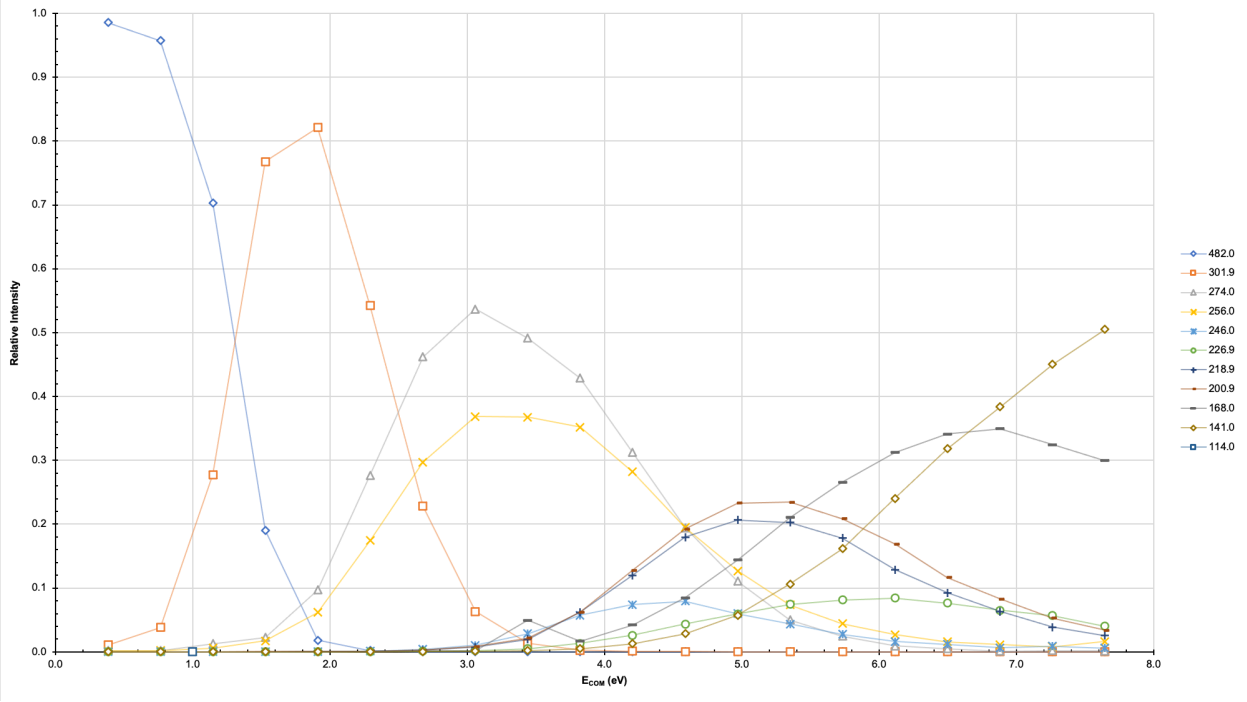

A8.8. Breakdown diagram for the nitrated 1:2 complex ($NiC_{12}H_8N_2C_{12}H_8N_2NO_3^+$) at 482.0 *m/z* in the transfer from 0-100eV.

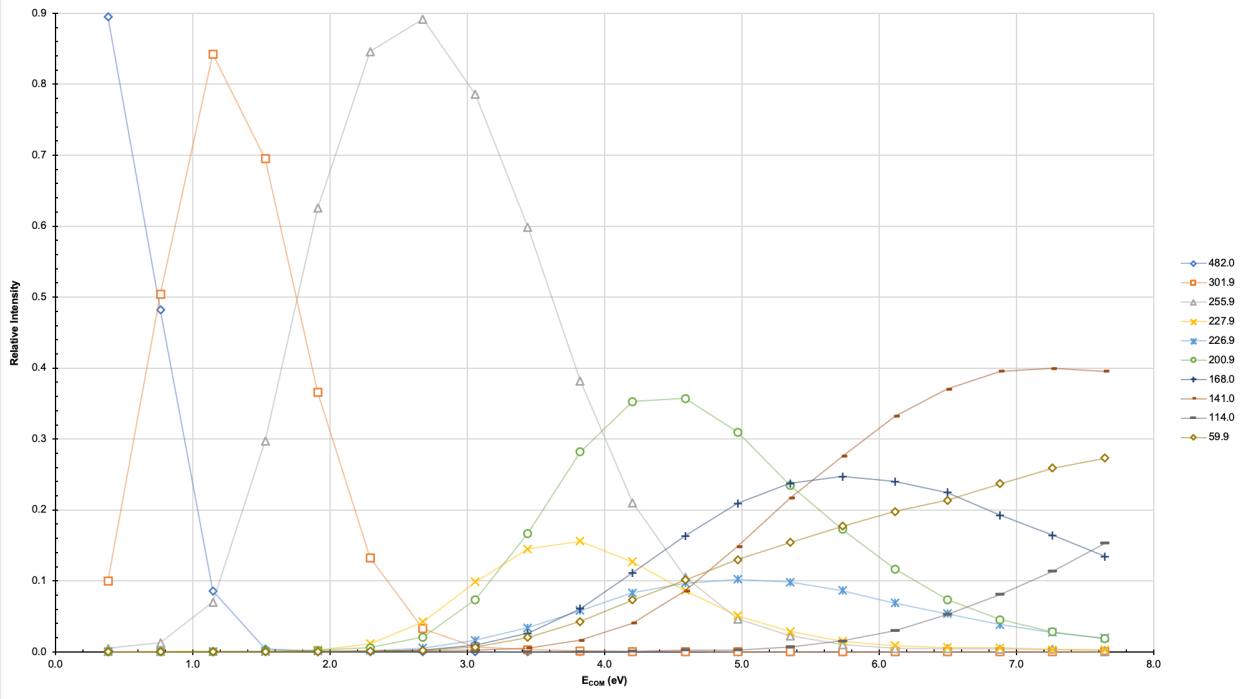

Appendix IX. Breakdown diagrams for Nickel (II) Nitrate and 1,10-Phenanthroline, dual-spray.

A9.1. Breakdown diagram for the 1:1 complex ($NiC_{12}H_8N_2^+$) at 240.0 *m/z* in the transfer from 0-40eV.

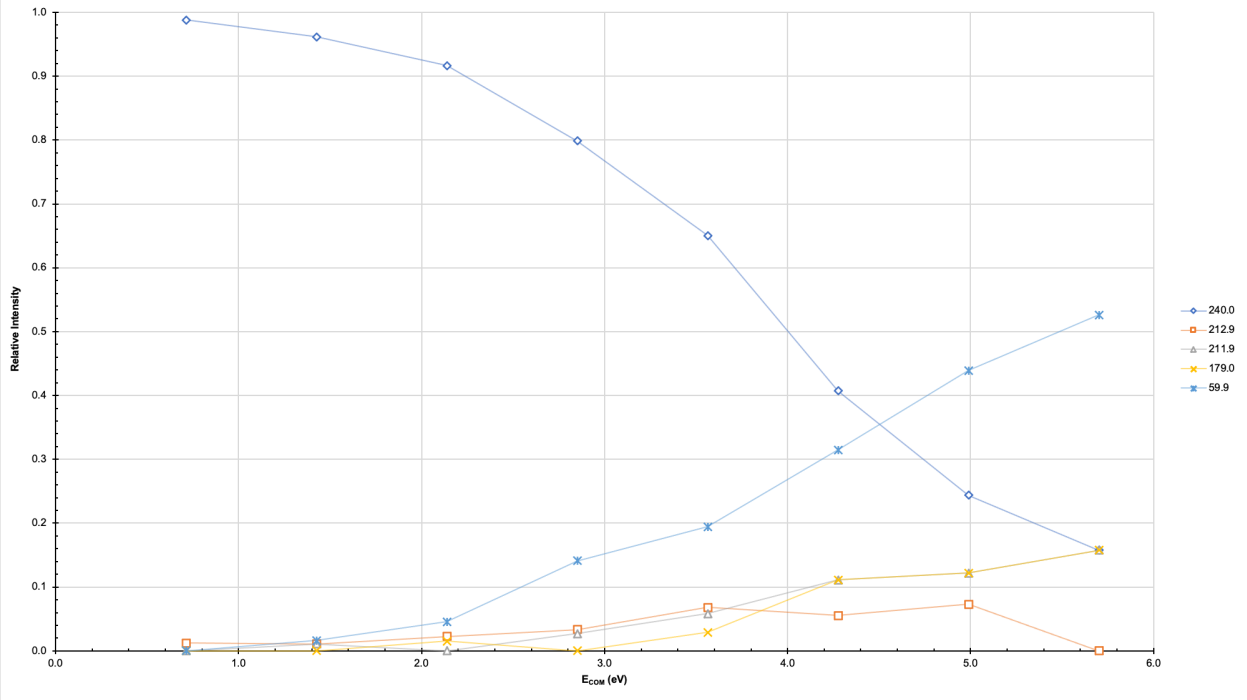

A9.2. Breakdown diagram for the nitrated 1:1 complex ($NiC_{12}H_8N_2NO_3^+$) at 302.0 *m/z* in the transfer from 0-100eV.

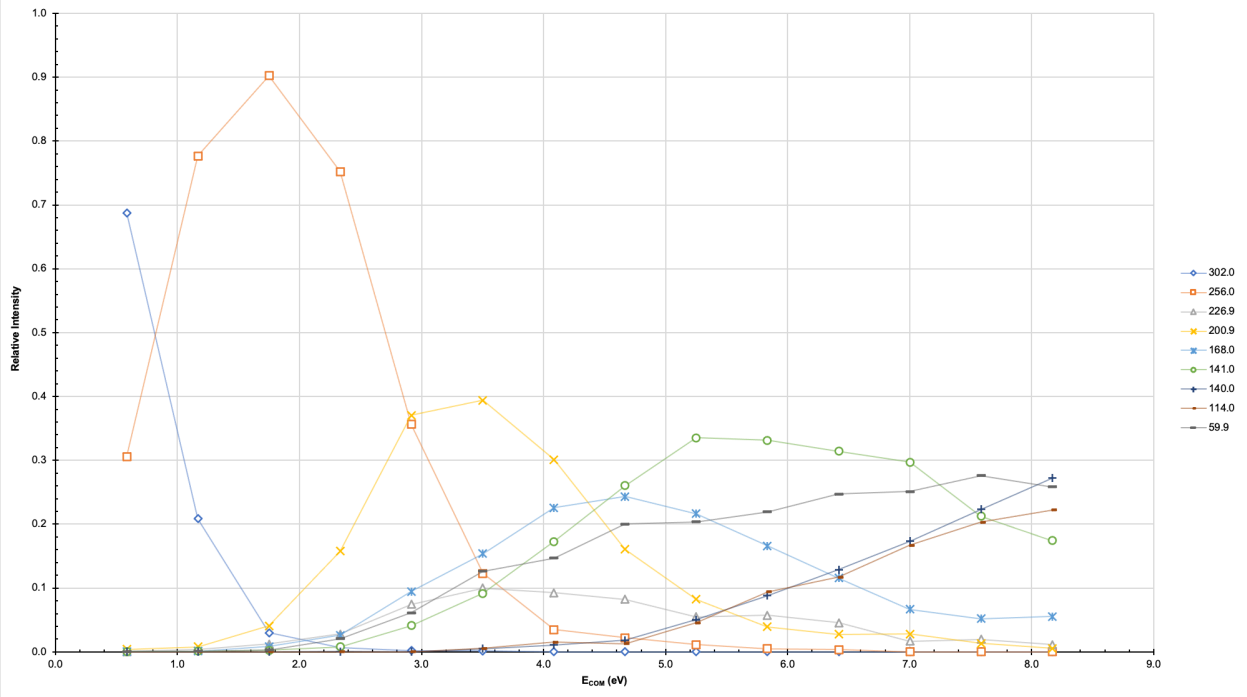

A9.3. Breakdown diagram for the 1:2 complex ($NiC_{12}H_8N_2C_{12}H_8N_2^+$) at 420.0 *m/z* in the transfer from 0-80eV.

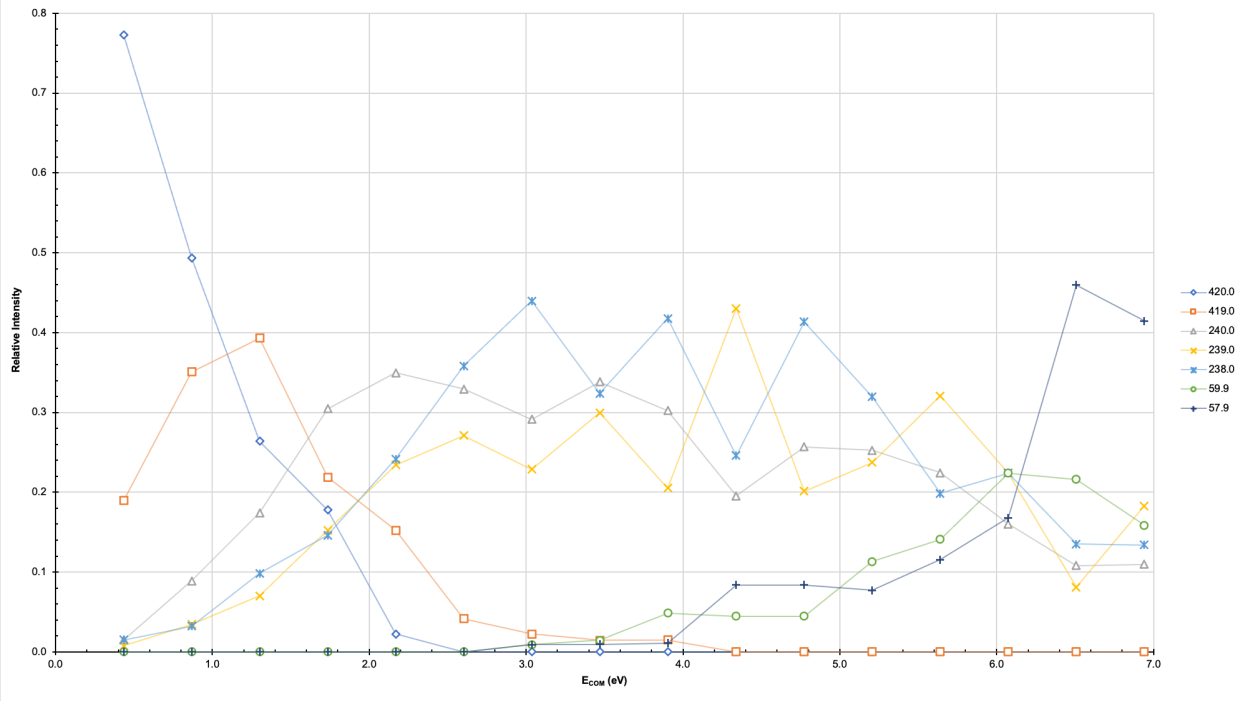

A9.4. Breakdown diagram for the nitrated 1:2 complex ($NiC_{12}H_8N_2C_{12}H_8N_2NO_3^+$) at 482.0 *m/z* in the transfer from 0-100eV.

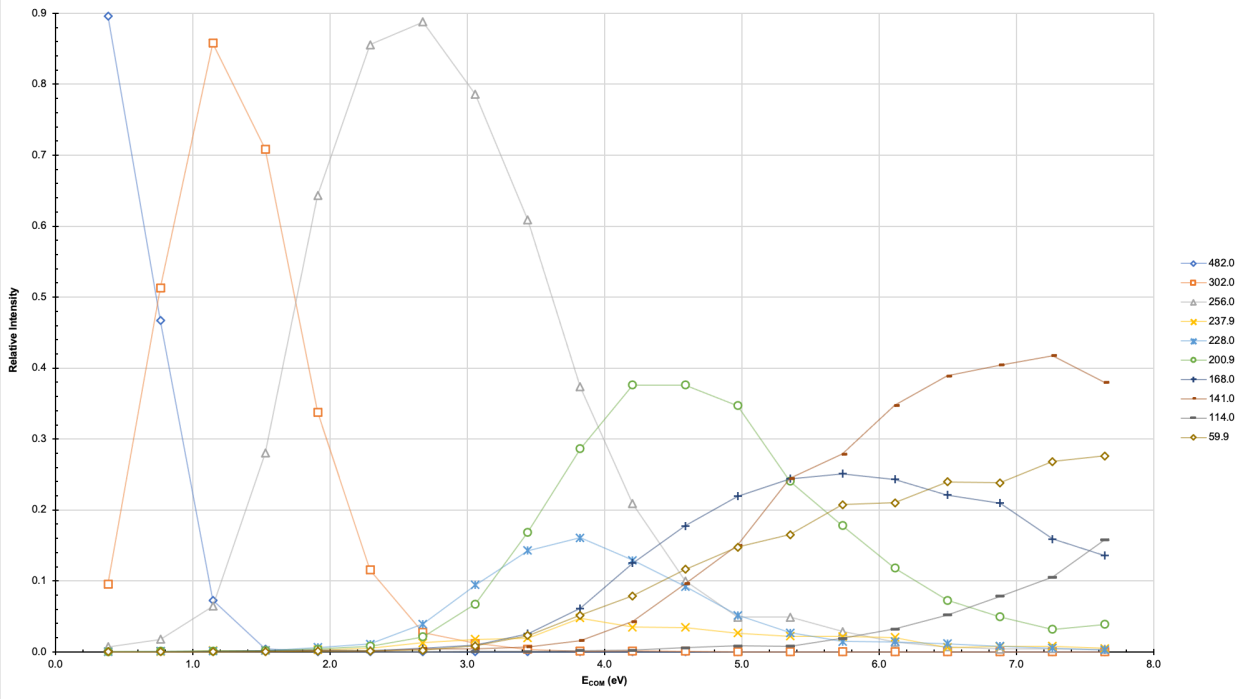

Appendix X. Breakdown diagrams for Nickel (II) Nitrate and SNS, single-spray.

A10.1 Breakdown diagram for the 1:1 complex ($NiC_{14}H_{12}NS_2^+$) at 317.9 *m/z* in the trap from 0-75eV.

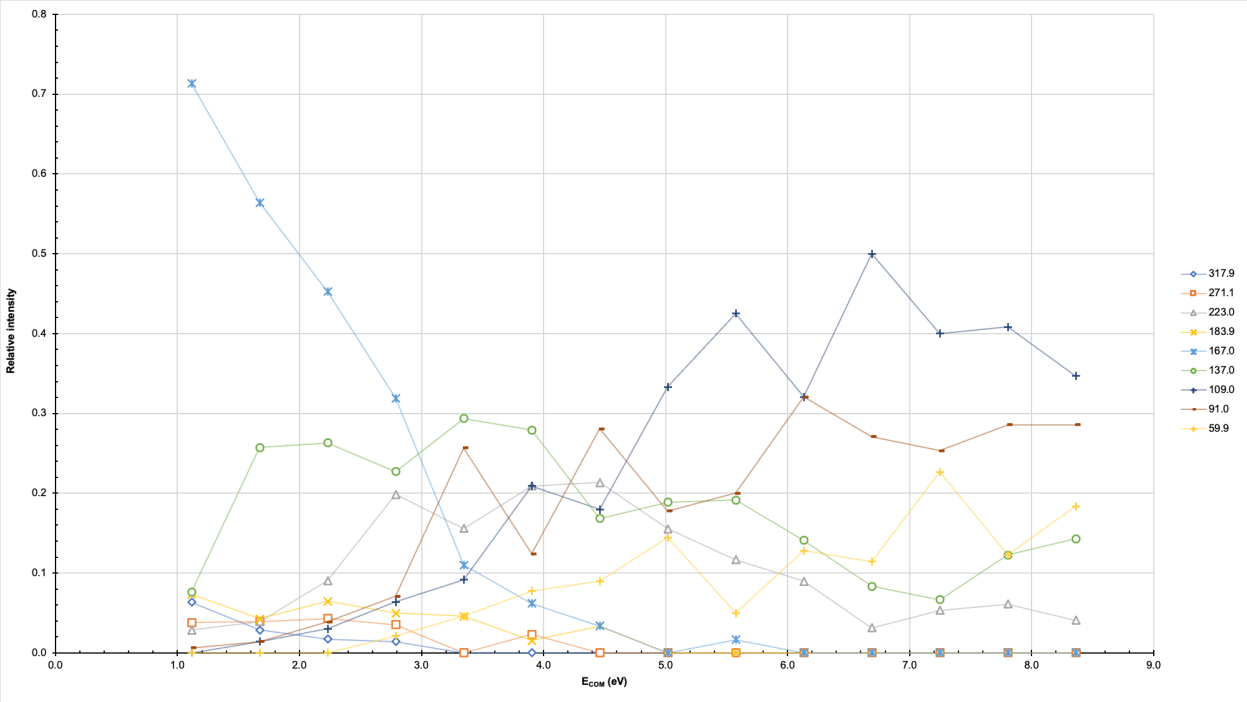

A10.2 Breakdown diagram for the 1:1 complex ($NiC_{14}H_{12}NS_2NO_3^+$) at 378.9 *m/z* in the transfer from 0-75eV.